Heat Transfer Parameters of Cylindrical Catalyst Particles with Internal Voids in Fixed Bed Reactor Tubes

A Major Qualifying Project Report

Submitted to the Faculty of the
WORCESTER POLYTECHNIC INSTITUTE

in partial fulfillment of the requirements for the
Degree of Bachelor of Science
In Chemical Engineering

By

Michael Ashman _____

Dmitriy Rybak _____

William Skene _____

Date: December 2009

Approved:

_____
Dr. Anthony G. Dixon, Advisor

Abstract

This study measured and analyzed fixed bed heat transfer parameters for different size and shape packing materials that might be used for steam methane reforming. These parameters were compared to those found in the literature for similar packing types with fair agreement. The monoliths and 4-hole cylinders gave better radial heat transfer than the raschig rings; however the monoliths are too brittle for industrial processes.

Executive Summary

Steam methane reforming is a very important process for the industrial world and has many large scale applications. This process requires a very high operating temperature, high process flow rates, and also requires the presence of a catalyst. It is therefore necessary to optimize the process by finding a suitable catalyst shape and size that has a high surface area and a low pressure drop. The catalyst particle must be durable enough to withstand the process conditions, and it must also be able to transfer heat evenly and effectively to ensure uniformity throughout the process.

To more accurately study how different shaped particles transfer heat through fixed bed reactors, we employed a column with a heated air flow through the middle of the bed with a water cooled jacket to regulate temperature. The column was packed with different shaped packing materials and the heat dispersion was measured across the cross section of the column using an array of thermocouples that measured the temperature at several radial positions. The process was conducted using four different packing materials, each at four different bed depths and six different air flow rates. This process was conducted in a column with a diameter of 4 inches, and again in a column with a diameter of 2 inches.

Once the system was at steady state for each run, the temperature readings for each run were collected and analyzed. We used the Inlet Profile Plug Flow model to analyze the data and compared results for the different packing types. When fitted to the data, the IPPF model allowed us to determine which packing had the best heat transfer through the column. Overall, we found that the monoliths and 4-hole cylinders had better heat transfer characteristics than the raschig rings; however, we noted that the monoliths are too brittle to be considered for an industrial process as they are very prone to break and create dust (causing large problems in this type of setting).

Contents

List of Figures

List of Tables

Introduction

In many cases, it is beneficial to convert natural gas into syngas (H_2 and CO) and then into a liquid through use of the Fischer-Tropsch process. The most common method used to convert natural gas into hydrogen is through conventional steam reforming (SR). Other methods similar to SR include Autothermal Reforming (AR) and Gas Heated Reforming (GHR). Commercial hydrogen production is also necessary for the production of ammonia, the production of methanol, as a reducing agent in metal ores, to increase the level of saturation in unsaturated fats and oils (such as margarine) and in hydrogen fuel cell research (New York Energy Research and Development Authority, 2009). The reaction taking place is shown below.

$$CH_4 + H_2O \leftrightarrow CO + 3H_2 \qquad \Delta H = +206 \text{ kJ/mol}$$

At high temperatures, above 700 degrees Celsius and with the use of a nickel catalyst, steam reacts with methane to produce hydrogen and carbon monoxide in fixed bed reactors. The process is highly endothermic, therefore this process consumes a lot of energy as heat. Thus, large amounts of energy are required to heat the reactors; over half of the plant's operating cost will be used for the syngas generation section alone. (US DOE, 2009) Production of hydrogen from methane has an efficiency of about 70%, and is the most common and cheapest method to produce hydrogen.

Fixed bed reactor tubes can have very high radial temperature gradients, and it is very important to ensure that there is effective heat transfer from the wall to the packing so that the reactor does not overheat and fail. A steam reformer facility usually has several hundred of these fixed bed reactor tubes and they each usually cost about $6,000-$7,000 due to the high process temperature that they are designed for. It is therefore very important to fully understand how the packing shape affects the radial heat transfer to maximize the lifespan of the reactors. Since altering the wall temperature of one of these tubes by 20 K can shorten the lifespan of the tubes from ten years to less than five, this can save the company millions of dollars over time (Dixon, 2009).

A lot of effort is therefore spent researching the best methods to heat the reactor tubes, so that the tubes are heated evenly and efficiently. There are several different approaches to the design of burners, including top, side and terraced wall firing for the steam reformers. Hundreds of burners are used to ensure that the heating is done in a uniform manner through the reformer.

In order to improve the interaction between the steam and the methane within the fixed bed, the reactor is filled with catalyst coated packing (Smirnov, 2003). The shape of the packing determines the amount of interaction between the steam and methane, and also determines the heat flow through the reactor. In order to control the process most efficiently, it is necessary to analyze how the shape and size of the packing alters the flow of heat through the reactor. In addition, the packing must function practically within the tube. The strength and durability of the packing are serious concerns and the packing must also be shaped properly to avoid sharp edges on the packing that lead to particle deterioration and dust that would contaminate the equipment.

Another vital concern in the development of a steam reformer is ensuring that the catalysts are loaded into the reactor tubes in a uniform manner (Stitt, 2005). If any tubes are packed tighter or less densely than another, then the reactant flow to the tubes which are in parallel would tend to have higher flows in some of the tubes than others which lead to hot spots and eventually system failure. To overcome this challenge, technicians perform highly accurate tests to ensure that the pressure drop across each tube for a given flow rate is as uniform as possible to ensure that the reactant flow does not tend towards certain reactor tubes over others.

There is a difficult tradeoff when deciding what kind of catalyst packing to use in a packed bed reactor. Catalysts are more effective with higher surface area, which would indicate that smaller particles with a larger surface area would be beneficial. But it is also true that larger packing particles require a lower pressure drop across the column, which allows for higher flow rates through the column. In addition, the tube to particle diameter ratio also determines the efficiency of the radial heat transfer (Stitt, 2005).

Research in the past regarding heat transfer modeling in packed beds is lengthy. Some of the first significant research was conducted by Coberly and Marshall in 1951, who were the first

engineers to use h_w and k_r as prior work had utilized k_r and $k_r(r)$. In 1972 DeWasch and Froment were the first to question the perceived dependence of k_r and h_w to bed height. In 1975, Gunn and Khalid were the first to introduce the concept of axial thermal dispersion, represented by the term k_a. In 1978, Bauer and Schünder developed what is today the standard model for k_r. Also in 1978, Dixon and Creswell introduced the theory that k_r and h_w ware not height dependant. In 1985, Dixon showed that k_a had little physical basis, he also measured heat leaks through the calming section to eliminate height dependence. In 1988, Dixon reviewed Pe_r and Bi with a significant amount of heat transfer data. In 1993, Borkink, Borman and Westerterp introduced the Inlet Profile Plug Flow model to eliminate height dependence of the packing. In 1993, Martin and Niles found a relationship to describe Nu_w. In 1996, Landon, Hebert and Adams published results for different shaped packing materials. In 1997, Dixon looked at the effect that a low tube-to-particle ratio has on heat transfer for spheres.

There are many different shapes of packing used industrially for steam reforming, but there has been little research done exploring the heat transfer through fixed beds containing cylindrical packing with internal holes and domes. The main purpose of the team's research is to analyze the heat transfer across a fixed bed with different shaped packing. From these findings, optimal designs for catalyst particles can be suggested, which is a major step in the effort to develop more efficient steam reforming technology.

Background

Heat transfer is categorized into three types: conduction, convection, and radiation. For these experiments, radiation does not apply as the temperatures were relatively low. Through research done over the years, models have been created using Fourier's law where conduction and convection parameters are strictly based on packing size and shape as well as fluid flow. The effective radial thermal conductivity, k_r, represents all mechanisms of heat transfer in the center of the bed (unaffected by wall effects). The wall heat transfer coefficient, h_w, is a parameter representing the increased heat transfer resistance close to the wall. Both of these parameters can be found from data using models such as the Plug Flow (PF) model or the Inlet Profile Plug Flow (IPPF) model.

In order to model the heat transfer using the equipment and model used, the following assumptions were made:

- The system was in steady state
- No reaction took place
- There is no radiation
- The pressure throughout the bed was constant
- No radial variation of the superficial gas velocity (Reynolds number)
- The wall temperature was constant and steady for each run
- The physical properties of the gas and solid were independent of temperature

IPPF Model

The standard model used to analyze the temperature profile data acquired was the Inlet Profile Plug Flow (IPPF) model. The PF model uses the temperature of the inlet air as the inlet temperature; however, with the apparatus in the laboratory, it was impossible to determine the temperature of the air flowing into the packing at $z = 0$ due to heat loss in the calming section. The IPPF model uses the first height temperature profile as the inlet temperature profile, and compares it to the temperature profiles at consequent heights.

The IPPF model is derived from the following dimensional energy balance:

$$GC_p \frac{\partial T}{\partial z} = k_r \left(\frac{\partial^2 T}{\partial r^2} + \frac{1}{r} \frac{\partial T}{\partial r} \right)$$

With the following boundary conditions:

$$T = T_{z,o}(r) \; at \; z = z_o$$

$$\frac{\partial T}{\partial r} = 0 \; at \; r = 0$$

$$-k_r \frac{\partial T}{\partial r} = h_w (T - T_w) \; at \; r = R$$

These equations are usually made dimensionless by defining the following:

$$\vartheta = \frac{(T - T_w)}{(T_o - T_w)}$$

$$y = \frac{r}{R}$$

$$x = z/R$$

$$Pe_R = \frac{GC_p R}{k_r}$$

$$Bi = \frac{h_w R}{k_r}$$

In this case, using the first measurement height at $z=z_o$ as the inlet temperature, we get:

$$\zeta = \frac{{}^{z}/_{L} - {}^{z_o}/_{L}}{1 - {}^{z_o}/_{L}}$$

$$\frac{\partial \zeta}{\partial z} = \frac{1}{L} \frac{1}{1 - {}^{z_o}/_{L}}$$

So:

$$\frac{\partial T}{\partial z} = \frac{\partial T}{\partial \zeta}\frac{\partial \zeta}{\partial z} = \frac{1}{L}\ \frac{1}{1 - {}^{z_o}/_{L}}\frac{\partial T}{\partial \zeta}$$

Then:

$$GC_p\frac{1}{L}\frac{1}{1 - {}^{z_o}/_{L}}\frac{\partial \vartheta}{\partial \zeta} = k_r\frac{1}{R^2}(\frac{\partial^2 \vartheta}{\partial y^2} + \frac{1}{y}\frac{\partial \vartheta}{\partial y})$$

i.e.

$$\frac{\partial \vartheta}{\partial \zeta} = \frac{k_r L}{GC_p R^2}\left(1 - {}^{z_o}/_{L}\right)(\frac{\partial^2 \vartheta}{\partial y^2} + \frac{1}{y}\frac{\partial \vartheta}{\partial y})$$

Define:

$$Bo_{h,r}^{\theta} = \frac{GC_p R^2}{k_r L}$$

$$\theta = \frac{\vartheta}{\vartheta_o}$$

Where:

$$\vartheta_o = \frac{(T|_{r=o} - T_w)}{(T_o - T_w)}$$

Gives:

$$\frac{\partial \theta}{\partial \zeta} = \frac{1}{Bo_{h,r}^{\theta}}\left(1 - \frac{z_o}{L}\right)\left(\frac{\partial^2 \theta}{\partial y^2} + \frac{1}{y}\frac{\partial \theta}{\partial y}\right)$$

With boundary condition:

$$-k_r\frac{\partial T}{\partial r} = h_w(T - T_w)$$

This can be made dimensionless into:

$$-k_r\frac{1}{R}\frac{\partial \vartheta}{\partial y} = h_w\vartheta$$

This may be reduced to the following:

$$\frac{\partial \vartheta}{\partial y} + Bi\vartheta = 0$$

And then:

$$\frac{\partial \theta}{\partial y} + Bi\theta = 0$$

Assume a parabolic profile at $z = z_o$:

$$T = T|_{r=o} + A'r^2$$

Where A'<0 for cooling.

$$\frac{(T - T_w)}{(T_o - T_w)} = \frac{(T|_{r=o} - T_w)}{(T_o - T_w)} + \frac{A'}{T_o - T_w} R^2 y^2$$

$$\vartheta = \vartheta_o + \frac{A'R^2}{T_o - T_w} y^2$$

So:

$$\theta = \frac{\vartheta}{\vartheta_o} = 1 + \frac{A'R^2}{(T_o - T_w)\vartheta_o} y^2 = 1 - Ay^2$$

Where $A = \frac{A'R^2}{(T_o - T_w)\vartheta_o} > 0$ always.

The IPPF model is incorrect as given by Borkink (1993). It may be made correct by defining:

$$Bo^{\theta}_{h,r}(corrected) = \frac{GC_pR^2}{k_rL} \frac{1}{1 - {z_o}/{L}} = Bo^{\theta}_{h,r} \frac{1}{1 - {z_o}/{L}}$$

Convert into present variables using corrected $Bo^{\theta}_{h,r}$:

$$Bo^{\theta}_{h,r} = Pe_R \frac{R^2}{Ld_p} \frac{1}{1 - {z_o}/{L}} = Pe_R \frac{R}{L} \frac{1}{1 - x_o\, {R}/{L}}$$

$$\zeta = \frac{x\,{}^{R}/_{L} - x_o\,{}^{R}/_{L}}{1 - x_o\,{}^{R}/_{L}}$$

$$\frac{\partial \zeta}{\partial x} = \frac{R}{L}\,\frac{1}{1 - x_o\,{}^{R}/_{L}}$$

$$\vartheta = \frac{(T - T_w)}{(T_o - T_w)} \Big/ \frac{(T|_{r=o} - T_w)}{(T_o - T_w)}$$

$$= \left[\frac{(T_w - T_o)}{(T_w - T_o)} - \frac{(T - T_o)}{(T_w - T_o)}\right] \Big/ \left[\frac{(T_w - T_o)}{(T_w - T_o)} - \frac{\left(T|_{y=o} - T_o\right)}{(T_w - T_o)}\right]$$

$$= (1 - \vartheta)/(1 - \vartheta_o)$$

Equations become:

$$\frac{\partial \vartheta}{\partial x} = \frac{1}{Pe_R}\left(\frac{\partial^2 \vartheta}{\partial y^2} + \frac{1}{y}\frac{\partial \vartheta}{\partial y}\right)$$

With:

$$\vartheta = 1 - (1 - \vartheta_o)(1 - Ay^2)\ at\ x = x_o$$

$$\vartheta\ finite\ at\ y = 0.$$

$$\frac{\partial \vartheta}{\partial y} + Bi(\vartheta - 1) = 0\ at\ y = 1$$

This reduces to the conventional PF model if $x_o = 0$, $A = 0$, and ϑ_o. The solution is:

$$\vartheta = 1 - 2(1 - \vartheta_o)\sum_{i=1}^{\infty}\{\frac{[(Bi\lambda_i^2 + 4ABi - 2A\lambda_i^2 - ABi\lambda_i^2)J_o(\lambda_i y)]}{\lambda_i^2[\lambda_i J_o(\lambda_i) + BiJ_i(\lambda_i)]} e^{\left[-\frac{\lambda_i^2}{Pe_R}(x - x_o)\right]}\}$$

$$= 1 - 2(1 - \vartheta_o)\sum_{i=1}^{\infty}\{\frac{(Bi + 4ABi/\lambda_i^2 - 2A - ABi)}{[Bi^2 + \lambda_i^2]}\frac{J_o(\lambda_i y)}{J_o(\lambda_i)} e^{\left[-\frac{\lambda_i^2}{Pe_R}(x - x_o)\right]}\}$$

Dimensionless Parameters

The Reynolds number (Re) is a dimensionless fluid mechanics parameter that is directly proportional to the superficial velocity of the fluid. The equation for the Reynolds number of the air flowing through a fixed bed is:

$$Re = \frac{v_s \rho d_p}{\mu}$$

Where v_s is the superficial velocity of the air in ft/min, ρ is the density of the air, d_p is the diameter of the particle in inches, and μ is the dynamic viscosity of the air

The Peclet number (Pe_r) is given by the following equation:

$$Pe_r = \frac{Re * Pr}{k_r / k_f}$$

Assuming kr/kf is linearly related to Re, and Pr is assumed to be constant at 0.71 for air at 60 °C:

$$Pe_r = \frac{Re * Pr}{m * Re + b}$$

Where m and b are the slope and intercept respectively of the line fitting our k_r/k_f versus Re data. The Peclet number should increase rapidly for a low range of Reynolds numbers and stay relatively constant with respect to Reynolds number after reaching a certain velocity. This is because when Re is low, the intercept (b) has more of an effect on Pe_r.

The Biot Number (Bi) is a relationship between the wall heat transfer coefficient and the thermal conductivity of the packing. It is given by the following equation:

$$Bi = \frac{h_w R}{k_r} = Nu_w \frac{R / d_p}{k_r / k_f}$$

Since k_r is assumed to be linearly proportional to the Reynolds number, and h_w increases at a slower rate with Reynolds number, we would assume the Biot number to decrease with respect to the Reynolds number. If Nu_w was linearly proportional to Re, the Biot number would decrease linearly, but theoretically Nu_w should fit the equation:

$$Nu_w = Nu_w^o + ARe^B Pr^C$$

Where A, B, and C are experimentally determined constants. With only six data points, it is impossible to create an accurate fit line with this model for Nu_w, so we just assume that the Biot number will decrease with respect to Reynolds number.

The dimensionless parameter N is a ratio of tube diameter to particle diameter.

$$N = \frac{2 * R}{d_p}$$

Several studies completed have given various parameters that must be met in order to receive accurate data when using models such as the IPPF. Many of these studies suggest that the first bed depth used should be at least 1.5 times the diameter of the column (Borkink & Westerterp, 1993). This being said, the optimum first height for the 4 inch column would be 6 inches. With the limited number of particles available, the first height chosen was 4 inches, which could have had an effect on the accuracy of our data.

Methodological Procedure

Equipment

The apparatus used in a cooling experiment with a fixed bed reactor tube is shown in Figure 1.

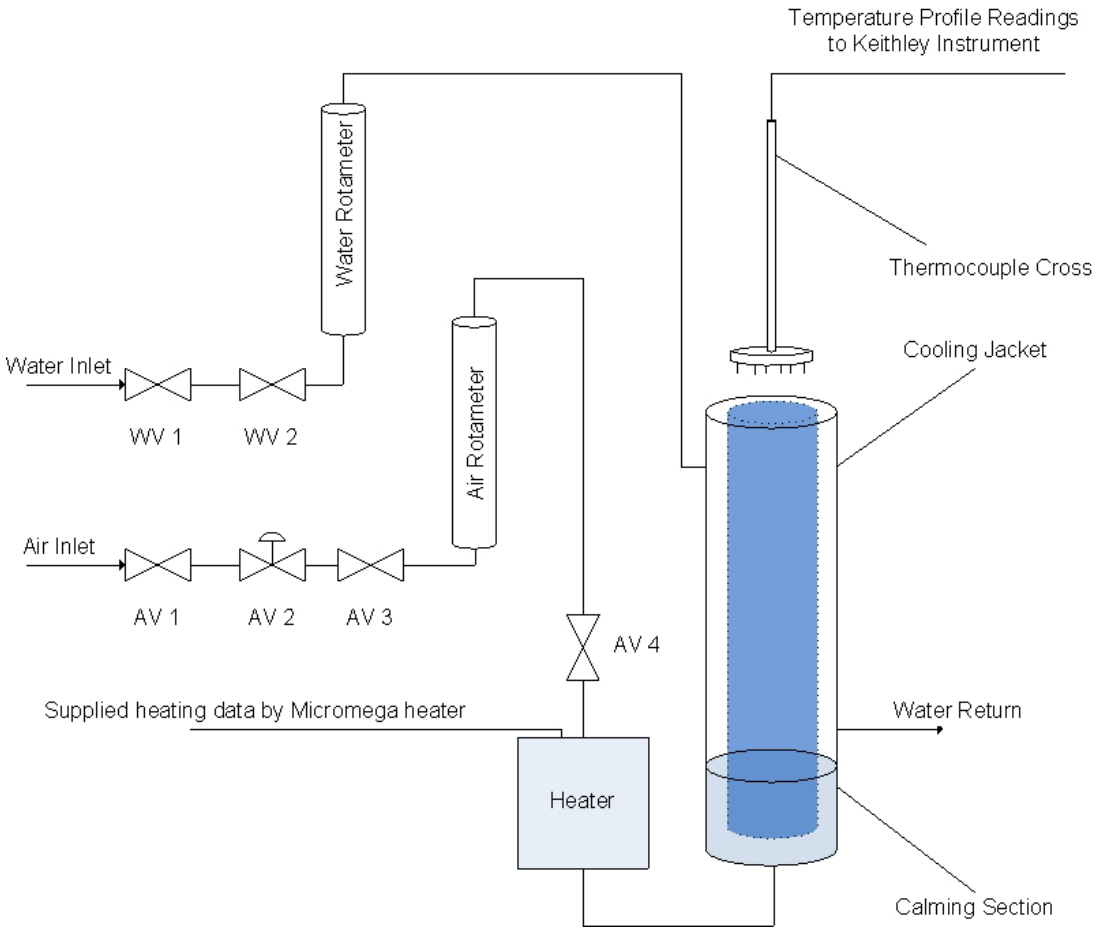

Figure 1: Schematic of Laboratory Apparatus

Columns

Each column used was constructed using two concentric brass tubes to form an annular space between the two (water jacket). The columns were attached to calming sections using four screws. Screws used in the 4 inch column were constructed from nylon, whereas the screws used in the 2 inch column were constructed from steel. The calming sections were constructed out of nylon and filled with ¼ inch steel spheres. The steel spheres were separated from the test packing by a circular piece of steel mesh. The calming section allowed for the airflow to be evenly

dispersed over the cross-section of the column. The columns had internal diameters measuring 2 inches (50.8mm) and 4 inches (101.6mm).

Determining Reynolds number of inlet air flow

To measure the flow rate of the air entering the column, it was passed through a ½-27-G-10 rotameter tube with a ½-GSVT-48A float. Depending on the pressure of the air, different amounts of air would flow through the rotameter at 100% of the total flow. These values are listed in Table 1.

Table 1: Flow data for a ½-27-G-10 rotameter tube with a ½-GSVT-48A float

Gauge pressure	MAX	Gauge Pressure	MAX
0	44.9	26	2.94
1	4.73	27	2.91
2	4.6	28	2.88
3	4.46	29	2.84
4	4.34	30	2.8
5	4.23	31	2.78
6	4.13	32	2.75
7	4.03	33	2.72
8	3.94	34	2.69
9	3.86	35	2.67
10	3.78	36	2.64
11	3.7	37	2.61
12	3.64	38	2.59
13	3.57	39	2.56
14	3.51	40	2.54
15	3.45	41	2.52
16	3.39	42	2.49
17	3.34	43	2.47
18	3.28	44	2.45
19	3.23	45	2.43
20	3.19	46	2.41
21	3.15	47	2.39
22	3.1	48	2.37
23	3.06	49	2.35
24	3.02	50	2.34
25	2.98	51	2.32

The volumetric flowrate of air flowing through the column (SCFM) was found using the following equation:

$$SCFM = \% * Max * (\frac{14.7 + psig}{14.7})$$

Where % is the percentage read on the rotameter tube for air, Max is the maximum flow rate (at 100% on the rotameter, which can be found in Table 1) for the rotameter tube and float used, and psig is the pressure read off of the pressure gauge downstream from the rotameter. The percentage of airflow is read from the "knife-blade edge" of the float (which is at the widest diameter of solid on the float).

Since the column area, and the density and viscosity of air were assumed constant for air flowing though the column, the Reynolds number was then determined using the following equation derived for each column:

$$Re = C * SCFM * d_p$$

Where C is 380 for the 2 inch column and 95 for the 4 inch column.

Packings

Four different packing shapes were examined throughout the course of the project:

- ½ inch ceramic spheres
- Raschig rings
- Johnson Matthey K-57 4-hole pellets (4-hole cylinders)
- Monoliths

The ½ inch ceramic spheres measured 12.7mm in diameter and were porous in nature. There have been many studies completed using spheres with N=8 (in our case, the spheres were used in the 4 inch column only). By comparing our data to these studies, we could verify that our data is consistent with past experiments.

Raschig rings in this study are brittle non-porous ceramic cylinders with a single hole in the middle. The rings we used had heights and outer diameters equal to 13mm, with a wall thickness of 3mm. There have also been some studies with raschig rings with various values of N, which

allows us to do a comparison to verify our data is relatively consistent and will give values for the N we used.

The Johnson Matthey K-57 4-hole pellets were porous ceramic 4-hole cylinders. These were 17mm tall, with an outer diameter of 14mm and hole diameters of 4mm. Packings such as these are typical support for steam reforming.

The monoliths are ceramic cylinders, measuring 7mm tall with a diameter of 6mm and a hole density of 0.563holes/mm^2 (56.3 holes/cm^2). The monoliths used in this study are illustrated in Figure 2.

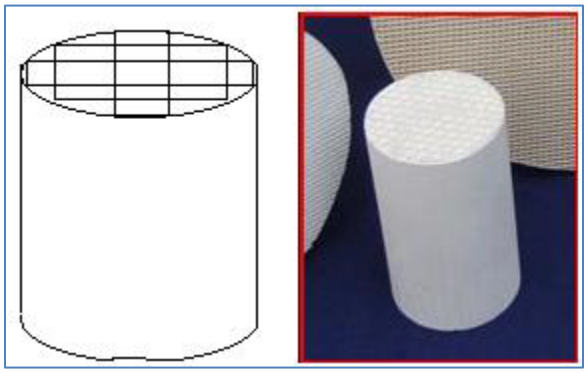

Figure 2: Monoliths (http://www.made-in-china.com/showroom/hisina88/product-detailKoXmSOuGZzVf/China-Automobile-Exhaust-Catalyst-Carrier.html)

The Inlet Profile Plug Flow model requires a particle diameter to complete calculations. This diameter is referred to as the equivalent spherical diameter. In other words, this is the diameter required in a sphere to obtain the same volume as the particle (without accounting for any internal voids). The three non-spherical packings were all cylindrical in shape, so the equivalent spherical diameter could be found using the following equation:

$$\pi \frac{d_c^2}{4} h = \frac{4}{3} \pi \frac{d_p^3}{8}$$

Where d_c is the diameter of the cylinder and d_p is the equivalent spherical diameter.

Table 2 lists the equivalent spherical diameters of the packings, as well as the ratio of each column to said diameters.

Table 2: Packing to column diameter ratios

Packing	Equivalent Spherical Diameter	N in the 2 inch column	N in the 4 inch column
Spheres	12.7	--	8.0
Raschig Rings	14.5	3.5	7.0
JM 4-hole cylinders	17.4	2.9	5.8
Monoliths	7.3	7.0	14.0

Micromega Heater

The heater used to heat the inlet air flow was controlled by an Omega Micromega CN77000 Series Controller. Complete instructions to use the controller may be found on Omega's website at http://www.omega.com/Manuals/manualpdf/M2491.pdf. The purpose of the heater in this experiment is to heat the inlet air to approximately 100 ˚C. There are two settings that may be altered to acquire this: the desired temperature and the rate at which it takes to get to the desired temperature (ramp and soak). Our desired temperature was set to 100 ˚C. The rate will affect how long it will take the system to reach equilibrium. Since it is impossible to get the temperature of the air to be exactly 100 ˚C at all times, the heater heats until the air is 100 ˚C and hinders heating until the flow is cooled below 100 ˚C, in which case it will start heating again. This creates an oscillation in temperature over time, and after infinite time the temperature will approach 100˚C. With a faster heating rate, the air flow will reach 100 ˚C sooner; however, larger oscillations will occur. Conversely, with a slower heating rate, the air flow will reach 100 ˚C slower, but smaller oscillations will occur. The ramp and soak configuration was disabled, which allows the heater to reach the desired setting as fast as possible.

Thermocouples

A diagram of the thermocouple cross can be seen in Figure 3.

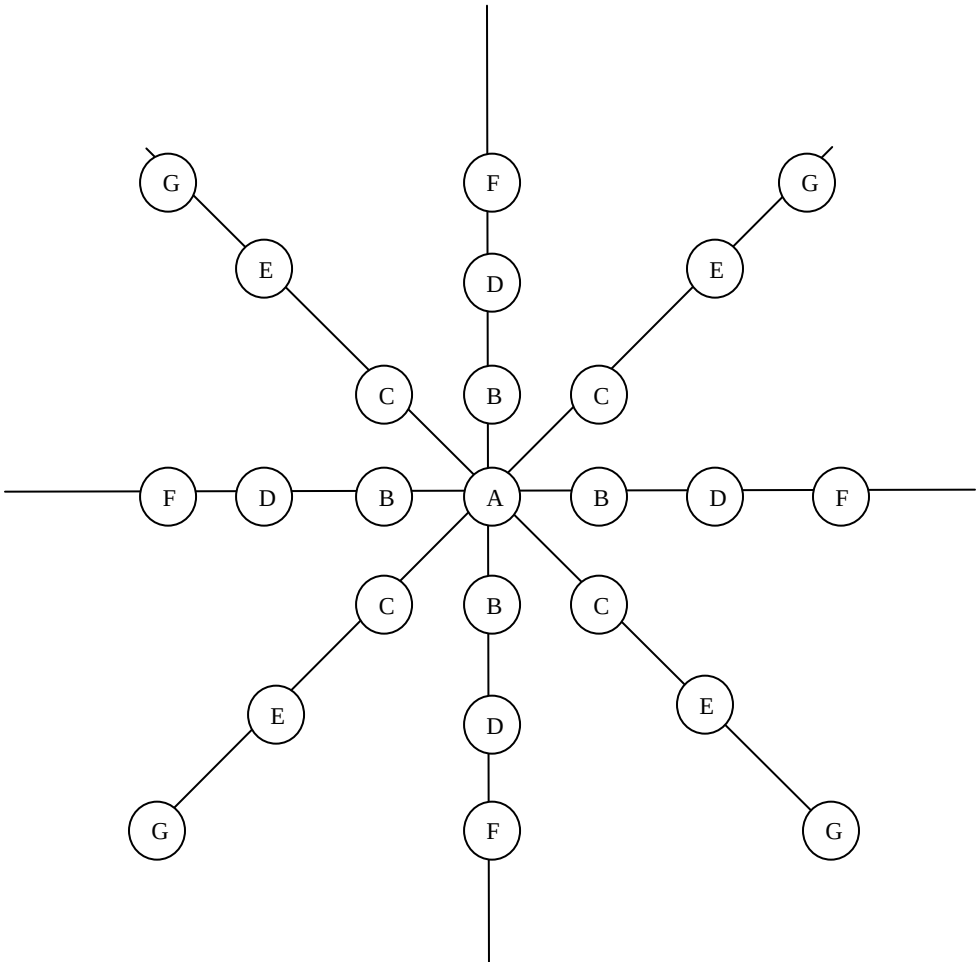

Figure 3: Thermocouple Cross

The thermocouple cross consisted of two sets of four arms set 45 degrees apart from each other. Each arm had three thermocouples attached, measured at different radii. The radii for each thermocouple in millimeters are shown in Table 3.

Table 3: Radial position of each thermocouple represented in Figure 2 in both columns

Thermocouple	2 inch column (mm)	2 inch column (dimensionless)	4 inch column (mm)	4 inch column (dimensionless)
A	0	0.00	0	0.00
B	8.5	0.33	9.5	0.19
C	12	0.47	19	0.37
D	15	0.59	28	0.55
E	18	0.71	41	0.81
F	21.5	0.85	44	0.87
G	24	0.94	48	0.94

Not counting the center thermocouple, data is collected by 24 thermocouples at six different radial positions. By rotating the thermocouple cross 45° and taking a second set or readings, 48 thermocouple readings are recorded (i.e. eight angular replicates of six radial positions). This allows for a more accurate measurement of the average temperature of each radial position across the cross-section of the column. The thermocouples were held in place by thin plastic tubing (like a small straw) connected to two nylon bars (each arm consisted of two bars) with holes drilled at the same radial position. A side view of the thermocouple cross (one of the eight arms) is shown in Figure 4.

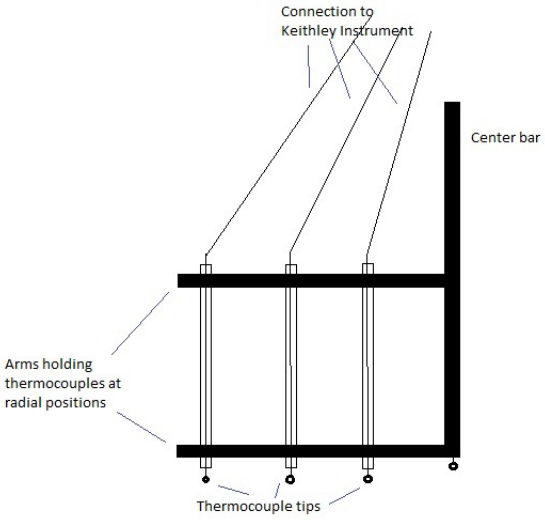

Figure 4: Side view of one arm in the thermocouple cross

Consecutive thermocouples used in these experiments are placed at radii very similar to the ones before and after (within 3mm). These thermocouples must be verified before inserting the thermocouple cross into the column each time to ensure that they are not bent, as reading temperatures from 1 or 2 mm different than expected will yield faulty results.

Three thermocouples were placed in the cooling water jacket. These were placed 7.5, 24.5, and 37.5 mm from the bottom of the column. All three were averaged for each set of data in order to determine the wall temperature.

Temperature Profile Collection

The data acquisition device used was a Keithley Integra Series 2700 Datalogger. This device combines functions of DMM, switch system, and datalogger, and allows for the collection of

thermocouple data for up to 200 channels (35 of these channels were utilized in this experiment). The device worked in conjunction with ExceLINX (an add-in designed for Microsoft Excel) to collect data over time.

To install ExceLINX, the program file ExceLINX.xla must be placed in the Excel Add-ins folder. This can be found in explorer: C→Documents and Settings→All users→Application Data→Microsoft→Add Ins. Then in Excel, go to Tools→Add In. Click browse and select ExceLINX.xla from the menu. Now the ExceLINX tab should be available from the menu at the top of Excel.

The Keithley instrument must now be configured to use with the ExceLINX program. Start by turning on the Keithley instrument. Then, at the top of the Excel screen, select ExceLinx→DMM Config and complete as shown in Figure 5.

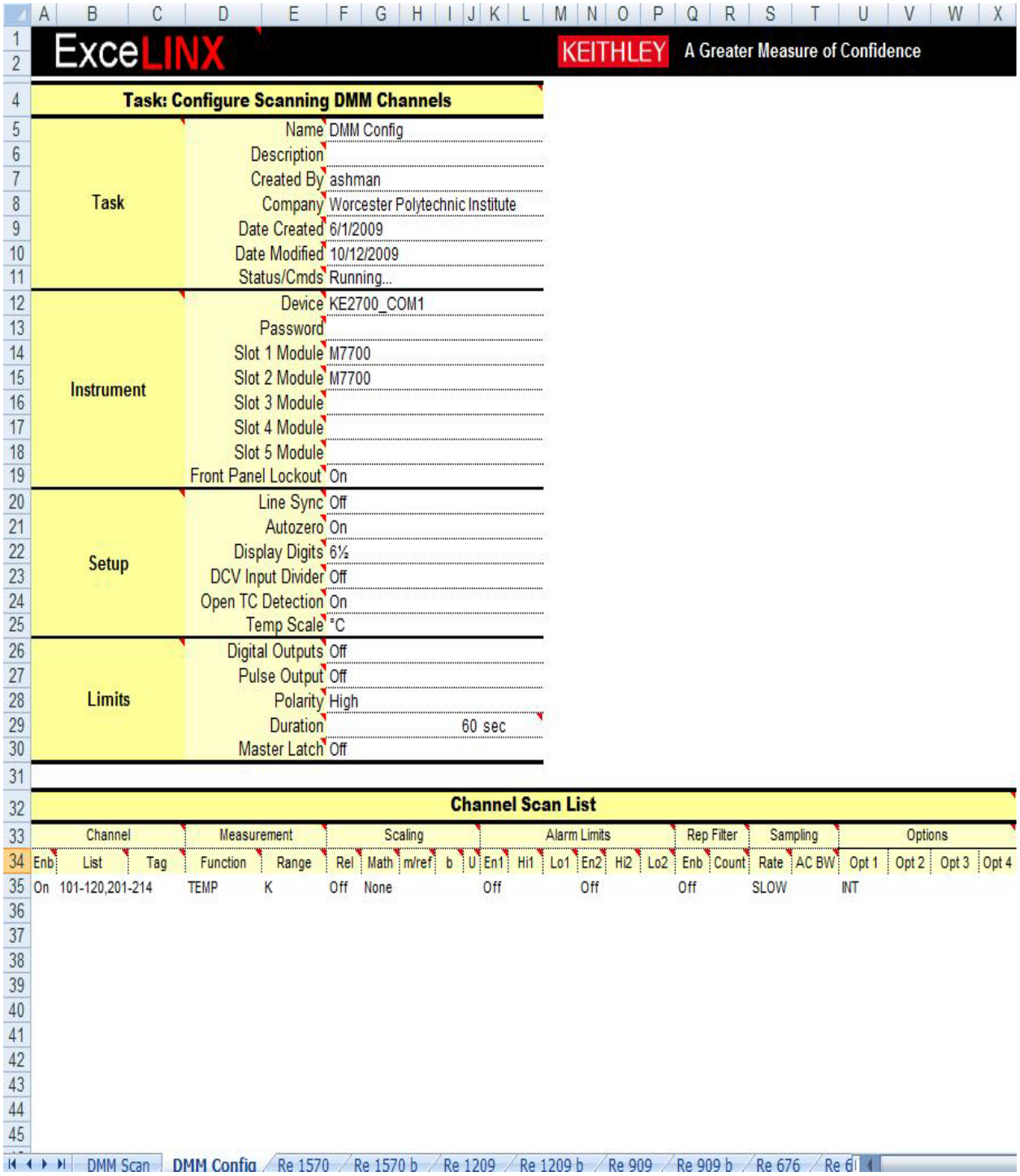

Figure 5: DMM Config Screenshot

Then click ExceLINX→DMM Scan and complete as shown in Figure 6.

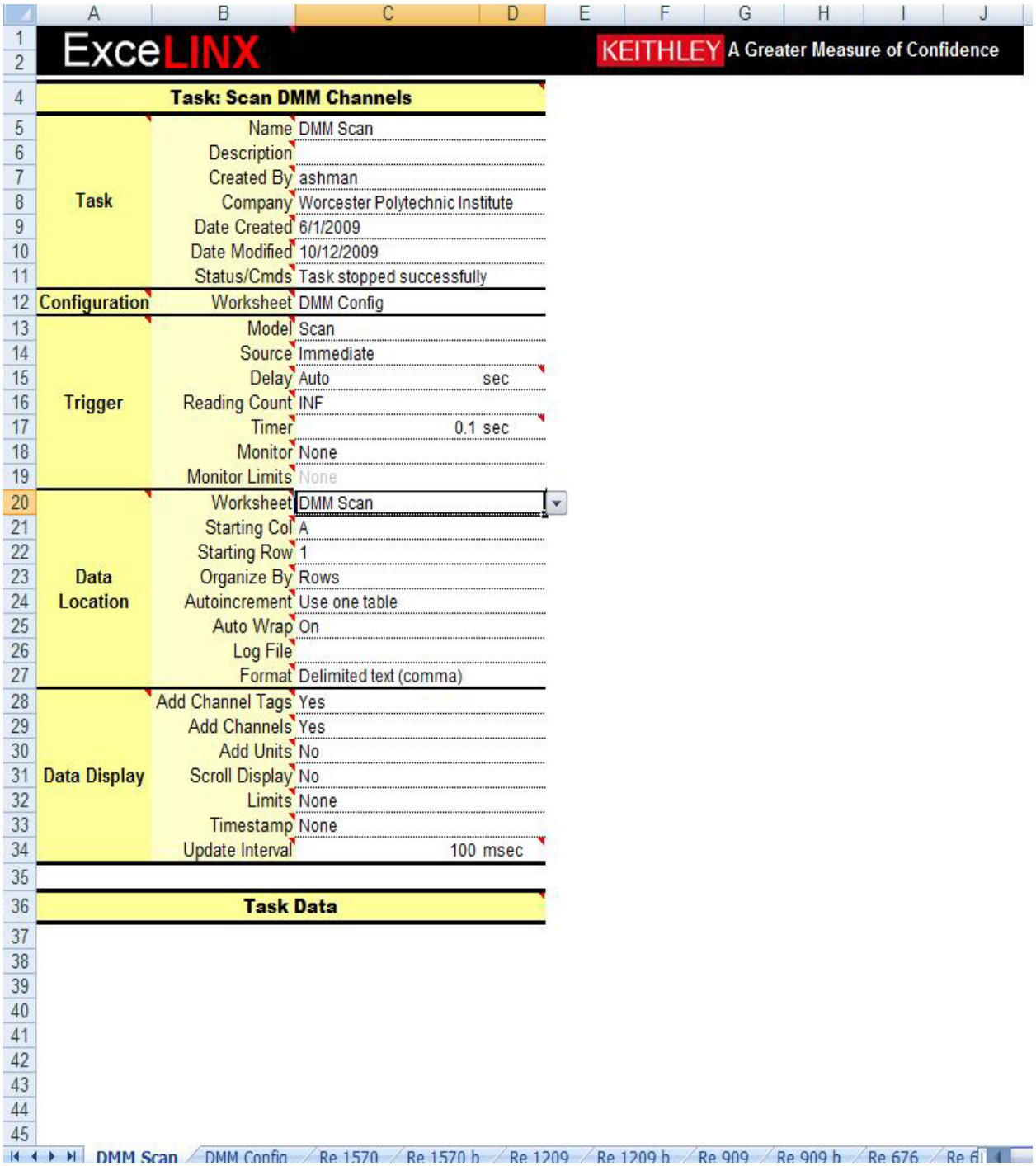

Figure 6: DMM Scan Screenshot

To record data, select the dropdown menu “Status/Cmds”, select “Start”, and then press enter. Data will be recorded in the selected sheet under “Worksheet”. To stop collecting, choose “Stop” from the “Status/Cmds”drop down menu and press enter very shortly after (almost instantaneously). Each column of data represents temperatures read at specific thermocouples

depending on their placement. In order to determine which thermocouple corresponded to each column, each thermocouple was tested by touching one by one with a finger-tip and checking ExceLINX to determine which column's temperature changed. The ambient temperature in the lab was usually close to 20 °C and after being touched by a finger-tip, the temperature reading for that thermocouple would read about 30 °C. There were five thermocouples removed from the column, but still connected to the Keithley instrument. Temperatures for these thermocouple connections read 9E31 on ExceLINX. After the channels on ExceLINX for these five thermocouples and the 25 thermocouples from the thermocouple cross were determined, the channels for the wall thermocouples and the inlet airflow needed to be determined. These were found by removing the connecting wires one by one and seeing which channel read 9E31.

Procedure

In order to ensure a good fit for our data, six different Reynolds numbers were measured during each day of column operation, and four bed depths were taken for the packings in each column. A table of all runs completed during the course of the project is shown in Table 4.

Table 4: Table of runs

Column Diameter (mm)	Packing	Re Values	Bed Depths (mm)
101.6	½" spheres	75, 145, 195, 260, 335, 425	92, 150, 200, 225
101.6	Raschig Rings	85, 142, 190, 258, 341, 432	100, 150, 200, 250
101.6	JM 4-hole cylinders	102, 198, 268, 358, 460, 584	100, 150, 200, 250
101.6	Monoliths	43, 71, 95, 129, 171, 216	100, 160, 200, 260
50.8	Raschig Rings	350, 490, 676, 909, 1209, 1570	80, 150, 210, 255
50.8	JM 4-hole cylinders	409, 775, 1052, 1412, 1822, 2275	80, 150, 200, 265
50.8	Monoliths	170, 323, 439, 589, 760, 948	95, 155, 210, 260

It has been determined that the minimum packing depth should be 1.5 times the column diameter to let the parabolic temperature profile develop (Borkink & Westerterp, 1993). This must be

done so that the IPPF model would fit the data (requires parabolic temperature profiles). Although the minimum packing depth was determined to be 1.5 times the column diameter, this could not be done with some of the packings in the 4 inch column due to a lack of packing quantity. To ensure enough deviation in bed depths, and keeping consistency throughout the runs, runs in the 4 inch column started at a height close to 4 inches (only 1 times the column diameter).

Operating the Column

1. If running the tower for the first time, carefully unscrew and remove the top section of the tower.

2. Fill the calming section of the tower with metal spheres and cover the calming section with a wire mesh to keep it separate from the test packing.

3. Re-attach the top section of the tower.

4. Measure the inside height of the empty tower and record the value.

5. Add the desired amount of the packing you are working with to the tower. To do this properly you should:

    a. Add the packing little by little and gently compact it from the top after each addition to assure for uniformity of packing.

    b. Regularly measure the height of the empty space left in the column (space from packing to top) to ensure that you do not surpass your desired packing height. (Packing height=height of empty tower - empty space left)

6. Set up the thermocouple cross so that once it is inside the tower the thermocouples are just above the packing (no more than 3-6 mm). To do this measure the distance from the cross bar that will support the cross to the bottom of the thermocouples and set it so that this distance is slightly less that the empty space remaining in the tower. Before lowering the thermocouple cross into the column each time, straighten all thermocouple tips and ensure that they are centered with the guide tubes.

7. Carefully lower the thermocouples cross into the tower. If you feel it hit the top of the packing remove it from the tower, re-adjust the height of the cross bar, and straighten all thermocouple tips.

8. Open ExceLINX. If you have not yet set up ExceLINX as described in the ExceLINX section take the time to do so now.

9. Turn on and configure the Keithley 2700 Multimeter/Data Acquisition System.

10. Prior to starting any flows make sure that all the valves are in the fully shut position. For Water Valves (WV) 1&2 as well as Air Valves (AV) 1&3 this means that the valve is perpendicular to the tube on which it is located. For AV 2 this means that the valve is turned fully in the CLOCKWISE direction.

11. Slowly fully open WV 1.

12. Slowly open WV 2 until the rotameter reads a flow of 80%.

13. Slowly fully open AV 1. At this point if the pressure gauge following AV 1 is showing a non-zero pressure reading it means that AV 2 is not fully shut, in which case take the time to fully shut it now.

14. Slowly fully open AV 3.

15. If you are running the column for the first time adjust AV 4 so that at the desired setting it allows for a full range of desired Re values to be obtained using only AV 2 to adjust the flow. The following things should be noted:

    a. Once this has been set AV 4 should not be touched in further runs to ensure for uniformity of values.

    b. Never allow the rotameter to reach or exceed 100%.

    c. The pressure gauge that should be used to calculate the Re values is the one that is right before entering the heater (i.e. downstream from the rotameter).

16. Turn on the heater. If you have not yet set up the Omega Micromega heating control unit take the time to do so now.

17. Set the flow to the desired amount by adjusting only AV 2.

18. Using ExceLINX start recording the data.

19. Once the system has reached steady state stop the data recording. This should take anywhere from 1 to 3+ hours depending on the flow rate, packing height, and if it's the first run of the day.

20. Carefully rotate the thermocouple cross 45 degrees. The top of the column has markings for 0 and 45° in which the cross is to be lined up with to accurately measure the 45° rotation.

21. Commence recording data in ExceLINX. Make sure to do this in a different Excel sheet then the one used for the previous data.

22. Once the system has once more reached steady state stop the data recording. This should only take about 5min after the angular rotation.

23. Repeat Steps 17-22 for all desired Re values.

24. Shut the system down in the reverse order that you started it in.

Safety Precautions

The spheres, raschig rings, and monoliths were all inert ceramic packings. However, the 4-hole cylinders contained a white powdered metal on the surface of each particle. Labels on the container provided by Johnson and Matthey warn that exposure may cause irritation. Although it has not been classified as hazardous, it is good practice to minimize exposure to this metal. In order to do so, gloves were worn at all times when handling the 4-hole cylinders. Also, in order to prevent inhalation, the first set of runs performed with this packing was done using the largest bed depth. Once packed for the first time, painter's masks and safety glasses were worn and then the air was set to the highest flowrate achievable. Visibly, no dust came from the column at the highest flowrate, so the air was left at a high flowrate overnight so that any particles that did get

blown up were not breathed in by anyone. No dust was visible anywhere in the lab the next day; a miniscule amount was actually loose enough to be blown off the particles.

The heater would reach temperatures of 115˚C, and even though was insulated on all sides, could cause minor burns if touched. These surfaces were not touched for any reason, and if a particle or other object were to fall on top of the heater, it was immediately removed with pliers.

Data file format for model fitting

The IPPF model was fit to the temperature profile readings using an existing program written in FORTRAN. In order to run the program, it was required to create a text file in the correct format with data collected. A template of this format is shown in Table 5. In order to smooth the steady state thermocouple temperatures, the last five time values in our ExceLINX data collection sheet were averaged.

Table 5: FORTRAN input template

# of Profiles	# of Radial Positions	# of wall Temperature Readings	# of Angles		
Column Diameter	Particle Diameter				
Radius 1	Radius 2	Radius 3	Radius 4	Radius 5	Radius 6
Reynolds Number	Bed Depth	Angle of Rotation			
Inlet Temperature					
Radius 1 Thermocouple 1	Radius 1 Thermocouple 2	Radius 1 Thermocouple 3	Radius 1 Thermocouple 4		
Radius 2 Thermocouple 1	Radius 2 Thermocouple 2	Radius 2 Thermocouple 3	Radius 2 Thermocouple 4		
Radius 3 Thermocouple 1	Radius 3 Thermocouple 2	Radius 3 Thermocouple 3	Radius 3 Thermocouple 4		
Radius 4 Thermocouple 1	Radius 4 Thermocouple 2	Radius 4 Thermocouple 3	Radius 4 Thermocouple 4		
Radius 5 Thermocouple 1	Radius 5 Thermocouple 2	Radius 5 Thermocouple 3	Radius 5 Thermocouple 4		
Radius 6 Thermocouple 1	Radius 6 Thermocouple 2	Radius 6 Thermocouple 3	Radius 6 Thermocouple 4		
Wall Thermocouple 1	Wall Thermocouple 2	Wall Thermocouple 3			

One text file could be made for all packing depths and Reynolds numbers for each packing in each column. Therefore, when using this template, the top three lines were only needed once at the top of the file. To indicate the end of the file, a “-1” was inserted on the last line to notify the program to stop. A sample text file is shown in Appendix A: Sample Fortran Input Text File (for JM 4-hole cylinders in the 2 inch column).

Fitting the IPPF model to collected data

In order to obtain a solution for the program in FORTRAN, the IPPF program uses iterations to minimize the sum of squares function given below:

$$\min(Pe_r, Bi)\, S = \sum(T_{calc} - T_{measured})^2$$

Where the measured temperatures are taken at each angular and radial position for the different bed depths. The temperatures are made dimensionless by:

$$\vartheta = \frac{(T - T_w)}{(T_o - T_w)}$$

The IPPF model can now be solved analytically. The program performs two sets of functions: first solving the partial differential equation, and the second minimizing the sum of squares shown above as a function of input parameters. The sequence in which this is performed is:

1. Guess Pe_r and Bi
2. Solve partial differential equation
3. Form S
4. Is S at a minimum? If not, start back at 1 and reiterate

For the IPPF model, Pe_r and Bi vary for each packing and initial values are needed before running the program. . The Biot number was assumed to be anywhere between 1 and 2, so was usually guessed to be 2 (unless iterations were not able to be completed). The Peclet number has been suggested from past research to be about 10 for spheres, and 6 for rings.

The function for the sum of squares is then solved using the guessed values for Pe_r and Bi. This sum is ended dependent on the user's desired accuracy.

The sum of squares function is in the category of target functions $S(\underline{x})$ with $\underline{x}=(x_1,x_2\ldots x_n)$

$$S(\underline{x}) = \sum_{i=1}^{m} f_i(\underline{x})^2 = \underline{f^T f}$$

Where m is the number of data points and n is the number of parameters to be estimated. Then, a m*n Jacobian matrix is formed with the first partial derivatives:

$$J_{ij}(\underline{x}) = \left(\frac{\partial f_i}{\partial x_j}\right)_{\underline{x}}$$

Using this, the gradient of S is given by:

$$G = 2J^T J + 2\sum_{i=1}^{m} f_i K^i$$

Where K^i is the matrix of second derivatives of f_i (under some conditions, may be zero). S is minimized by the Levenberg-Marguardt algorithm. The accuracy of this solution is then determined by the accuracy of the radial temperature measurements used in the iterations. The approximate error (E) is then obtained by solving the following:

$$\left(J(\underline{x})^T J(\underline{x})\right)\underline{E} = -J(\underline{x})^T \underline{f}(\underline{x})$$

The second derivative of the target function must be available to approximate x. The actual method for calculating E depends on which of J, J^TJ, or $(J^TJ)^{-1}$ is available. The accuracy of x_i values is determined by observing how x_i changes over iterations. Values for x_i should not change over the last few iterations (Van Dongeren, 1994).

Although these iterations allow the determination of accurate values for Peclet and Biot numbers, it is important to determine confidence intervals for these parameters. As long as the hessian of S is available in some form, variances may be calculated. If J is known, $G=2J^TJ$ can be evaluated. Letting H be the inverse of G and S be the sum of squares, then an estimate of the uncertainty in the i^{th} parameter x_i is:

$$var(x_i) = \frac{S}{m-n} H_{ii}$$

Now that the variance is known, the values for a t-distribution with m-n degrees of freedom can be used to give 100(1-β) confidence intervals for x:

$$x_i - \sqrt{var(x_i)}\, t_{(\beta/2, m-n)} < x_i^* < x_i + \sqrt{var(x_i)}\, t_{(\beta/2, m-n)}$$

Where x_i^* is the true solution. For these calculations, a 95% confidence interval was used, meaning 2.5% is tolerated on each side (Van Dongeren, 1994).

F-test

For each flowrate observed, data collected at the same radial and axial positions, but different angular positions, are considered to be "replicates". Therefore, each data set for a given column, packing, and bed depth yields eight replicate sets of six measurements, if two angular positions are used. A first test of model adequacy is to perform an F-test to show adequacy of fit. The pure-error sum of squares is calculated by:

$$SSPE = \sum_{1}^{N}\left(\sum_{1}^{6}\sum_{1}^{8}\left(T_{observed} - T_{average}\right)^2\right)$$

Where N is the number of bed depths. Indices are omitted for clarity and averages are taken over each set of eight replicate measurements for each position. The mean square pure error is then calculated by:

$$MSPE = \frac{SSPE}{n_2}$$

Where n_2=m-(number of averages found). The mean square pure error is an estimate of the error variance. Since this varies weakly over the bed depths, it must be estimated by averaging the error variance over the bed-depths for the "overall" analysis case. The mean lack-of-fit sum of squares is then calculated by:

$$MSLF = \frac{S - SSPE}{n_1}$$

Where $n_1 = m - number\ of\ parameters\ estimated - n_2$. If the model is linear in the parameters, the mean lack-of-fit sum of squares is an independent estimator of error variance. However, if the model is nonlinear, then it is a biased estimator, and a test of model inadequacy may be stated as:

$$F_c = {}^{MSLF}/_{MSPE} > F_{0.05}(n_1, n_2)$$

With values of $F_c > F_{0.05}$, either the model is a poor fit or the data has a low amount of variability. This indicated a lack of fit error is significant compared to inherent scatter in the data.

Results

In order to proceed *with* any results, it was necessary to first prove that the data collected was representative of what was expected compared to past experiments. This includes the following:

- Plots of θ vs. y should show a parabolic fit at the first bed depth
- On the Plots of θ vs. y for each Reynolds number, temperatures should be lower with a higher bed depth
- On a height to height basis, k_r/k_f and Nu_w should be height independent
- Peclet and Biot numbers are in line with previously found literature figures

Parabolic Fit

Over the vast amounts of experiments done with fixed bed reactor tubes, it has been found that temperature profiles in the tubes fit a parabolic curve of the form $T = A * r^2 + B$, or in dimensionless form, $\theta = A * y^2 + B$. Figure 7 shows an example of a parabolic fit for the first depth for raschig rings in the 4 inch column. As expected, the data follows a parabolic fit very closely with a coefficient of determination of 0.99. It would also be expected that $\theta_{y=0} = 1$ for the best fit, this is due to how the θ is calculated in terms of the center temperature and as so would only hold true if the center of the column had not cooled more than the surrounding locations. This example has an intercept (A) of 1.005, very close to 1. Some temperature profiles for other packings are not as parabolic as expected. Figure 8 is an example of a parabolic fit for the first height of JM 4-hole cylinders. This poor parabolic fit was uncommon however and only occurred in two instances, the raschig rings and the JM 4-hole cylinders in the 2 in column, both of which were instances with a particularly low N value. Graphs expressing the parabolic fit for first depth temperature profiles for each packing/column combination can be found in Appendix B: θ vs. y for First Heights.

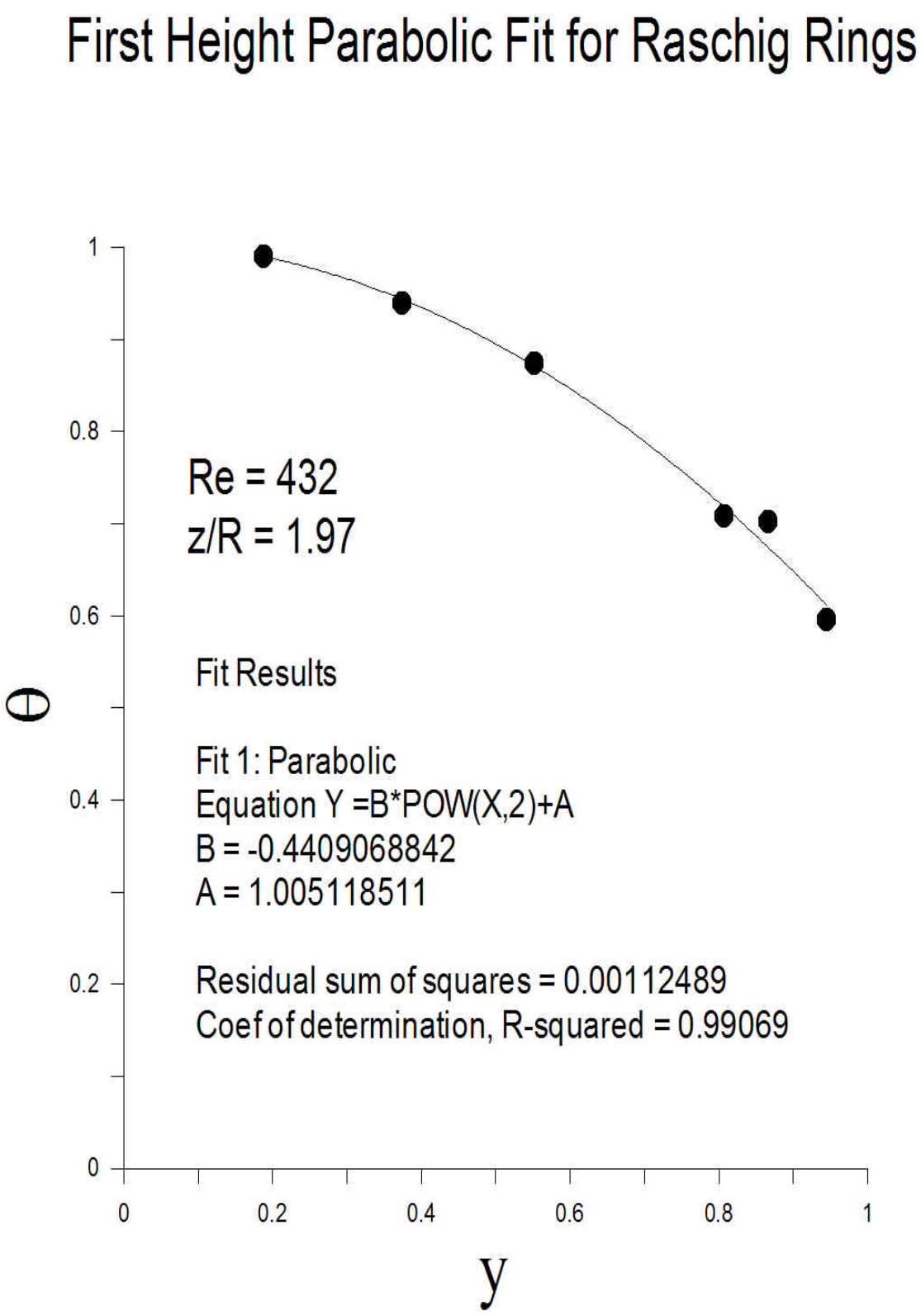

Figure 7: Temperature Profile Parabolic Fit for Raschig Rings in the 4 inch column with Reynolds Number 432

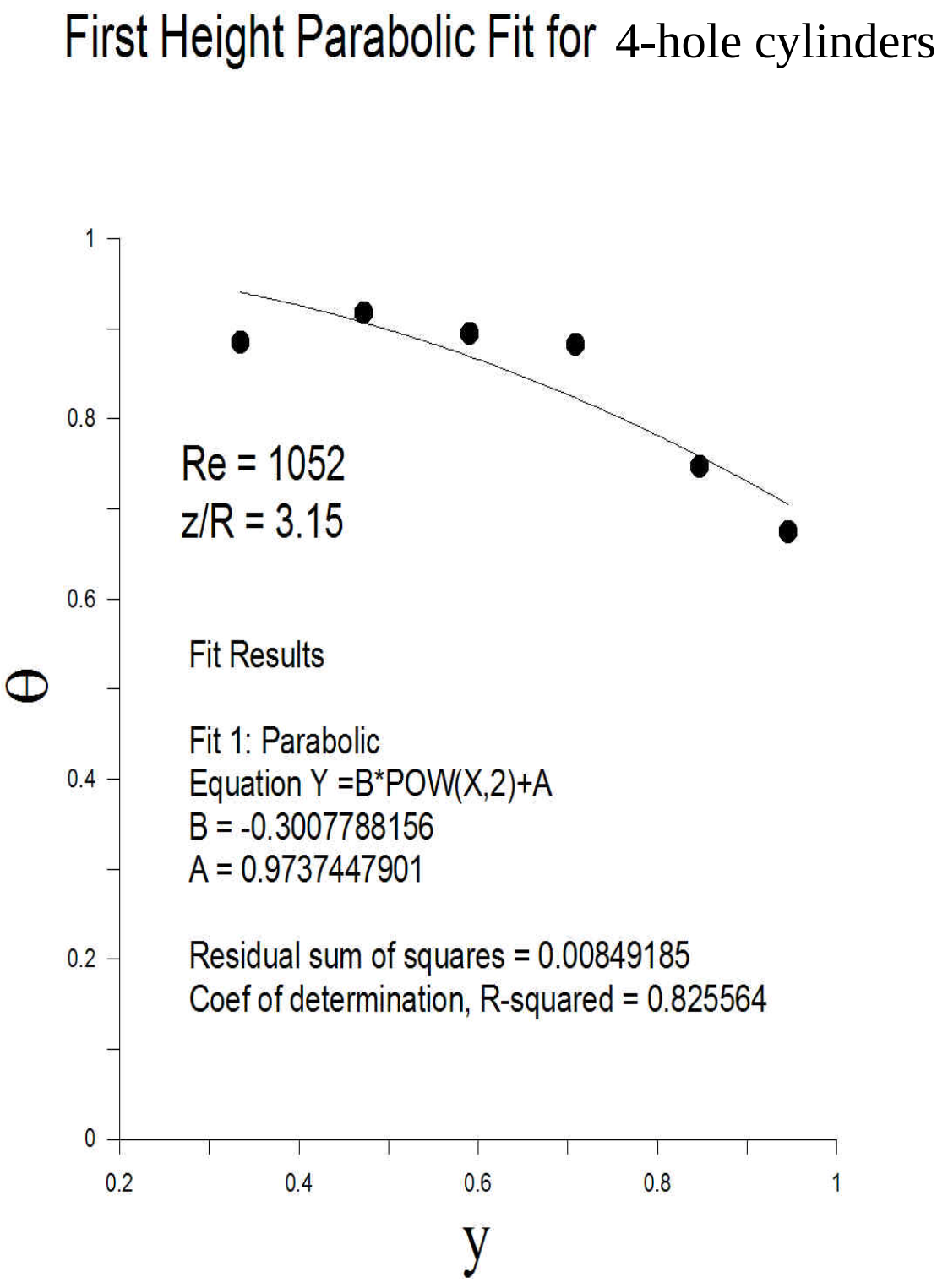

Figure 8: Poor parabolic fit for temperature profile of JM 4-hole cylinders in the 2 inch column with Reynolds Number 1052

The dimensionless profiles should also make physical sense. Since this is a cooling experiment, higher bed depths should yield lower temperatures. Temperatures should also decrease farther from the center of the tubes. It would also make sense for temperature differences between successive bed depths to be lower at greater bed depths. As air travels through the tube, the temperature difference between the center of the tube and the walls is decreased, lowering the driving force of the heat transfer. This means that the rate of temperature decrease with increasing radial position should also decrease with increasing bed depths. A sample radial temperature profile is shown in Figure 9.

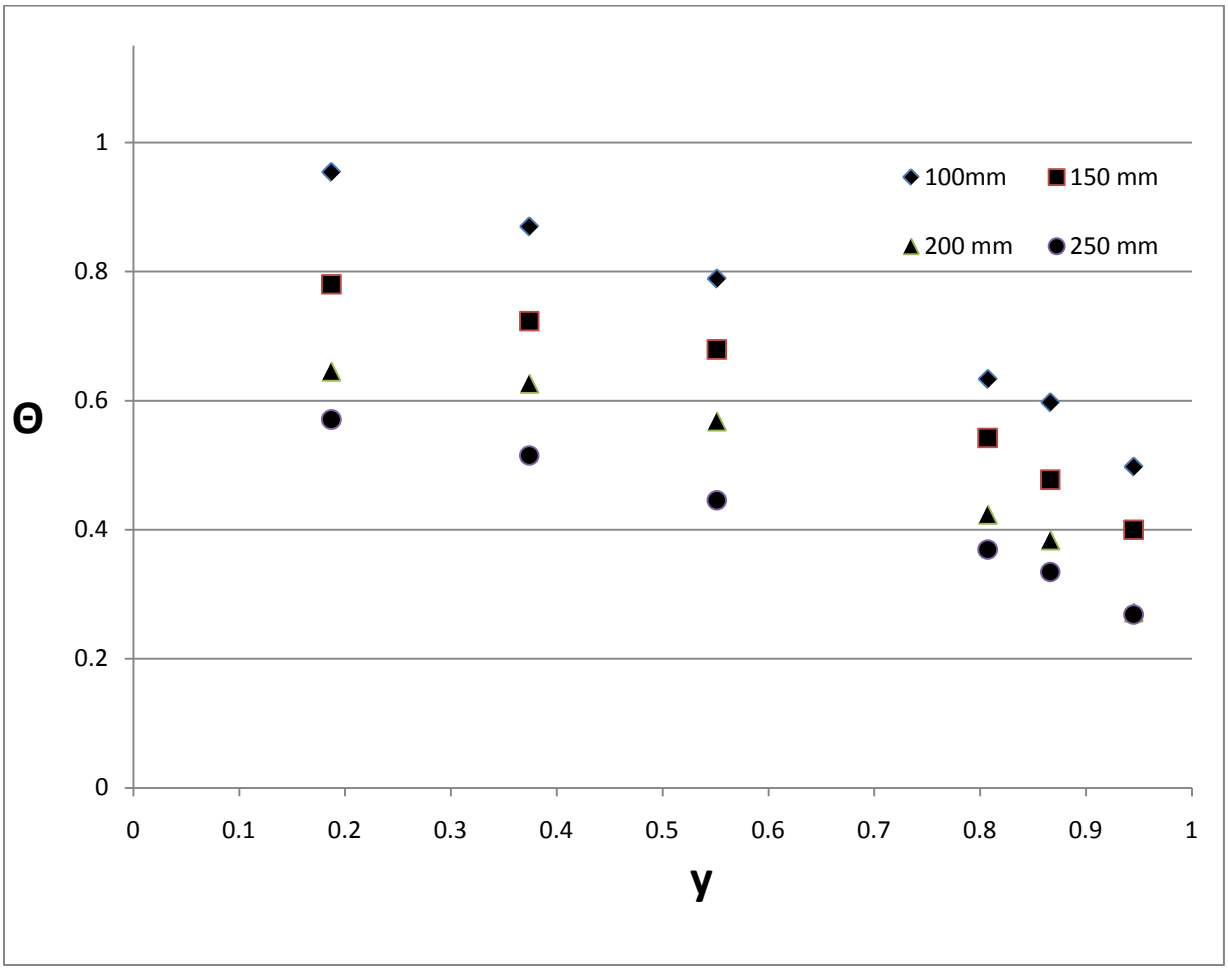

Figure 9: Temperature Profile for JM 4-hole cylinders in the 4 inch column for Reynolds Number 268

Figure 9 is representative of the majority of our temperature profiles, and shows the expected trends for radial profiles obtained during the experiment. It would also be expected for higher

Reynolds numbers to yield higher temperatures. Figure 10 is a temperature profile of the same packing/column as Figure 9 but with a higher Reynolds number.

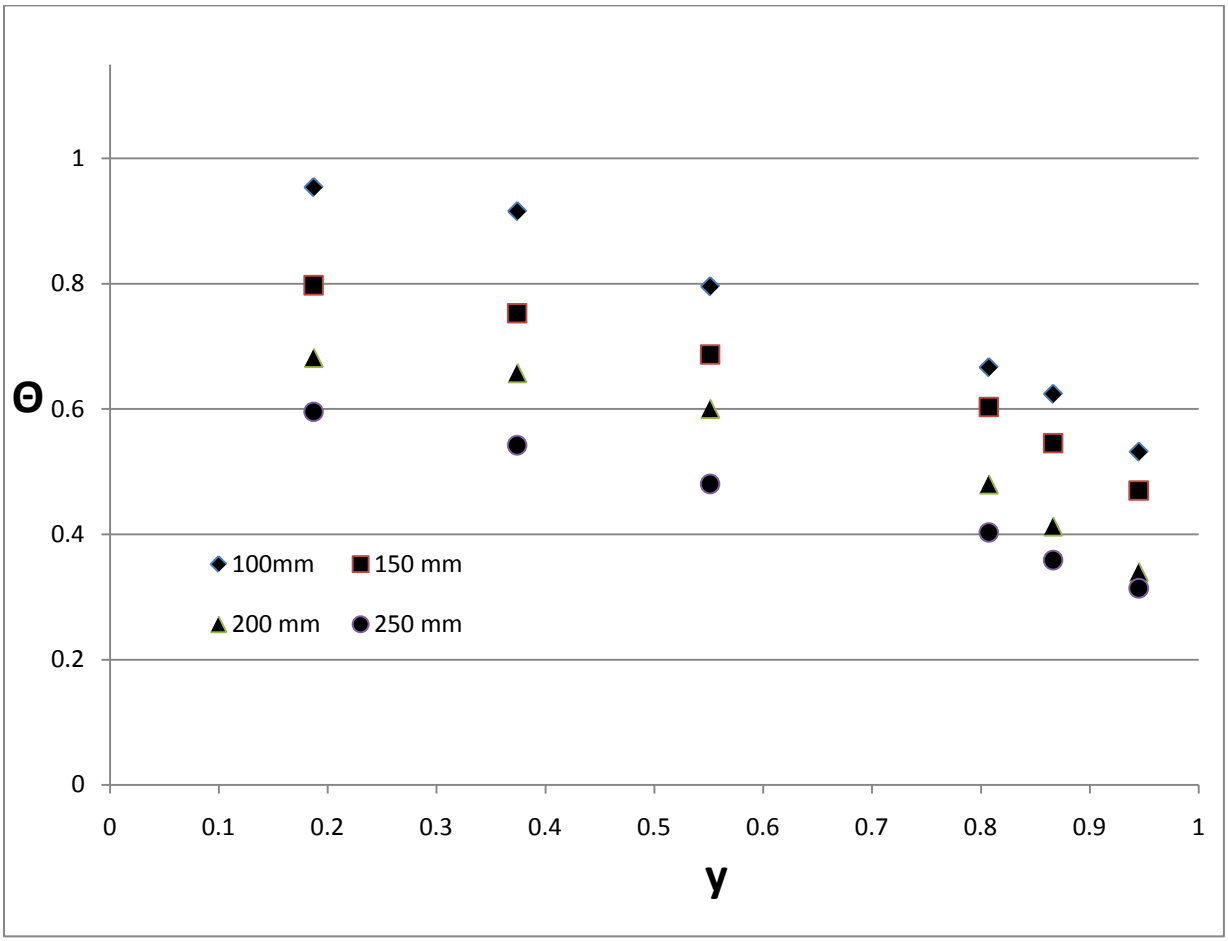

Figure 10: Temperature Profile for JM 4-hole cylinders in the 4 inch column for Reynolds Number 358

Each data point on Figure 10 corresponding with the same bed depth and radius as points on Figure 9 have higher temperatures. Figure 11 displays a temperature profile for a given bed depth rather than Reynolds number.

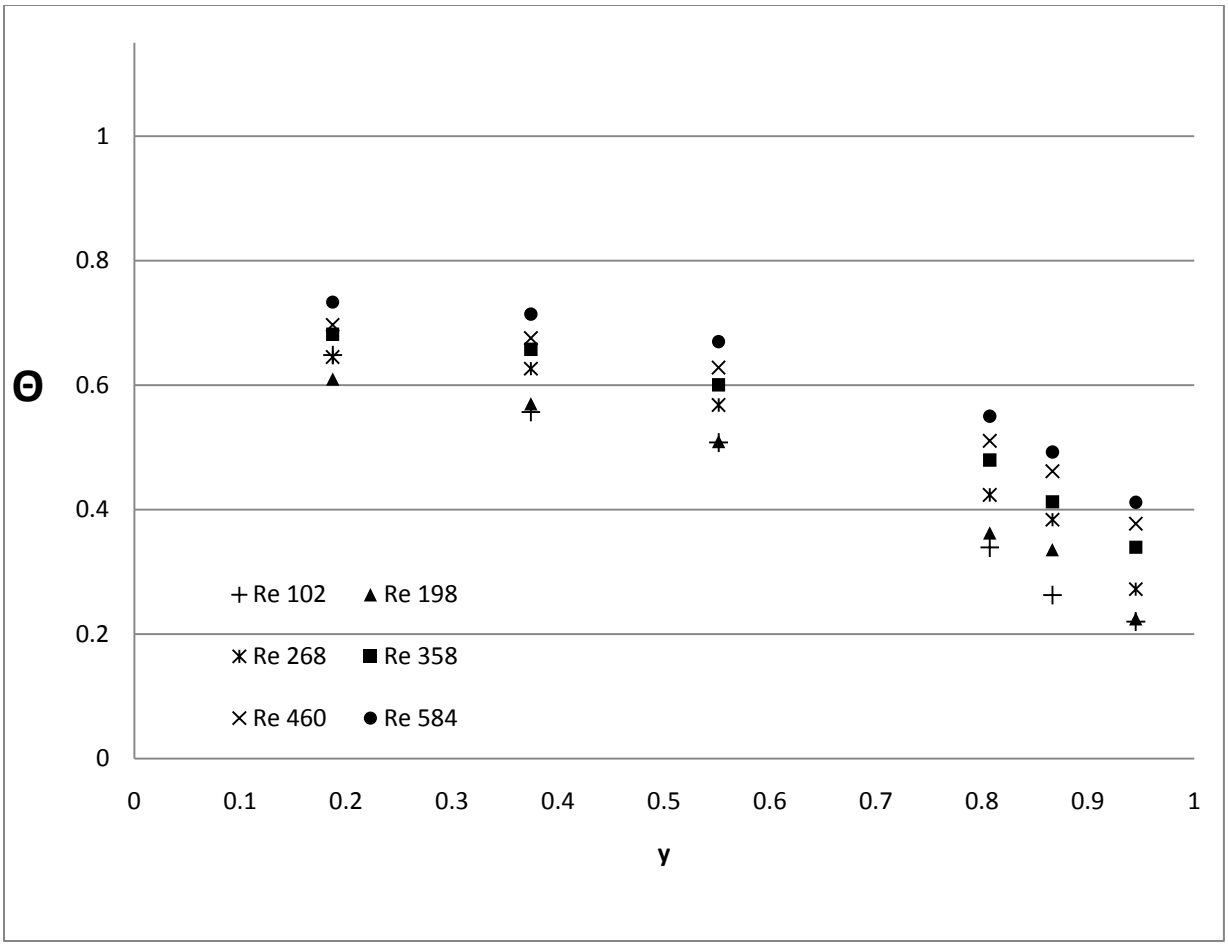

Figure 11: Temperature Profile for JM 4-hole cylinders in the 4 inch column for Bed Depth 200mm

There were few temperature profiles that did not represent our expected findings. Some of the temperatures for higher bed depths would be higher than those for lower bed depths, as well as some temperatures at higher radii being higher than those closer to the center of the tube. This can be a result of bent thermocouples where even a slight deviation from their expected position would cause such a discrepancy. Furthermore since most of the uncharacteristic behavior was seen in the near wall region it could be the result of wall effects dominating this portion of the tube. Figure 12 is an example of these findings.

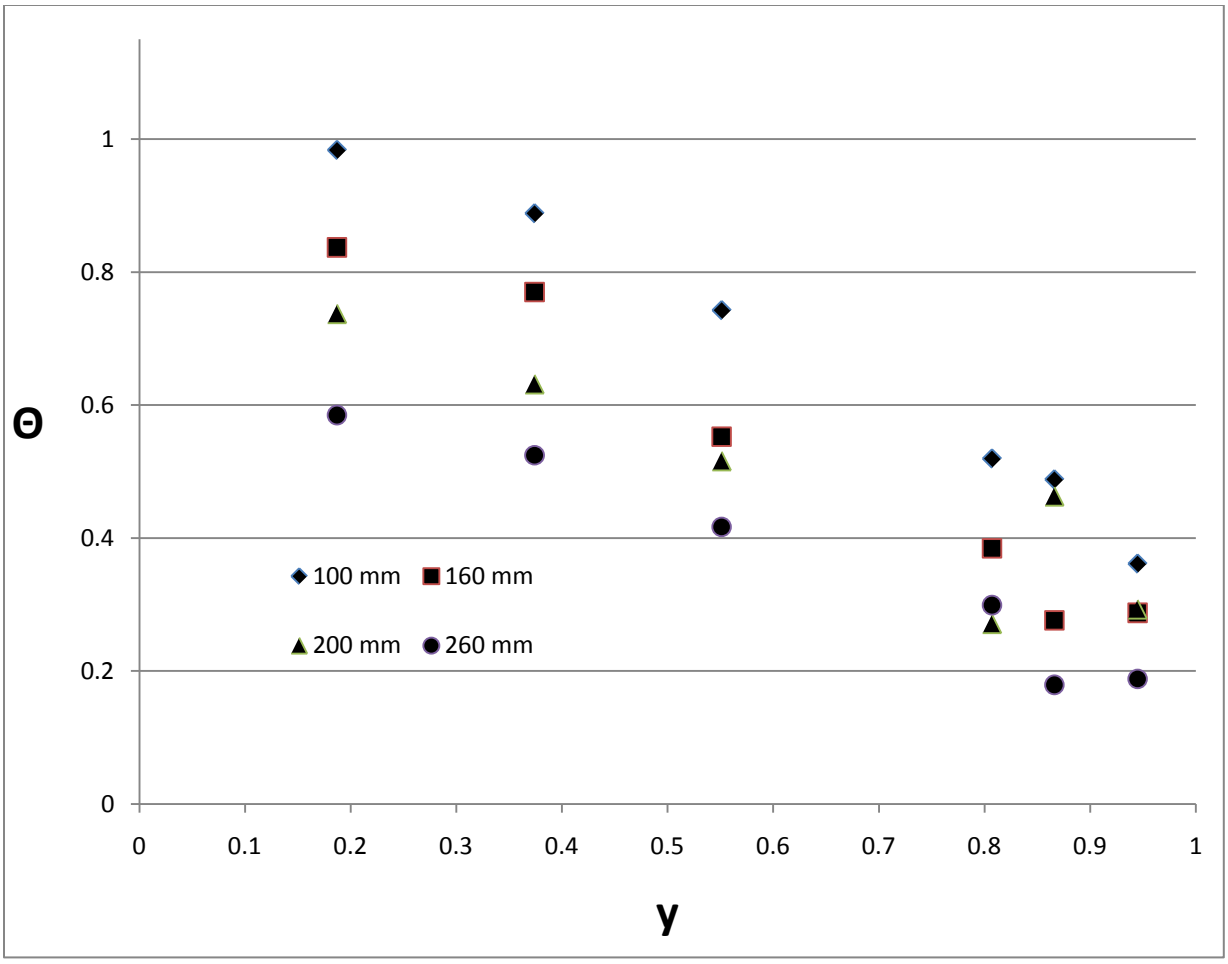

Figure 12: Temperature profile for Monoliths in the 4 inch column with Reynolds Number 129

It is also understood that θ should not exceed 1, as T_o should be the greatest temperature recorded; however, for some packings, θ values of greater than 1 were recorded. This also contradicts prior statements regarding the fit being parabolic with an intercept of 1. Larger than expected θ values were only recorded for raschig rings in the 2 inch column (N=3.5). An example of this is shown in Figure 13. This could be the result of the larger currents created by the larger packing. Because the larger packing takes up a much larger fractional area of the tube cross section it can in effect, if positioned in a certain manner, channel the hot air around the center thermocouple effectively creating a cool spot in this region and resulting in θ of over 1.

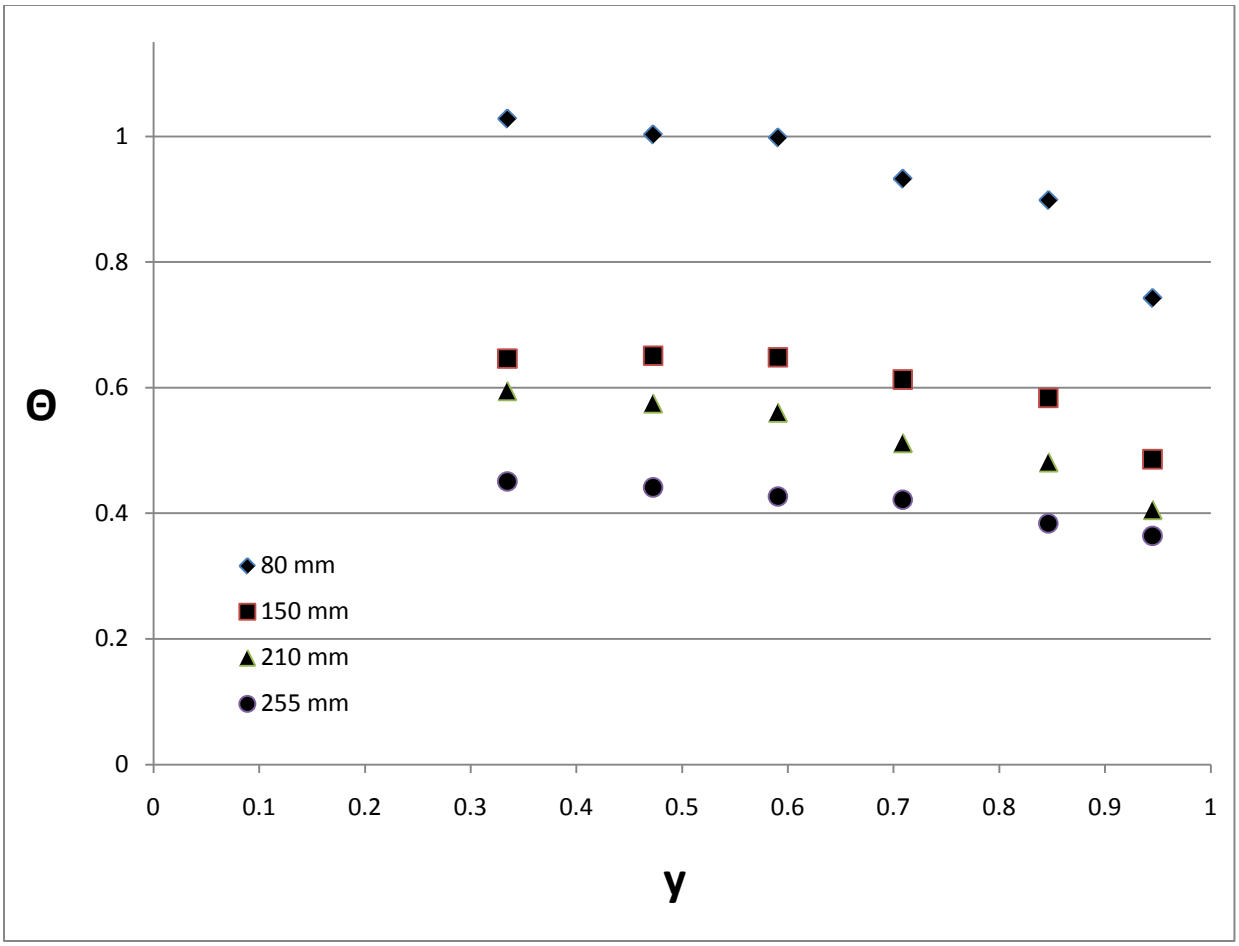

Figure 13: Example of θ exceeding 1; Raschig Rings in the 2 inch column with Reynolds number 1570

41 different sets of Reynolds numbers were examined over this course of this project (5 for the spheres, 6 for the other 6 packing/column combinations). Radial temperature profiles for all 41 sets of Reynolds numbers can be found in Appendix C: θ vs. y by Reynolds Number.

Depth independence on heat transfer parameters

The heat transfer coefficients k_r/k_f and Nu_w are strictly based on the packing size and shape, and airflow. It was once assumed that these parameters were both expected to decrease with bed depth because the models using to fit the parameters were not accounting for the axial dispersion of heat (DeWasch & Froment, 1972; Gunn & Khalid, 1975). However, it has been shown that bed depth should not be a factor in determining the heat transfer coefficients if the IPPF model is used. In order to show this, the data for the second, third, and fourth heights completed were

compared directly to the first height and values were found for the coefficients. Sample graphs of height by height analysis are shown in Figures 14 and 15, using IPPF model. The vertical error bars for all data collected in this study represent 95% confidence intervals.

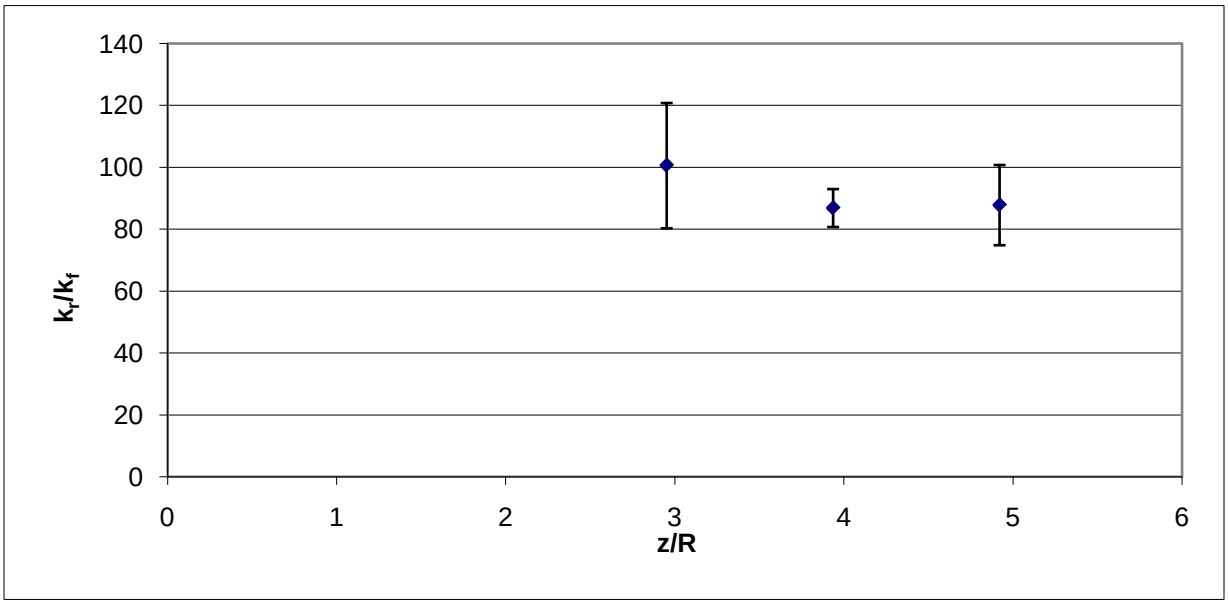

Figure 14: Height by height analysis of kr/kf for JM 4-hole cylinders in the 4 inch column with Reynolds Number 584

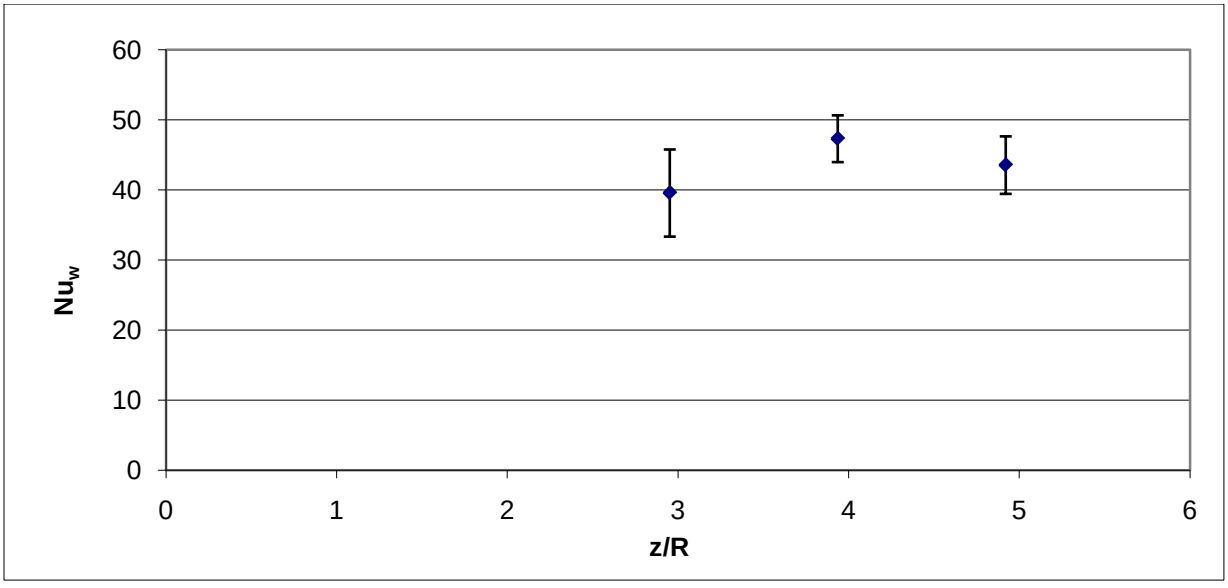

Figure 15: Height by height analysis of Nu_w for JM 4-hole cylinders in the 4 inch column with Reynolds Number 584

Most data obtained presents no strictly positive or negative trends. For respective bed depths, if k_r/k_f decreased, Nu_w would usually increase, and vice versa. Since the overall heat transfer coefficient, U, is dependent on both of these, increasing one and decreasing the other will not affect this parameter. Figure 16 represents how h_w and k_r/k_f are representative of this, showing that using the following equation for the overall heat transfer coefficient:

$$\frac{1}{U} = \frac{1}{h_w} + \frac{\alpha R}{k_r}$$

An increase in Nu_w and decrease in k_r/k_f will yield the same value for U. This has also been seen in the literature. Landon (1996) also showed this; this is shown in Figure 16.

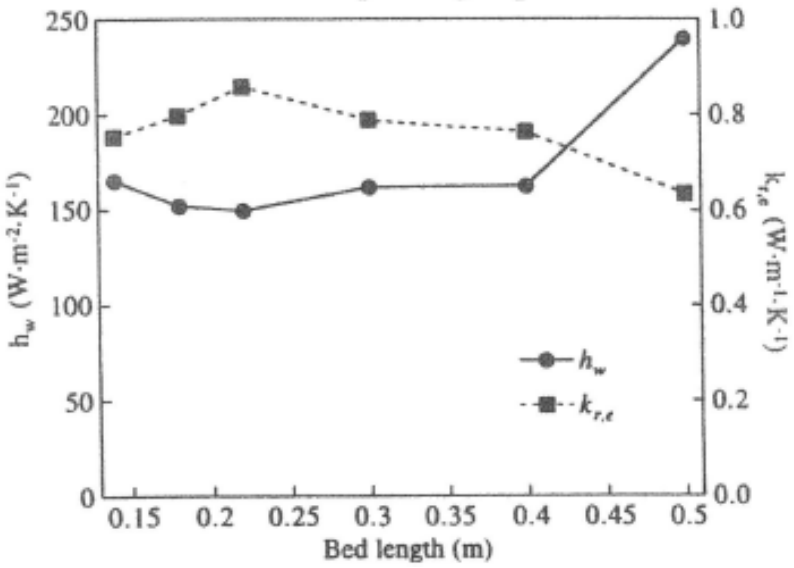

Figure 16: Illustration of bed depth dependence for heat transfer parameters (Landon, 1996)

Peclet and Biot number analysis

Graphs of the Peclet and Biot numbers were also compared to expectations. All except for one, the graphs are representative of our expectations. As stated before, it was expected according to their definitions that the Peclet number would increase rapidly at low Reynolds numbers and

level out at a certain value of the Reynolds number. Figure 17 presents the Peclet number over a range of Reynolds numbers for 4-hole cylinders in the 4 inch column.

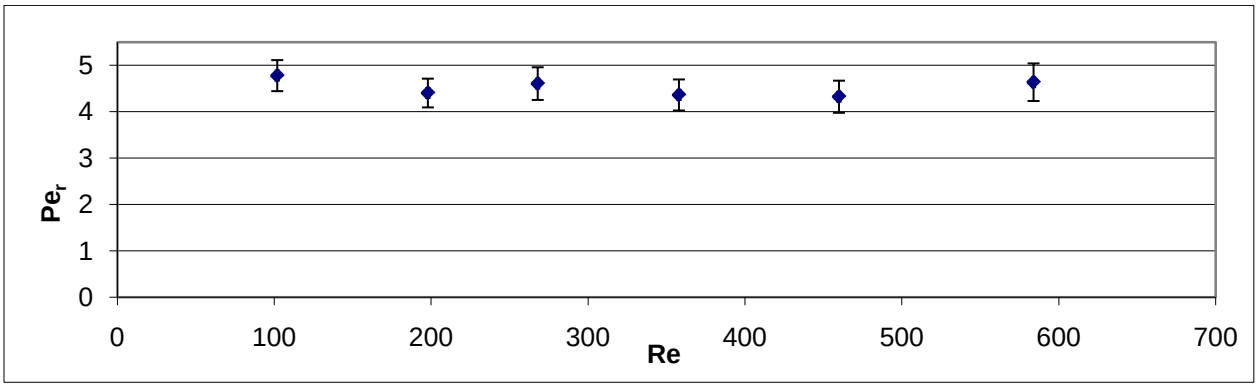

Figure 17: Peclet number versus Reynolds Number for JM 4-hole cylinders in the 4 inch column

The data presented above shows that the Peclet number does not deviate with respect to Reynolds number. The data also shows that the Peclet number for Monoliths is approximately 4.5, which is believable compared to the expected 6 for ceramic particles. This lower value indicates superior heat transfer and as such would make the particle more appealing. Since lower Reynolds numbers were found not to yield reliable data, the values at which Peclet increases rapidly with respect to Reynolds number were not examined. One of the packing/column combinations yielded data unrepresentative of our expectations. This is shown in Figure 18.

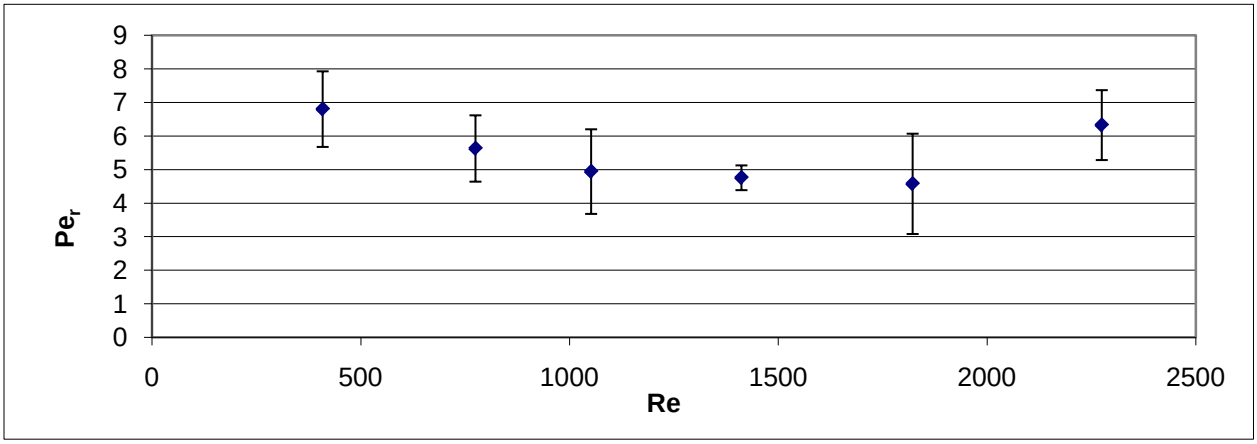

Figure 18: Peclet Number versus Reynolds Number for JM 4-hole cylinders in the 2 inch column

It is very unlikely that Pe_r would behave in such a manner, and the reasoning for such behavior is uncertain. This might be due to the small N value not allowing the heat to disperse evenly across the cross section of the column, causing a discrepancy in parameters at different flowrates.

The Biot number is expected to decrease with respect to Reynolds numbers. All data of Biot number versus Reynolds number obtained in these experiments expressed this behavior. A sample of these graphs is shown in Figure 19.

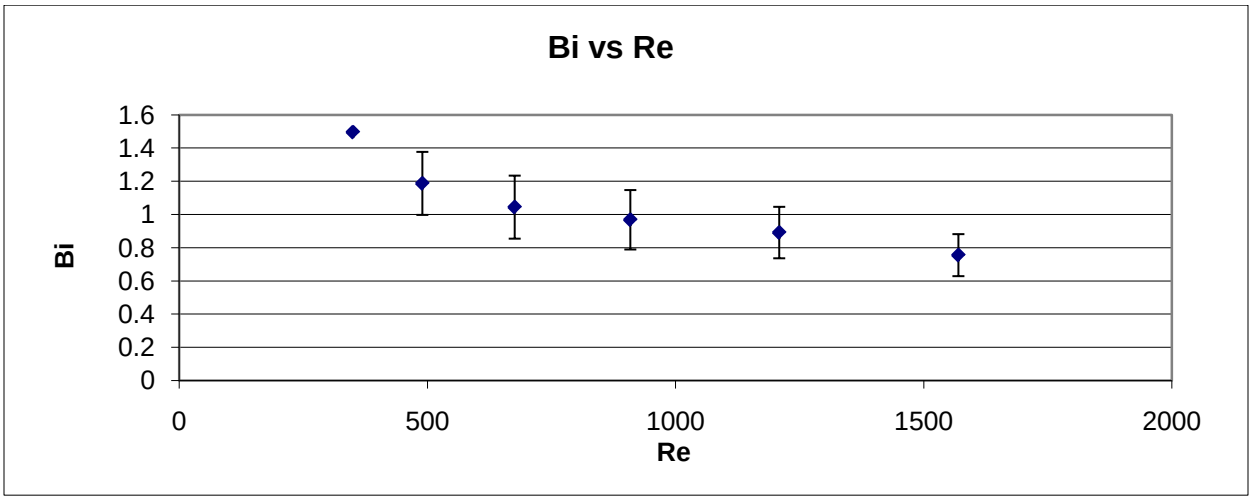

Figure 19: Biot Number versus Reynolds Number for Raschig Rings in the 2 inch column

Most values for the Biot number fall in the range of 1-2, which is close to the expected value. All graphs of Peclet and Biot numbers plotted against Reynolds numbers can be found in Appendix E: kr/kf, Nuw, Bi, and Per for all Packings and Columns.

The Bauer/Schlunder Method

A study done by Smirnov (2002) showed an equation for finding k_r/k_f:

$$k_r/k_f = k_r/k_{f,bed} + K * Re * Pr$$

Where Pr is the Prandtl number for air, which is assumed constant at 0.71. The parameter $k_r/k_{f,bed}$ is the effective radial thermal conductivity of the packing with stagnant air. This parameter must be determined experimentally by plotting k_r/k_f versus Reynolds number and finding the y intercept of the best fit line. In Smirnov's (2002) study, this was assumed to be 10 for ceramic particles (regardless of shape or size) and 20 for glass particles. Although this is much less significant than the slope of the line (considering steam methane reforming is undergone at very high Reynolds numbers), it is important to verify that this value is close to expected to ensure that the slope is accurate. This means that having a negative $k_r/k_{f,bed}$ value will yield a slope that cannot be assumed to be perfectly accurate, and therefore extrapolating will not be precise.

This leaves K, which may be determined experimentally or mathematically through the Bauer/Schlunder method. K varies for each packing, and depends on size (N), shape, and material. Experimentally, this would be the slope of the k_r/k_f versus Re plot divided by the Prandtl number. The Bauer/Schlunder method (Bauer & Schlunder, 1978) for determining K can be expressed by:

$$K_{Bauer} = \frac{X}{8 * \left\{ 2 - \left[1 - \left(\frac{1}{R/d_p} \right) \right]^2 \right\} * d_p}$$

Where X for cylindrical particles can be expressed as:

$$X = \frac{\varepsilon_{bed}}{\varepsilon_{hbed}} F_{cyl}\, d_p + \frac{\varepsilon_{hole}\,(1 - \varepsilon_{bed})}{\varepsilon_{hbed}} F_{hole}\, d_{hole}$$

Where $F_{cyl} = 1.75$, $F_{hole} = 2.8$, $d_{hole} = \sqrt{2}l$, ε_{bed} can be assumed as 0.40 for cylindrical particles, ε_{hole} is the porosity of one particle, and $\varepsilon_{hbed} = \varepsilon_{bed} + \varepsilon_{hole}\,(1 - \varepsilon_{bed})$. For Spherical particles, X can be expressed as:

$$X = 1.15 d_p$$

Experimental K values were compared with those found mathematically using the aforementioned equations. The Bauer/Schlunder equation does not correlate our results well. However, correcting the equation to read:

$$K_{Bauer\ ,corrected} = \frac{X}{7 * \left\{ 2 - \left[1 - \left(\frac{1}{R/d_p} \right) \right]^2 \right\} * d_p}$$

By correcting the K_{Bauer} equation, it was found that the equation correlates our experimentally found K values nicely. This yields the following K values:

Table 6: Comparison of K_{Bauer} and K_{exp} to account for corrected equation

Packing	K_{Bauer}	$K_{Bauer,corrected}$	K_{exp}	N
Raschig Ring (4 inch)	0.226	0.258	0.252	7.0
JM 4-hole cylinders (4 inch)	0.195	0.223	0.225	5.8
Raschig Ring (2 inch)	0.185	0.212	0.175	3.5
JM 4-hole cylinders (2 inch)	0.161	0.184	0.183	2.9

The value of 8 used in the denominator of the K_{Bauer} equation has been found for an ideal model. Since the experiment was not ideal, changing this value to 7 works similar to that of a correction factor to correct for the reality of this experiment.

A study completed by Borkink et al. (1993) compared Peclet number (Note that this is not the radial Peclet number, but instead $Pe = Re * Pr$) to the effective radial thermal conductivity for different packings including raschig rings with an equivalent spherical diameter of 6.2mm in a 49.9mm column (N=8). This was compared to data obtained in this study for raschig rings in the 4 inch column (N=7). To obtain the Peclet number, the Reynolds number was multiplied by the Prandtl number for air. This comparison is displayed in Figure 20.

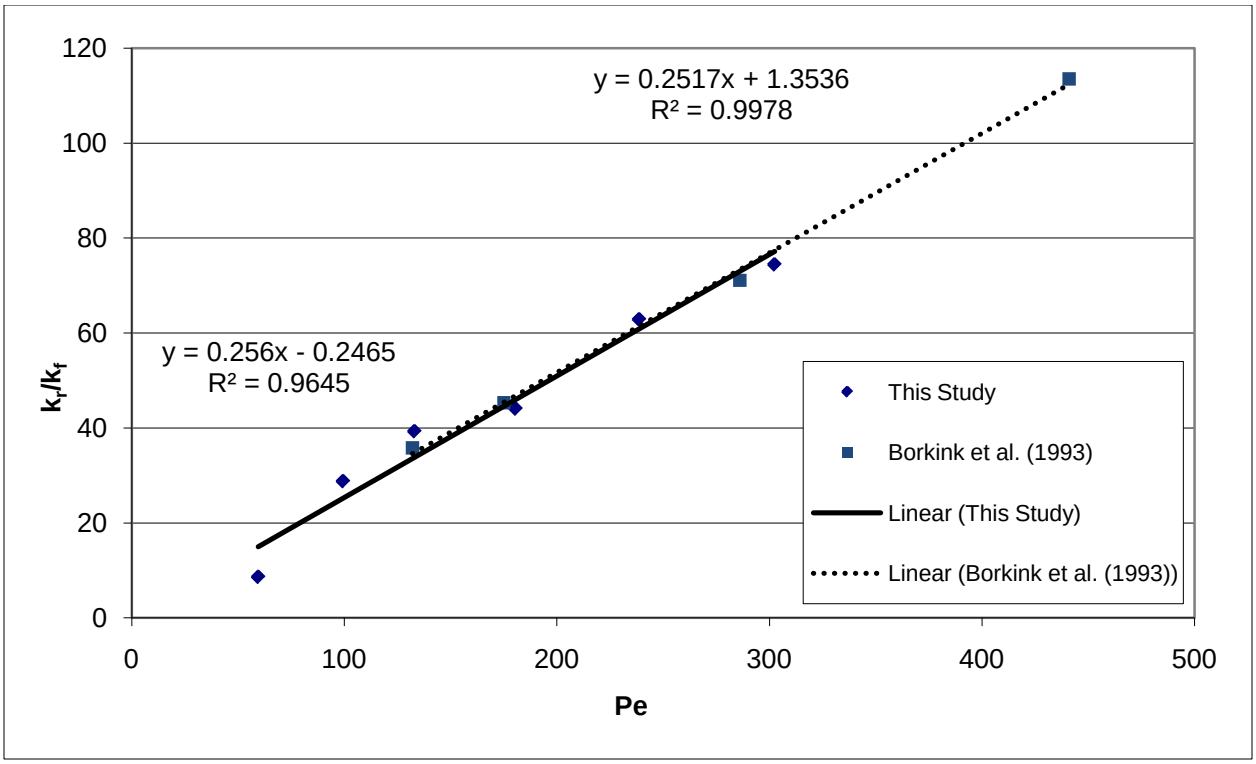

Figure 20: Comparison of Borkink Raschig Ring effective radial thermal conductivity to values from this study

The slopes for both best fit lines are nearly identical, verifying that the value determined for K (which is the slope for the best fit lines above) using the corrected Bauer and Schlunder equation is accurate (according to this and Borkink et al.).

Comparison to past experiments using spheres

The data from this experiment was also compared to various other studies which used ½ inch porous ceramic sphere packing in the 4 inch column. These studies were performed by Hans Van Dongeren (1994) and Darryl Pollica (Dixon, Personal Communication). The two studies were both performed using a heating method rather than cooling; cool air entered the column at the inlet and steam in the jacket heated the air up. Although these were not cooling experiments as this study was, the two are comparable as the IPPF model adjusts all variables to be dimensionless.

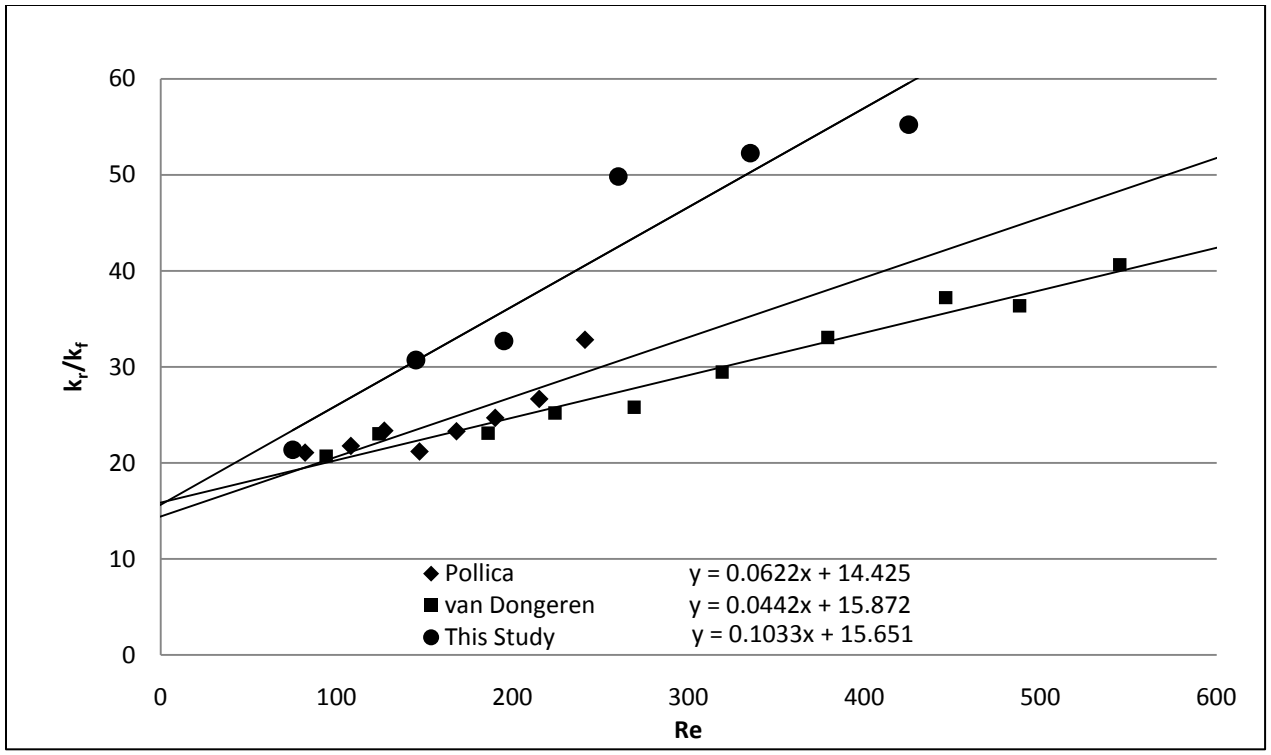

Figure 21: Comparison of k_r/k_f for spheres

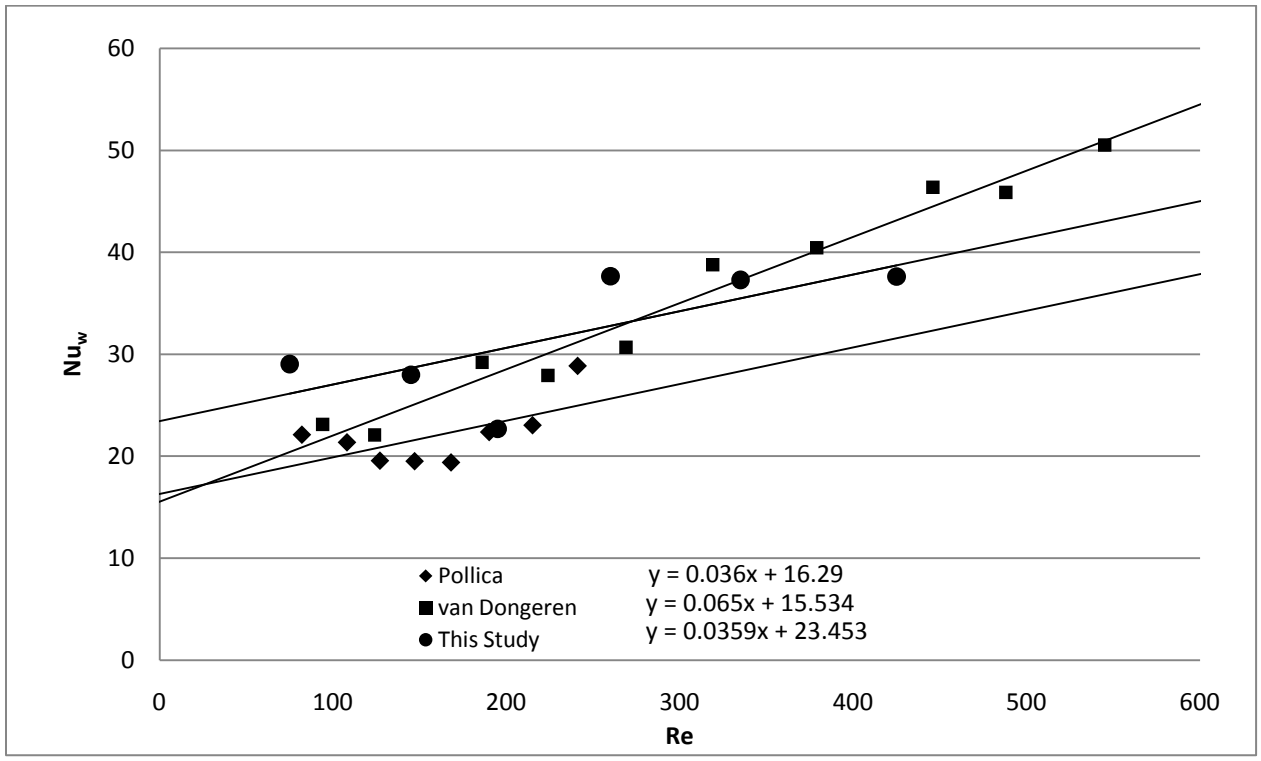

Figure 22: Comparison of Nu_w for spheres

The k_r/k_f comparison illustrates that this study, Pollica, and van Dongeren all determined that the intercept should lie somewhere around 15, however, none of the slopes strongly correlate from one study to another. Although it appears that van Dongeren has a stronger correlation with more data points than the other two studies, a slope (where slope = K*Pr) of 0.044 is far less than the expected 0.07 for a spherical packing with N=8 (Bauer & Schlunder, 1978).

Although Nu_w is not linear in nature with respect to Reynolds number, it can be compared using linear trends at low flowrates. The intercept collected in this study deviates greatly from the intercepts obtained by Pollica and van Dongeren (which are both about 16). However, disregarding the first data point (at a Reynolds number less than 100), the intercept is less than 20. The slope in this study is identical to that of Pollica, which shows that both our study and Pollica's will yield similar Nu_w values at very high flowrates.

Asymptotic radial Peclet relationship to k_r/k_f

Von Landon (1996) stated that at high Reynolds numbers, one may disregard $k_r/k_{f,bed}$ in calculating k_r/k_f by using the equation:

$$k_r \Big/ k_f = \frac{Re * Pr}{Pe_{r,f}^{\infty}}$$

Where $Pe_{r,f}^{\infty}$ is the radial asymptotic Peclet number at high Reynolds numbers. This equation states that $Pe_{r,f}^{\infty} = \frac{1}{K}$ .There are empirically derived equations for $Pe_{r,f}^{\infty}$, such as Bauer and Schlunder, but when using different shaped particles, these equations cannot be assumed accurate. To determine this value, these experiments need to be run at high Reynolds numbers. However, with varied data for Pe_r at higher Reynolds numbers, this calculation cannot be assumed perfect. With the data taken in this study, $Pe_{r,f}^{\infty}$ is the approximate average of Pe_r values over the last 4 Reynolds numbers in which data was recorded. For example, for 4-hole cylinders in the 4 inch column (Figure 17), values for Pe_r average 4.5.

Table 7: Correlation between experimentally found slopes and radial Peclet numbers

Packing	K_{exp}	$Pe_{r,f}^{\infty}$	$1/Pe_{r,f}^{\infty}$	N
Raschig Ring (4 inch)	0.252	4	0.25	7.0
JM 4-hole cylinders (4 inch)	0.225	4.5	0.22	5.8
Monoliths (4 inch)	0.225	3.5	0.29	14.0
Raschig Ring (2 inch)	0.175	6	0.17	3.5
JM 4-hole cylinders (2 inch)	0.183	6	0.17	2.9
Monoliths (2 inch)	0.225	4.5	0.22	7.0

The only packing that greatly deviates from K_{exp} is the monoliths in the 4 inch column. The correlation between Peclet and Reynolds numbers is shown in Figure 23.

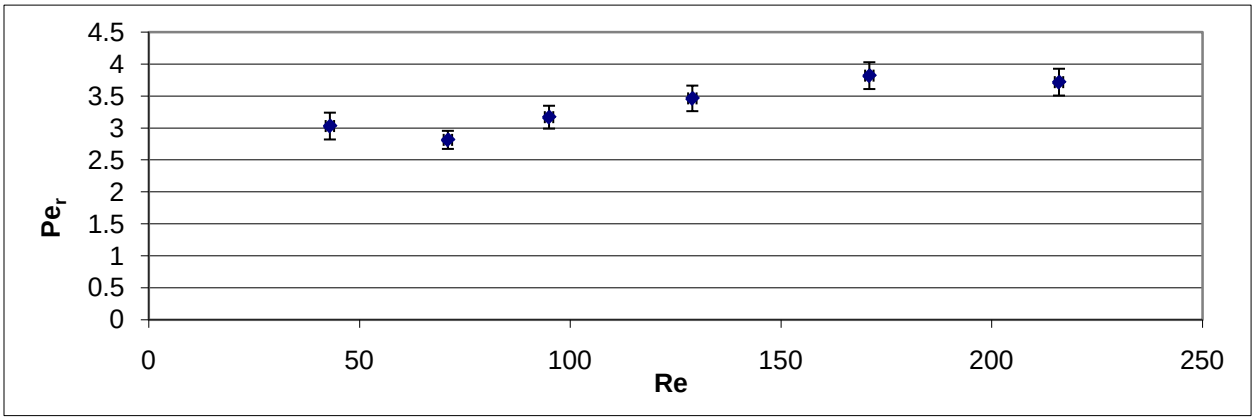

Figure 23: Peclet versus Reynolds number for monoliths in the 4 inch column

As shown in Figure 23, the Peclet number is increasing over Reynolds numbers instead of remaining constant. This is most likely due to the flowrates being too low for the Peclet number to asymptote, and therefore $Pe_{r,f}^{\infty}$ is not definable for this packing. According to the experimental K value determined by the slope, $Pe_{r,f}^{\infty}$ should be 4.5, and very well might be. Comparing $1/Pe_{r,f}^{\infty}$ and slopes of k_r/k_f to Reynolds number is also useful to confirm that the data has been collected at high enough flowrates where the flow is fully developed. The lower the value for $Pe_{r,f}^{\infty}$, the higher k_r/k_f is, meaning that the heat transfer would be overestimated for cases such as this.

Analytically determining a Nusselt wall value

Martin and Nilles (1993) proposed that Nu_w may be determined analytically by using the following equation:

$$Nu_w = \left(1.3 + \frac{5}{N}\right) {}^{k_r}\!/_{k_f, bed} + 0.19Re^{0.75}Pr^{0.33}$$

In a simpler form, this equation is:

$$Nu_w = A + 0.1697Re^{0.75}$$

Where A is the intercept based on the packing's N and $k_r/k_{f,bed}$ value. There are equations to determine theoretical values for $k_r/k_{f,bed}$, however, this study used the values of the intercepts from graphs of k_r/k_f versus Reynolds number. Since Prandtl is assumed constant for air at 60˚C to be 0.71, the second term is solely dependent on Reynolds number. The data collected in this study does not support the accuracy of this equation. An example of this equation compared to this study is shown in Figure 24.

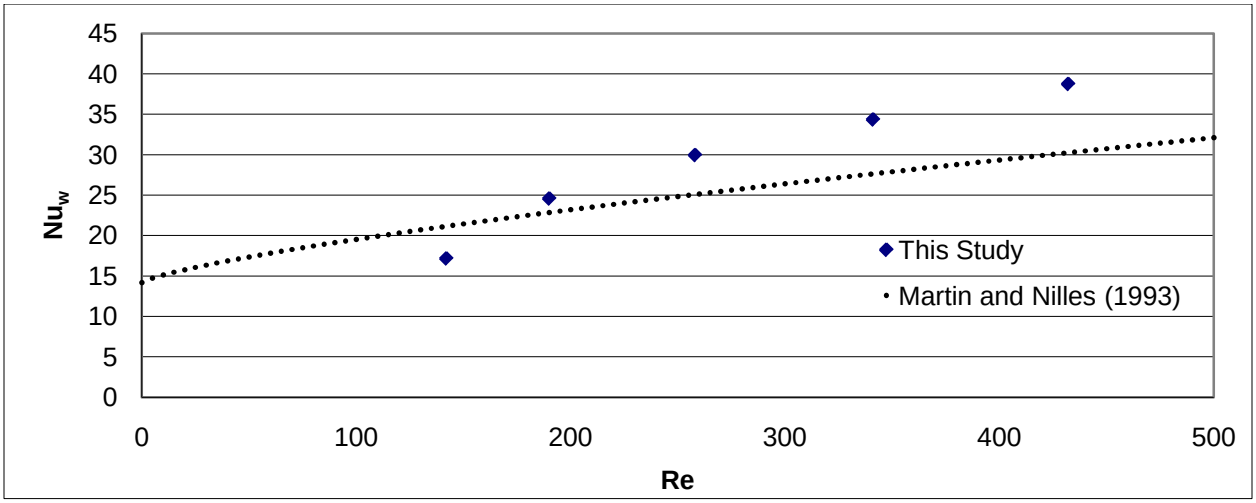

Figure 24: Nu_w versus Re for raschig rings in the 4 inch column

In order to determine correct values for Nu_w, the intercept of k_r/k_f versus Re graphs must be accurate. Some of the data in this study yielded intercepts far lower than expected (some negative) which causes the Martin and Nilles comparison to be far off from the collected Nu_w data. The Martin and Nilles equation compared to this study's data for 4-hole cylinders in the 4 inch column is shown in Figure 25.

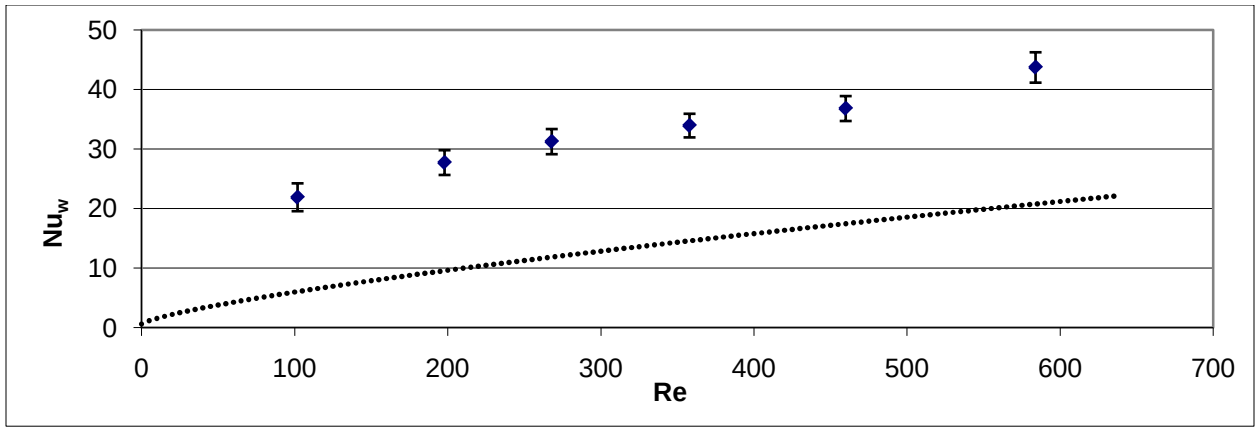

Figure 25: Nu_w versus Re for 4-hole cylinders in the 4 inch column

It can be seen that the series created by the Martin and Nilles is relatively parallel to the data obtained in this study; this deviation of the equation to collected data is solely dependent on the intercept ($k_r/k_{f,bed}$). After correcting the $k_r/k_{f,bed}$ value to be 8 instead of the obtained 0.2835 for the 4-hole cylinders in the 4 inch column, a much better correlation was found. This is shown in Figure 26.

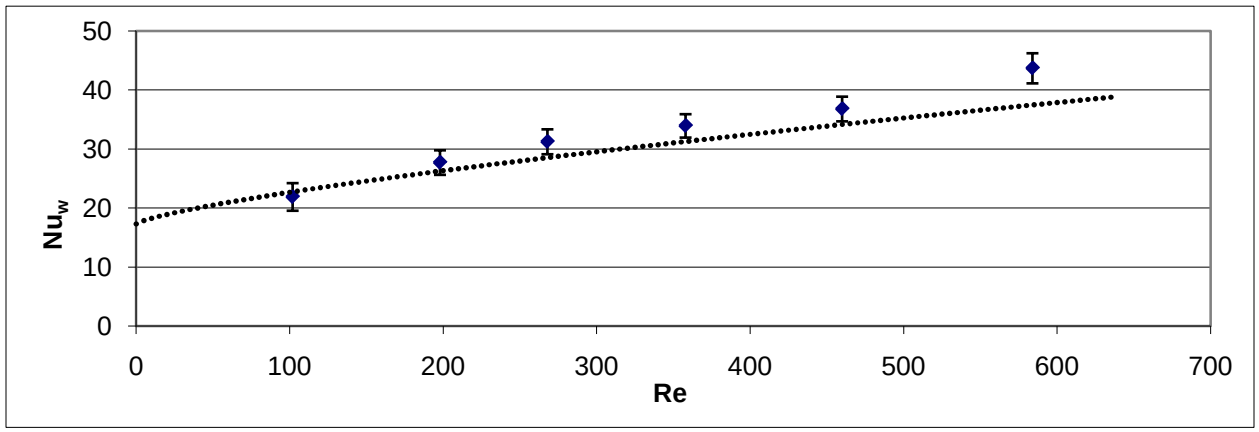

Figure 26: Nu_w versus Re for 4-hole cylinders in the 4 inch column with corrected k_r/k_f bed

N Dependence

Through the course of the experiment the value of N ranged from 2.9 to 14 depending on the packing and tube, the full list can be found in Table 2. Typically N can be expected to fall in the range of 5 to 15 (Von Landon, 1996) and it is generally accepted that this range will produce the desired heat dispersion profiles. As the N drops significantly lower than this range you start to encounter data that does not fit the predicted profiles. This is largely due to the wall effects which dominate the region within a particle diameter of the tube wall (Smirnov, 2002).

Therefore, for any N≤2, the entire tube region would be affected entirely by wall effects; N must be large enough so that the majority of thermocouple readings are not affected by this phenomena. This can be observed by looking at the parabolic fits for the runs where the Raschig Rings and the JM 4-hole cylinders in the 2in column, N=3.5 and N=2.9 respectively (figures 5 and 6), by far produced the least parabolic curves at the first bed heights. Further evidence of poor model prediction in this region comes from values of θ larger than one found for the Raschig Rings in the 2 inch column as well as an uncharacteristic Peclet versus Reynolds correlation for the JM 4-hole cylinders in the 2 inch column. These findings come in contrast to a study done by Dixon (1997) which concluded that an N of as low as 2 for non-sphere particles will still produce the desired results.

Particle Durability

All the particles in this study were composed of ceramics however they varied in both shape and size. It was found that the monolith packing, being of smallest size and having the thinnest walls was far more brittle than the other packings. While the packing heights in this study remained below 300mm in all instances it was still found that many monoliths at the bottom of the column, whether as a result of weight or agitation cracked and crumbled. The raschig rings were far more durable than the monoliths however even these resulted in a few broken particles most likely during the initial packing of the tower. The JM 4-hole cylinders and the spheres were by far the most resilient of the particles as none of these showed cracking or breaking.

Analysis of Variance

In order to ensure that the data is accurate, the F-ratio of F/F_{95} should be less than 1. However, it was found that for packings in the two inch column, values larger than 1 were very common. It was also found that values larger than 1 were often found for monoliths in the 4 inch column. For the raschig rings and 4-hole cylinders in the 2 inch column, this was most likely due to the low N value, causing less uniform heat dispersion, causing the sum of squares to be very large. However, since this is not the case with the monoliths, the discrepancy may be attributed to the large voidage within the particle. A table with all F-ratio values can be found in Appendix F: F-test values.

Conclusion

The IPPF model requires that the lowest height of packing used should provide a z/R ratio of 3. It has been stated that a value below this results in insufficient development of the profile at the inlet height resulting in failure of the model. However, data collected in this study for z/R ratios of 2 showed parabolic profiles. In future studies, if this is found not to be the case, a new model would need to be utilized that does not require a parabolic fit of the temperature profile.

The value of N displays a positive correlation to Nu_w resulting in a distinctive rise in the latter when N was double by moving to the smaller tube. Furthermore an $N \leq 3.5$ is dominated by wall effects and results in data that does not fit the model while $N \geq 5.8$ fits the model well. Further studies would need to be conducted in the range of $3.5 \leq N \leq 5.8$ to determine at which point the wall effects start to dominate a sufficiently large portion of the tube to negate the model.

Analyzing our data for the packings in the 4 inch column, we were able to not only get nearly identical findings for raschig rings, but were able to determine analytical models for determining heat transfer parameters based on shape and size. The Bauer/Schlunder equation, when corrected, gave parameters identical to those collected experimentally. It was also found that Von Landon's $Pe_{r,f}^{\infty}$ correlation to k_r/k_f is a fair estimation. It was however found that the Martin and Nilles equation for determining Nu_w cannot be relied on for accurate measurements as it only depends weakly on particle shape.

The JM 4-hole cylinders and Monoliths studied provided the best heat transfer parameters. However, since the Monoliths are brittle and would be subjected to high forces during steam methane formation, these should not be considered for industrial processes. Further studies should compare the differences between similar shapes such as 3-hole, 4-hole, and 5-hole cylinders.

Nomenclature

Bi	Biot Number ($Nu_w \frac{R/d_p}{k_r/k_f}$)
$Bo_{h,r}^{\theta}$	Bodenstein Number ($\frac{GC_pR^2}{k_rL}$)
C_p	Heat capacity
d_p	Particle diameter
d_{hole}	Characteristic length of the particle ($\sqrt{2}l$)
d_t	Tube diameter
G	Mass flowrate of the gas
h_w	Wall heat transfer coefficient
k_r	Effective radial thermal conductivity
k_f	Effective thermal conductivity of the fluid
F	Variance
L	Largest bed length analyzed
N	Tube to particle diameter ratio (d_t/d_p)
Nu_w	Wall Nusselt number ($\frac{h_w d_p}{k_f}$)
Pe_r	Radial Peclet number ($\frac{Re*Pr}{k_r/k_f}$)
$Pe_{r,f}^{\infty}$	Asymptotic radial Peclet number($\frac{Re*Pr}{k_r/k_f}$ $at\ high\ Re\ values$)
Pr	Prandtl number (0.71 for air at 60 ˚C)
r	Radial position
R	Radius of the tube
Re	Reynolds number ($\frac{v_s\rho d_p}{\mu}$)
T	Temperature
T_o	Center temperature of the first bed depth
T_w	Wall temperature
U	Overall heat transfer coefficient
v_s	Superficial velocity
x	Dimensionless bed depth (z/R)
y	Dimensionless radial position (r/R)
z	Bed depth
α	Experimentally determined constant
ε_{bed}	Bed porosity without account of porosity of particle
ε_{hbed}	Overall bed porosity
ε_{hole}	Porosity of one particle
λ	Effective radial thermal conductivity (same as k)
μ	Viscosity
ρ	Density
θ	Dimensionless temperature ($\frac{(T-T_w)}{(T_o-T_w)}$)
ζ	Dimensionless bed depth ($\frac{x^{R}/_{L}-x_o{}^{R}/_{L}}{1-x_o{}^{R}/_{L}}$)

References

Bauer, R., & Schünder, E.U. (1978). Effective radial thermal conductivity of packings in gas flow. Part I Convective transport coefficient. *Int. Chem. Eng.*, 18, 181-188.

Borkink, J.G.H., Borman, P.C., Westerterp, K.R. (1993). Modeling of the Radial heat Transport in Wall-Cooled packed beds. *Chemical Engineering Communications,* 121, 135-155.

Coberly, C.A., & Marshall Jr., W.R. (1951). Temperature gradients in gas streams flowing through fixed granular beds. *Chem. Eng. Prog.*, 47, 141-150.

DeWasch, A.P., & Froment, G.F. (1972). Heat transfer in packed beds. *Chem. Eng. Sci.*, 27, 567-576.

Dixon, A.G., Cresswell, D.L., & Paterson, W.R. (1978). Heat transfer in packed beds of low tube/particle diameter ratio. *ACS Symp. Ser.*, 65, 238-253.

Dixon, A.G. (1985). The length effect on packed bed effective heat transfer parameters. *Chem. Eng. J.*, 31, 163-173.

Dixon, A.G. (1988). Wall and particle-shape effects on heat transfer in packed beds. *Chem. Eng. Comm.*, 71, 217-237.

Dixon, A.G. (1997). Heat transfer in fixed beds at very low (<4) tube-to-particle diameter ratio. *Ind. Eng. Chem. Res.*, 36, 3053-3064.

Dixon, A.G. (2009). MQP Projects in Catalyst and Reactor Design for Hydrogen Production by Methane Reforming.

Gunn, D.J., & Khalid, M. (1975). Thermal dispersion and wall heat transfer in packed beds. *Chem. Eng. Sci.*, 30, 261-267.

Focus Technology Co., Ltd. *Automobile Exhaust Catalyst Carrier*. Made-in-China. (2009, December 13). http://www.made-in-china.com/showroom/hisina88/product-detailKoXmSOuGZzVf/China-Automobile-Exhaust-Catalyst-Carrier.html

Landon, Von G., Adams, C. Bryan, Hebert, Larry A. (1996). Heat Transfer Measurement for Industrial packed Bed Tubular Reactor Modeling and Design. *AIChE Symposium Series*, 92, 134-144.

Martin, H., & Nilles, M. (1993). Radiale Wärmeleitung in durchströmten Schüttungsrohren. *Chem.-Ing.-Tech.*, 65, 1468-1477.

New York State Energy Research and Development Authority. (2009, November 23). Hydrogen production- Steam Methane Reforming. Retrieved from: http://www.getenergysmart.org/Files/Schools/Hydrogen/6HydrogenProductionSteamMethaneReforming.pdf

Smirnov, E.I., Kronberg, A.E., Kuzmin, V.A., Muzykantov, A.V., Zolotarskii, I.A. (2003). Radial Heat Transfer in Packed Beds of Spheres, Cylinders and Raschig Rings. *Chemical Engineering Journal*, 91, 243-248.

Smirnov, E.I., Kuzmin, V.A., Zolotarskii, I.A. (2004). Radial Thermal Conductivity in Cylindrical beds packed by Shaped Particles. *Chemical Engineering Research and Design*, 82(A2), 293-296.

Smirnov, E.I., Koning, G.W., Kronberg, A.E., Kuzman, V.A., Muzykantov, A.V., Zolotarskii, I.A. (2003). Radial Heat Transfer in Packed Beds of Shaped Particles. *Chemistry for Sustainable Development*, 11, 293-296.

Stitt, E.H., (2005). Reactor Technology for Syngas and Hydrogen. *NATO Science Series II*, 191, 185-216.

US Department of Energy, Hydrogen Production. (2009, November 23). Natural Gas Reforming. Retrieved from: http://www1.eere.energy.gov/hydrogenandfuelcells/production/natural_gas.html

Van Dongeren, J.H.. (1994). Influence of Tube and Particle Diameter at fixed Ratios on Heat transport in Packed Beds. *Final Year project Report, University of Twente.*

Appendices

Appendix A: Sample Fortran Input Text File (for JM 4-hole cylinders in the 2 inch column)

4 6 3 2
50.8 17.4244
8.5 12 15 18 21.5 24
2275 80 0
98.6993515
73.51792602 78.67514038 77.5713257 77.86281738
77.3210266 80.45686036 76.06216734 73.99614106
76.99973906 74.60718994 76.78083646 77.72229768
69.05369872 79.96601562 77.00187682 68.09851226
69.2140457 69.6364151 69.71127474 71.04101106
63.0244606 60.36585998 72.53876342 60.9682289
19.60186308 21.4395725 25.94641496
2275 80 45
98.77065276
73.27800448 75.00024414 79.92648164 76.18695678
73.44379732 77.1693451 75.37802274 78.39521024
70.07826082 76.28060302 78.61668702 74.13243866
69.04063262 73.66384276 73.69291838 71.69318848
72.88054352 68.1328476 71.98683624 72.6760376
63.12102432 61.88073728 69.87362978 65.75786592
19.51357994 21.3685955 25.99892502
1822 80 0
99.0032837
72.00116424 73.03620758 78.05301664 74.74094236
71.51310426 75.45122678 74.21852876 77.48835146
67.20661316 74.16232908 78.2910904 73.26902616
69.28578644 71.16259612 73.7652176 71.61493072
70.35703428 71.04037018 68.31296846 69.6669754
60.4158493 60.79260866 72.35227966 65.32909394
20.29633062 22.00180892 25.93361932
1822 80 45
98.91923066
77.16016844 70.76894226 73.54588778 75.07192536
68.4898941 74.84447022 77.00720824 76.84577026
79.58320314 72.13587802 74.36732786 74.35321196
76.23908386 61.07149504 69.64187774 76.7695099
72.09566194 70.35791016 62.07328492 72.56248322
50.56270676 64.38652344 57.6177574 60.06700898
20.44216992 22.02308922 25.89328118
1412 80 0
98.76869048
73.5621277 67.0405426 70.00103302 71.15197754
65.63481446 71.73593292 73.14741362 73.5072876
76.6353195 68.17412874 70.96861876 70.14902648
72.67462006 57.41319732 66.3239807 73.62355348
67.15747682 66.8013733 58.54669038 68.66848298
47.83555144 60.07205964 53.94326248 57.07460404
19.71891554 21.07039492 24.4406624
1412 80 45
98.9111679
73.34187928 69.24677278 72.00898896 69.62782288
67.89277344 73.18645324 75.1600876 70.95996706
70.12002104 71.0735321 71.23355406 70.35523376
74.25852206 65.93112794 71.36910858 65.40884704
64.26127778 60.37468032 71.2966324 61.95517502
52.64456712 64.01000594 64.45240936 51.4372383

19.72838284 21.09444772 24.4977024
1052 80 0
98.8001999
68.29434206 65.19507292 66.60065306 66.83636778
64.68190612 68.25741732 69.82284546 70.71866304
63.92250366 67.90347598 68.50434264 68.65388334
69.14316408 63.49986954 65.06321718 68.72596892
62.48444292 56.15174638 67.8101944 52.43913954
51.44942398 64.33299254 53.92048034 54.6673523
20.2851219 21.36883354 24.19305116
1052 80 45
98.89687198
59.91440584 58.86440276 59.0906105 59.24870224
64.17294388 56.07076494 62.93479616 58.85851134
60.84555434 54.73794404 60.27732468 63.80253372
53.72100146 63.26296768 59.98911668 55.78862226
47.97101974 58.24943086 58.64743574 59.78501664
48.59130326 50.051342 56.23343276 48.8460846
20.27505568 21.15976448 23.92082404
775 80 0
99.43384704
59.45823746 61.6884689 62.73048478 62.46504518
65.95184784 61.06864318 65.21930846 58.41373674
59.70376434 57.51419678 64.41526184 63.91295698
59.09545746 63.09750598 58.552787 53.92599182
51.70502546 61.2921379 56.91301496 58.56207198
47.50985186 55.72848282 53.45356826 44.60525436
20.31828842 21.1653122 23.46459046
775 80 45
99.5616104
68.68361206 63.5823059 61.86362916 62.37270354
62.53291472 65.90697784 61.09473192 63.43332518
64.0926132 64.39998626 61.02958984 65.32199096
57.55845868 64.65750732 60.02675782 64.38395692
60.25372468 59.1067772 62.8616829 59.52434004
56.02996826 50.4035042 55.21190646 48.15922166
20.31336402 21.18619424 23.48711738
409 80 0
118.6779892
61.59536668 52.45747606 51.95164946 53.74286958
52.38668366 55.49029696 50.82851026 55.43695144
55.15008468 53.41965256 50.87927324 55.7397484
48.3984268 52.73624648 48.4462166 50.59808884
46.3868744 48.52955476 51.60263214 46.51319352
45.83642578 37.79503402 43.69383314 32.8810745
20.18028944 20.63690606 22.03336868
409 80 45
115.8672944
46.89469604 40.70767592 40.4937172 47.82091598
44.55739288 37.52248078 44.38219528 47.39627154
49.52509384 34.64694902 40.84518738 46.16904524
41.36538162 42.24956284 45.1345604 44.68399504
30.60537682 42.41700286 43.01247252 45.32846682
32.8019684 38.80463332 42.5204437 30.83472978
20.17482872 20.52550964 21.59088936
2275 150 0

98.91356508
58.43430328 60.83964308 63.91230622 63.82107468
61.44636842 61.42918168 64.08067014 59.02149506
55.13606186 59.46472624 65.10252836 62.940213
63.5492874 60.35691376 63.37976916 56.53418884
56.3140785 65.41085968 61.00628664 51.28270644
48.51304932 57.2770996 63.54102782 53.03800506
19.56986694 22.42404098 27.06655008
2275 150 45
98.62605742
58.73306882 60.26290054 64.38950196 64.7239746
57.95550918 61.47342226 65.20809022 64.25086974
55.06790694 58.79736326 63.9519615 62.98031006
59.12059098 57.87317044 64.7995209 61.86237182
59.14152144 64.8930344 59.46840822 52.28660656
53.22789 53.5156502 59.27845002 51.18025818
19.54683762 22.52379266 27.16913606
1822 150 0
98.6984726
50.67919006 51.93387604 59.05755616 59.44996874
50.29889906 56.62985916 60.96076582 58.29543536
47.95373078 51.76853638 58.13508528 58.63936234
56.99634626 49.17751694 60.99326704 58.00704422
54.63617708 60.73489074 55.4197731 47.53644486
45.08495408 50.19479218 56.01174318 46.6245842
19.2335289 21.498431 25.7419239
1822 150 45
98.6147278
56.77056808 49.41270372 57.39555436 58.6312027
52.338488 53.32281494 57.6699066 58.52672958
57.09482574 46.32721864 56.52928848 59.86500244
54.8510872 53.31860504 59.7137375 59.45969544
44.55054322 52.48655244 59.7456833 57.80756608
47.53789826 47.028257 54.29777374 56.67471468
19.12161484 21.57909472 25.69528312
1412 150 0
98.9509506
50.77979968 52.58001328 56.76442566 55.53376772
49.65307238 53.9867485 57.66937942 56.13626404
50.15673296 54.14580612 57.11678008 55.44091338
51.93353118 45.9466507 56.7082733 53.5809471
49.6351883 53.94620438 55.31752014 49.32602538
37.22709578 47.92097246 51.71604768 39.12158202
19.34335938 21.0656891 24.85866166
1412 150 45
98.57024386
48.80660018 52.86111146 53.3242119 52.78184662
52.836792 55.80041504 56.68186494 52.11970826
46.5125061 52.9849617 56.58839644 55.360421
56.12694856 51.27490998 57.5123207 52.21260302
51.89121474 56.30685654 50.99152144 42.50901564
40.20662996 53.07470704 55.34767456 42.76657564
19.38923264 21.12947806 24.85371858
1052 150 0
99.0073639
40.91475754 48.37804872 49.69394378 44.75125428

41.19297028 49.95391008 50.35421524 43.21306688
38.8451248 47.79931642 49.53569186 47.91036528
51.21306152 43.73466644 52.38024904 45.05809172
47.18281328 50.41306534 46.15266038 36.77309798
33.3092529 48.60114438 50.73813096 36.52398222
19.16157456 20.50416106 23.67472992
1052 150 45
98.62762146
46.55139084 50.37760542 48.8636734 41.72287138
45.81043778 50.49033814 48.18919678 40.85421524
46.73076936 50.27729416 51.40846788 43.54044876
51.33971708 47.48421098 48.51408158 38.6225525
50.43963316 52.52350996 45.03630522 42.02005766
38.76716766 49.8013588 42.7995491 31.79461822
19.2223526 20.58517952 23.8402817
775 150 0
100.4869492
45.82597198 48.88180924 48.64862902 43.62995148
45.46760638 49.50203702 48.50621186 42.58764344
46.45537264 49.10773392 49.6659912 45.5958679
49.3028244 45.623275 47.26775512 39.63362196
47.500325 49.26344376 45.51480788 42.73489836
37.46359254 46.86143492 40.74909362 32.50484694
19.61428872 20.74641036 23.3496689
775 150 45
97.4851593
48.8413147 49.661438 45.4838379 46.24140396
48.72106704 48.09358522 43.23610688 45.94310912
48.47971724 49.90555954 45.859346 46.2270523
47.4385887 48.55472716 40.49301912 44.75554962
48.4061447 45.473584 43.57394258 46.35172424
40.50546492 44.33735276 36.64361114 32.95051194
19.61437988 20.76703798 23.37957422
409 150 0
108.5689758
36.31838836 36.00875854 32.74766846 33.9221222
36.42999266 33.94670334 30.76653978 34.41045534
35.80542754 36.14849626 30.22783204 33.96519164
31.35536196 37.33917542 29.57197228 33.74812316
34.73056108 24.12475432 32.94790344 33.4170845
32.75461652 29.23967438 26.69602202 26.30184174
19.19199756 19.6527851 21.40013428
409 150 45
103.9985366
36.79264756 36.4160965 32.58012774 34.5112465
36.55339582 34.16837616 31.1742687 34.88336714
37.12656172 36.52278898 30.67872924 34.82304308
31.96548194 37.33473208 29.40726546 34.20025178
34.88130416 25.34253044 32.83948364 35.09132766
32.65042036 28.8647785 26.1234558 25.78597908
19.15955582 19.6281311 21.4826889
2275 200 0
99.16753998
56.80274048 56.5553627 55.35040894 55.66593932
56.48750994 55.8770172 54.6225708 55.54912872
55.06276856 55.50765228 53.97180328 51.80721436

53.6000389 56.02751234 55.77091596 54.49867782
53.37738264 50.68227464 48.56469346 52.22539214
50.68758774 47.39768144 53.3546509 42.7739067
19.9816288 24.27942428 27.3081413
2275 200 45
99.32751464
56.8763939 56.26218492 56.48807982 56.3740486
56.35706176 57.1123329 55.01497806 55.8926445
56.32222672 54.2671028 56.18304598 54.26648866
55.97688828 55.09260254 52.54919816 52.98763428
52.77218934 52.95060806 54.98386228 52.06026304
48.62270968 54.22021406 50.13025282 47.67022018
19.96664236 24.4571537 27.47696648
1822 200 0
98.75254518
52.77601622 52.2064331 52.1440544 51.74226988
52.39601898 52.94602584 50.73092422 51.81161346
52.09917146 49.93562622 51.71668168 49.73918764
50.47908556 50.70390778 48.12815628 48.78876494
47.19949416 46.8016281 50.37097092 48.32941208
43.98571776 47.95161056 46.1387558 44.51240924
19.47835502 22.96445274 25.7378071
1822 200 45
98.99816742
46.73545458 42.03614576 45.39466628 48.28736572
43.19481586 21.73489762 47.51638642 46.57336886
40.54960176 39.46253052 43.84951708 48.62294236
38.2229309 38.050766 44.00555876 44.44626692
39.54594574 43.10226364 46.77544478 36.17896652
32.50676192 32.80727462 38.04145966 41.05914232
19.2466503 22.3741989 25.6514675
1412 200 0
98.87921142
47.7934906 46.2575569 48.8368439 47.38877412
45.2327606 47.04674378 48.03281784 46.26497802
44.3535927 40.13817138 47.12823716 47.4955345
44.86109696 35.17089234 44.22092666 48.9150421
39.61377488 44.59798128 44.9947319 38.58955536
30.74430542 42.20111084 37.01335526 43.82090456
19.7666401 22.48489492 25.22439576
1412 200 45
98.5345642
46.32924804 48.3742035 48.14803698 47.5756569
46.00261536 48.96492462 46.95700226 46.0573738
42.17110368 46.27195664 48.52537918 44.81440962
46.5326851 38.79361878 45.09022902 41.37486496
43.4593918 44.30651016 45.34169312 34.4771507
37.65764236 44.62176666 43.78035812 34.187677
19.81744498 22.5064728 25.27298088
1052 200 0
98.90518646
41.69141464 43.93356322 43.96338578 43.00163726
42.08356248 44.7333618 42.92609786 41.22968826
38.4459564 41.72648162 44.28848724 40.32664414
42.73218156 40.75215912 41.01621246 36.77588576
38.96191406 39.5943901 40.25822066 30.58843956

33.66010284 40.84319838 40.1227333 30.39145394
19.6530487 21.6501873 24.25802344
1052 200 45
98.94475404
42.642659 40.93933562 43.49178466 42.71018754
40.83062362 41.8938591 42.83531266 41.70334852
39.34235308 35.26944732 41.42165374 43.3284668
40.17119906 36.29108656 39.35680158 42.1175003
33.46795576 39.31444244 41.46668244 34.50531998
28.95948334 35.94878388 32.84912796 37.29596784
19.65926816 21.48394086 24.13745194
775 200 0
98.44761658
38.6051117 37.4156601 39.48222732 38.845166
37.08525314 38.17751694 39.177832 37.64824982
35.41690064 32.3655525 37.5056557 39.48755798
36.19804 32.72103272 35.99720536 38.1797447
30.77688676 35.59904098 37.54720688 31.55895578
26.36857068 31.97444456 29.73430366 33.805246
19.45078966 20.87292788 23.20948906
775 200 45
99.293779
38.33902666 37.92753676 38.50621336 39.31750944
36.5863365 36.29005434 38.7314659 39.57939072
37.01532516 35.3193451 37.41386568 37.83820574
29.9499901 32.99298934 37.02521744 38.69386292
29.44973108 35.1542488 34.28367692 38.43269804
28.45227546 26.36058654 34.58326036 34.8159691
19.44895478 20.87421608 23.1486824
409 200 0
111.9536896
31.03306464 30.35135156 30.88413926 31.98917502
29.54854852 28.77385824 30.87115518 32.11796418
29.87023812 27.45694084 29.4767399 31.0357235
23.83875616 27.43690186 29.65249024 29.92760734
23.40657158 28.01109048 28.66285056 30.69504014
24.3244854 22.15790978 27.759346 27.32902602
19.34734918 20.1006733 21.720932
409 200 45
109.4164322
29.67201578 26.41555826 28.50524368 29.93023416
26.89048918 26.26057092 29.77409746 29.27373314
27.51098212 23.35940628 27.73017768 29.87352526
23.93672906 23.09819526 27.94829558 29.11346052
22.03939018 26.90578842 28.60467338 25.22316246
21.42739336 21.35714682 25.24629404 25.95150148
19.3326126 19.96550522 21.64152298
2275 265 0
98.93516996
51.52176742 49.21428452 50.76236496 49.38575362
48.88019104 49.23531266 50.61433334 49.36290664
50.31932298 46.08536074 51.42882308 49.4229492
50.92274398 45.73157654 52.48243558 48.54239732
42.85022354 50.2087555 48.30945514 46.24342498
38.42465594 47.09502638 47.69607544 41.99709398
19.15761566 22.83422852 25.63332102

2275 265 45
98.53293456
49.338488 49.26488418 50.10499344 49.98358612
51.07362212 47.37760314 52.17178114 49.77518692
49.5806618 47.7857712 50.11046524 50.6676811
46.00337676 48.51928712 51.20819552 49.48350982
45.03485108 50.19804764 50.2034294 47.94532014
40.21110228 42.11347884 49.10993194 43.37984618
19.14161796 22.82235376 25.6085289
1822 265 0
98.6812439
45.64598466 45.38593904 46.33173368 46.16474382
47.2903206 43.71267548 48.0881996 45.86076738
45.66292114 44.4619667 46.02790068 47.06360014
41.8697502 45.01825792 47.16648484 45.427948
41.13500598 45.99850846 46.4579643 43.97706374
36.88848192 36.26695482 45.13731002 38.98748628
19.13657722 22.81351854 25.60926932
1822 265 45
98.54974824
40.23674318 41.40471724 41.78658068 43.065905
40.36697006 42.1230606 40.6655464 43.69579698
39.12290878 41.32575532 39.48177186 42.29679184
40.51795654 38.9880913 38.06063768 43.35520782
41.0656563 39.80584792 44.13357772 37.30011594
32.17085114 36.9378525 34.38277056 40.00833436
19.16079788 22.79908218 25.6180031
1412 265 0
98.86578064
38.85801544 40.33667298 41.21251526 39.3657837
41.02693712 39.53769534 42.59932708 38.1136116
38.99116362 39.99701918 41.10022506 41.65617904
38.27532042 40.0788841 42.83440324 37.3191269
37.29112626 40.71051256 40.61609422 37.57031404
33.90524674 35.1454651 41.77336274 31.52881432
19.30854414 22.29714164 24.7952156
1412 265 45
98.84623718
40.84026108 40.28384552 40.93802412 38.18530426
40.0435661 40.25686796 40.24929352 38.56129454
40.50852966 38.9292061 42.20601348 37.72995224
41.57413102 38.55087358 42.70633698 37.83195952
37.91297914 42.59278488 36.45733796 38.74069826
32.4420685 38.94508132 38.72758942 32.00665246
19.34336056 22.30565488 24.81808052
1052 265 0
98.09759826
36.20451658 33.15526428 36.40771636 33.58348694
32.71285326 35.2932205 36.85055848 33.38526384
34.7976776 33.23992082 36.67690506 34.27435608
35.24885482 28.84222374 40.1488388 33.02709502
31.88615686 37.90348968 33.2546242 30.61848222
25.40261496 32.41366576 37.13974838 29.28974496
19.3337341 21.68404466 23.84773864
1052 265 45
97.96114348

35.79308546 32.31847306 35.40328292 35.34646988
35.32076034 32.20355608 38.20213088 34.305616
33.40152894 30.65407182 35.30542906 36.50457916
32.60639648 32.333667 37.0570244 34.15605394
29.6860058 37.62654956 37.27133942 32.78776094
26.0327778 31.92216798 35.86511306 28.8260361
19.38240816 21.70701676 23.86766778
775 265 0
99.89899596
31.82552604 28.38801652 30.5000683 31.62730332
31.06622048 27.57356606 33.3532692 30.88825838
29.44453966 26.32150536 30.79584962 32.26807864
27.96599694 28.06433906 32.06499098 30.6549839
25.32743416 32.47447206 33.15893628 28.53027764
23.201284 26.99083404 30.97368928 26.04771766
19.22278254 20.92047804 22.90697594
775 265 45
97.69941254
31.92369768 28.91629524 31.81234208 30.4450676
27.01779098 30.30033952 31.98719826 31.88331568
28.97728652 27.63662642 34.2344177 30.6048332
32.50058058 26.23759192 31.85536194 29.03033294
27.94880486 31.50609702 30.267054 24.08791198
23.96117554 31.70822486 31.33988838 26.99343032
19.26017456 20.96857226 22.96351282
409 265 0
112.4658508
24.88429414 23.86322706 24.40131724 23.95190508
22.69894904 24.37530212 24.39242288 24.7513981
23.15618592 22.77808152 25.97793732 24.04668348
25.1021969 21.79917872 24.2587055 23.52177584
22.74705086 24.2143673 23.62438622 21.05283624
20.57918664 24.04594078 24.72375946 21.10760954
18.73377798 19.5138748 21.00809098
409 265 45
109.804715
24.10503808 25.07635842 24.41656036 23.32913706
24.43660392 24.4563286 24.6548073 22.89769706
23.58973198 26.3138546 23.8388481 22.91086046
24.27376138 24.76650392 23.57692644 22.27217254
25.59636114 23.14626388 21.51476516 22.94084472
23.4987427 22.99370384 22.18857652 20.10545082
18.7401596 19.53059462 21.00464324
-1 -1 -1

Appendix B: θ vs. y for First Heights

First Height Parabolic Fit for Raschig Rings

In the 4inch Column

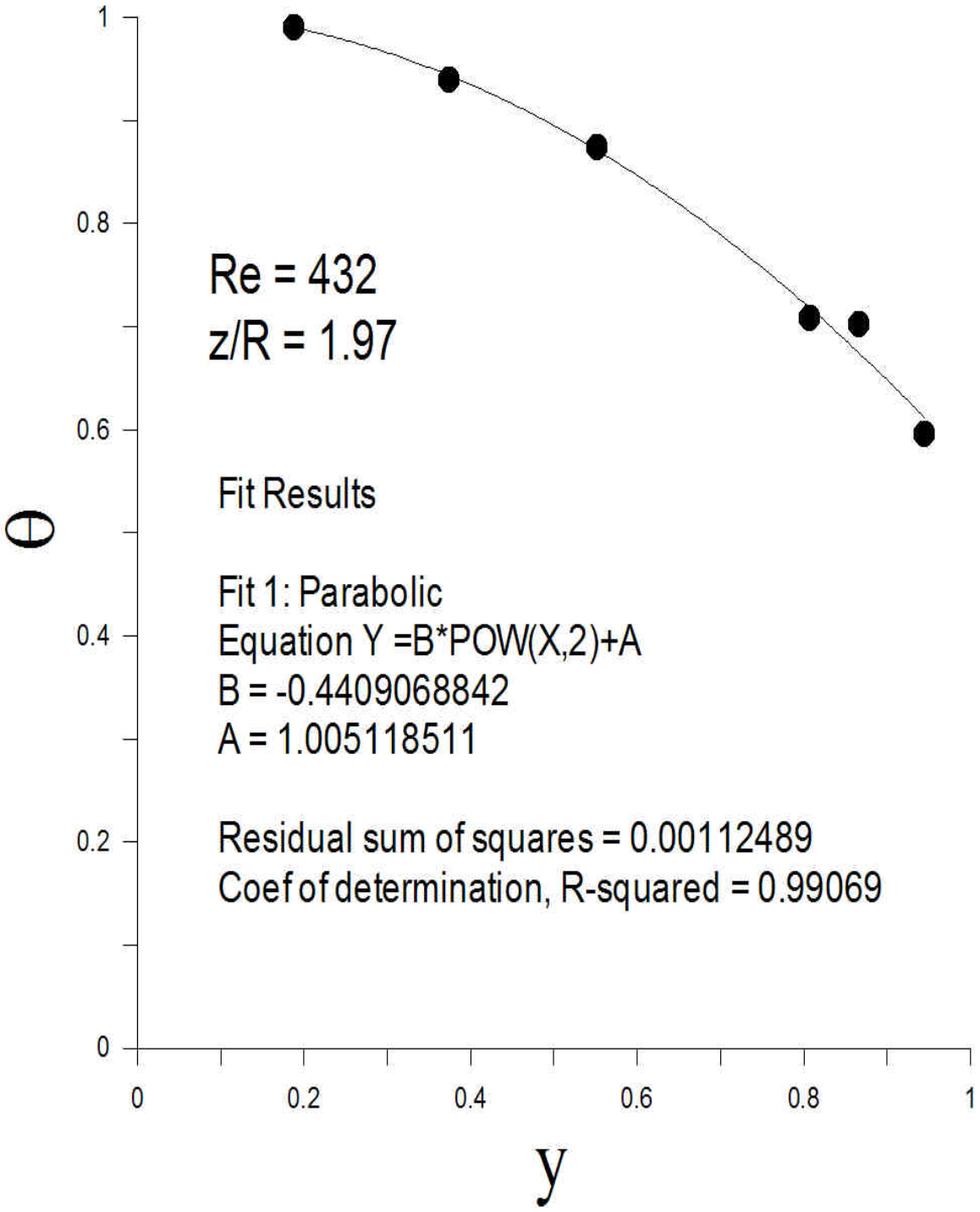

First Height Parabolic Fit for 4-hole cylinders

In the 4inch Column

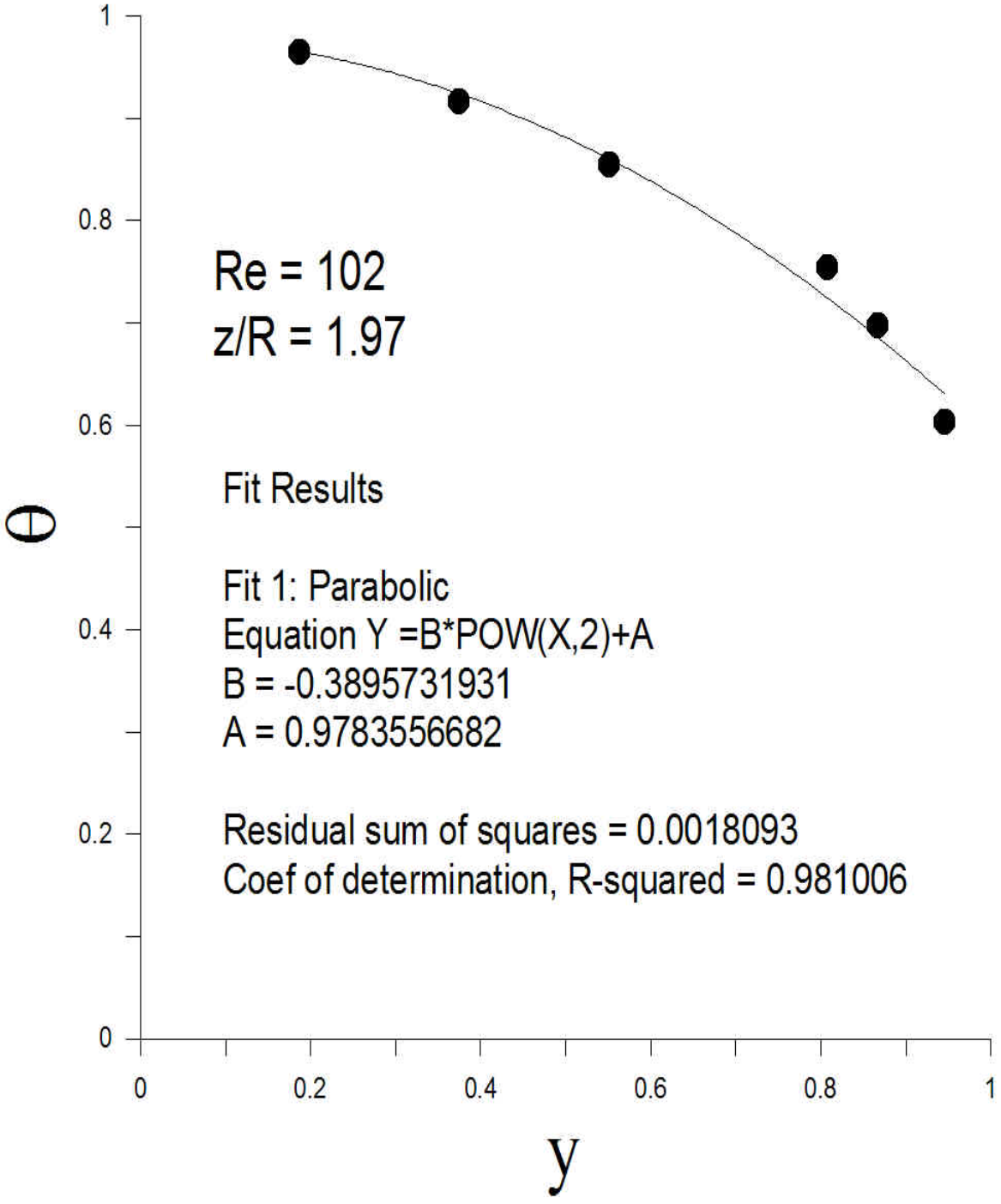

First Height Parabolic Fit for Monoliths

In the 4inch Column

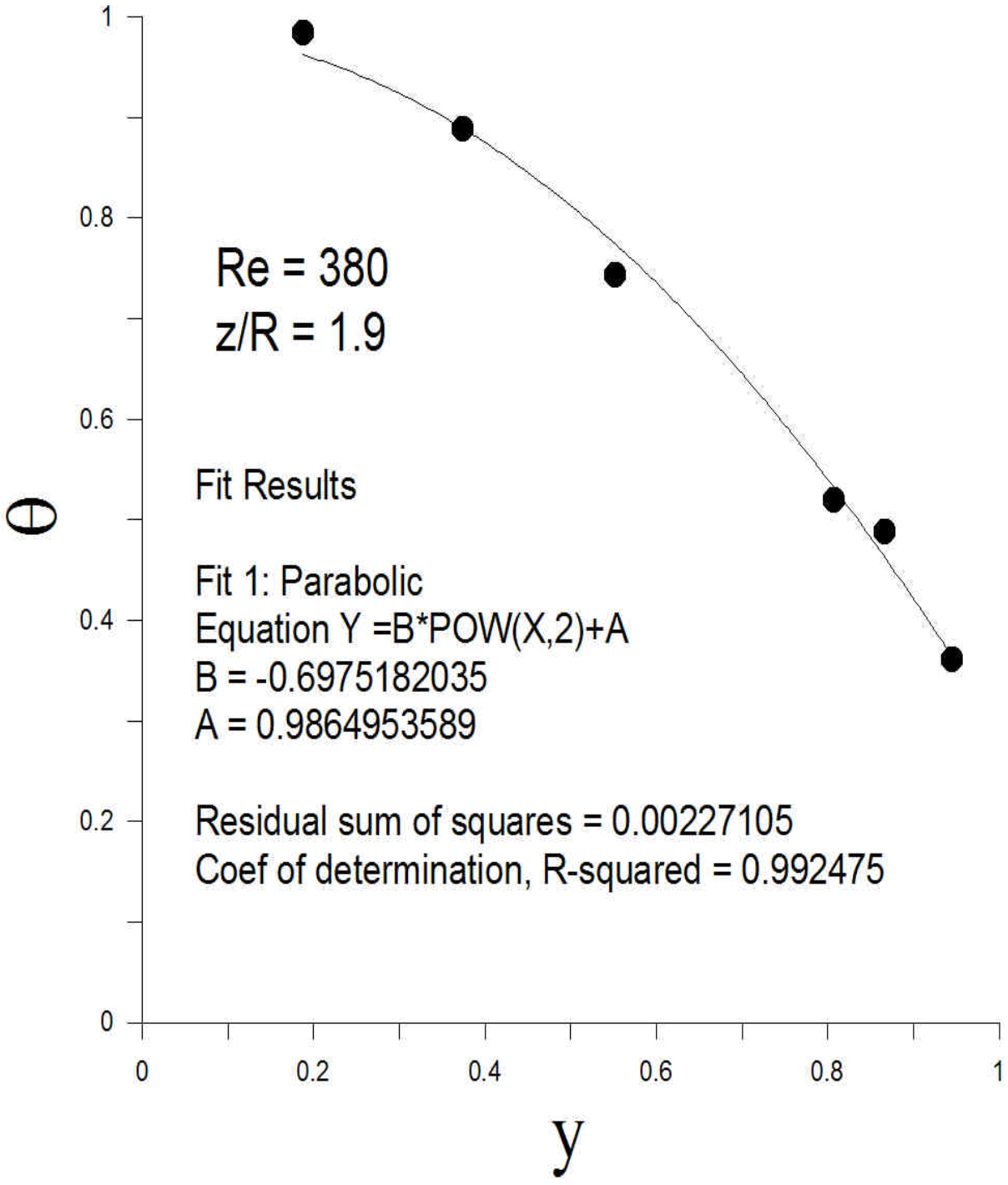

First Height Parabolic Fit for Raschig Rings

In the 2inch Column

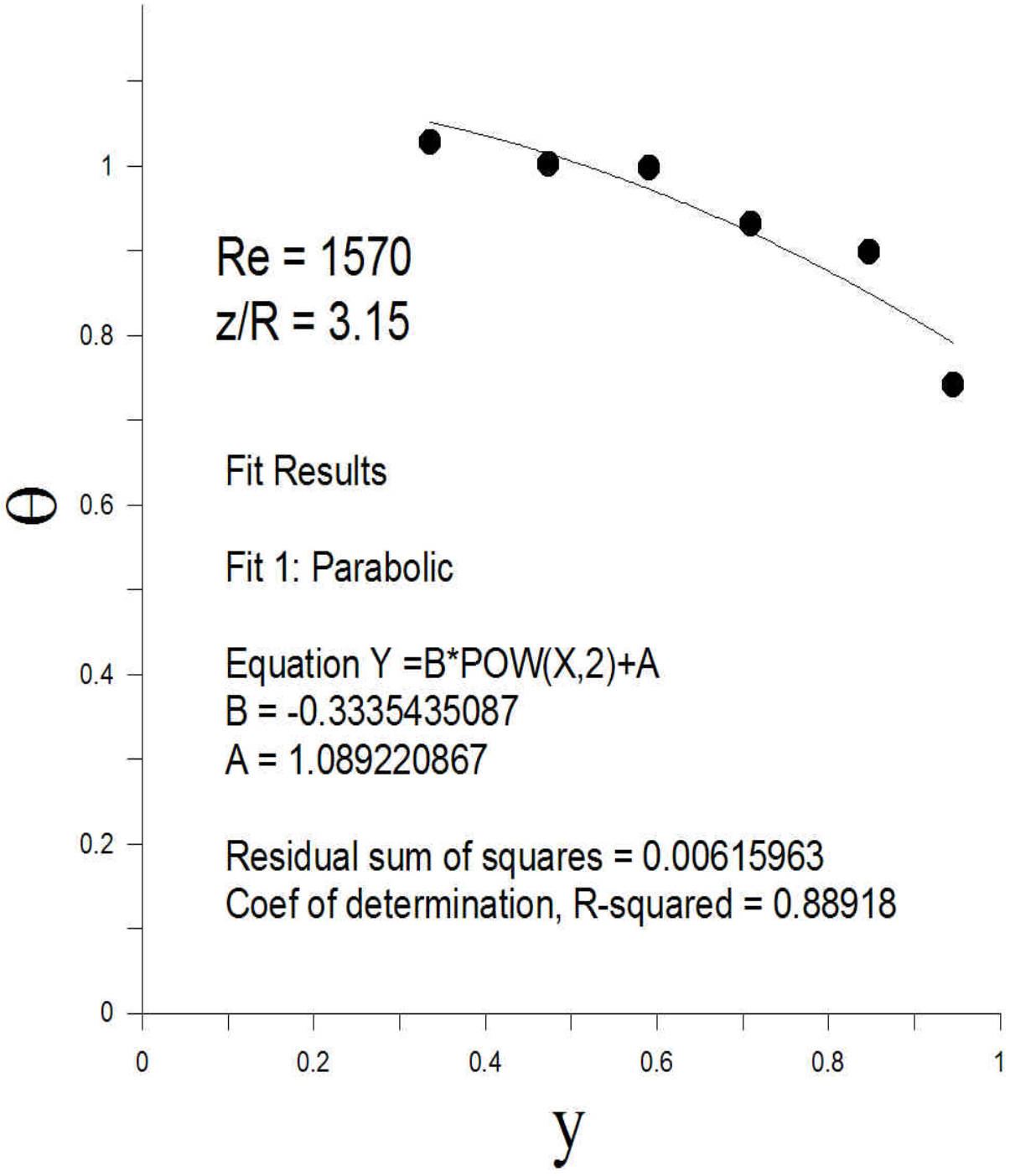

First Height Parabolic Fit for 4-hole cylinders

In the 2inch Column

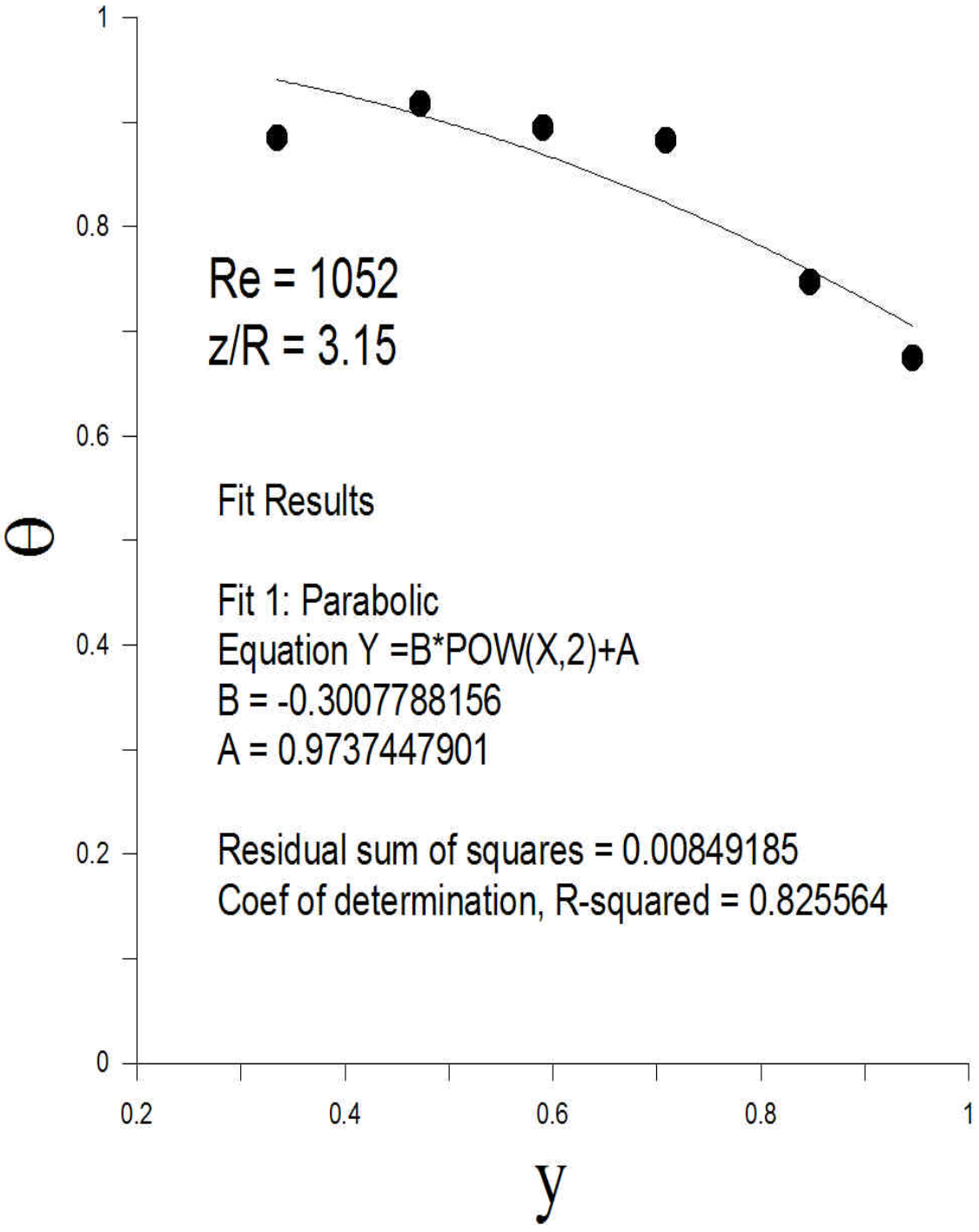

First Height Parabolic Fit for Monoliths

In the 2inch Column

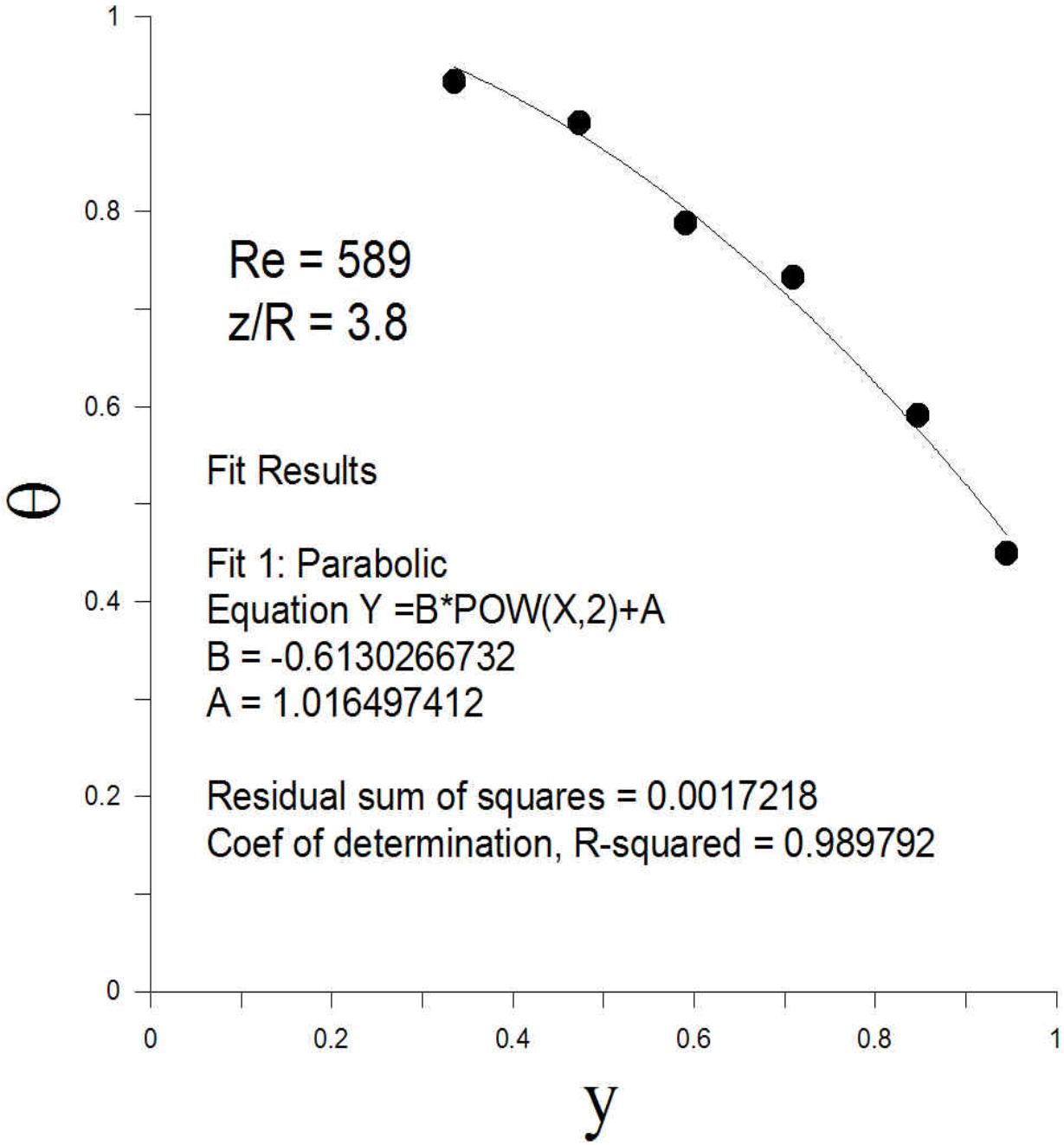

Appendix C: θ vs. y by Reynolds Number

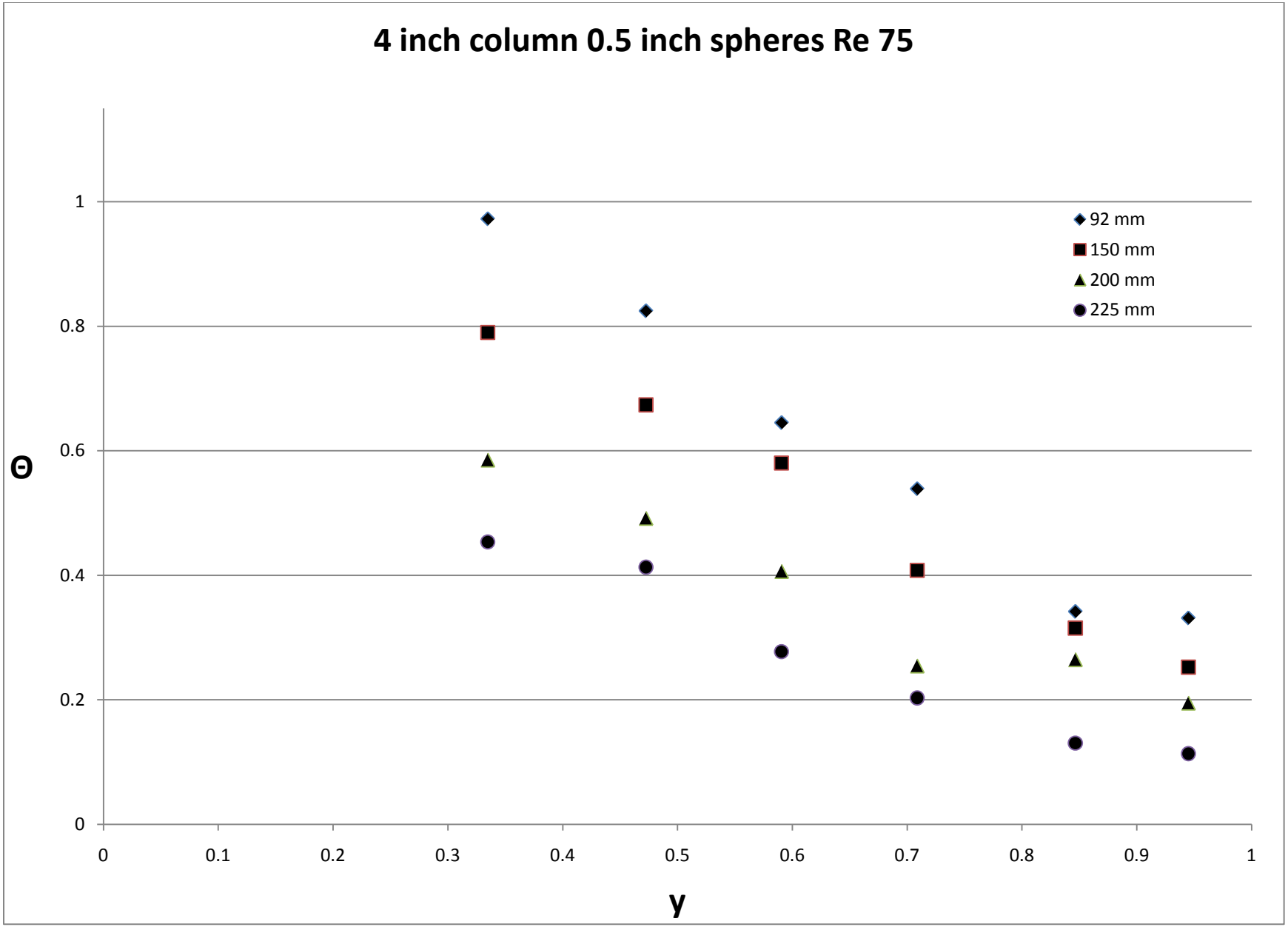
4 inch column 0.5 inch spheres Re 75
92 mm
150 mm
200 mm
225 mm
Θ
y
0
0.2
0.4
0.6
0.8
1
0
0.1
0.2
0.3
0.4
0.5
0.6
0.7
0.8
0.9
1

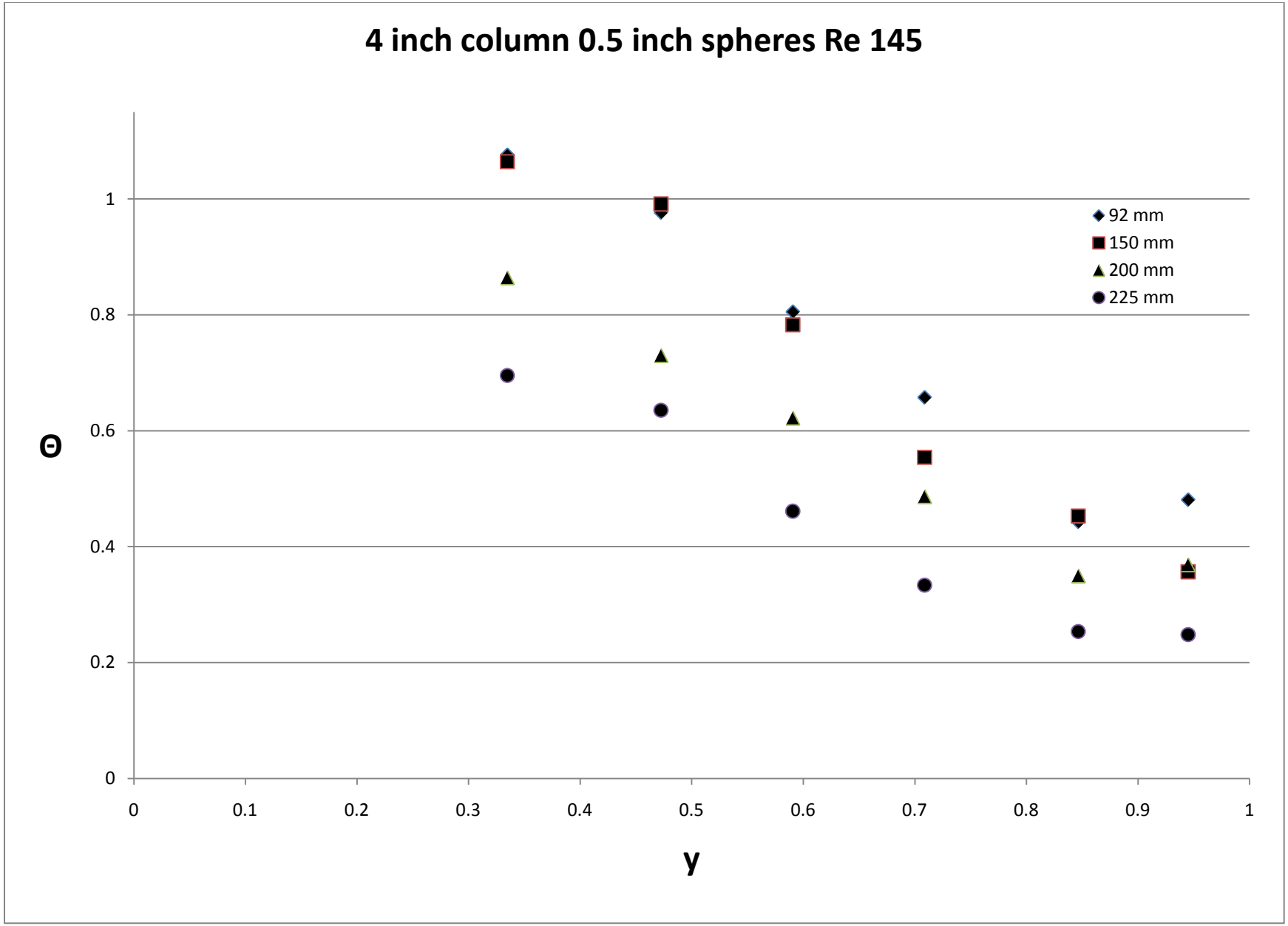
4 inch column 0.5 inch spheres Re 145
Θ
y
92 mm
150 mm
200 mm
225 mm
0
0.2
0.4
0.6
0.8
1
0
0.1
0.2
0.3
0.4
0.5
0.6
0.7
0.8
0.9
1

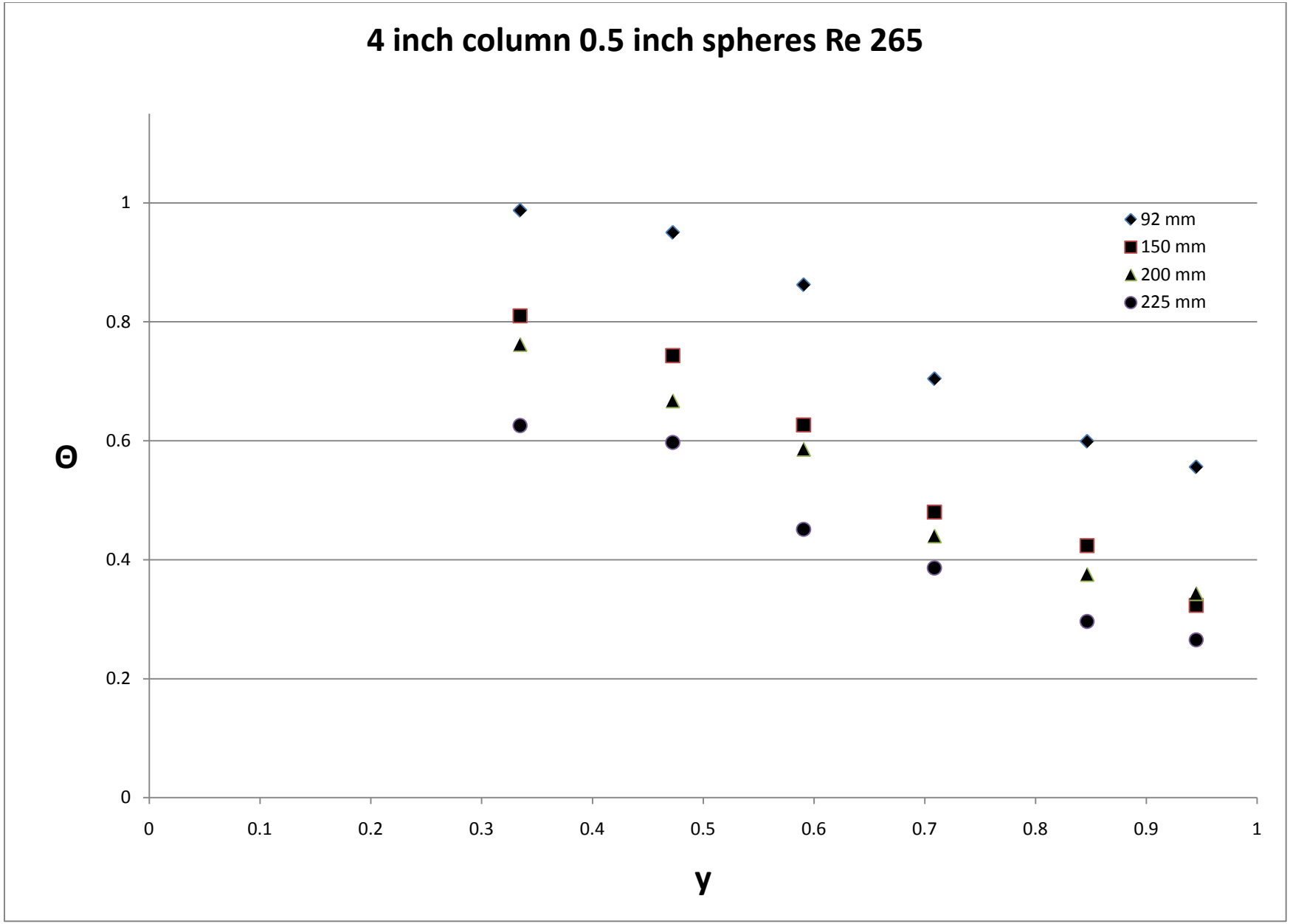
4 inch column 0.5 inch spheres Re 265
92 mm
150 mm
200 mm
225 mm
Θ
y
0
0.2
0.4
0.6
0.8
1
0
0.1
0.2
0.3
0.4
0.5
0.6
0.7
0.8
0.9
1

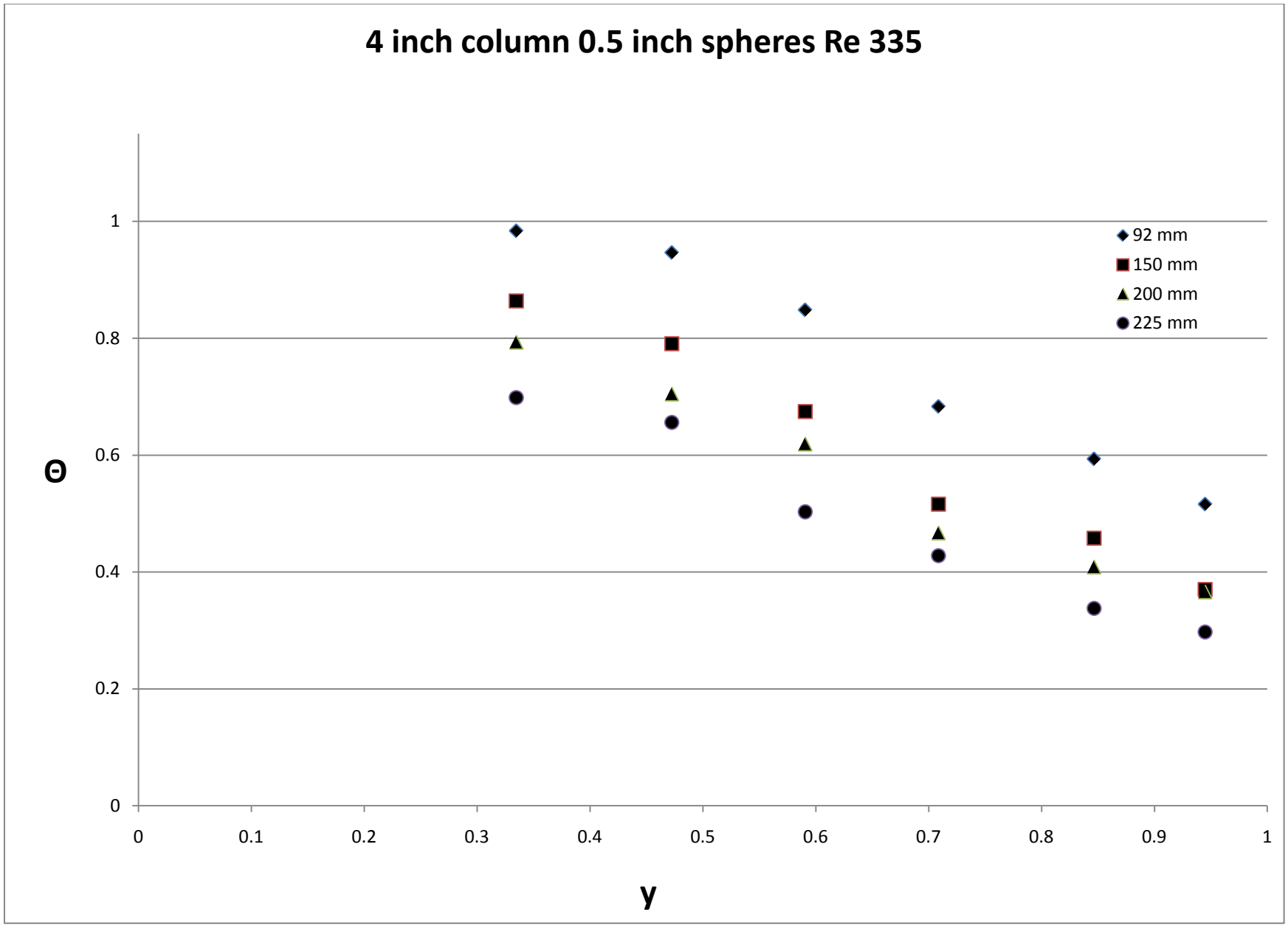
4 inch column 0.5 inch spheres Re 335
Θ
y
92 mm
150 mm
200 mm
225 mm
0
0.2
0.4
0.6
0.8
1
0
0.1
0.2
0.3
0.4
0.5
0.6
0.7
0.8
0.9
1

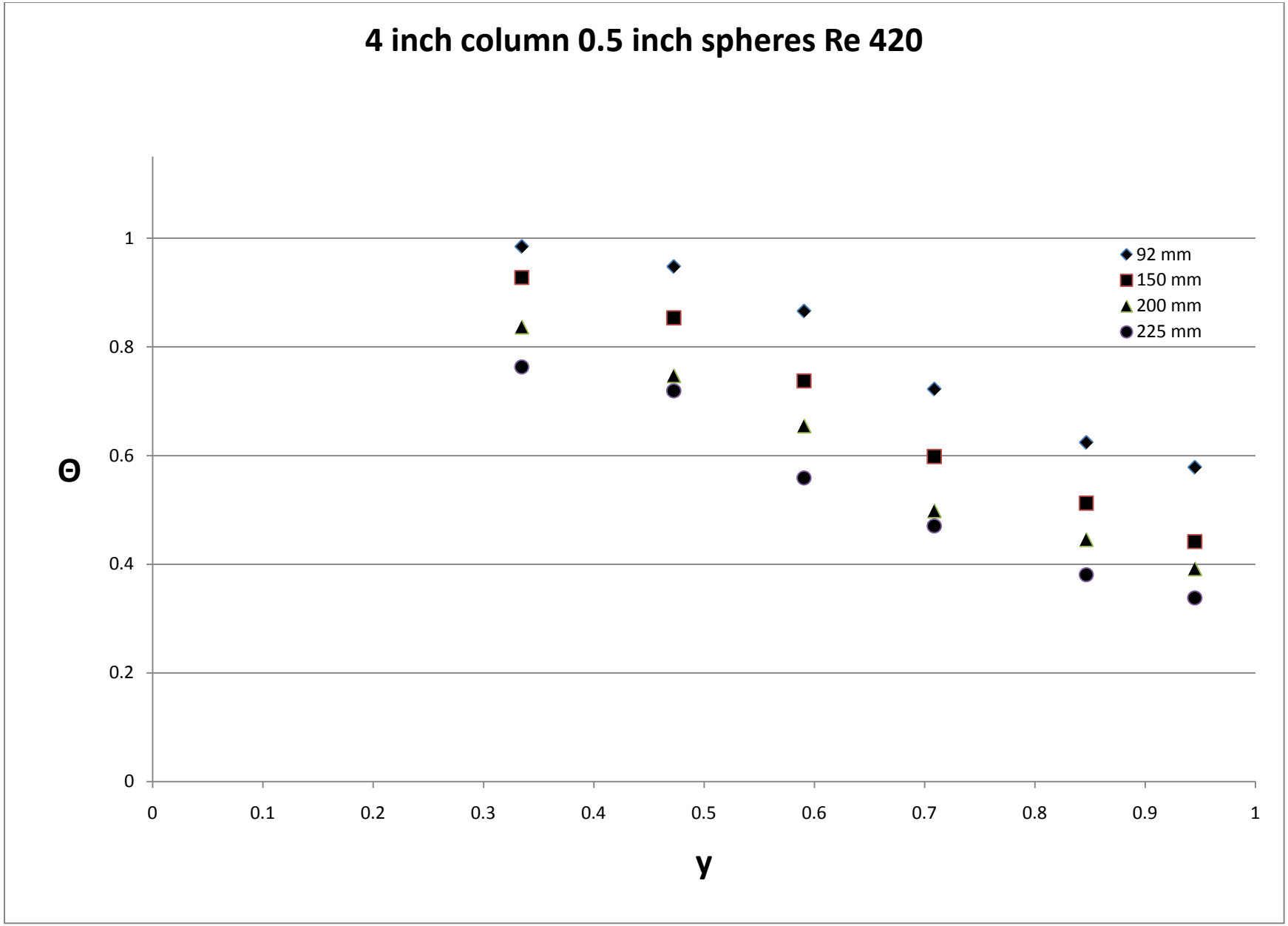
4 inch column 0.5 inch spheres Re 420
Θ
y
92 mm
150 mm
200 mm
225 mm
0
0.2
0.4
0.6
0.8
1
0
0.1
0.2
0.3
0.4
0.5
0.6
0.7
0.8
0.9
1

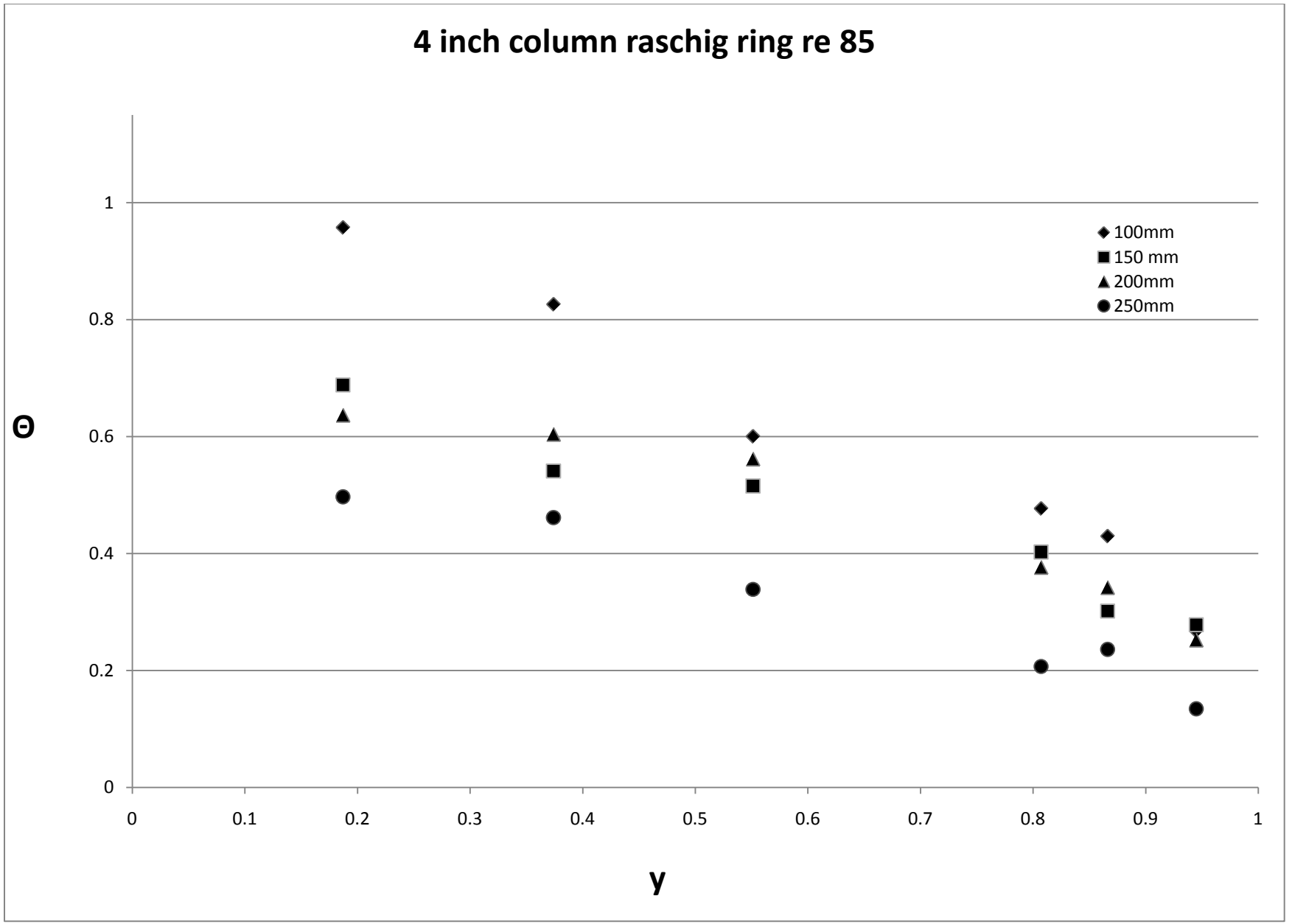
4 inch column raschig ring re 85
Θ
y
100mm
150 mm
200mm
250mm
0
0.2
0.4
0.6
0.8
1
0
0.1
0.2
0.3
0.4
0.5
0.6
0.7
0.8
0.9
1

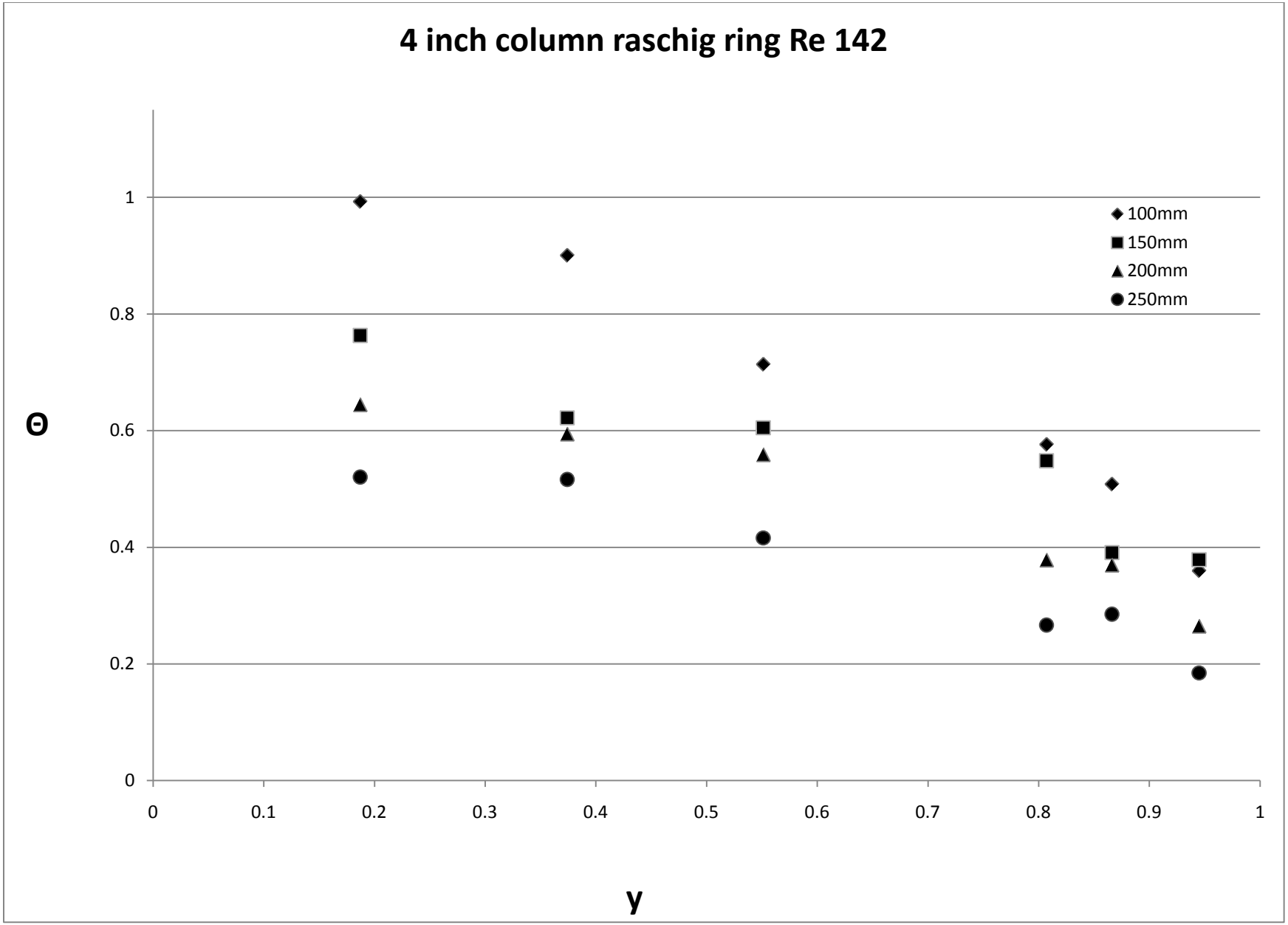
4 inch column raschig ring Re 142
Θ
y
100mm
150mm
200mm
250mm
0
0.2
0.4
0.6
0.8
1
0
0.1
0.2
0.3
0.4
0.5
0.6
0.7
0.8
0.9
1

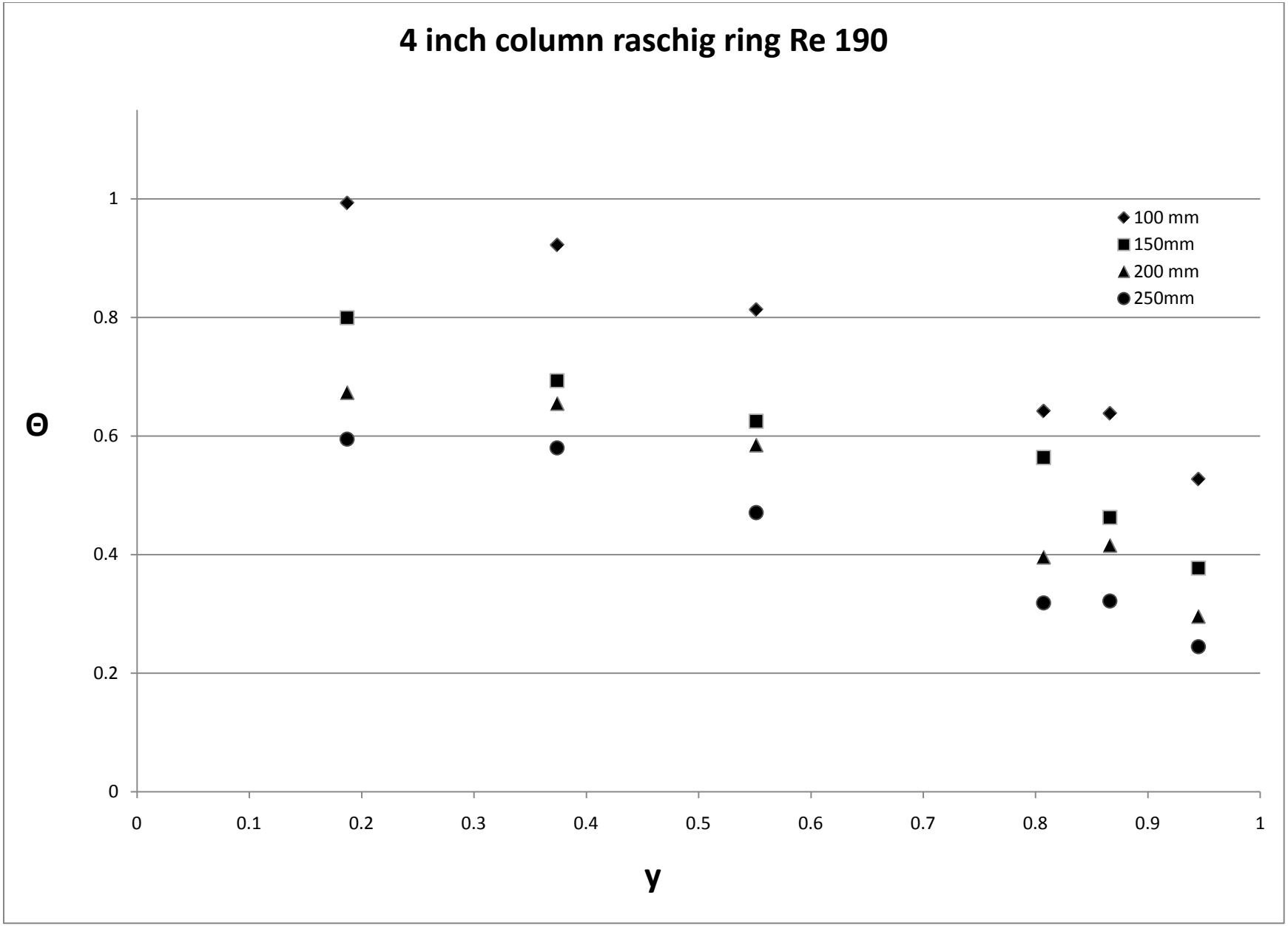
4 inch column raschig ring Re 190
Θ
y
100 mm
150mm
200 mm
250mm
0
0.2
0.4
0.6
0.8
1
0
0.1
0.2
0.3
0.4
0.5
0.6
0.7
0.8
0.9
1

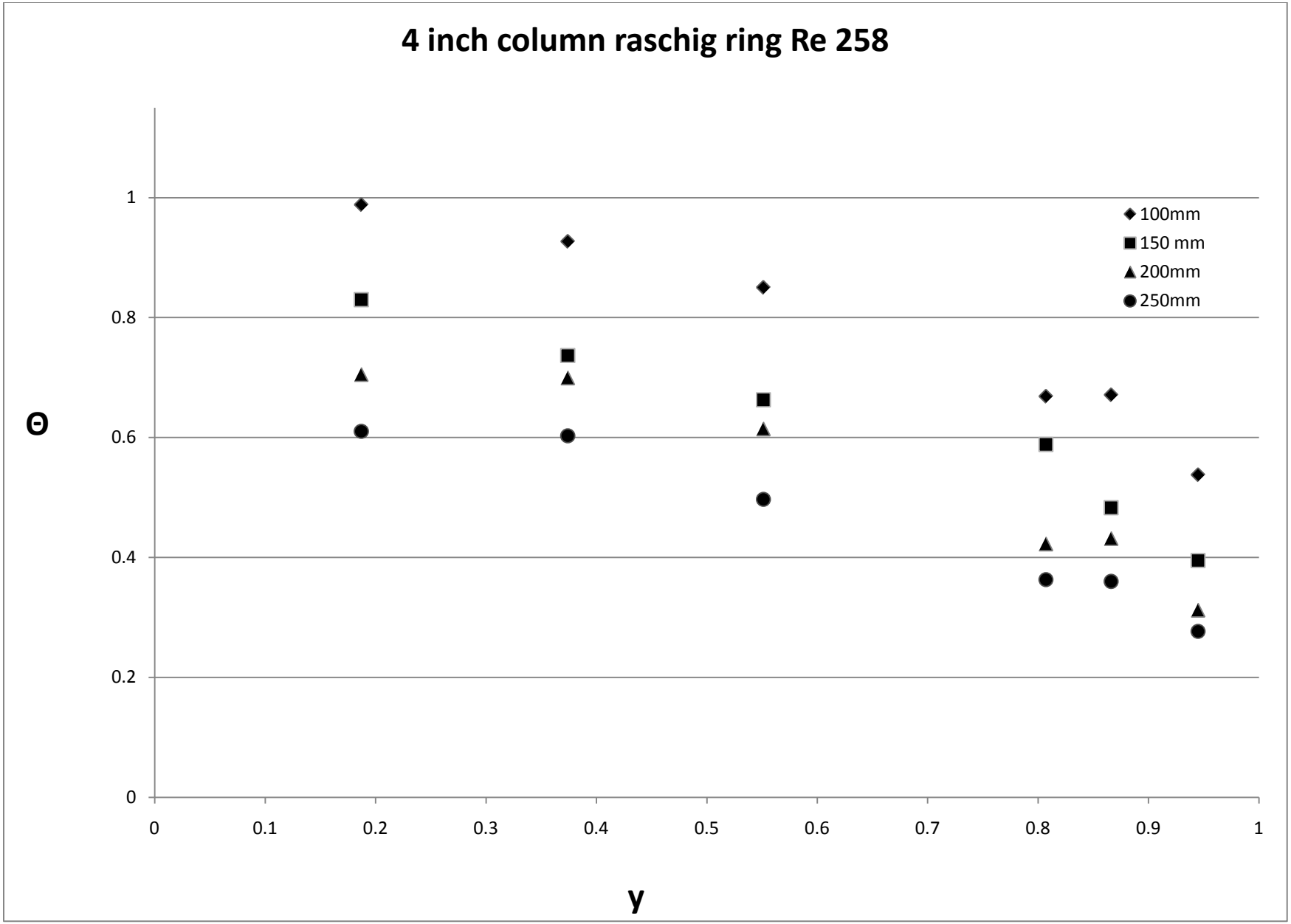
4 inch column raschig ring Re 258
Θ
y
100mm
150 mm
200mm
250mm
0
0.2
0.4
0.6
0.8
1
0
0.1
0.2
0.3
0.4
0.5
0.6
0.7
0.8
0.9
1

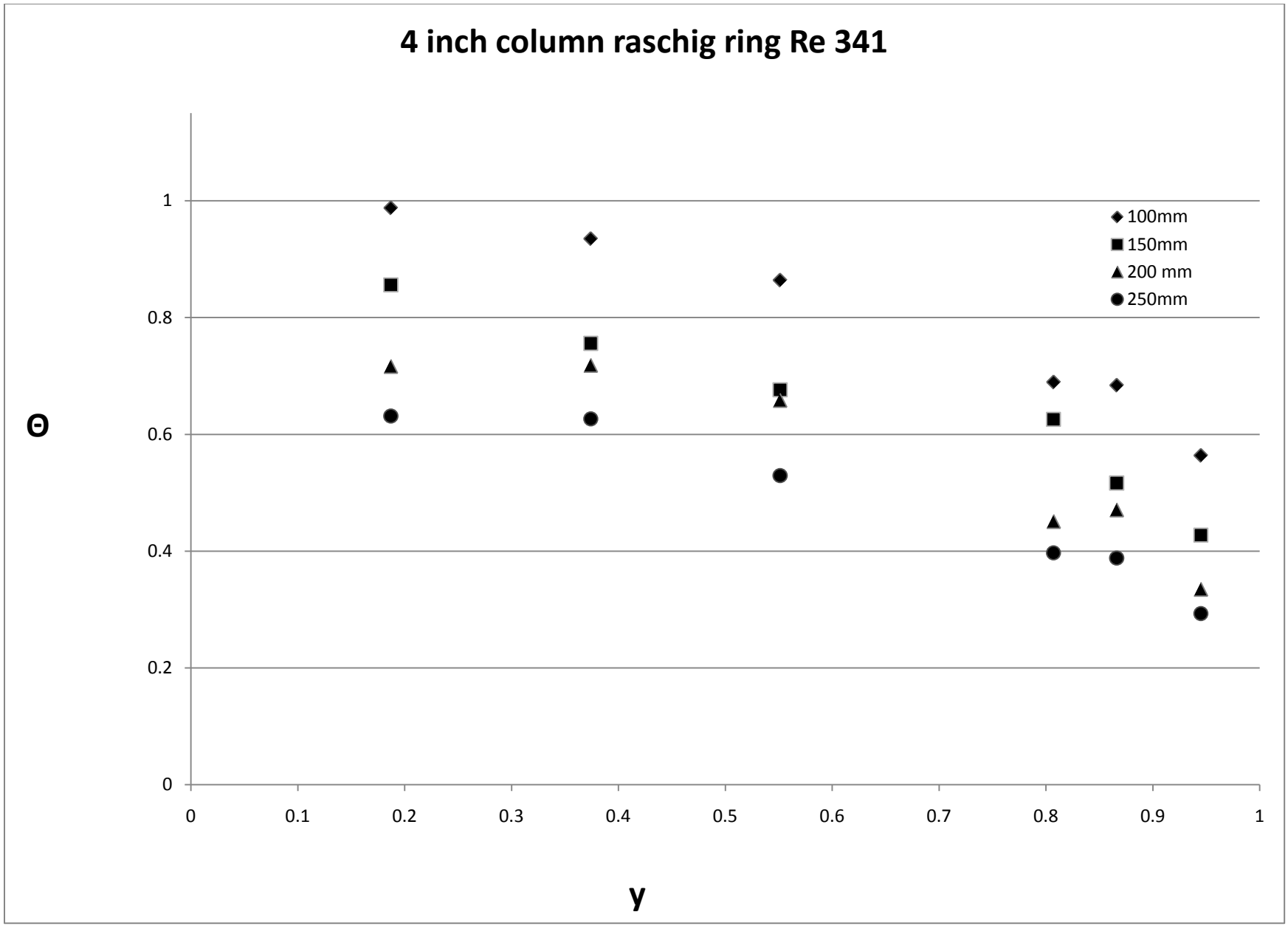
4 inch column raschig ring Re 341
Θ
y
100mm
150mm
200 mm
250mm
0
0.2
0.4
0.6
0.8
1
0
0.1
0.2
0.3
0.4
0.5
0.6
0.7
0.8
0.9
1

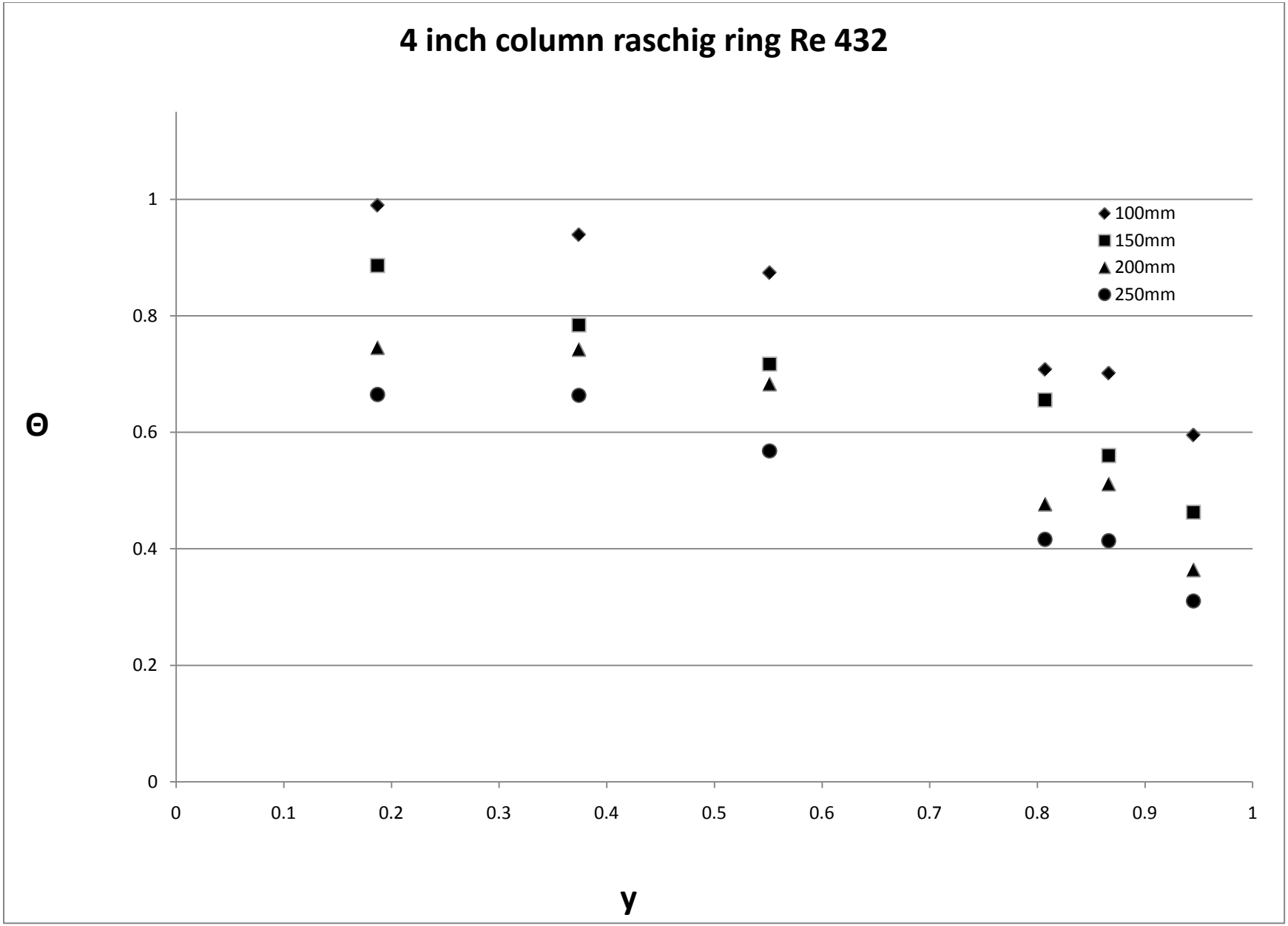
4 inch column raschig ring Re 432
Θ
y
100mm
150mm
200mm
250mm
0
0.2
0.4
0.6
0.8
1
0
0.1
0.2
0.3
0.4
0.5
0.6
0.7
0.8
0.9
1

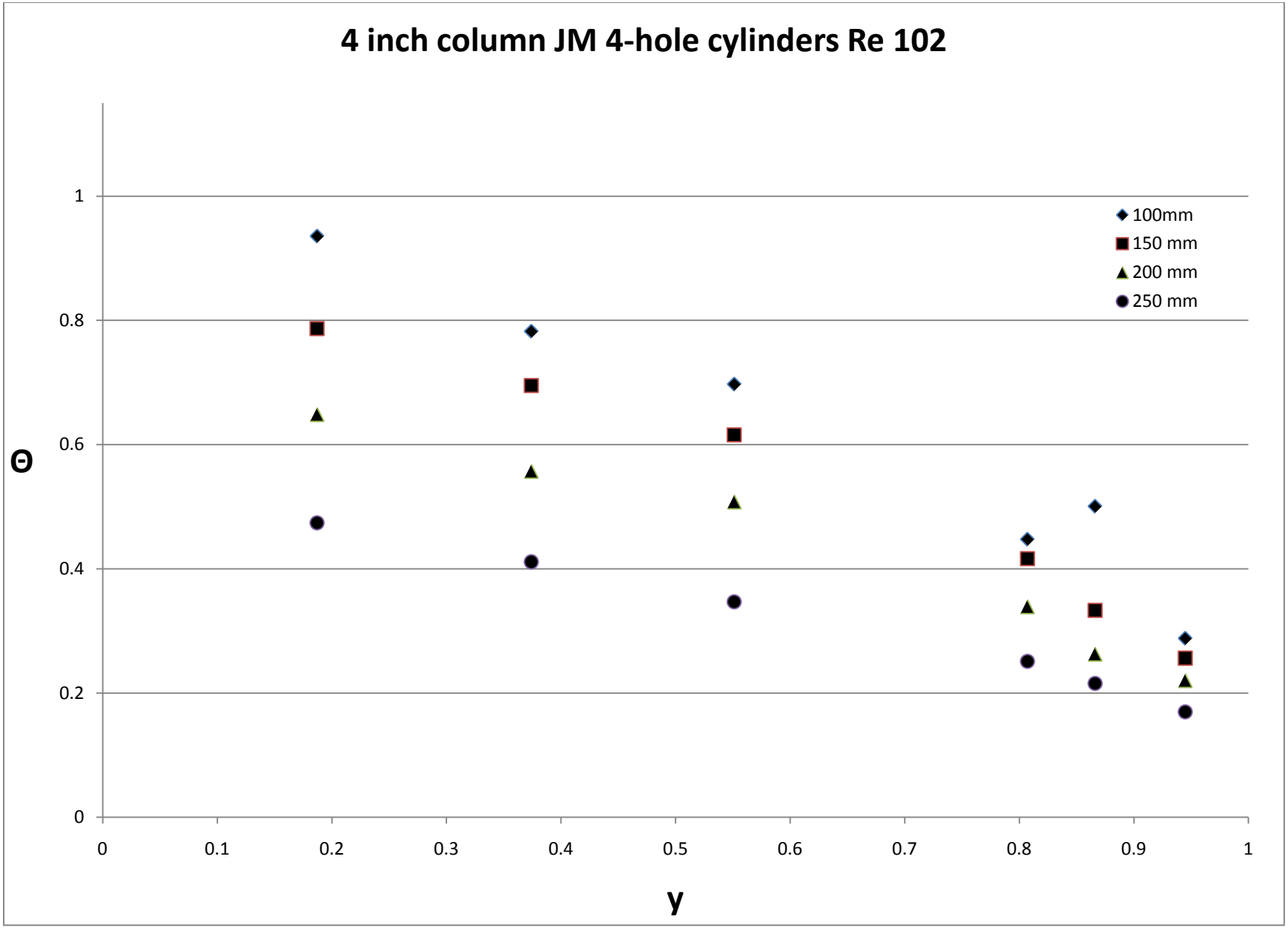
4 inch column JM 4-hole cylinders Re 102
100mm
150 mm
200 mm
250 mm
Θ
y
0
0.2
0.4
0.6
0.8
1
0
0.1
0.2
0.3
0.4
0.5
0.6
0.7
0.8
0.9
1

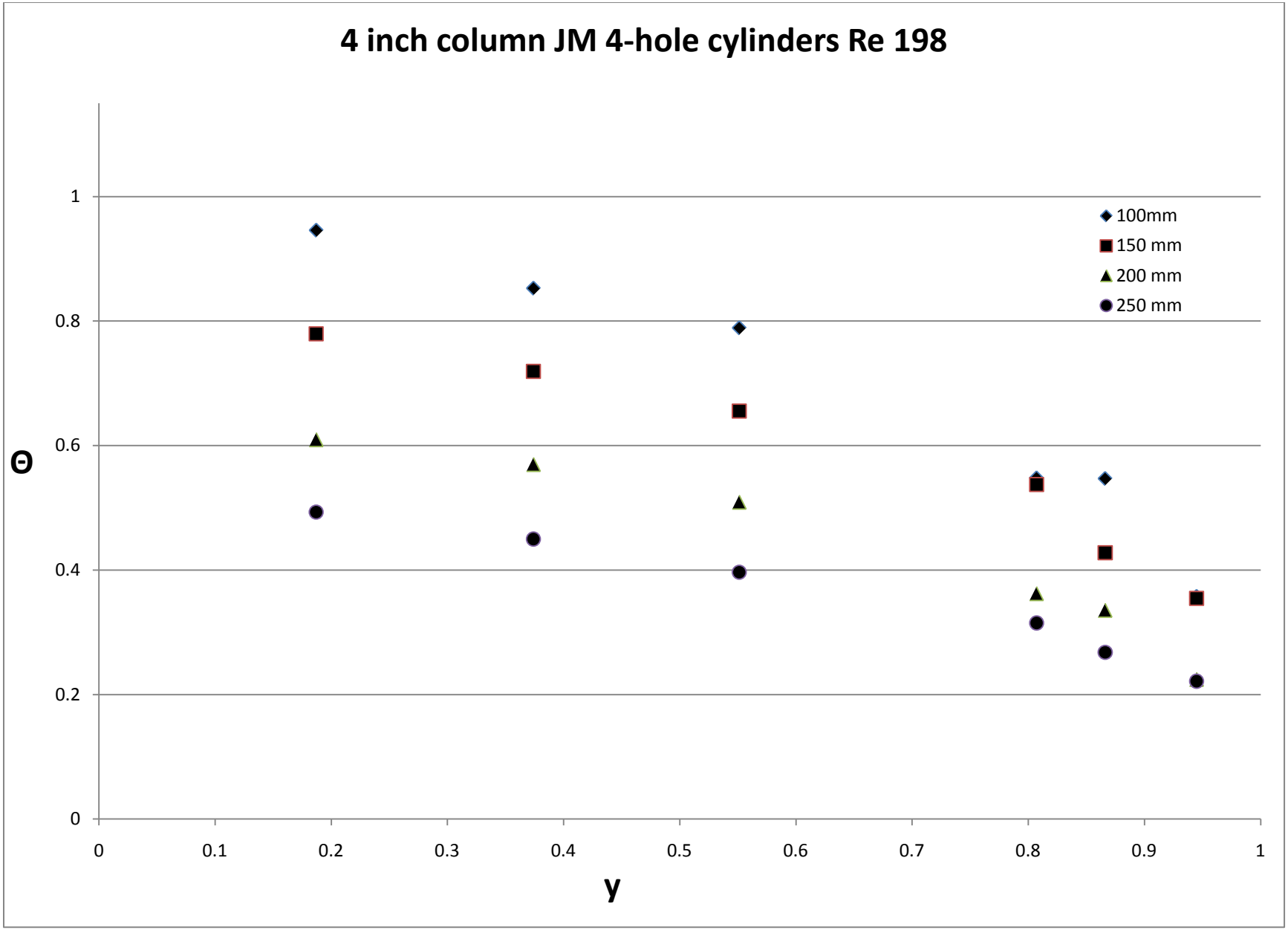
4 inch column JM 4-hole cylinders Re 198
Θ
y
100mm
150 mm
200 mm
250 mm
0
0.2
0.4
0.6
0.8
1
0
0.1
0.2
0.3
0.4
0.5
0.6
0.7
0.8
0.9
1

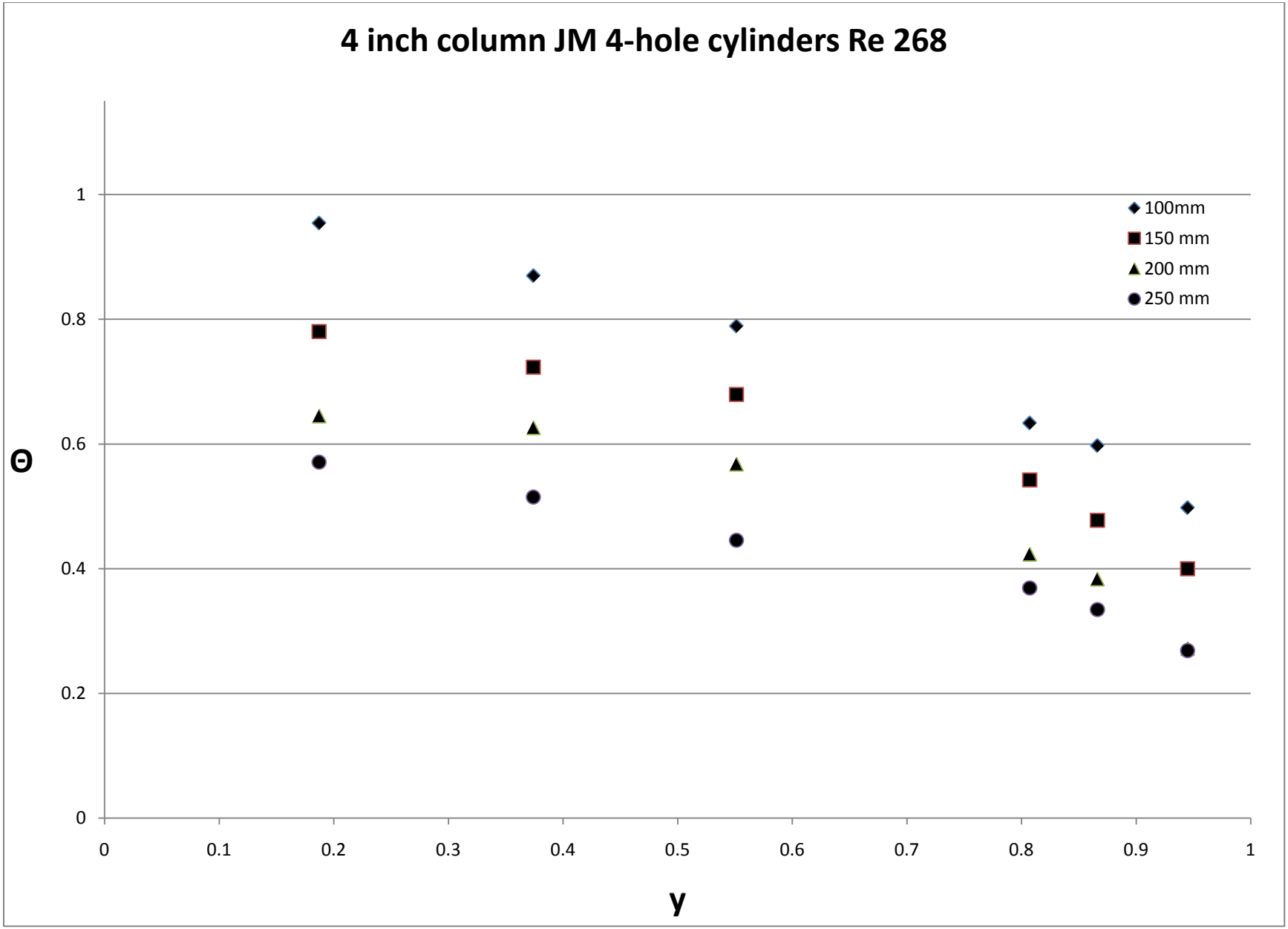
4 inch column JM 4-hole cylinders Re 268
Θ
y
100mm
150 mm
200 mm
250 mm
0
0.2
0.4
0.6
0.8
1
0
0.1
0.2
0.3
0.4
0.5
0.6
0.7
0.8
0.9
1

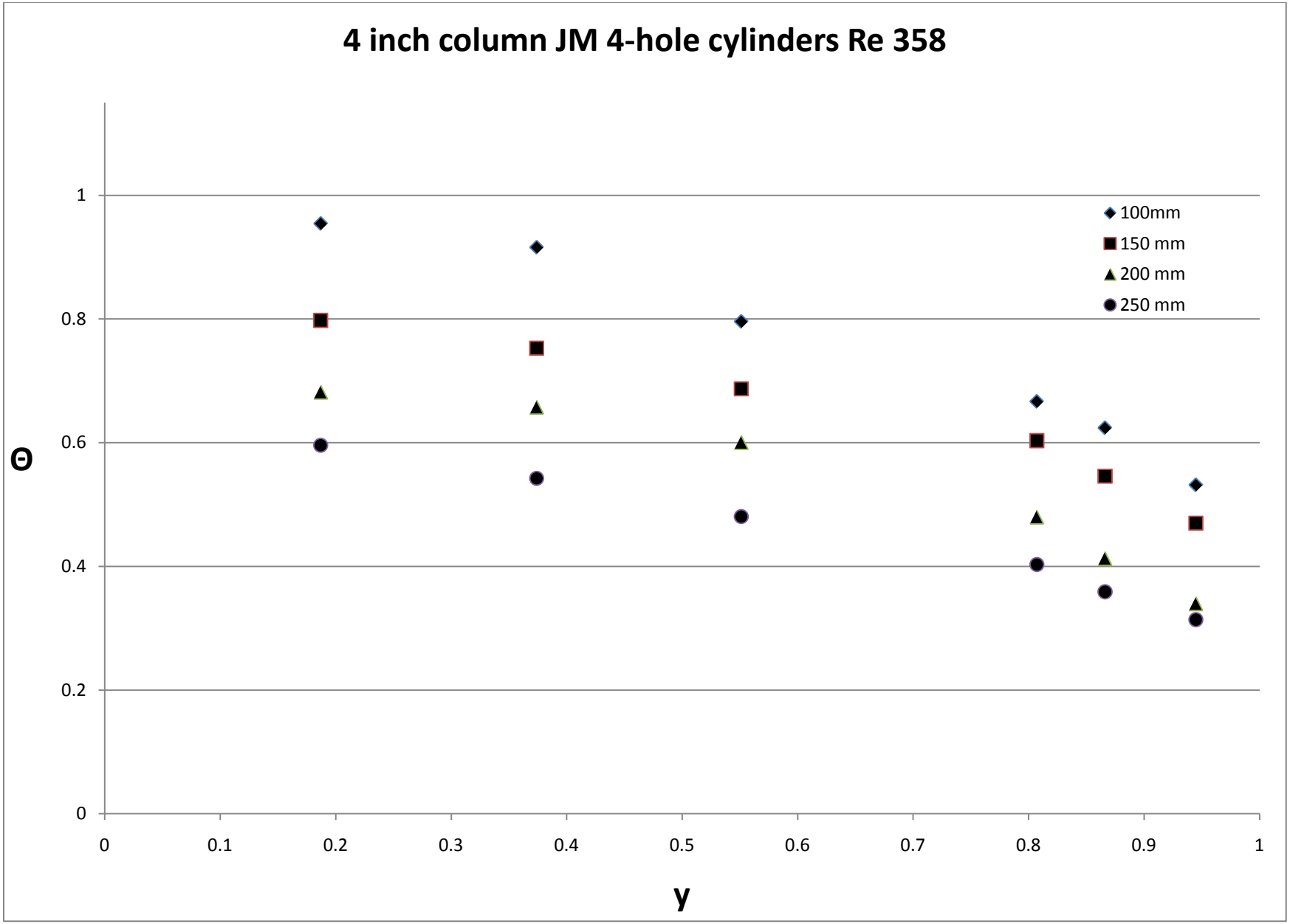
4 inch column JM 4-hole cylinders Re 358
Θ
y
100mm
150 mm
200 mm
250 mm
0
0.2
0.4
0.6
0.8
1
0
0.1
0.2
0.3
0.4
0.5
0.6
0.7
0.8
0.9
1

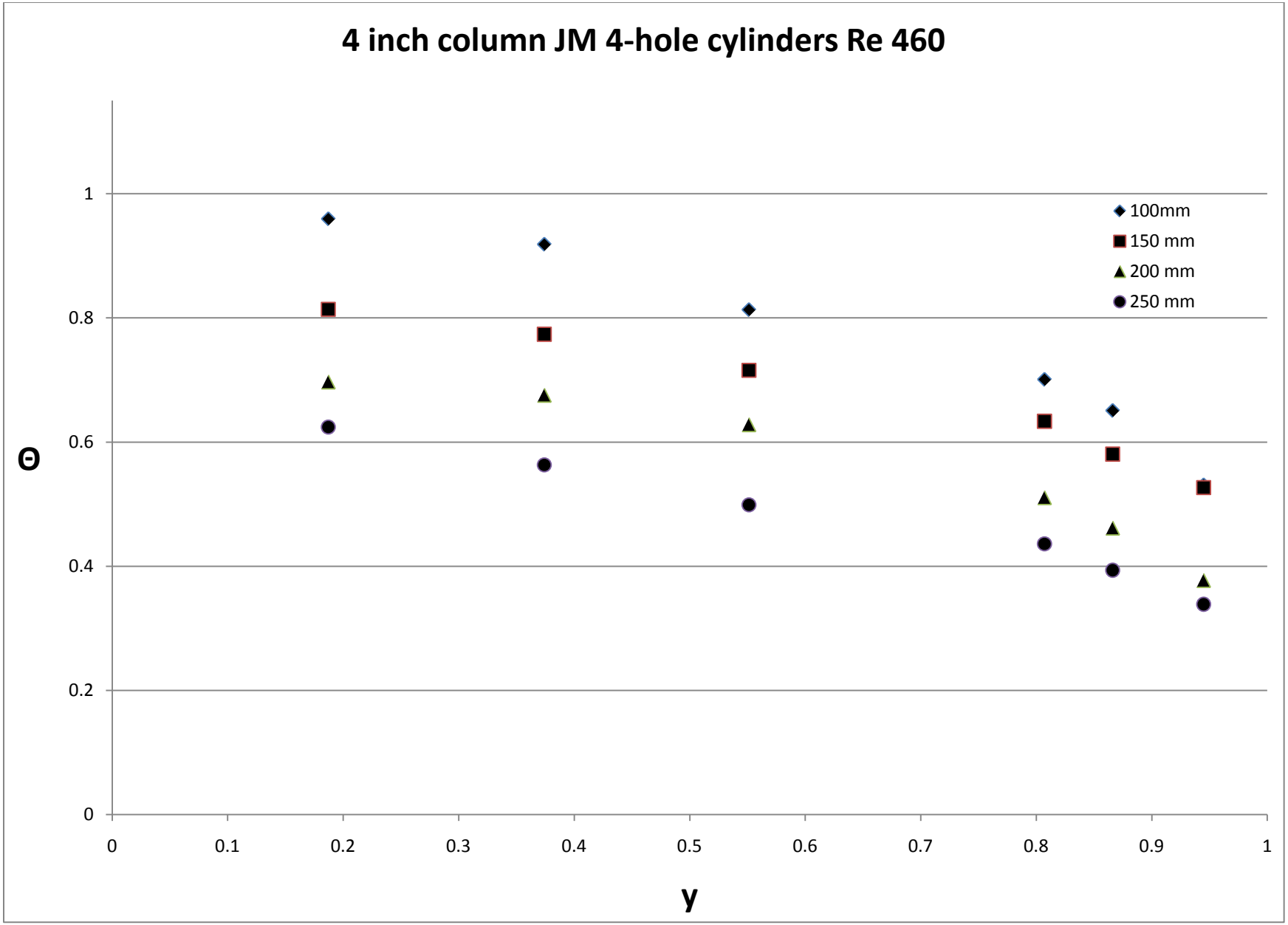
4 inch column JM 4-hole cylinders Re 460
100mm
150 mm
200 mm
250 mm
Θ
y
0
0.2
0.4
0.6
0.8
1
0
0.1
0.2
0.3
0.4
0.5
0.6
0.7
0.8
0.9
1

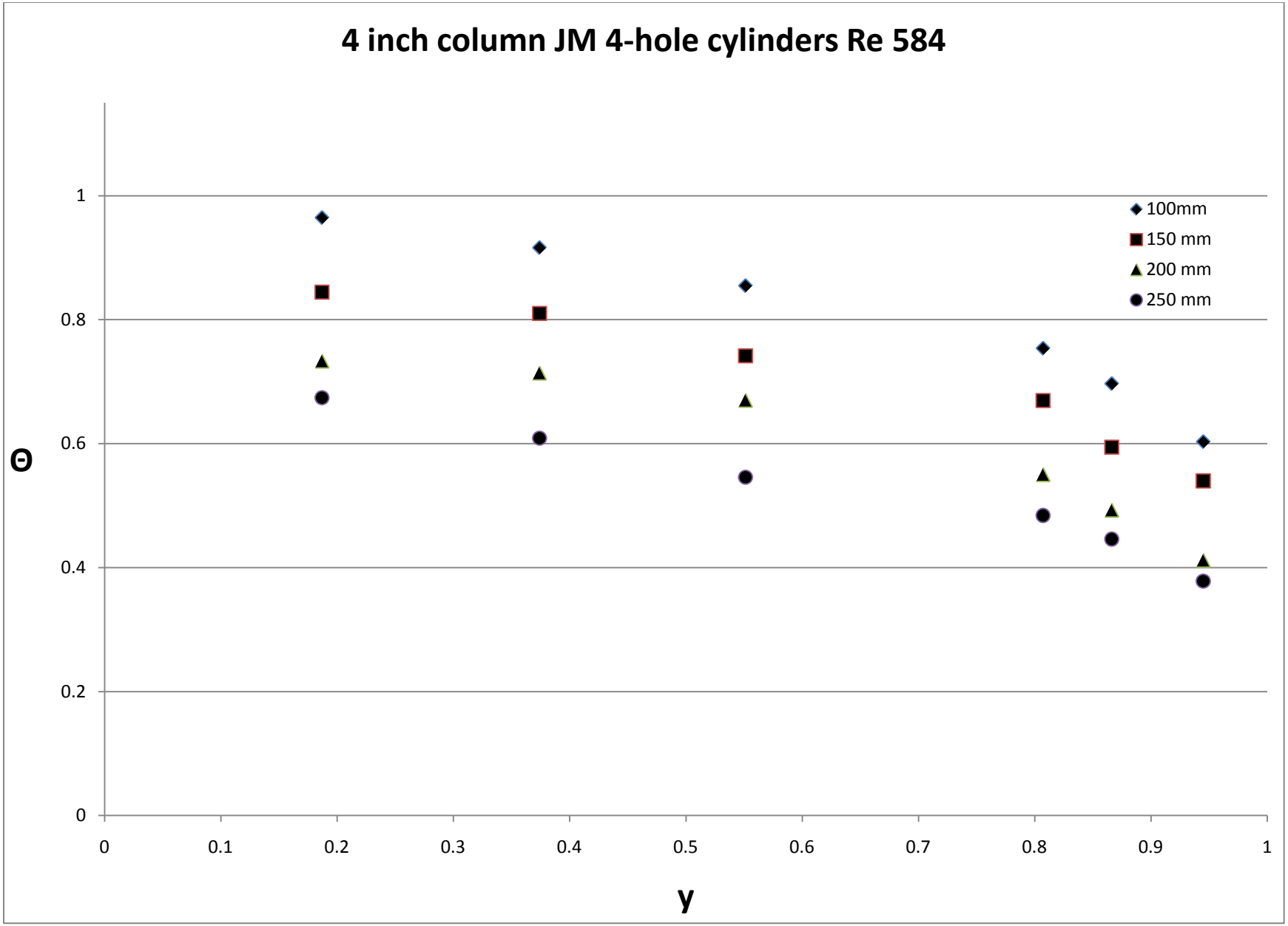
4 inch column JM 4-hole cylinders Re 584
100mm
150 mm
200 mm
250 mm
Θ
y
0
0.2
0.4
0.6
0.8
1
0
0.1
0.2
0.3
0.4
0.5
0.6
0.7
0.8
0.9
1

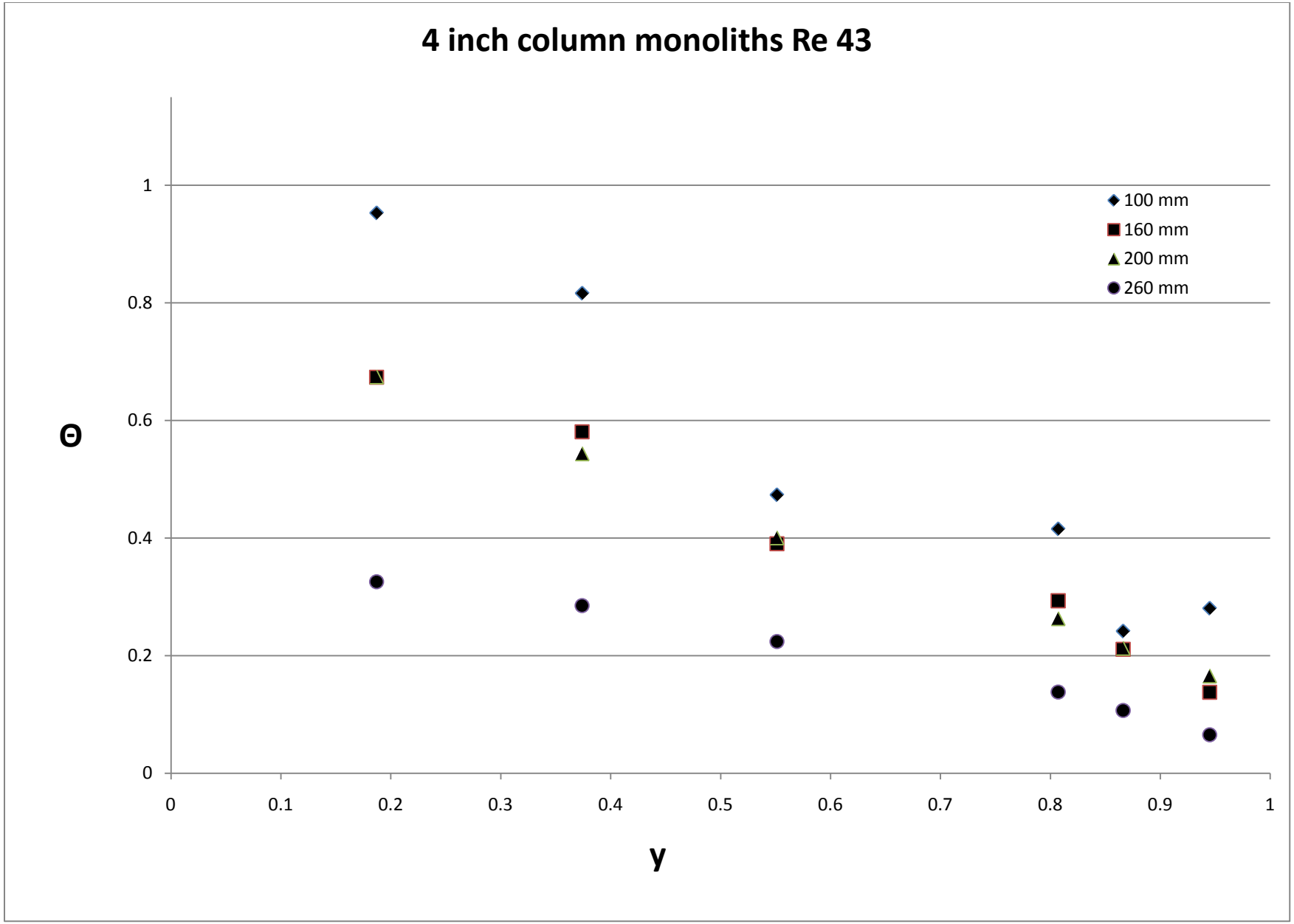
4 inch column monoliths Re 43
Θ
y
100 mm
160 mm
200 mm
260 mm
0
0.2
0.4
0.6
0.8
1
0
0.1
0.2
0.3
0.4
0.5
0.6
0.7
0.8
0.9
1

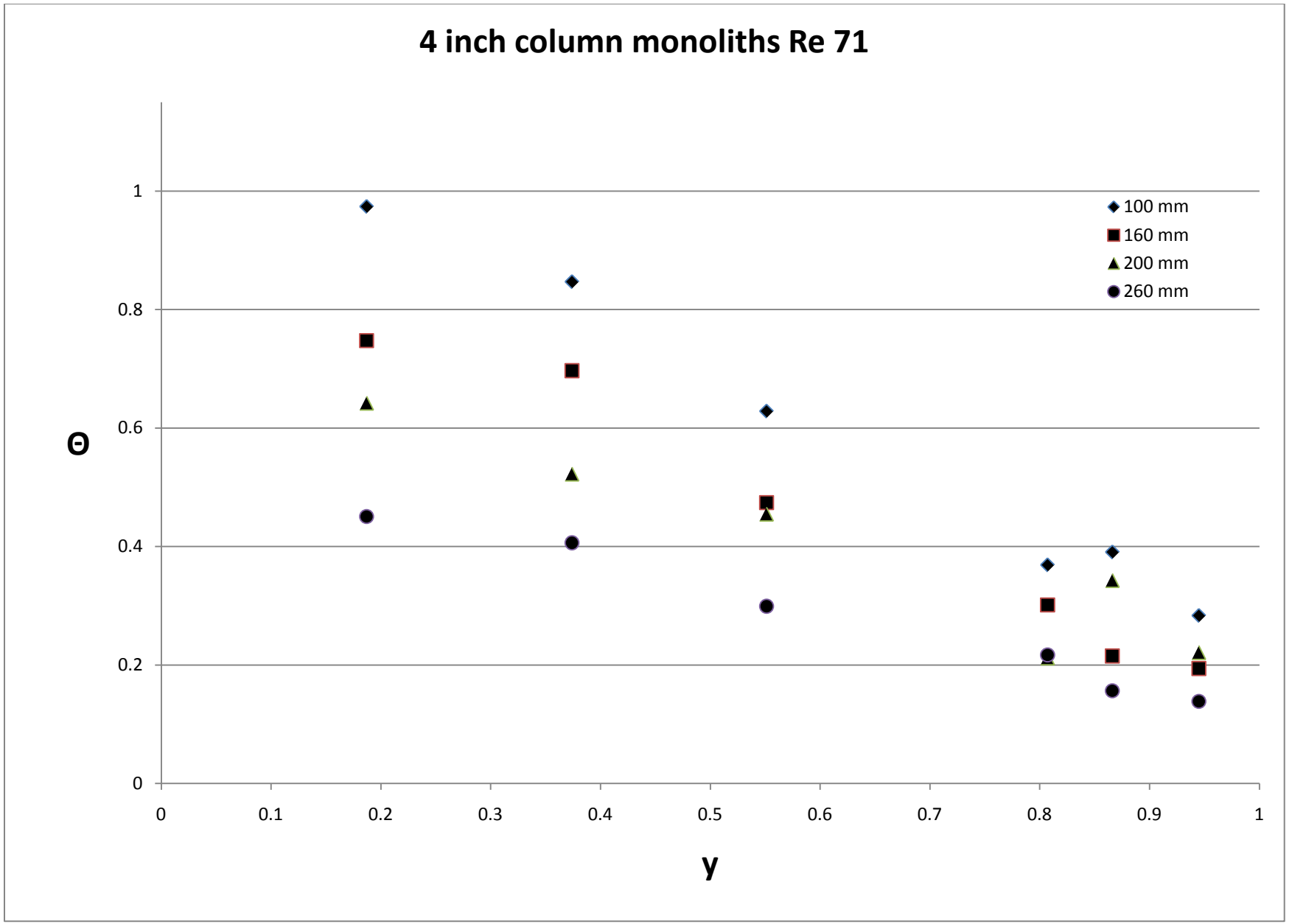
4 inch column monoliths Re 71
Θ
y
100 mm
160 mm
200 mm
260 mm
0
0.2
0.4
0.6
0.8
1
0
0.1
0.2
0.3
0.4
0.5
0.6
0.7
0.8
0.9
1

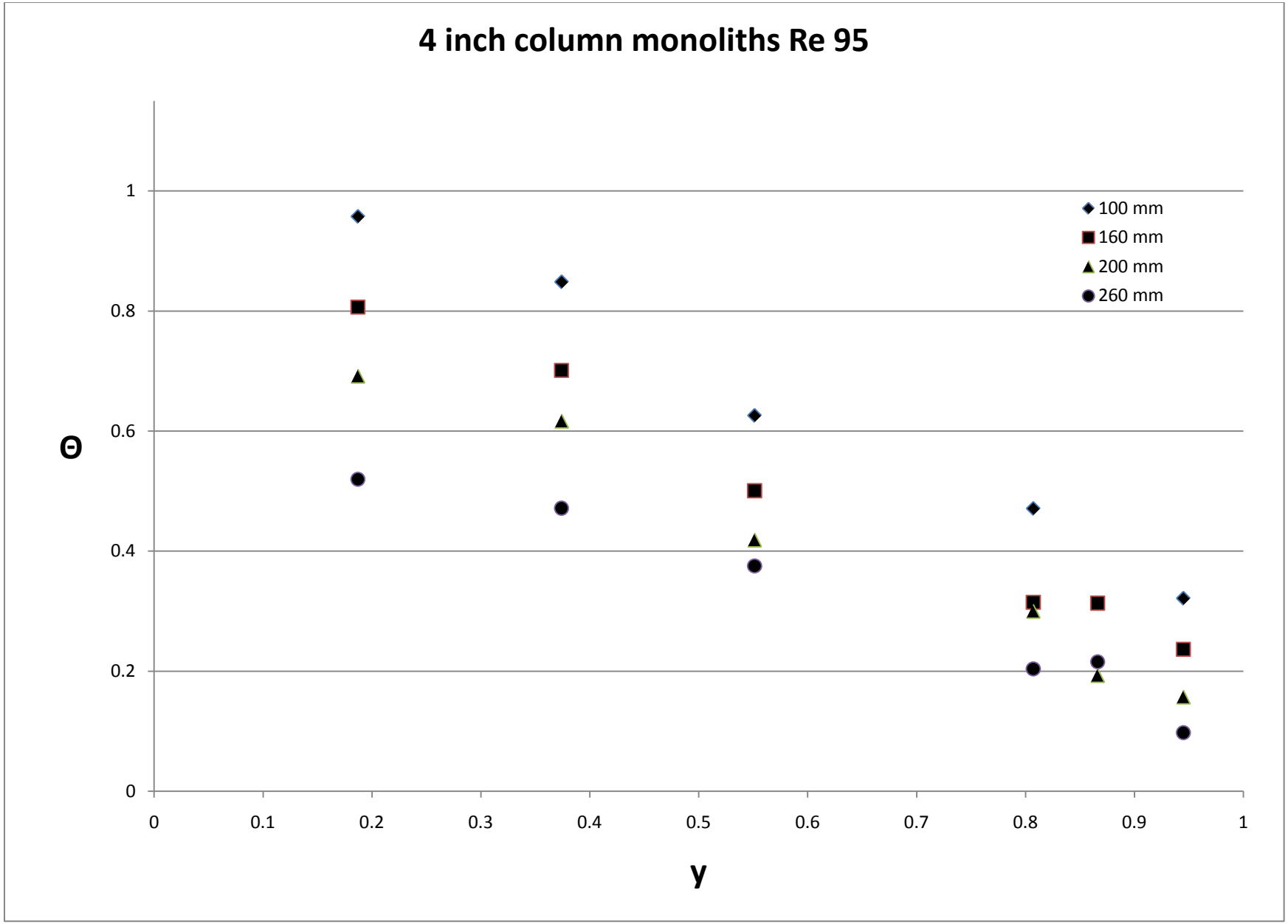
4 inch column monoliths Re 95
Θ
y
100 mm
160 mm
200 mm
260 mm
0
0.2
0.4
0.6
0.8
1
0
0.1
0.2
0.3
0.4
0.5
0.6
0.7
0.8
0.9
1

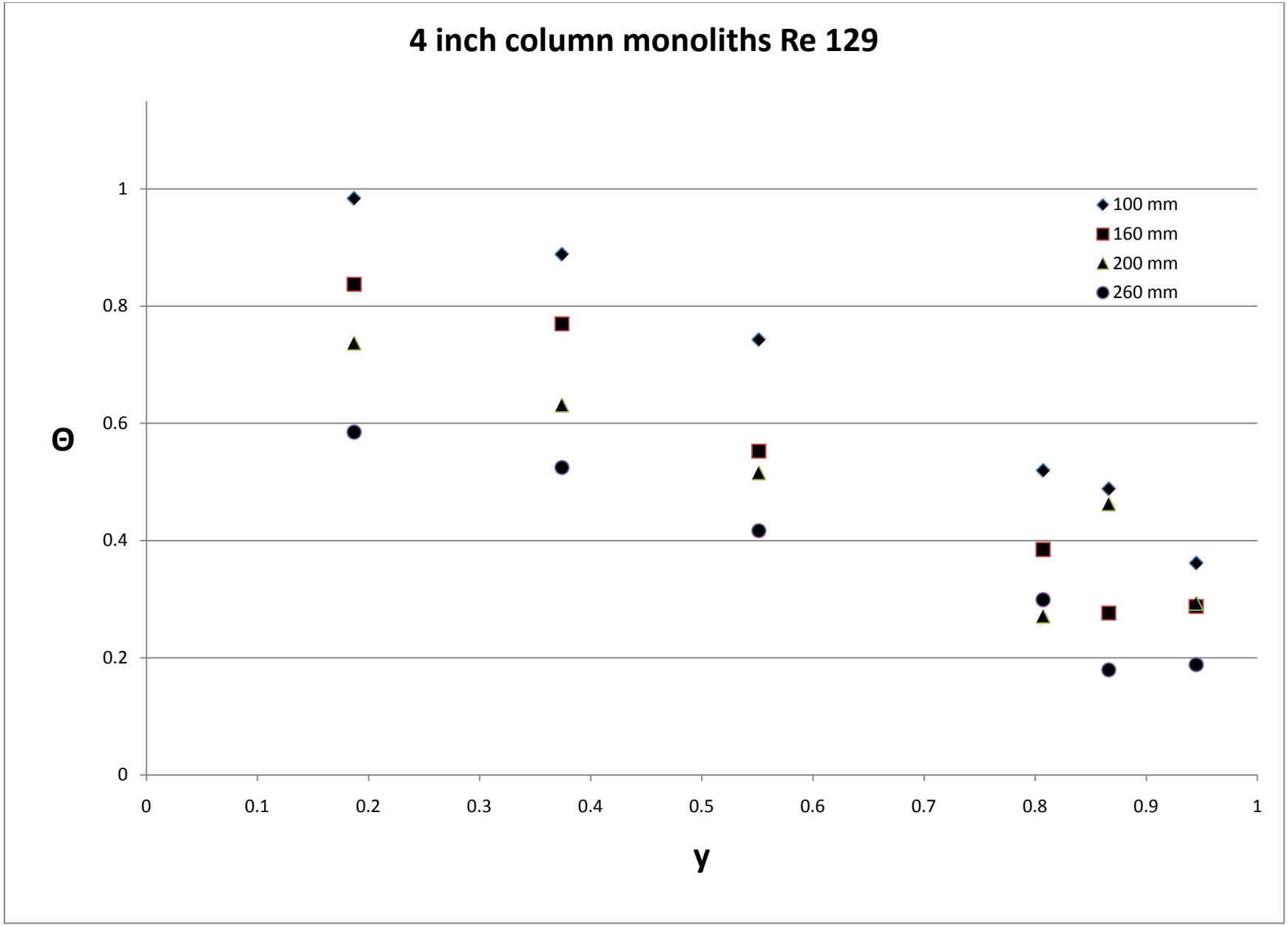
4 inch column monoliths Re 129
Θ
y
100 mm
160 mm
200 mm
260 mm
0
0.2
0.4
0.6
0.8
1
0
0.1
0.2
0.3
0.4
0.5
0.6
0.7
0.8
0.9
1

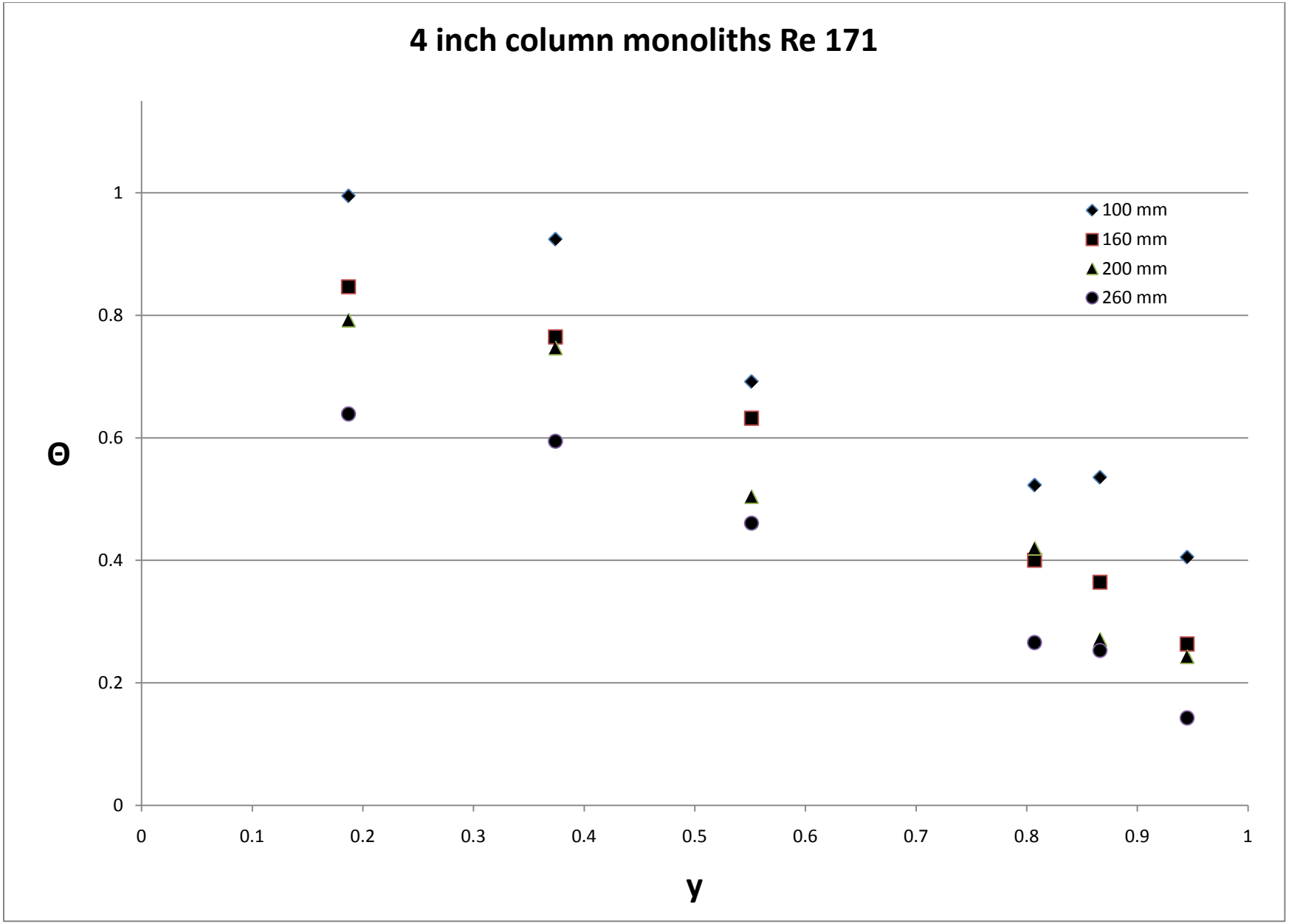
4 inch column monoliths Re 171
Θ
y
100 mm
160 mm
200 mm
260 mm
0
0.2
0.4
0.6
0.8
1
0
0.1
0.2
0.3
0.4
0.5
0.6
0.7
0.8
0.9
1

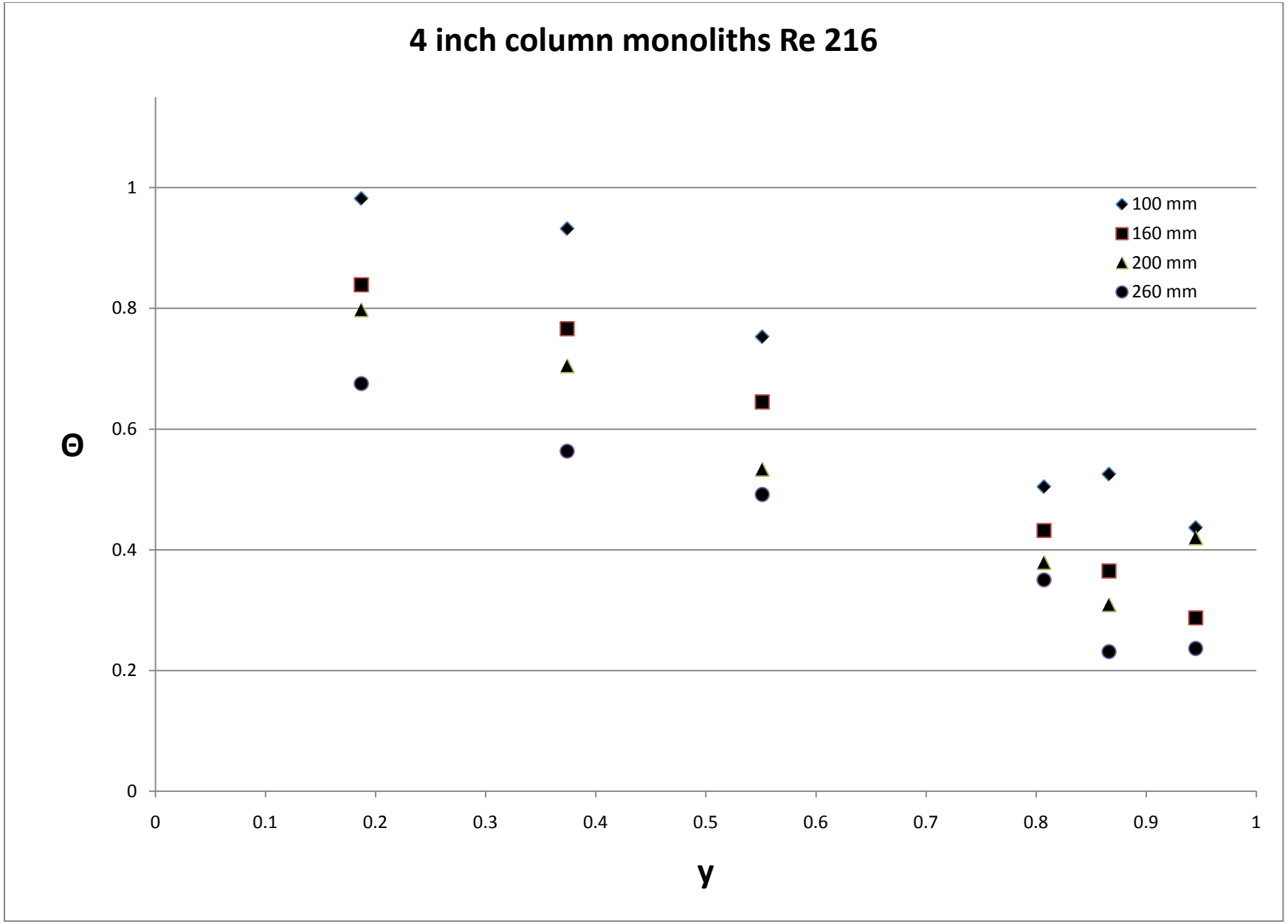
4 inch column monoliths Re 216
Θ
y
100 mm
160 mm
200 mm
260 mm
0
0.2
0.4
0.6
0.8
1
0
0.1
0.2
0.3
0.4
0.5
0.6
0.7
0.8
0.9
1

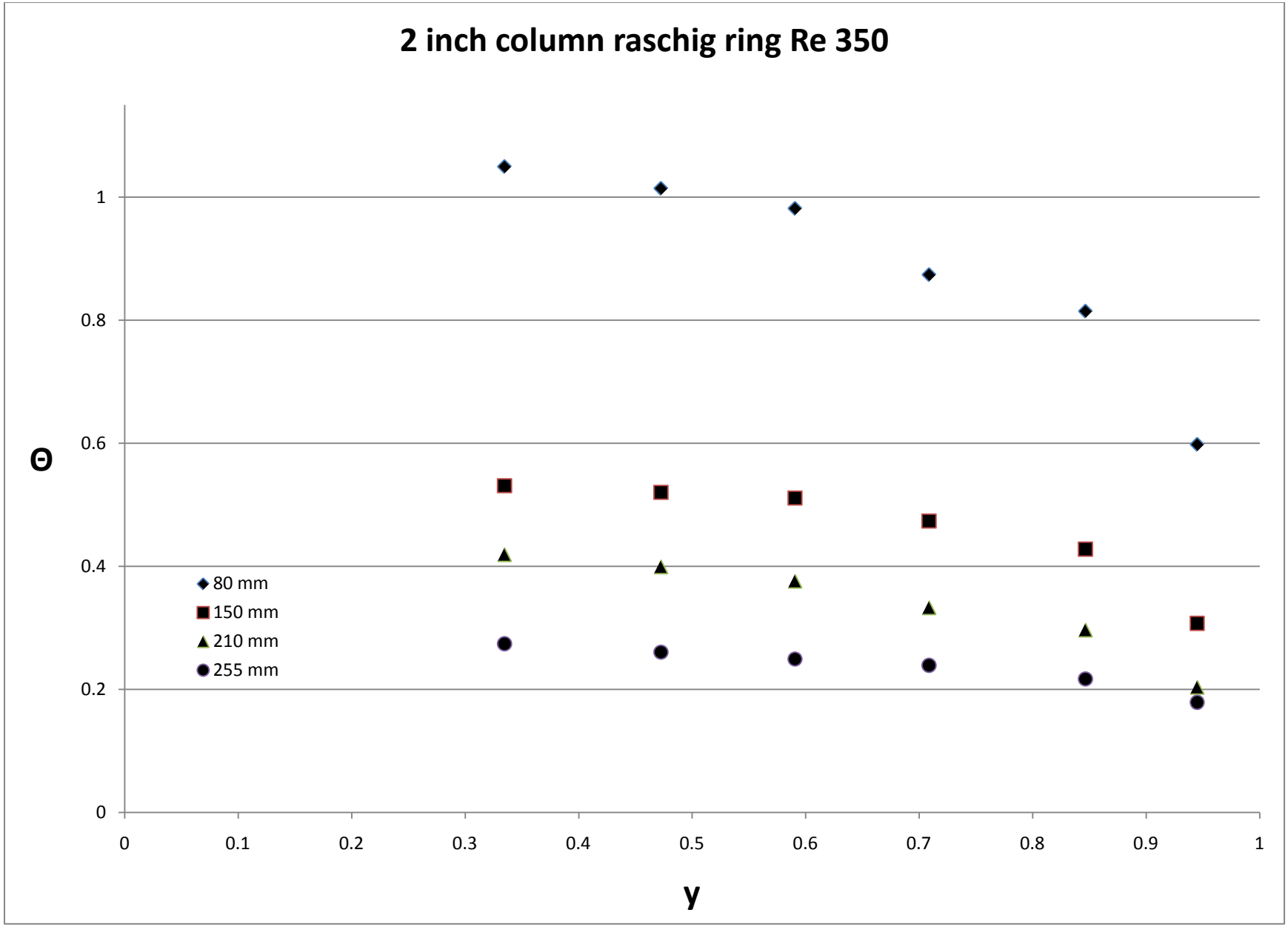
2 inch column raschig ring Re 350
Θ
y
80 mm
150 mm
210 mm
255 mm
0
0.2
0.4
0.6
0.8
1
0
0.1
0.2
0.3
0.4
0.5
0.6
0.7
0.8
0.9
1

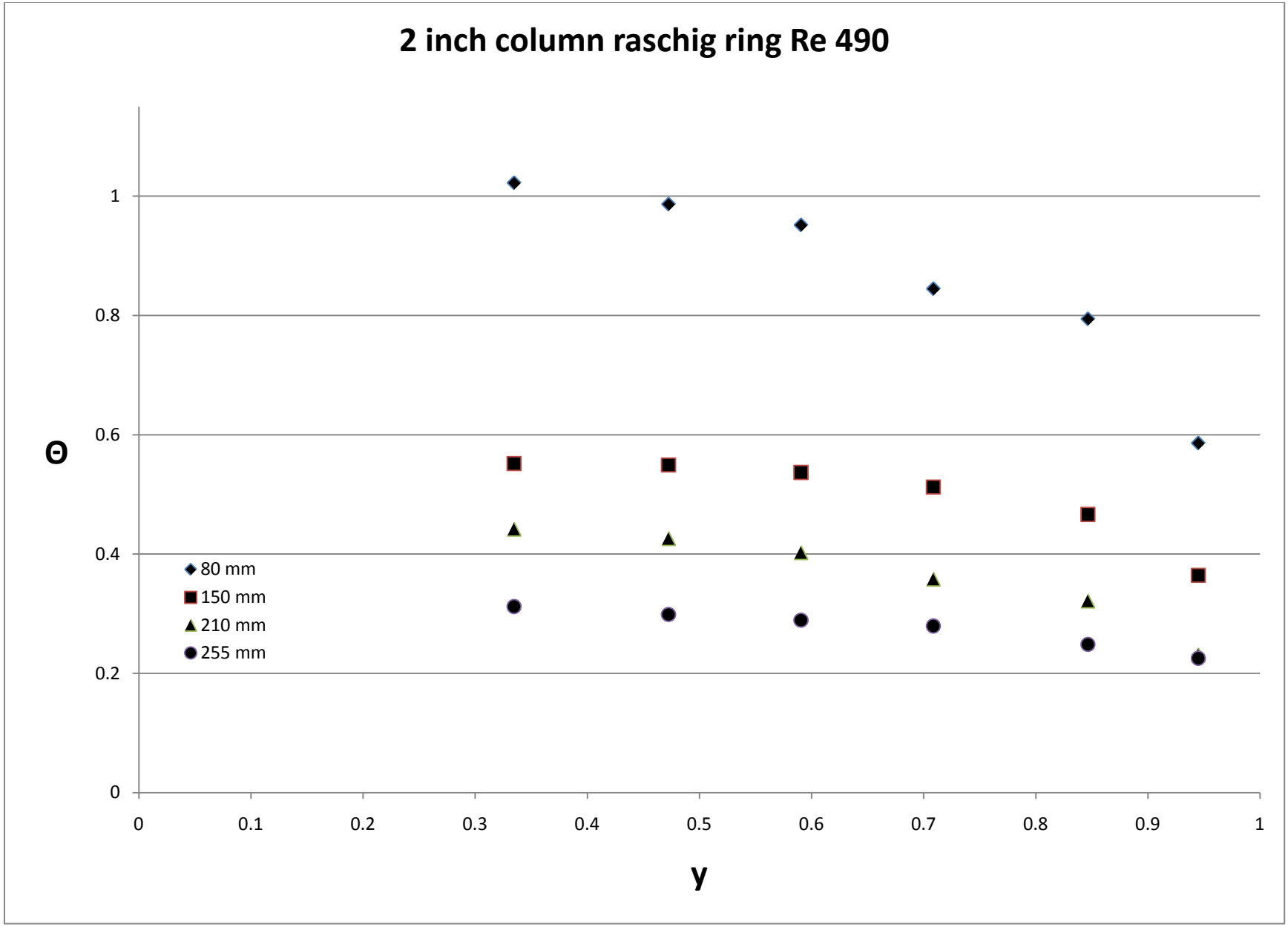
2 inch column raschig ring Re 490
Θ
y
1
0.8
0.6
0.4
0.2
0
0
0.1
0.2
0.3
0.4
0.5
0.6
0.7
0.8
0.9
1
80 mm
150 mm
210 mm
255 mm

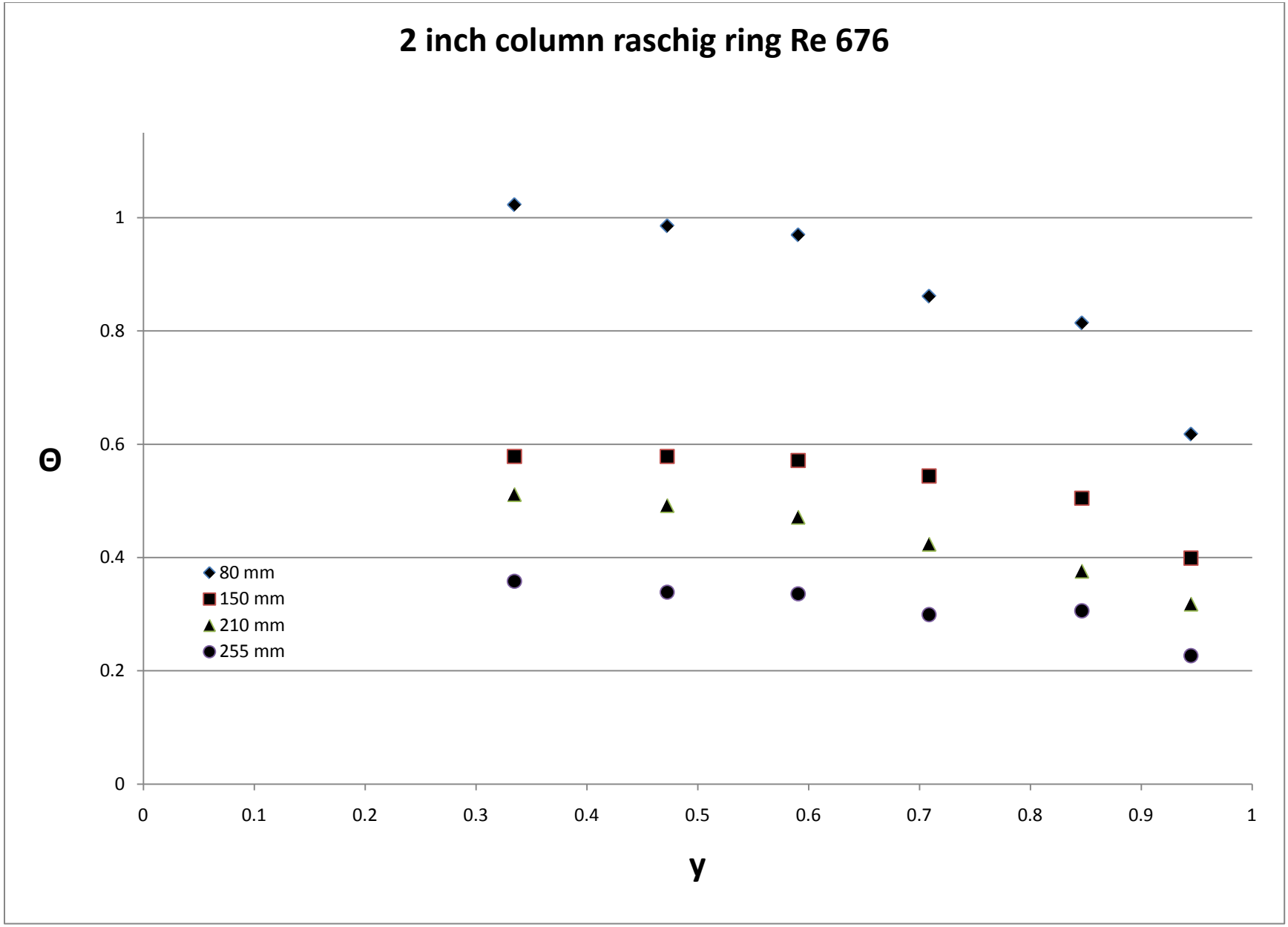
2 inch column raschig ring Re 676
Θ
y
1
0.8
0.6
0.4
0.2
0
0
0.1
0.2
0.3
0.4
0.5
0.6
0.7
0.8
0.9
1
80 mm
150 mm
210 mm
255 mm

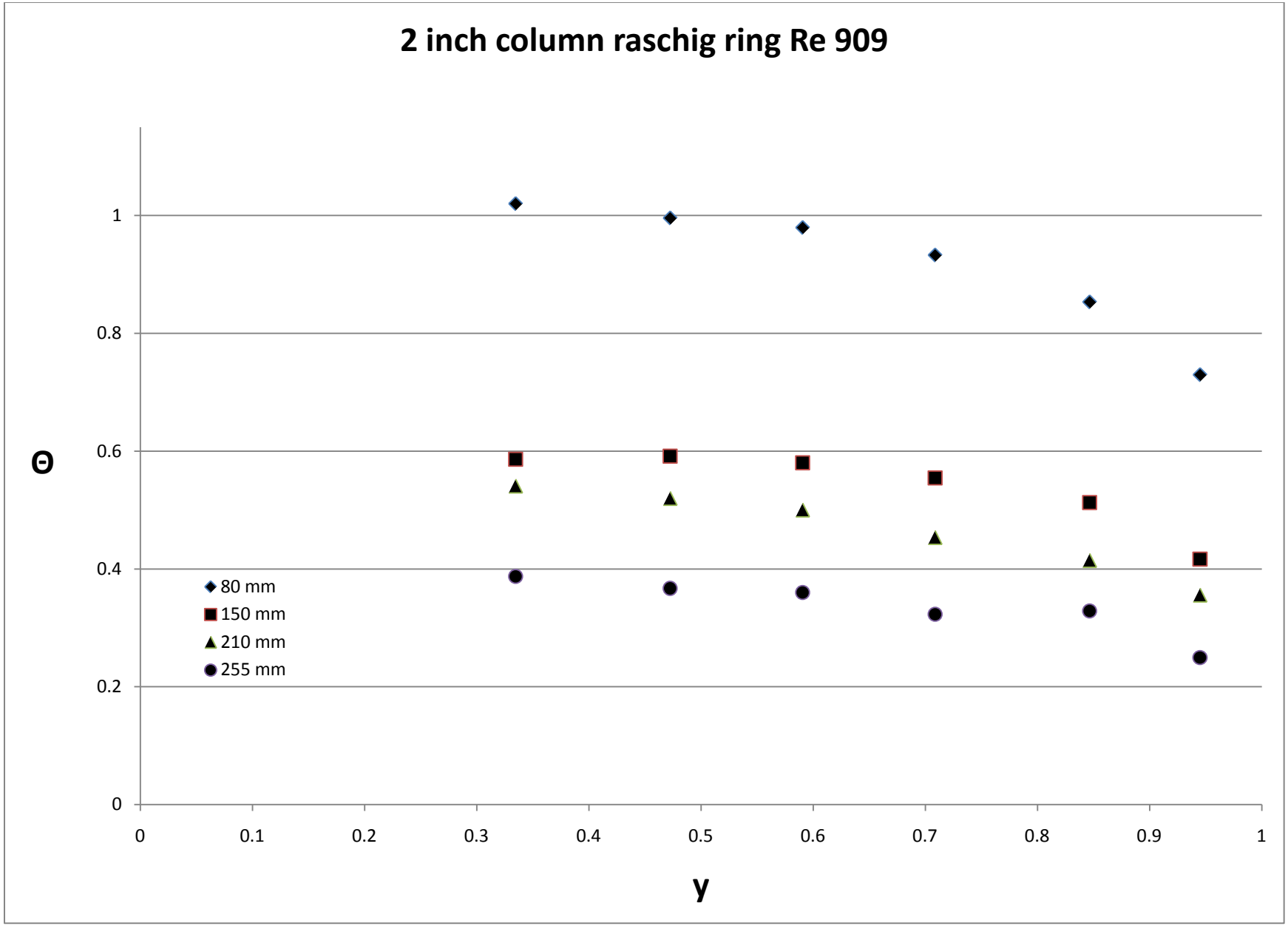
2 inch column raschig ring Re 909
Θ
y
1
0.8
0.6
0.4
0.2
0
0
0.1
0.2
0.3
0.4
0.5
0.6
0.7
0.8
0.9
1
80 mm
150 mm
210 mm
255 mm

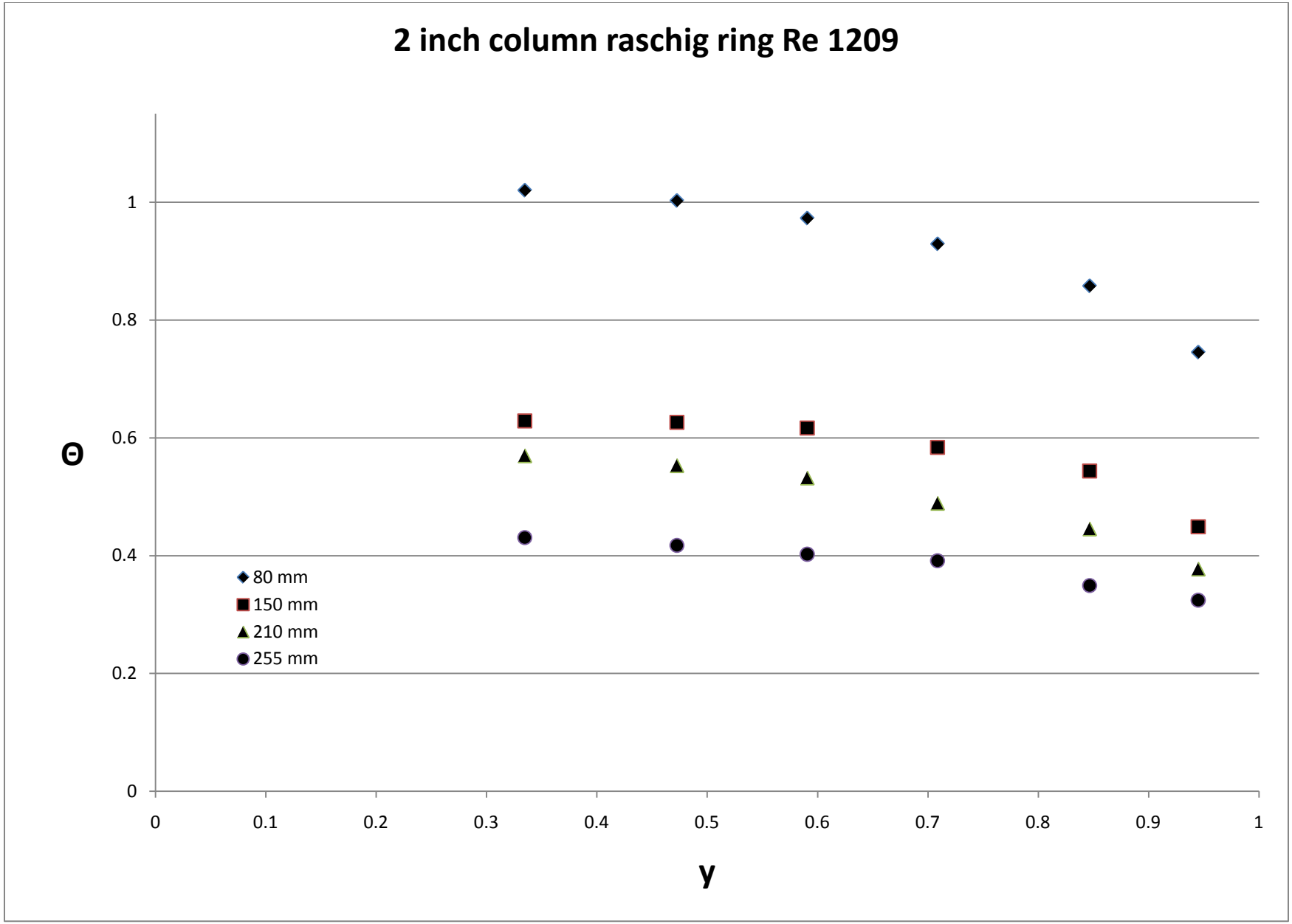
2 inch column raschig ring Re 1209
Θ
y
1
0.8
0.6
0.4
0.2
0
0
0.1
0.2
0.3
0.4
0.5
0.6
0.7
0.8
0.9
1
80 mm
150 mm
210 mm
255 mm

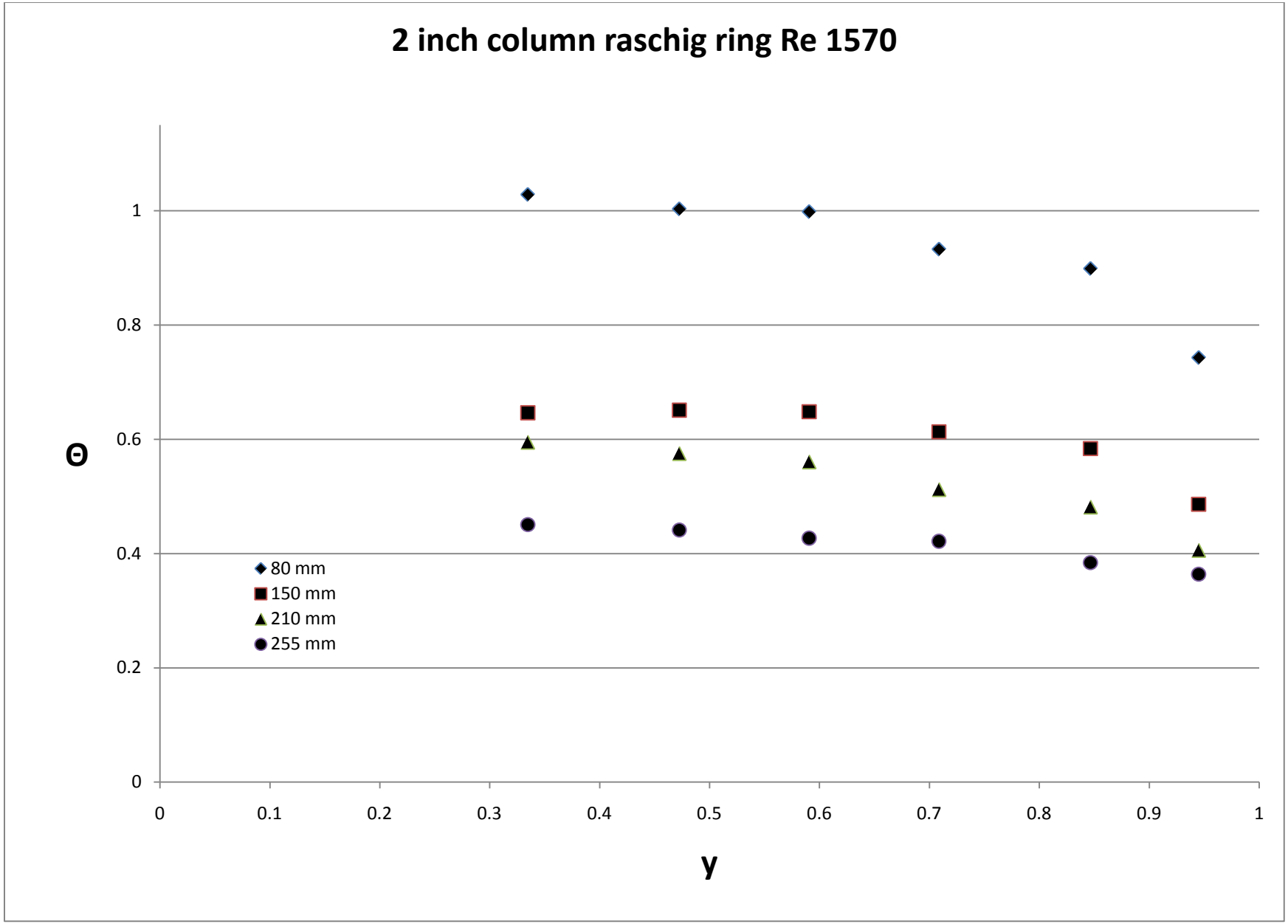
2 inch column raschig ring Re 1570
Θ
y
1
0.8
0.6
0.4
0.2
0
0
0.1
0.2
0.3
0.4
0.5
0.6
0.7
0.8
0.9
1
80 mm
150 mm
210 mm
255 mm

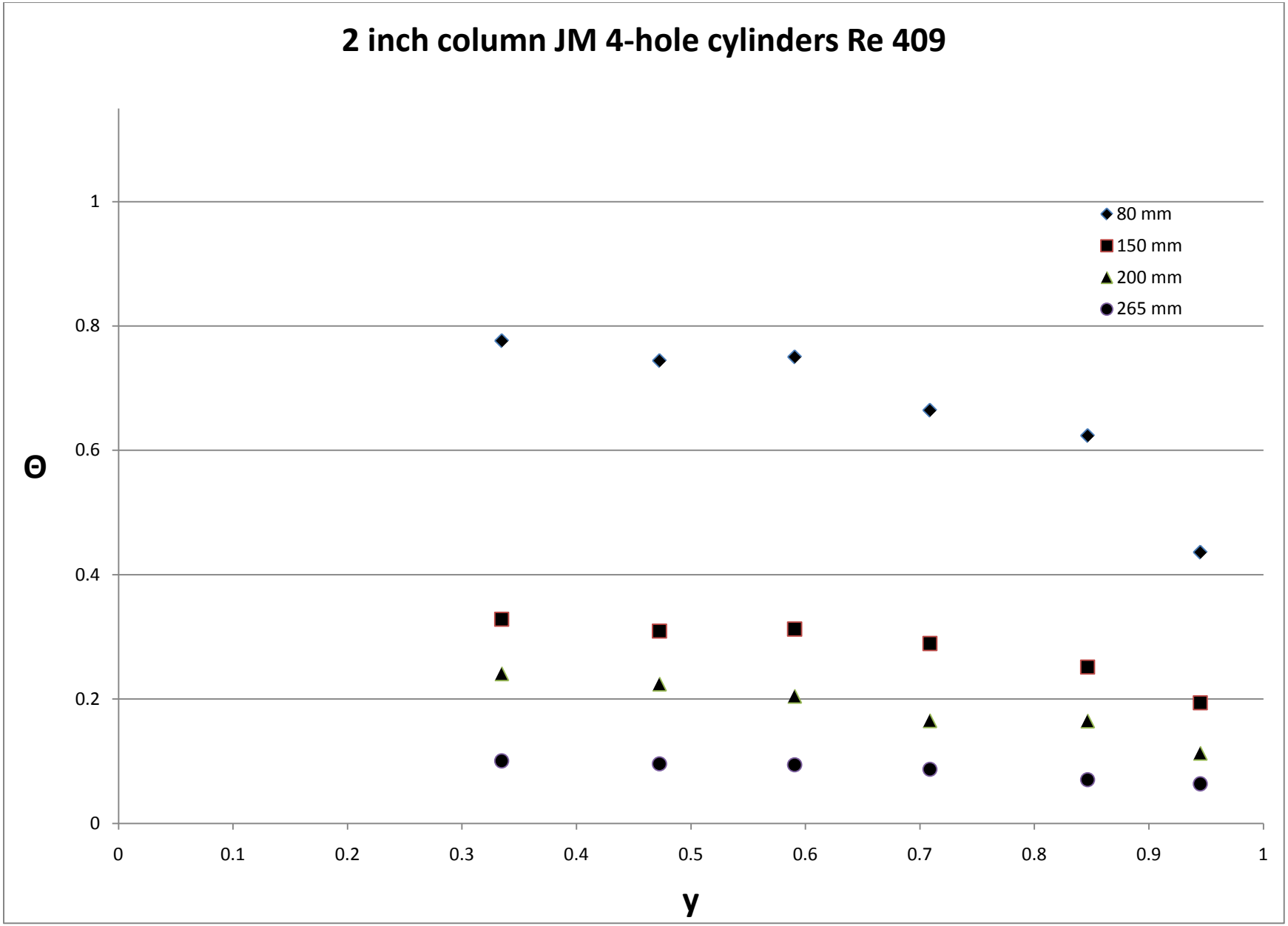
2 inch column JM 4-hole cylinders Re 409
Θ
y
80 mm
150 mm
200 mm
265 mm
0
0.2
0.4
0.6
0.8
1
0
0.1
0.2
0.3
0.4
0.5
0.6
0.7
0.8
0.9
1

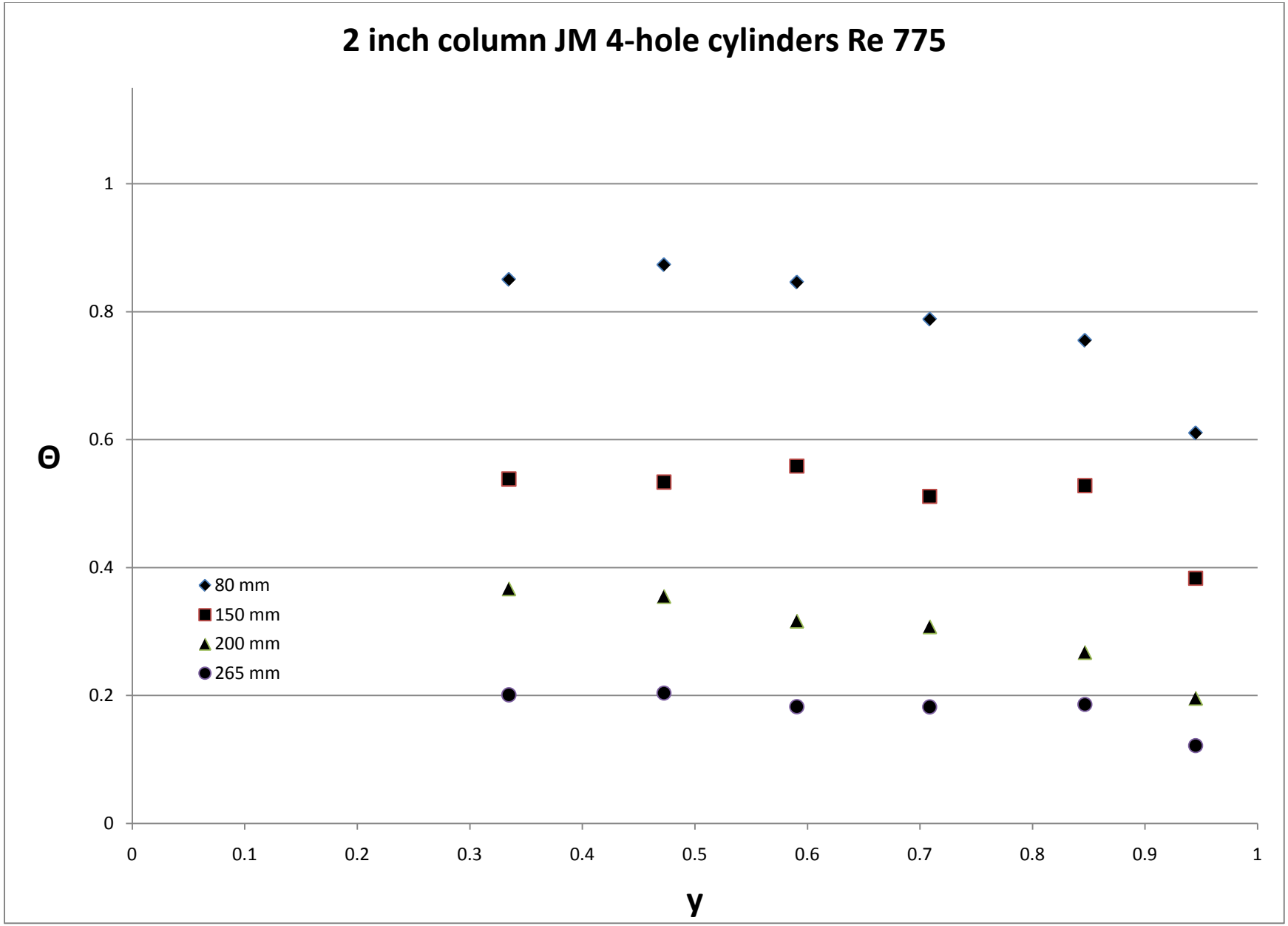
2 inch column JM 4-hole cylinders Re 775
Θ
y
1
0.8
0.6
0.4
0.2
0
0
0.1
0.2
0.3
0.4
0.5
0.6
0.7
0.8
0.9
1
80 mm
150 mm
200 mm
265 mm

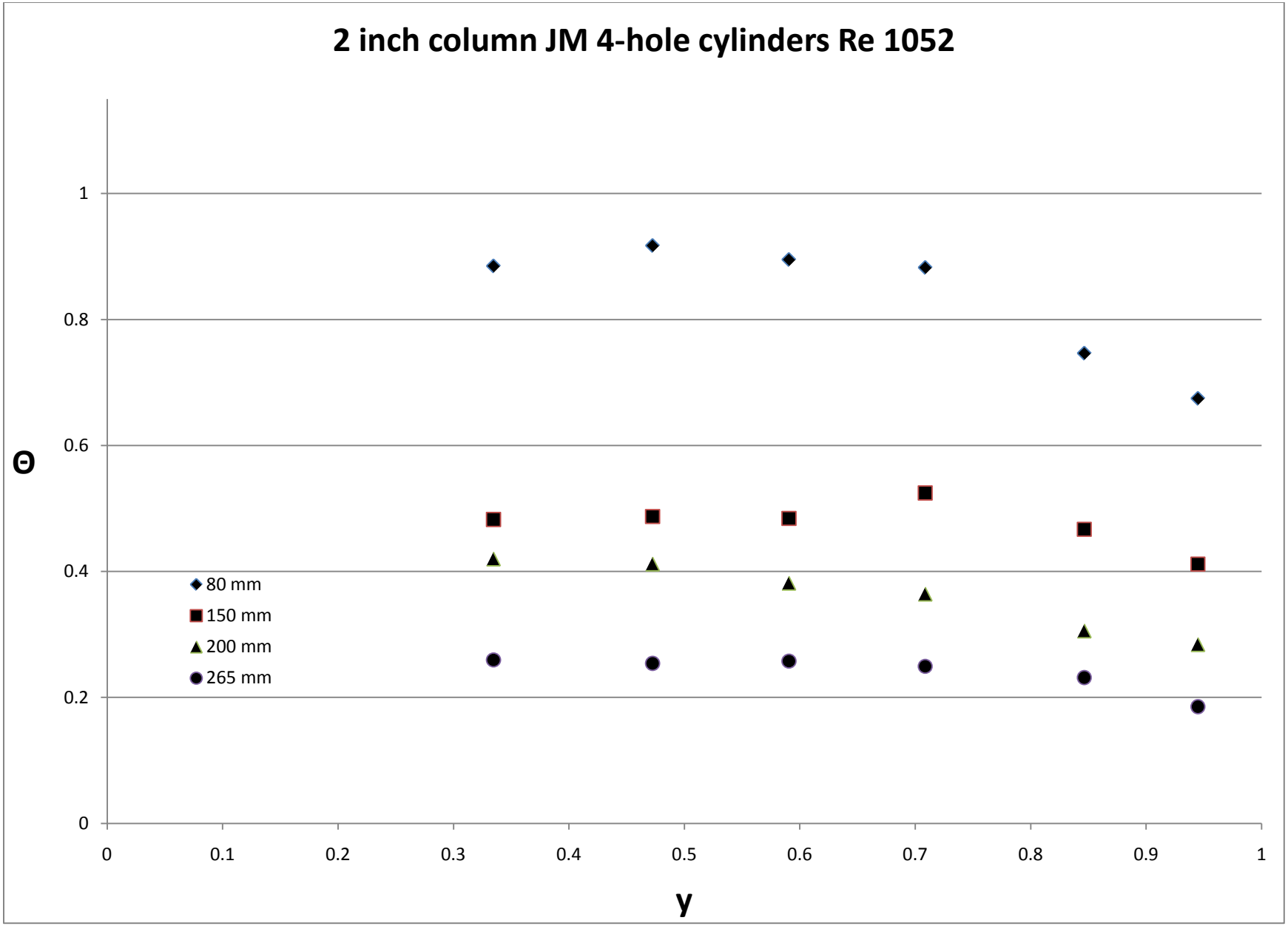
2 inch column JM 4-hole cylinders Re 1052
Θ
y
80 mm
150 mm
200 mm
265 mm
0
0.2
0.4
0.6
0.8
1
0
0.1
0.2
0.3
0.4
0.5
0.6
0.7
0.8
0.9
1

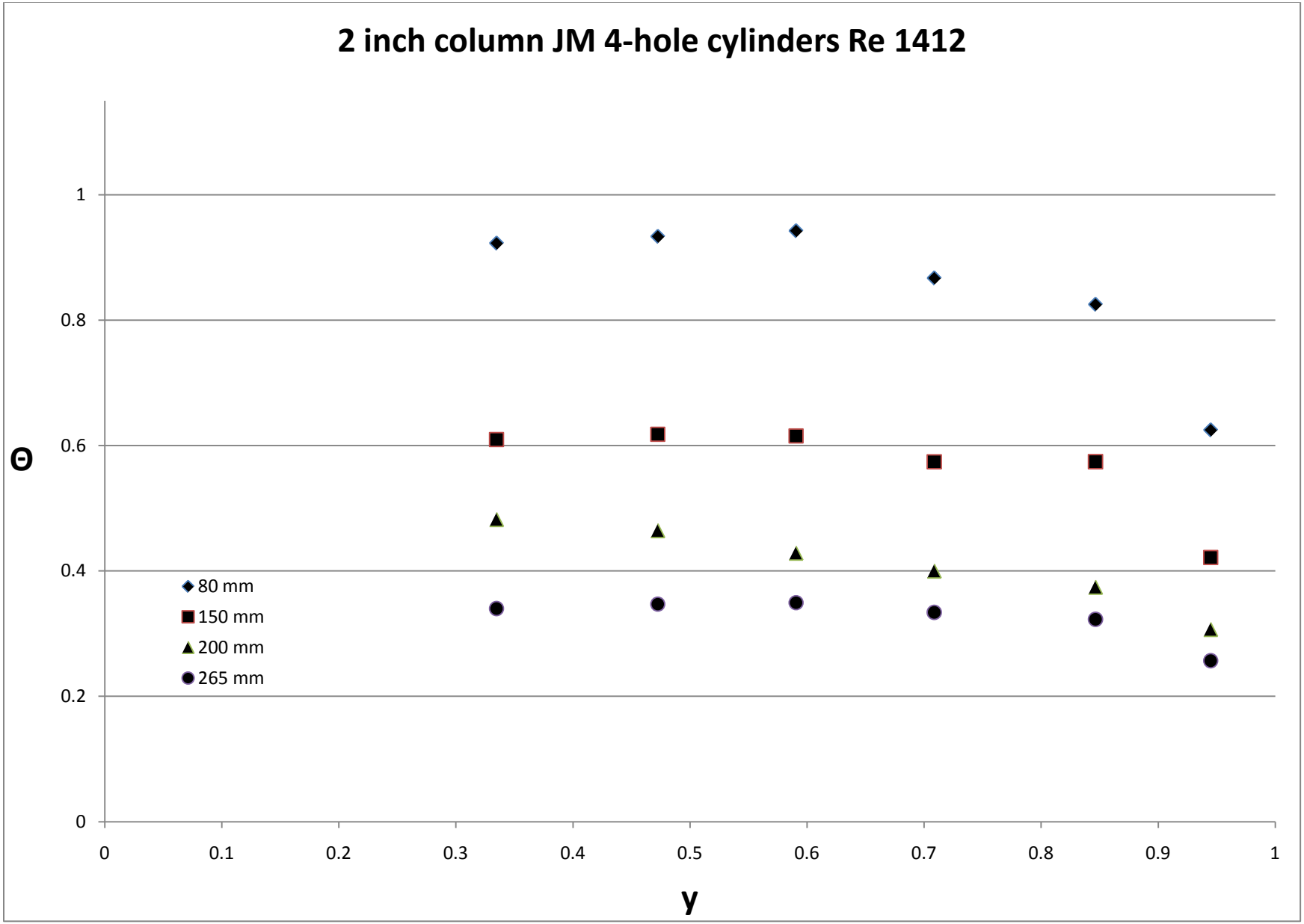
2 inch column JM 4-hole cylinders Re 1412
Θ
y
1
0.8
0.6
0.4
0.2
0
0
0.1
0.2
0.3
0.4
0.5
0.6
0.7
0.8
0.9
1
80 mm
150 mm
200 mm
265 mm

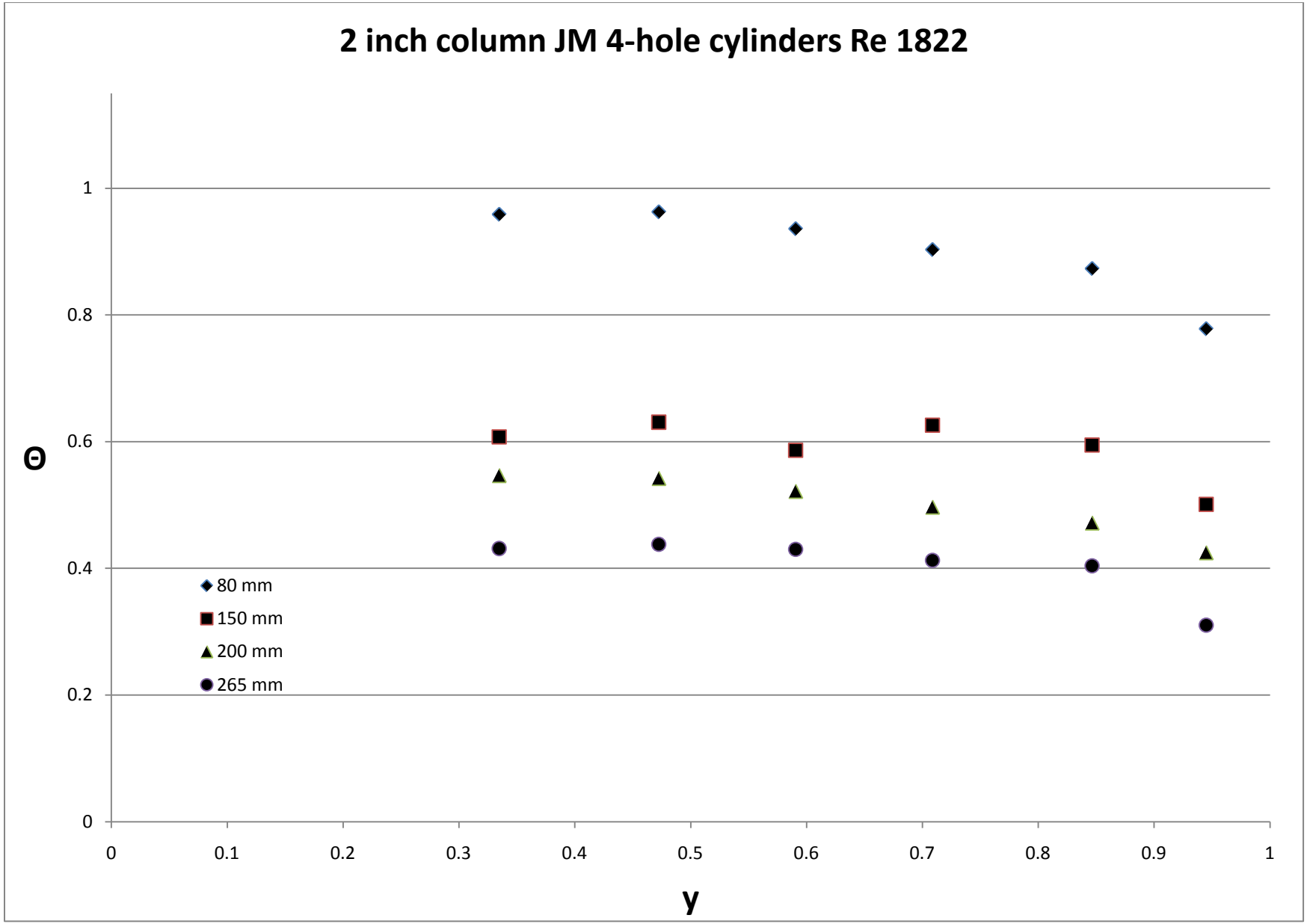
2 inch column JM 4-hole cylinders Re 1822
Θ
y
1
0.8
0.6
0.4
0.2
0
0
0.1
0.2
0.3
0.4
0.5
0.6
0.7
0.8
0.9
1
80 mm
150 mm
200 mm
265 mm

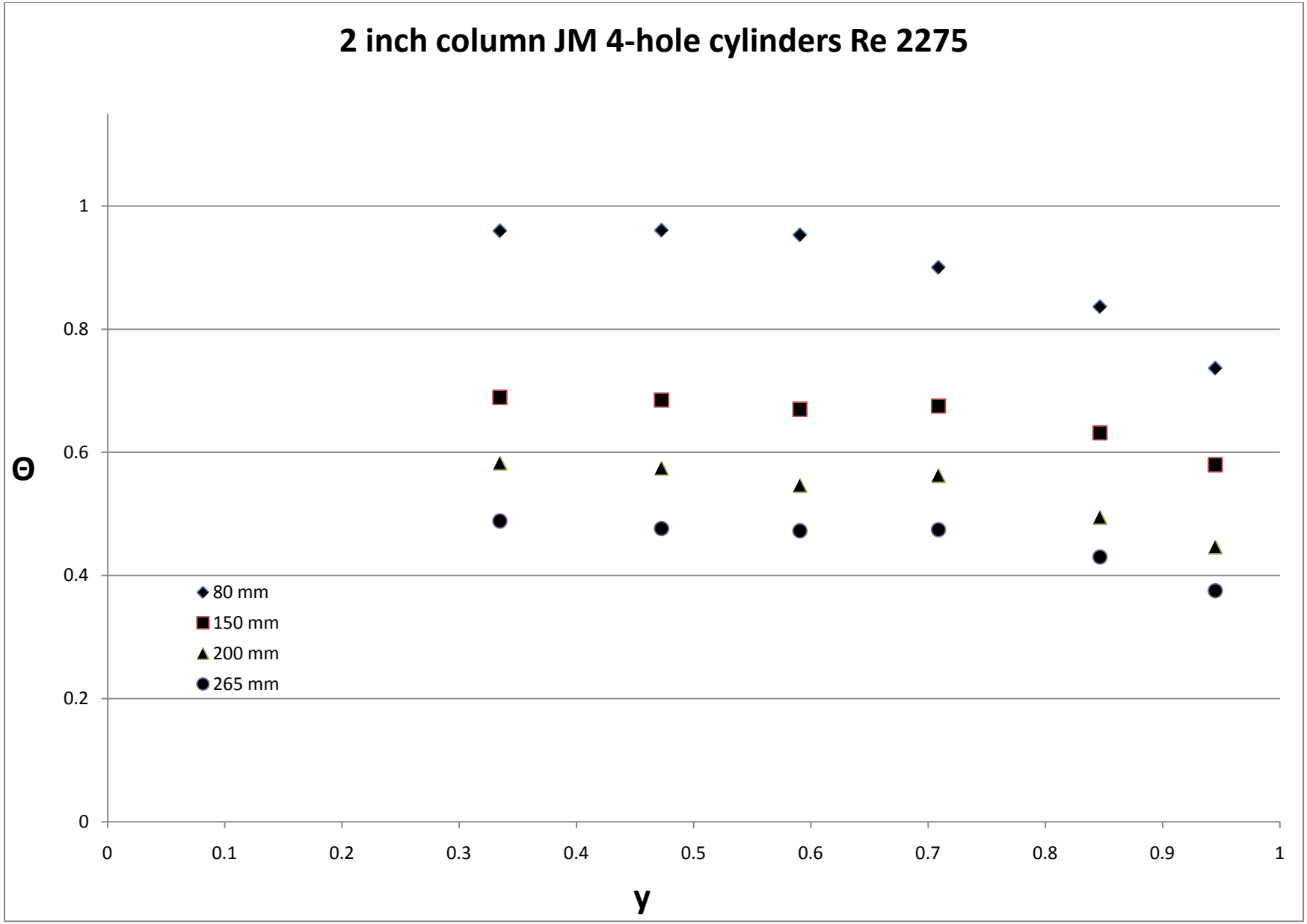
2 inch column JM 4-hole cylinders Re 2275
Θ
y
1
0.8
0.6
0.4
0.2
0
0
0.1
0.2
0.3
0.4
0.5
0.6
0.7
0.8
0.9
1
80 mm
150 mm
200 mm
265 mm

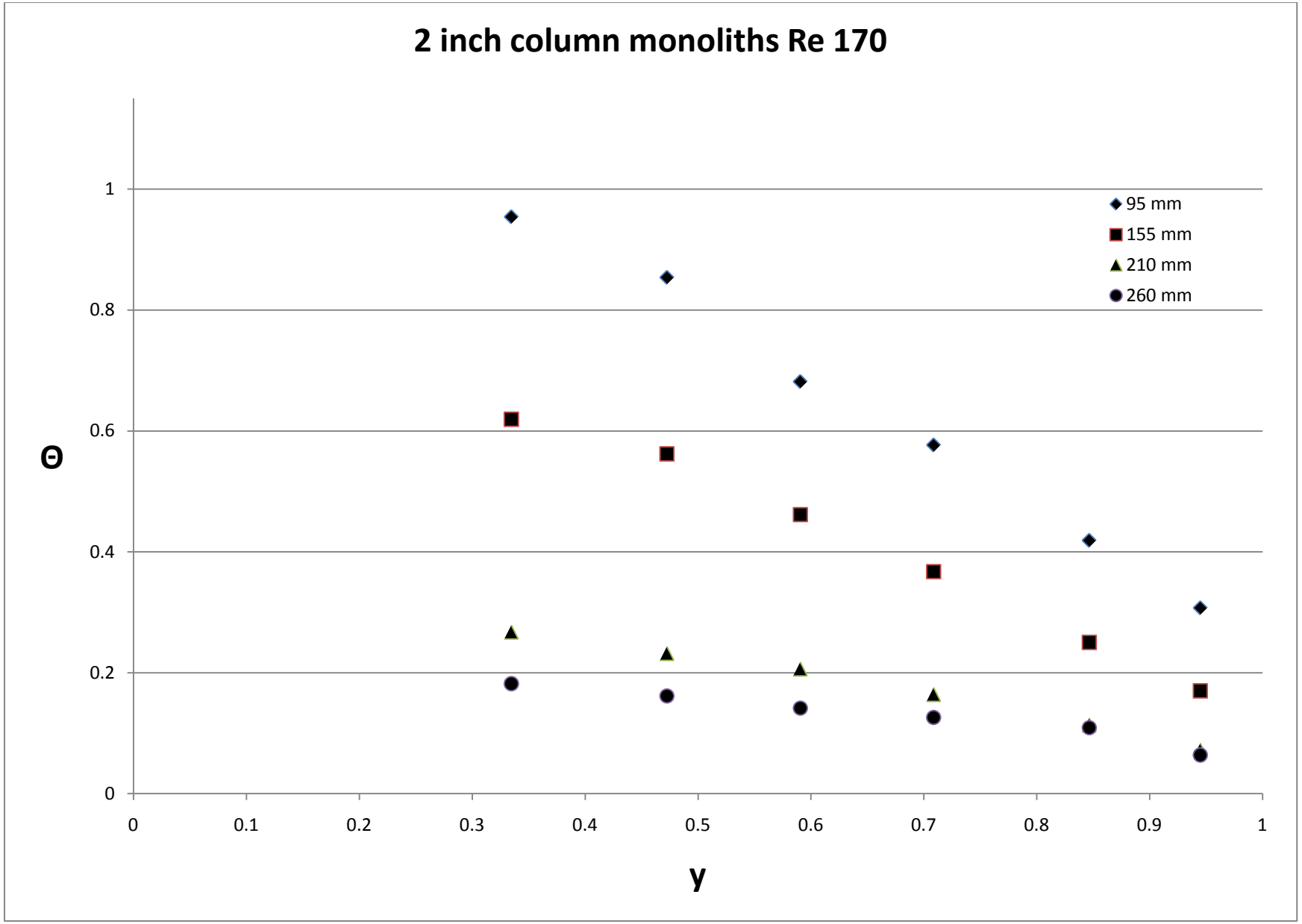
2 inch column monoliths Re 170
Θ
y
95 mm
155 mm
210 mm
260 mm
0
0.2
0.4
0.6
0.8
1
0
0.1
0.2
0.3
0.4
0.5
0.6
0.7
0.8
0.9
1

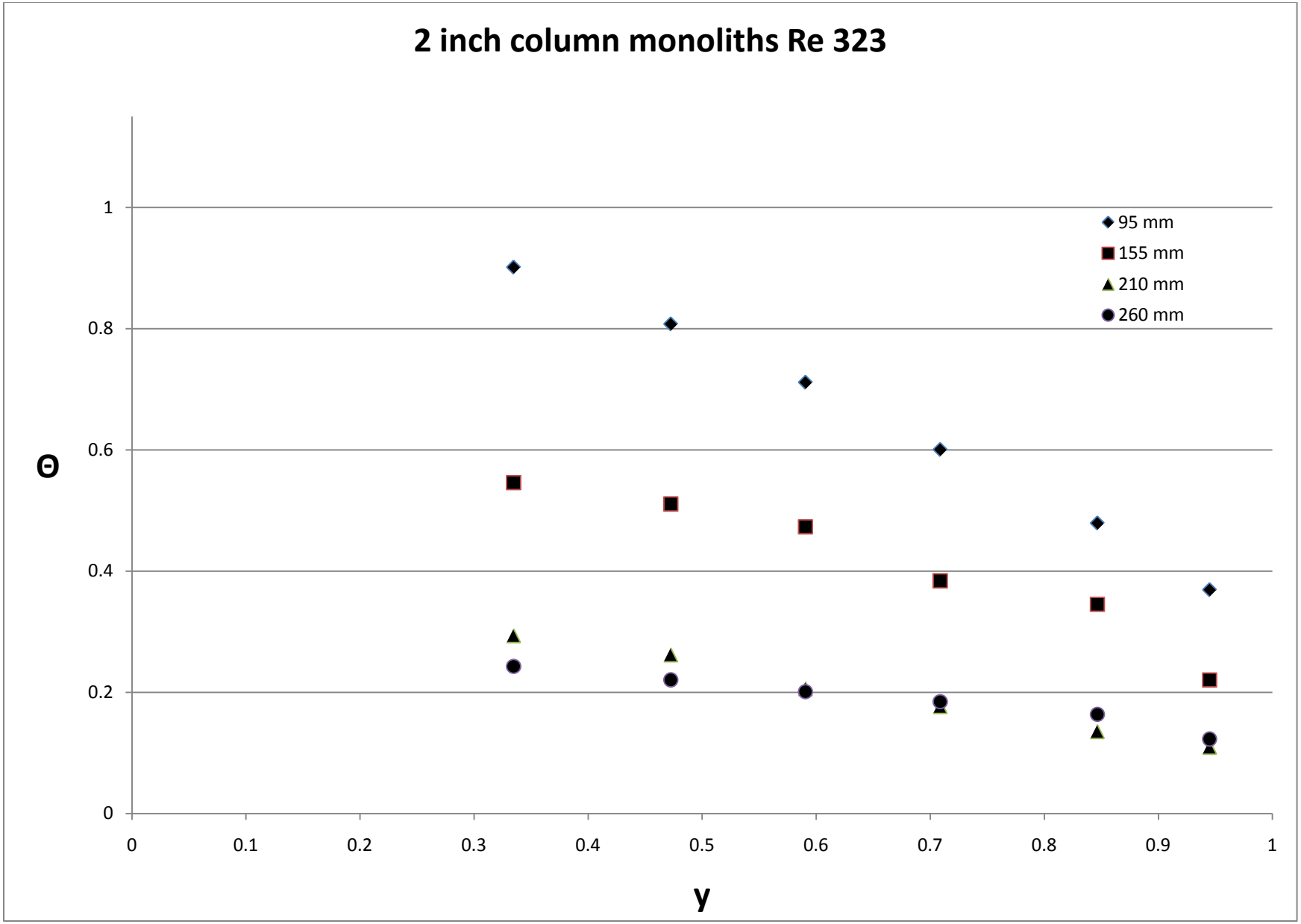
2 inch column monoliths Re 323
Θ
y
95 mm
155 mm
210 mm
260 mm
0
0.2
0.4
0.6
0.8
1
0
0.1
0.2
0.3
0.4
0.5
0.6
0.7
0.8
0.9
1

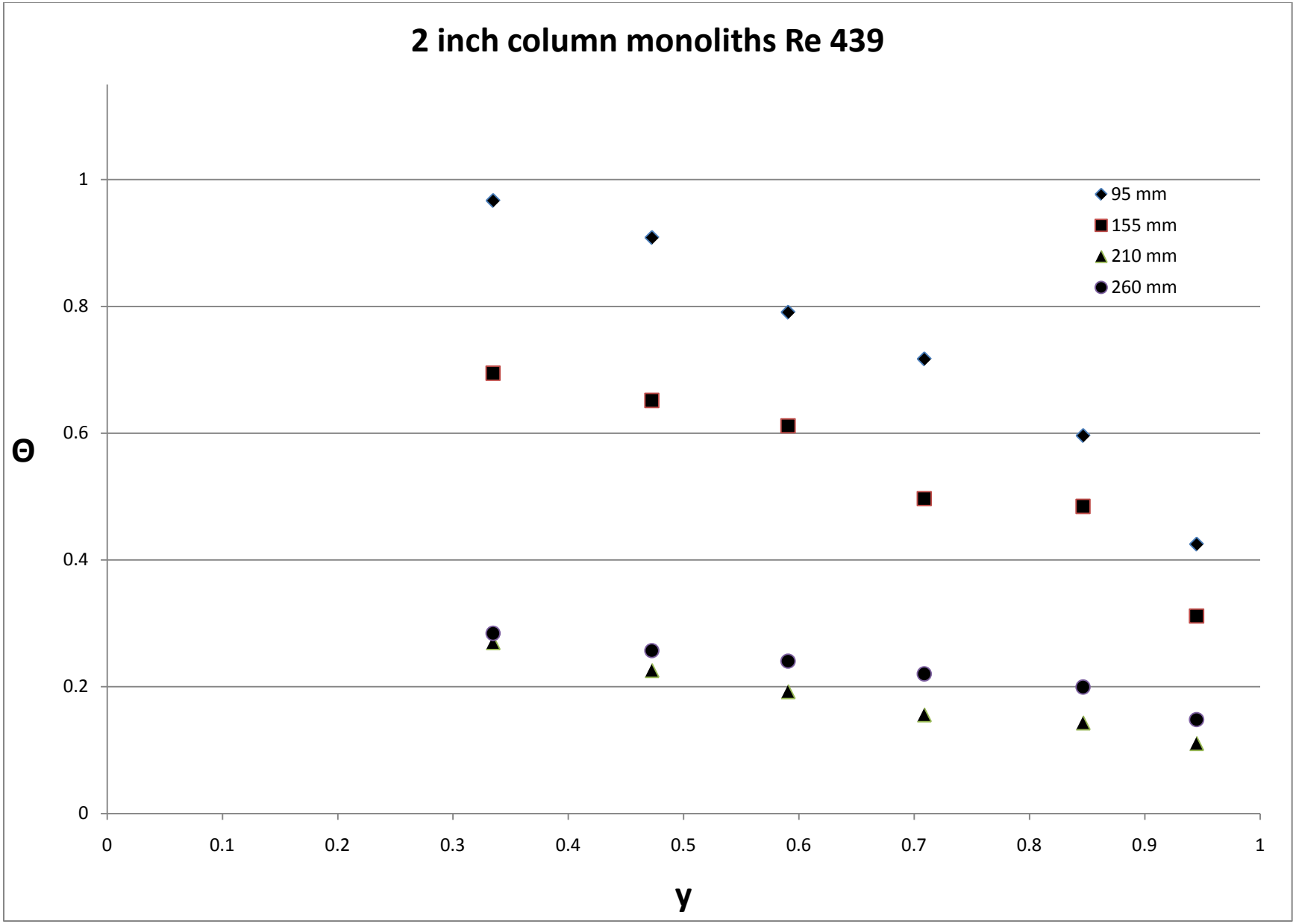
2 inch column monoliths Re 439
95 mm
155 mm
210 mm
260 mm
Θ
y
0
0.2
0.4
0.6
0.8
1
0
0.1
0.2
0.3
0.4
0.5
0.6
0.7
0.8
0.9
1

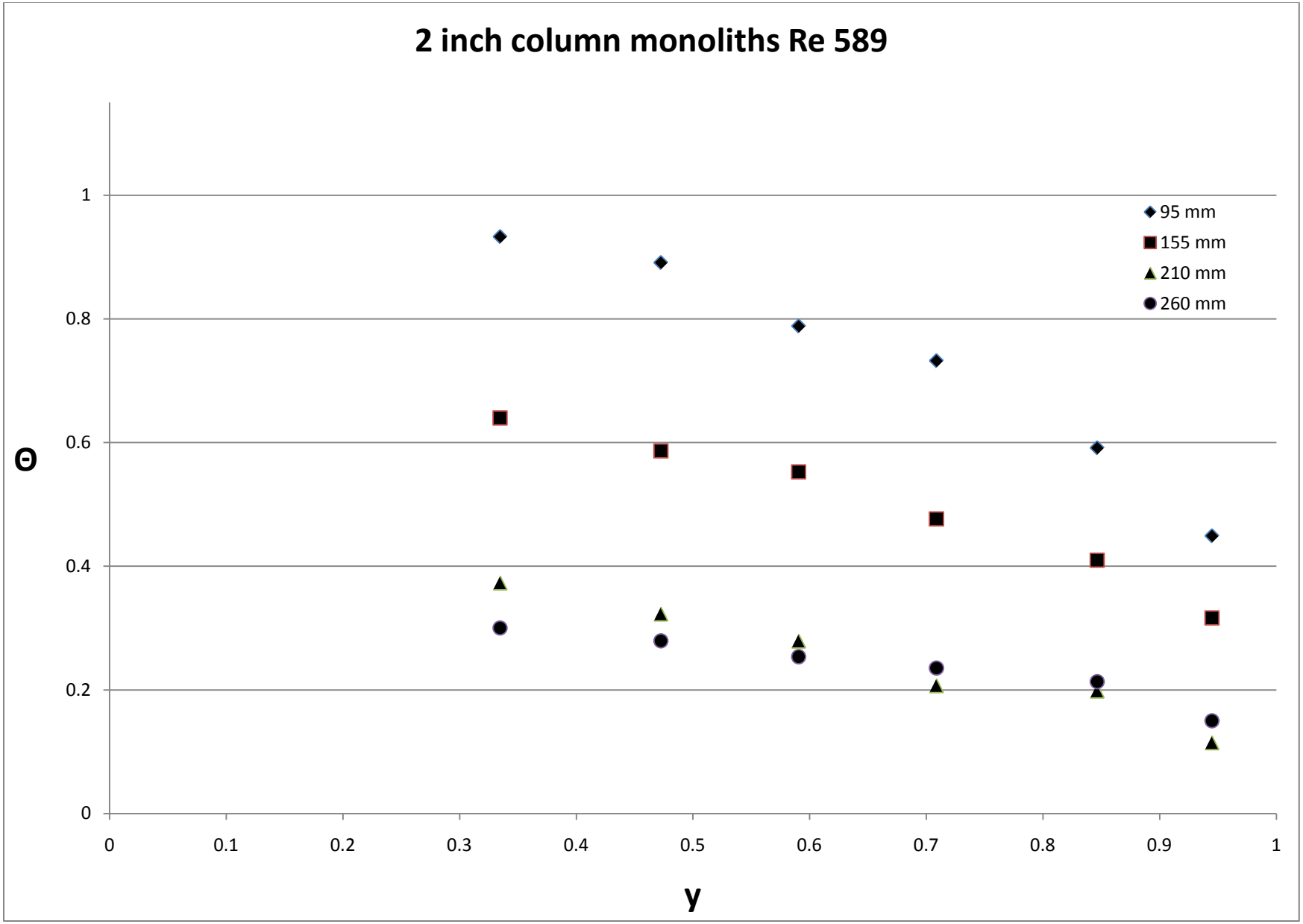
2 inch column monoliths Re 589
95 mm
155 mm
210 mm
260 mm
Θ
y
0
0.2
0.4
0.6
0.8
1
0
0.1
0.2
0.3
0.4
0.5
0.6
0.7
0.8
0.9
1

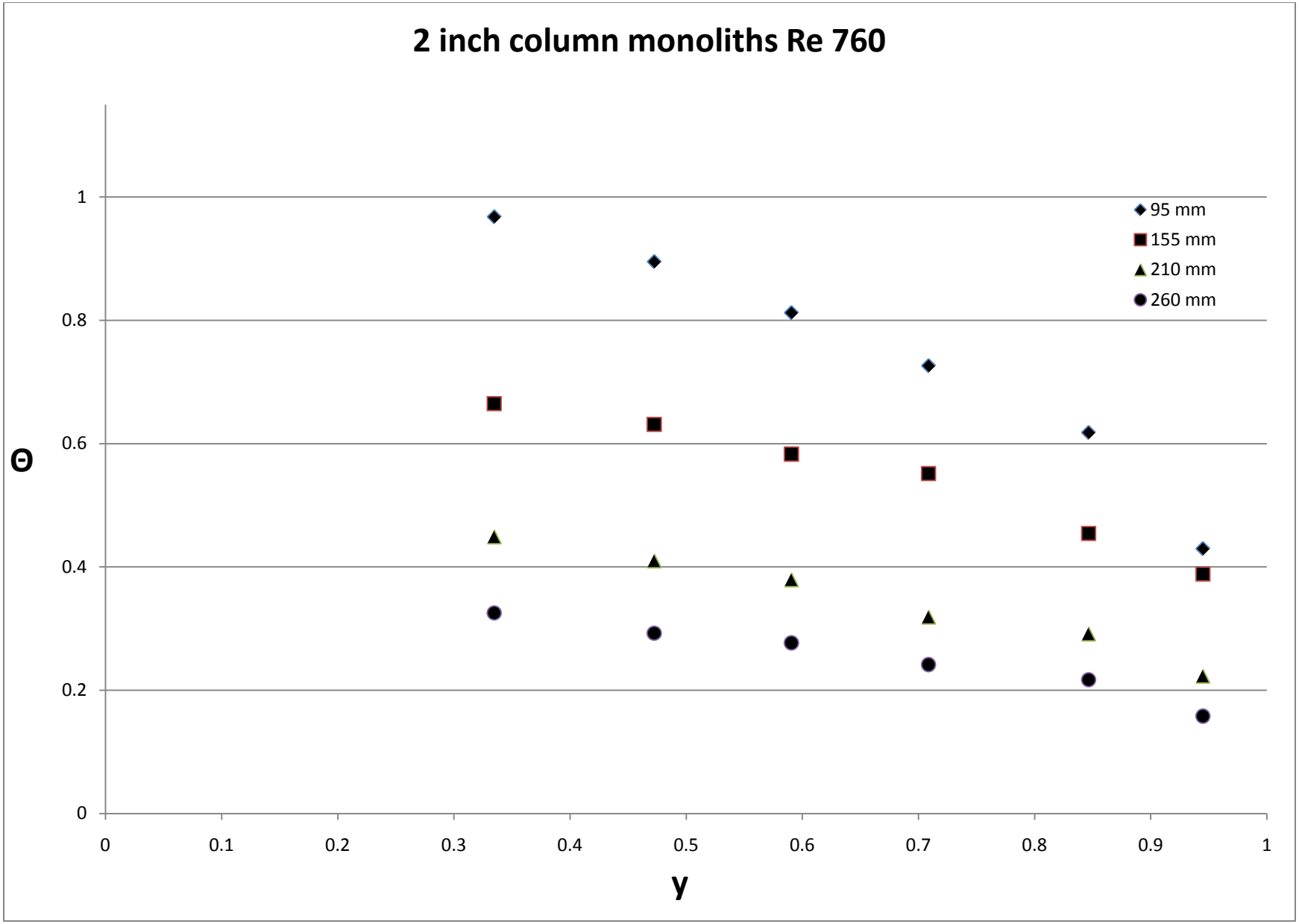
2 inch column monoliths Re 760
95 mm
155 mm
210 mm
260 mm
Θ
y
0
0.2
0.4
0.6
0.8
1
0
0.1
0.2
0.3
0.4
0.5
0.6
0.7
0.8
0.9
1

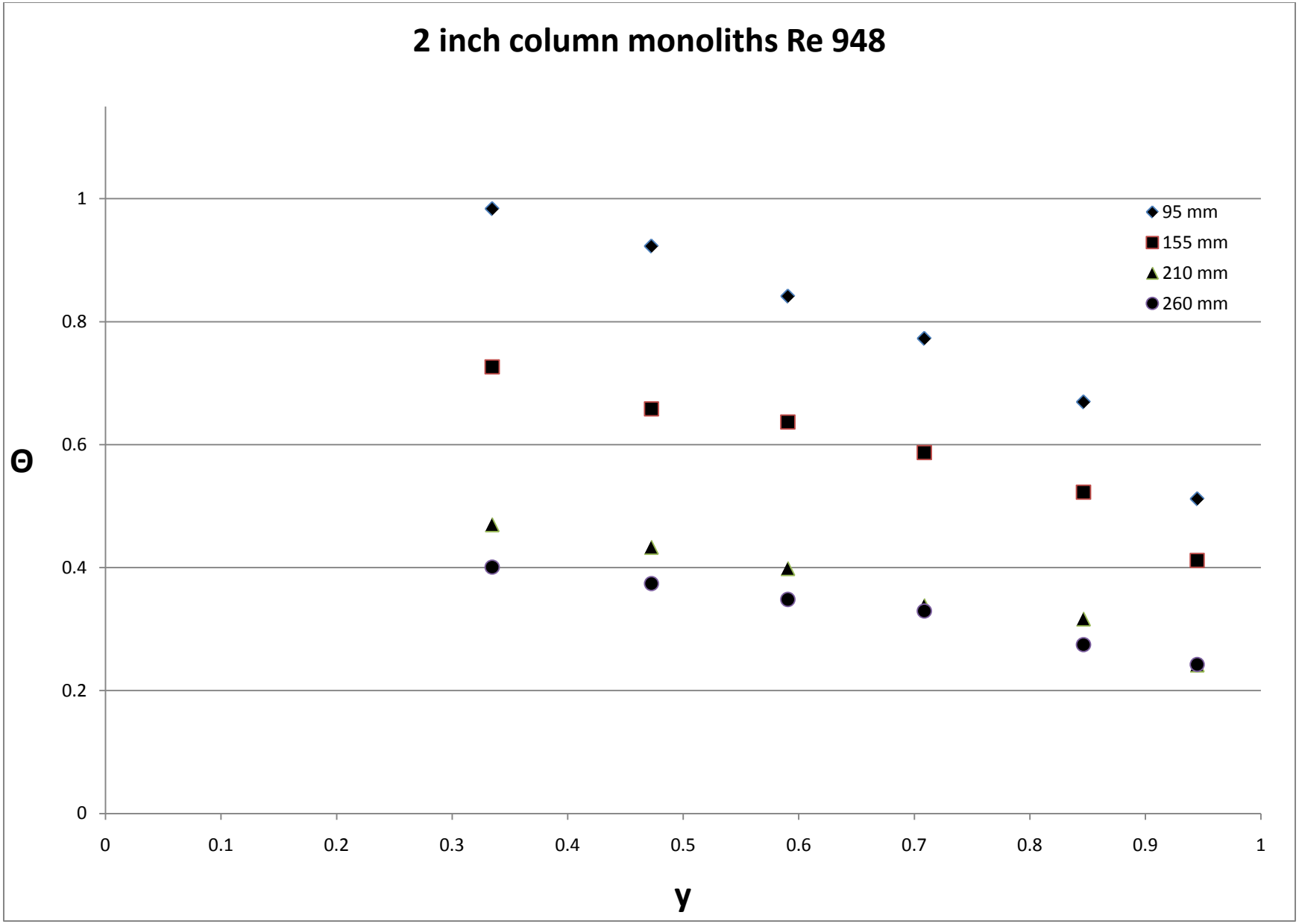
2 inch column monoliths Re 948
Θ
y
95 mm
155 mm
210 mm
260 mm
0
0.2
0.4
0.6
0.8
1
0
0.1
0.2
0.3
0.4
0.5
0.6
0.7
0.8
0.9
1

Appendix D: k_r/k_f and Nu_w Height by Height Analysis

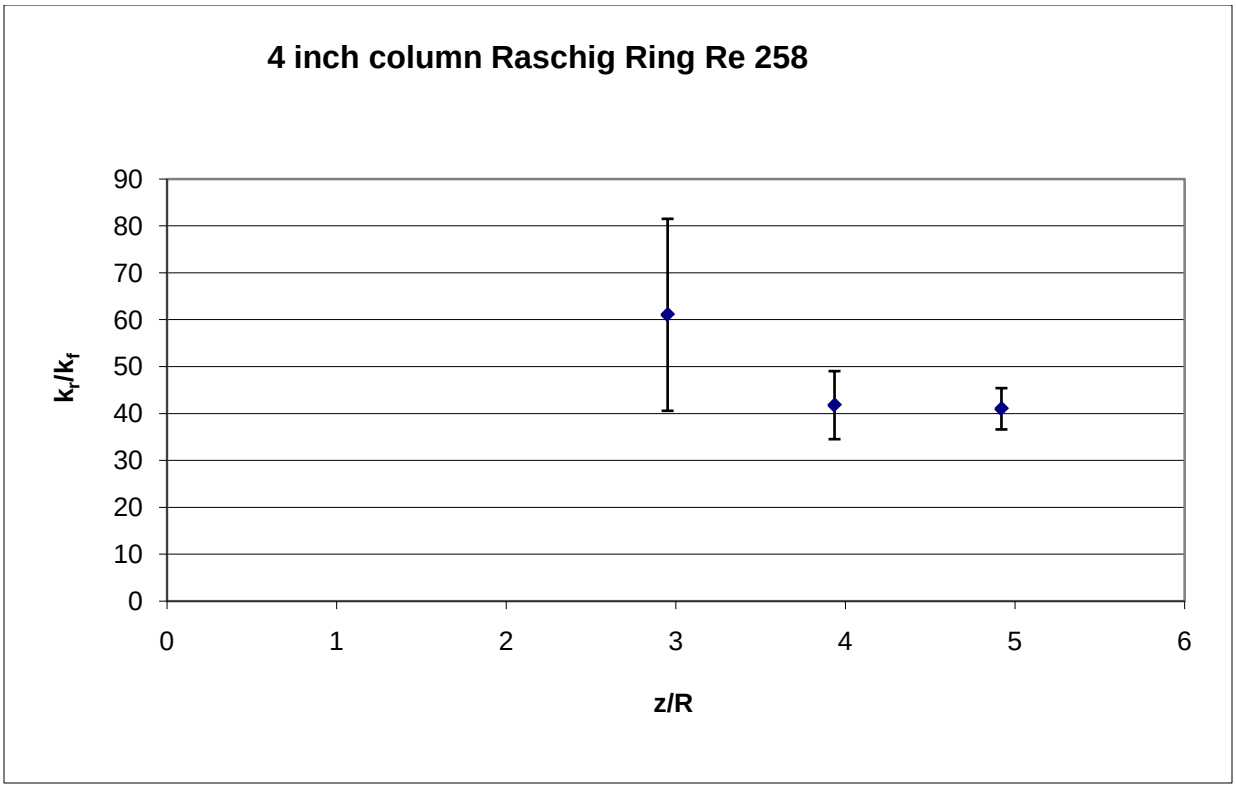
4 inch column Raschig Ring Re 258
90
80
70
60
50
40
30
20
10
0
k_r/k_f
0
1
2
3
4
5
6
z/R

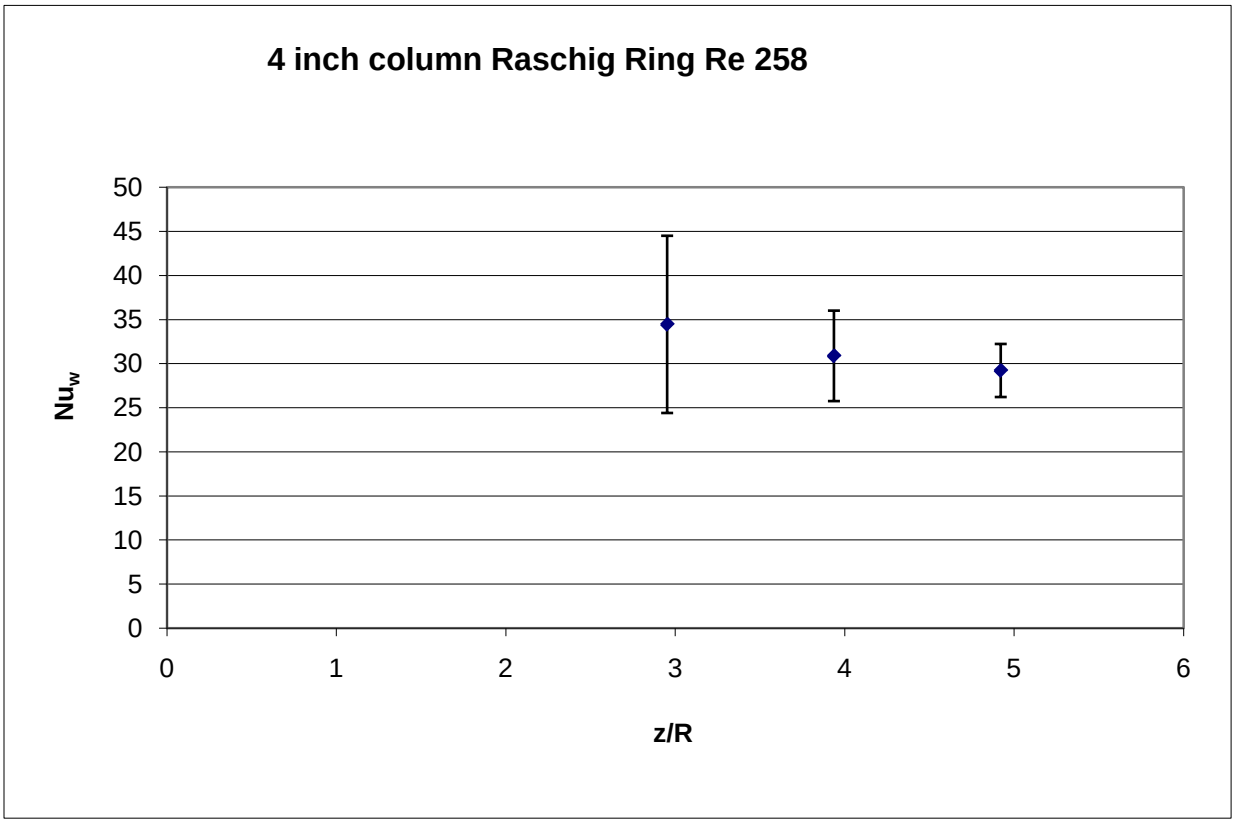
4 inch column Raschig Ring Re 258
50
45
40
35
30
25
20
15
10
5
0
Nu_w
0
1
2
3
4
5
6
z/R

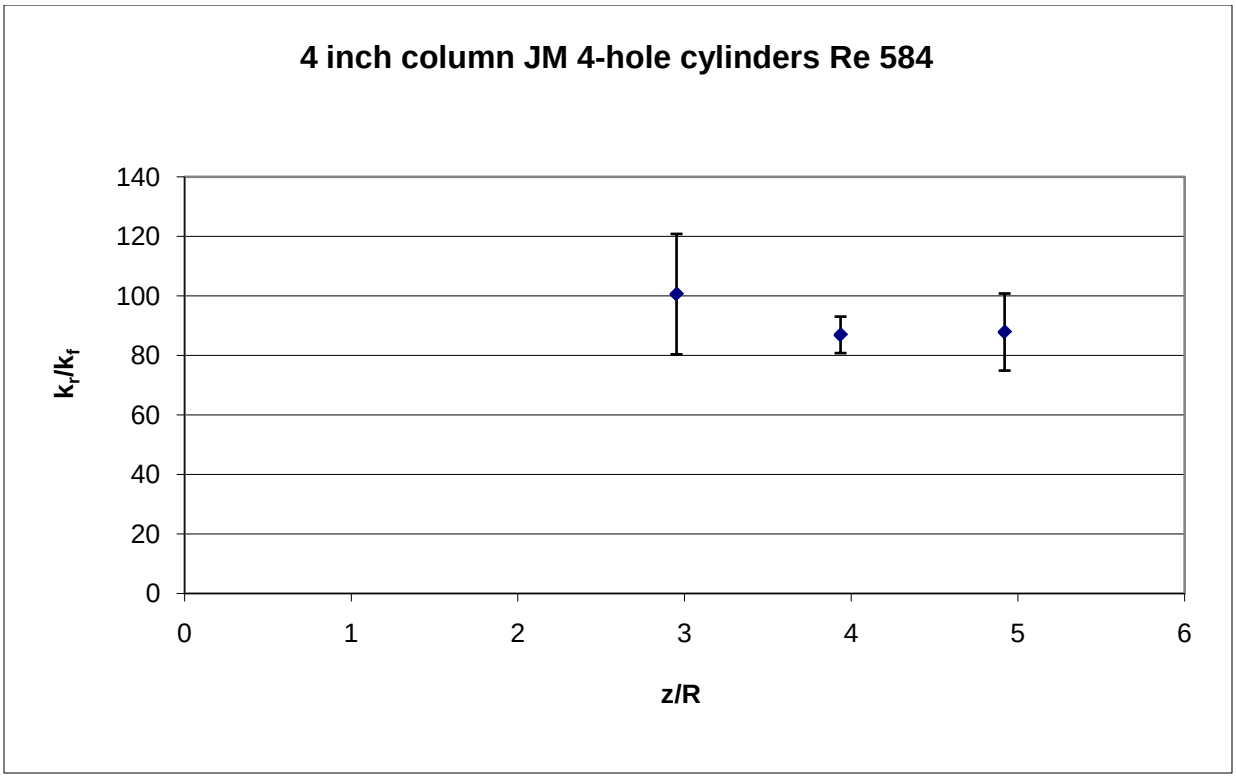
4 inch column JM 4-hole cylinders Re 584
140
120
100
80
60
40
20
0
k_r/k_f
0
1
2
3
4
5
6
z/R

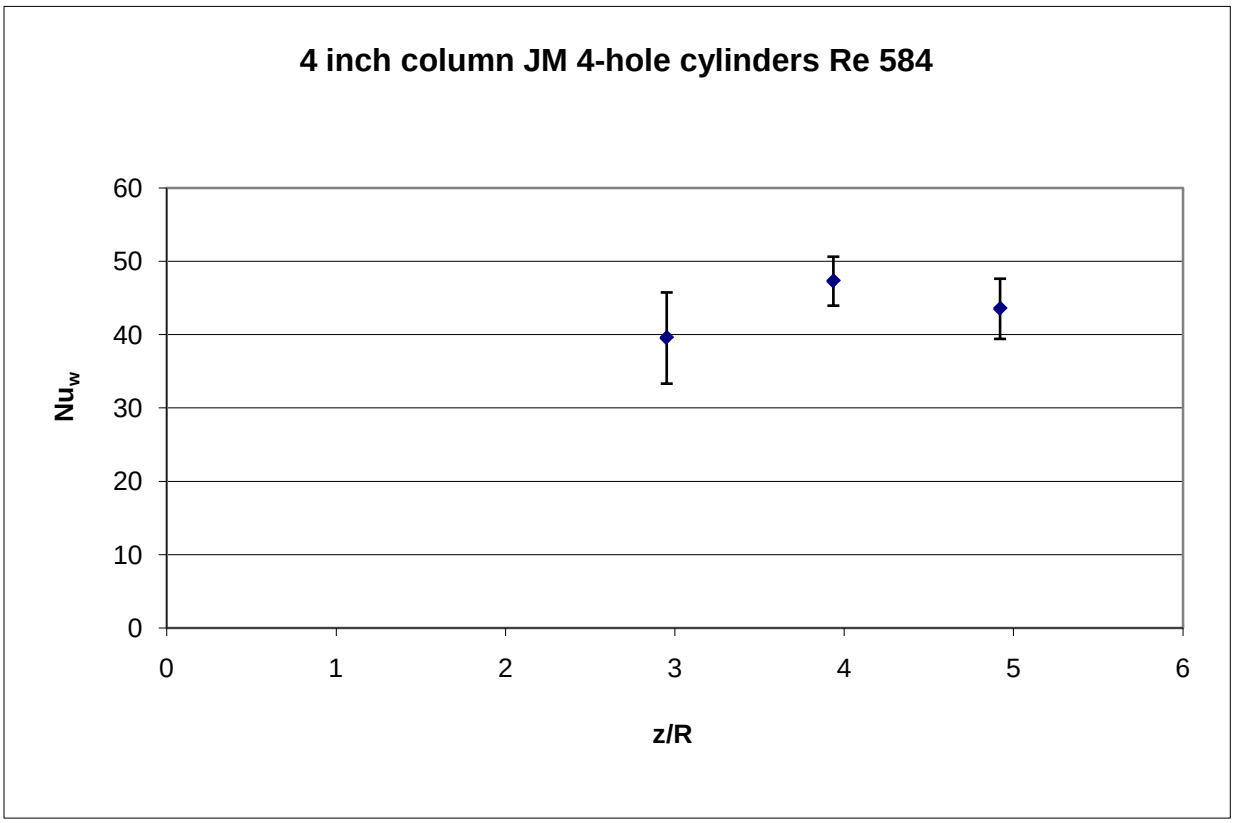
4 inch column JM 4-hole cylinders Re 584
60
50
40
30
20
10
0
Nu_w
0
1
2
3
4
5
6
z/R

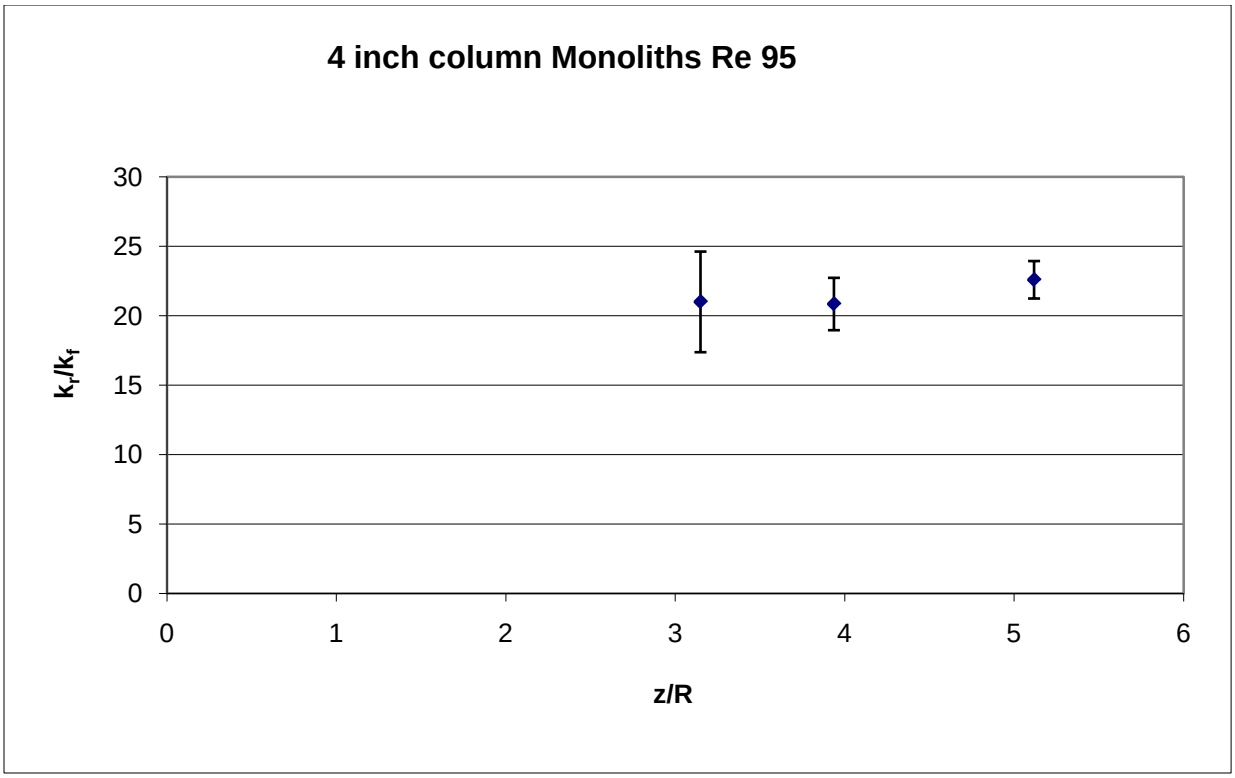
4 inch column Monoliths Re 95
30
25
20
15
10
5
0
k_r/k_f
0
1
2
3
4
5
6
z/R

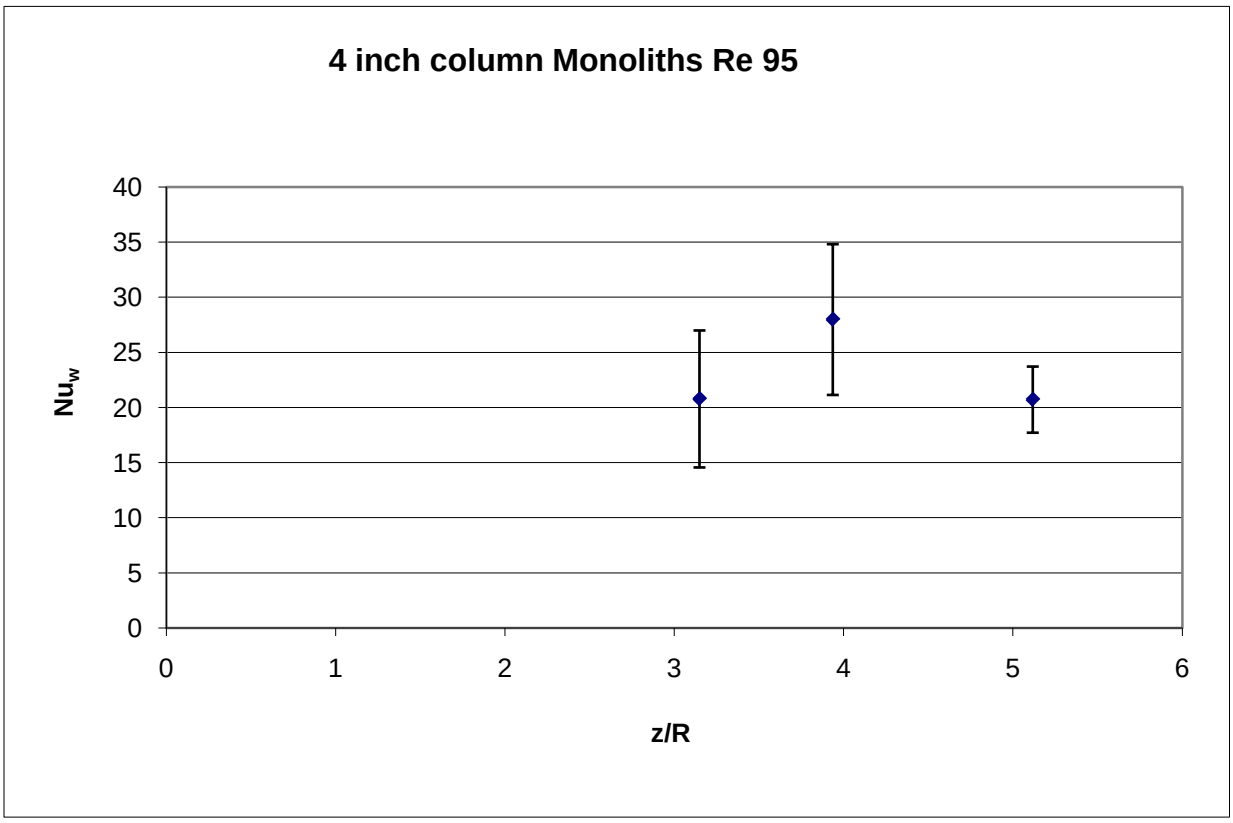
4 inch column Monoliths Re 95
40
35
30
25
20
15
10
5
0
Nu_w
0
1
2
3
4
5
6
z/R

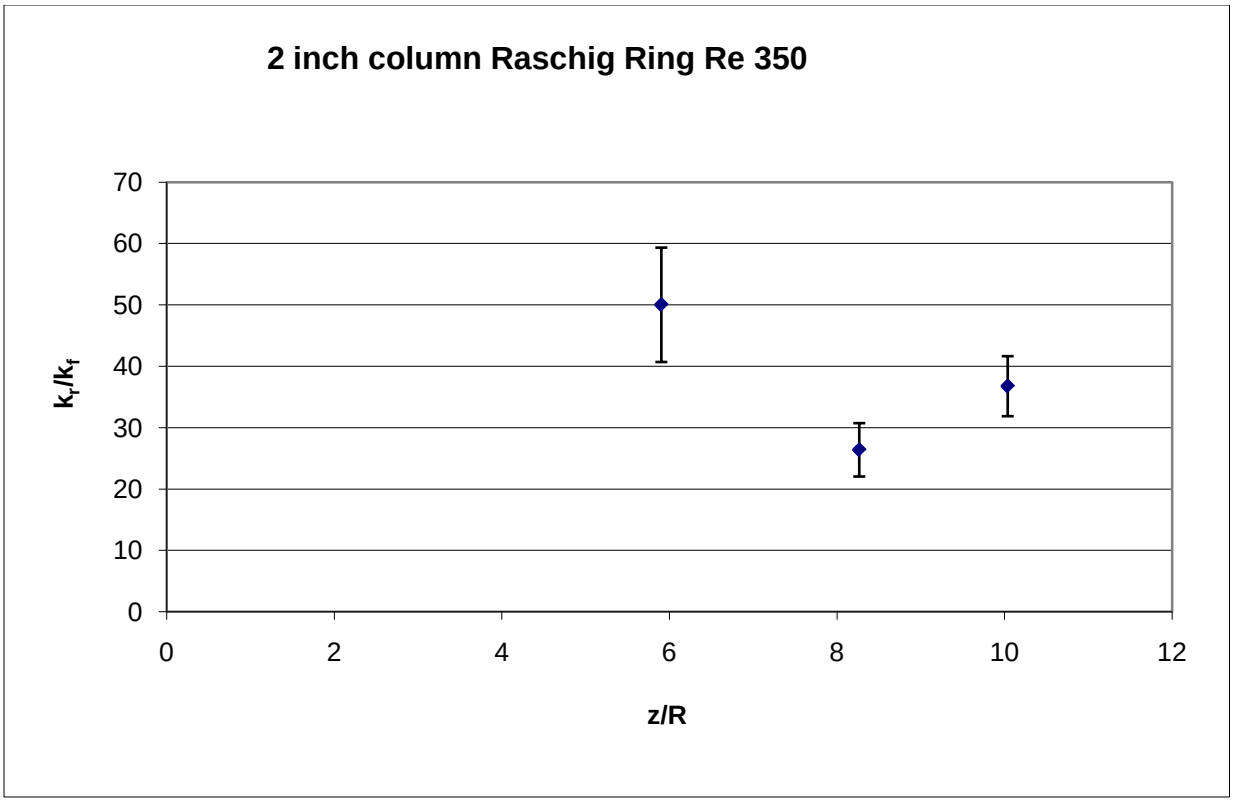
2 inch column Raschig Ring Re 350
70
60
50
40
30
20
10
0
k_r/k_f
0
2
4
6
8
10
12
z/R

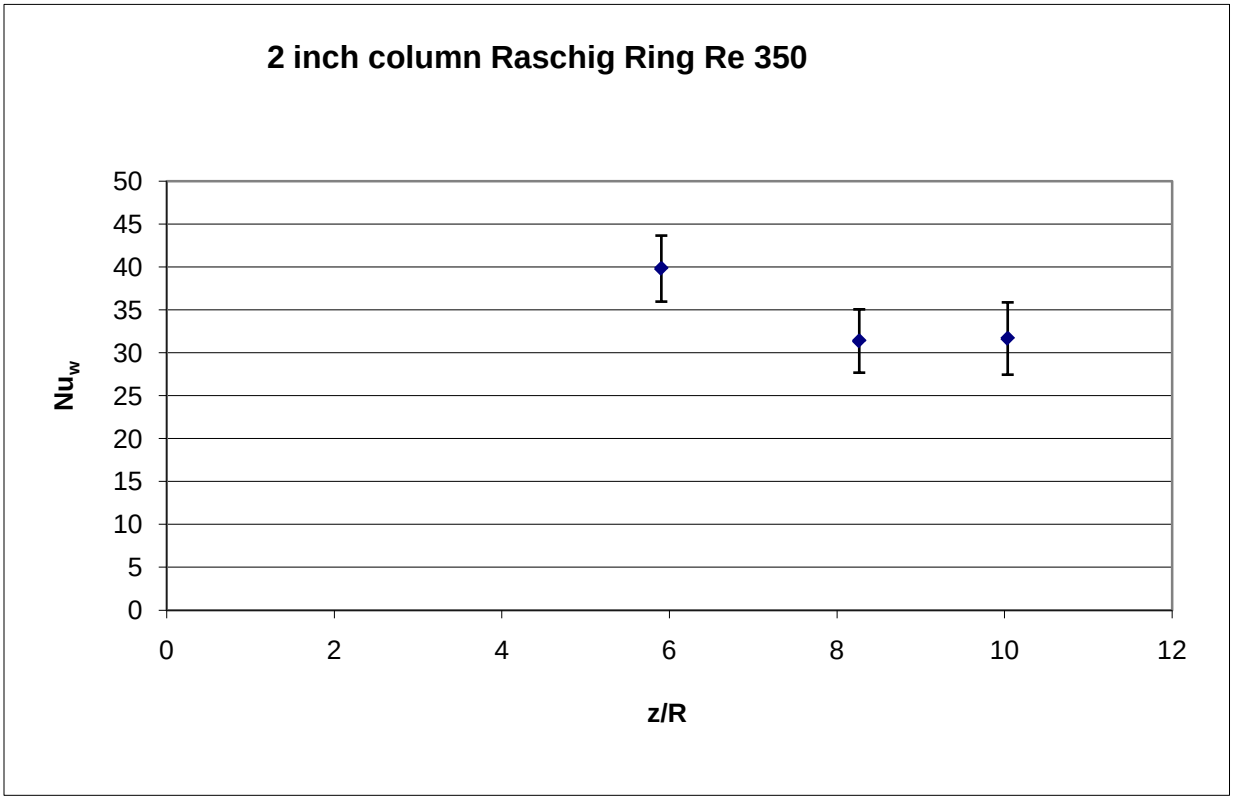
2 inch column Raschig Ring Re 350
50
45
40
35
30
25
20
15
10
5
0
Nu_w
0
2
4
6
8
10
12
z/R

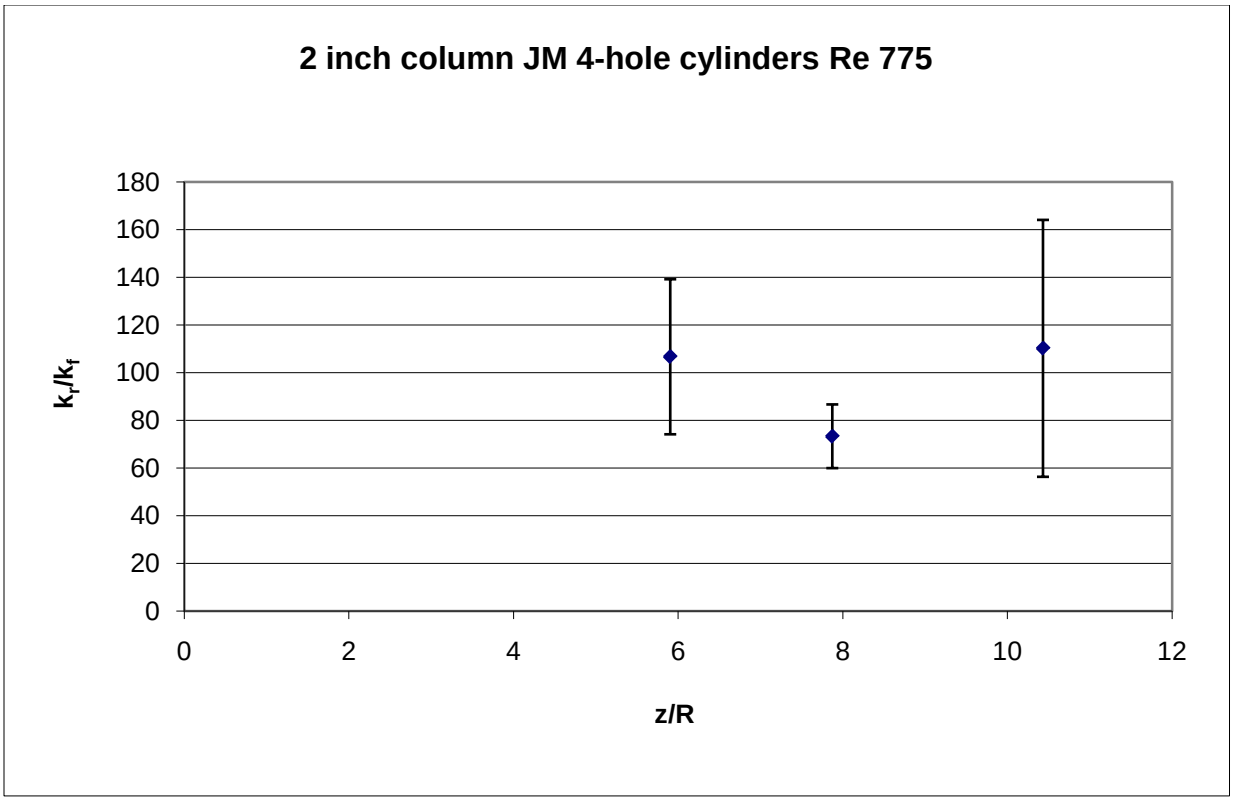
2 inch column JM 4-hole cylinders Re 775
180
160
140
120
100
80
60
40
20
0
k_r/k_f
0
2
4
6
8
10
12
z/R

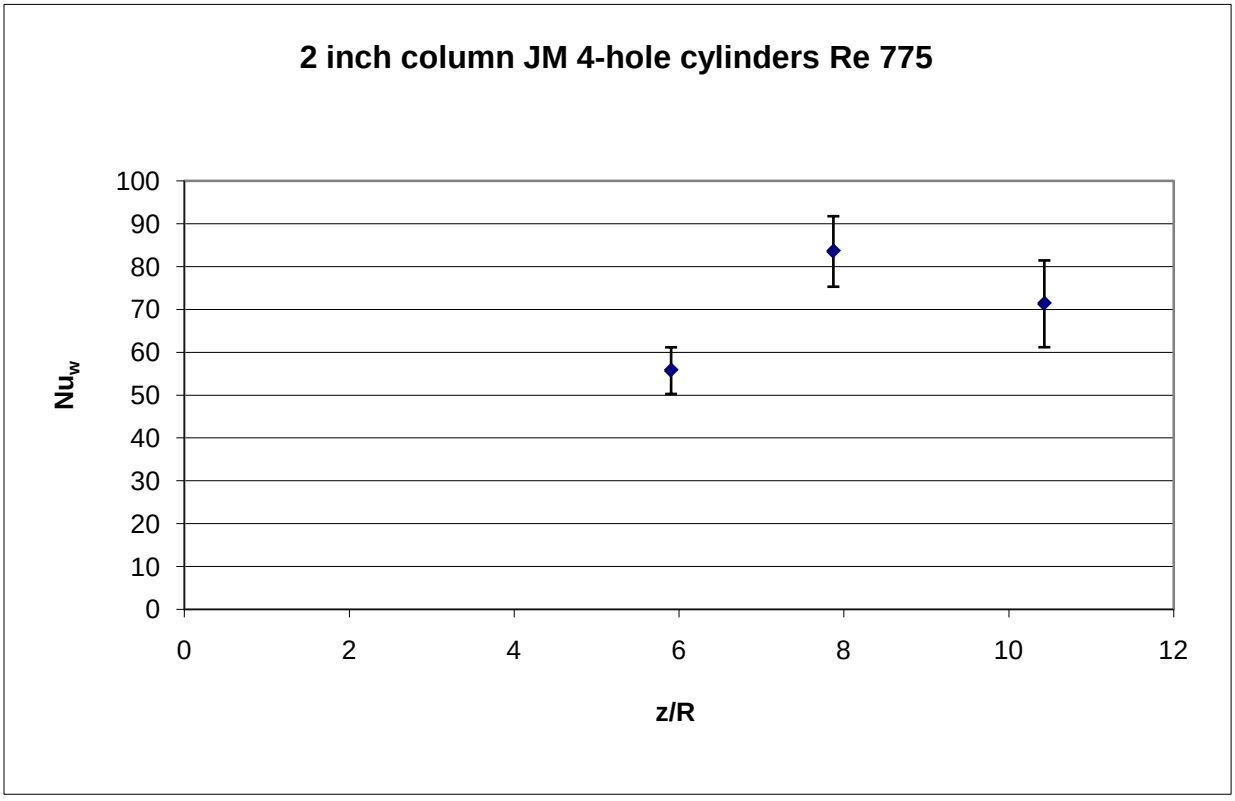
2 inch column JM 4-hole cylinders Re 775
100
90
80
70
60
50
40
30
20
10
0
Nu_w
0
2
4
6
8
10
12
z/R

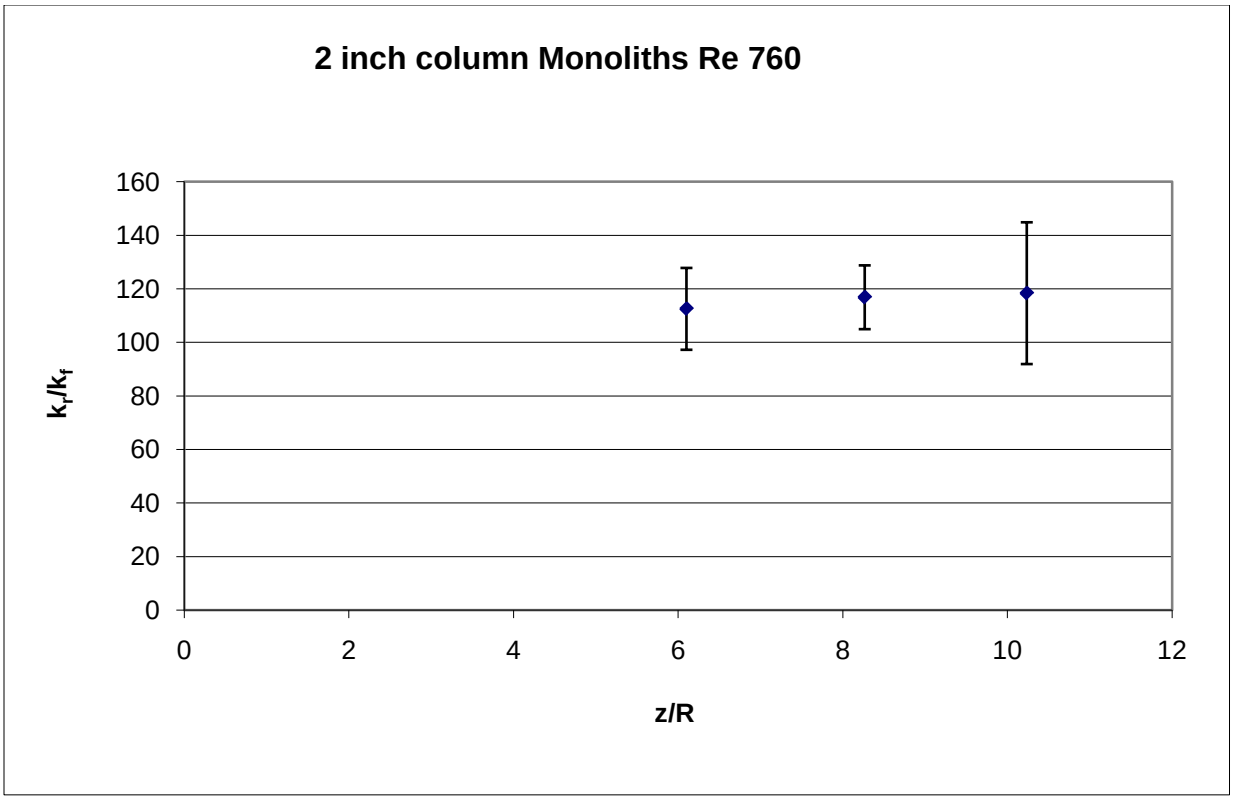
2 inch column Monoliths Re 760
160
140
120
100
80
60
40
20
0
k_t/k_f
0
2
4
6
8
10
12
z/R

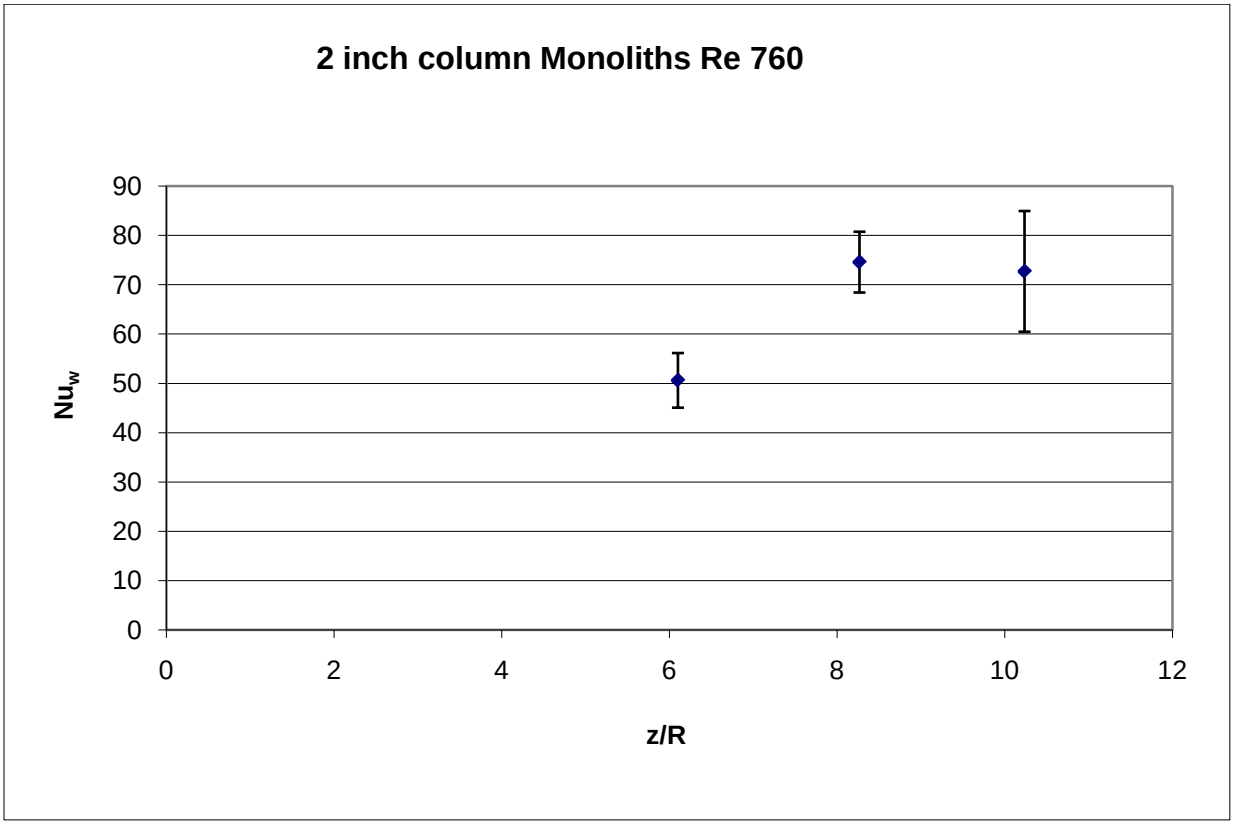
2 inch column Monoliths Re 760
90
80
70
60
50
40
30
20
10
0
Nu_w
0
2
4
6
8
10
12
z/R

Appendix E: k_r/k_f, Nu_w, Bi, and Pe_r for all Packings and Columns

4 inch column Spheres

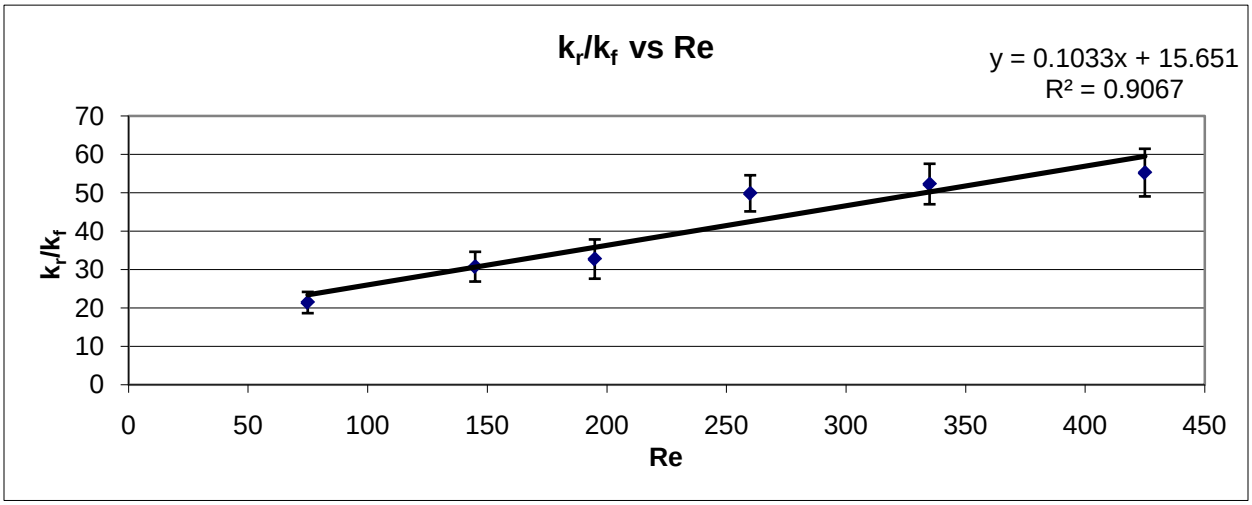

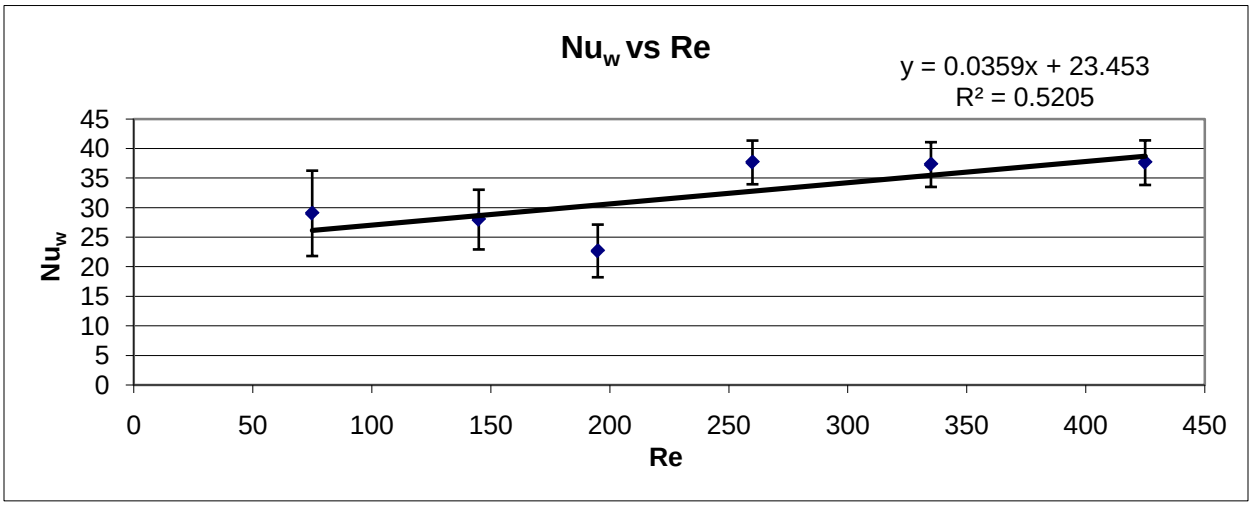

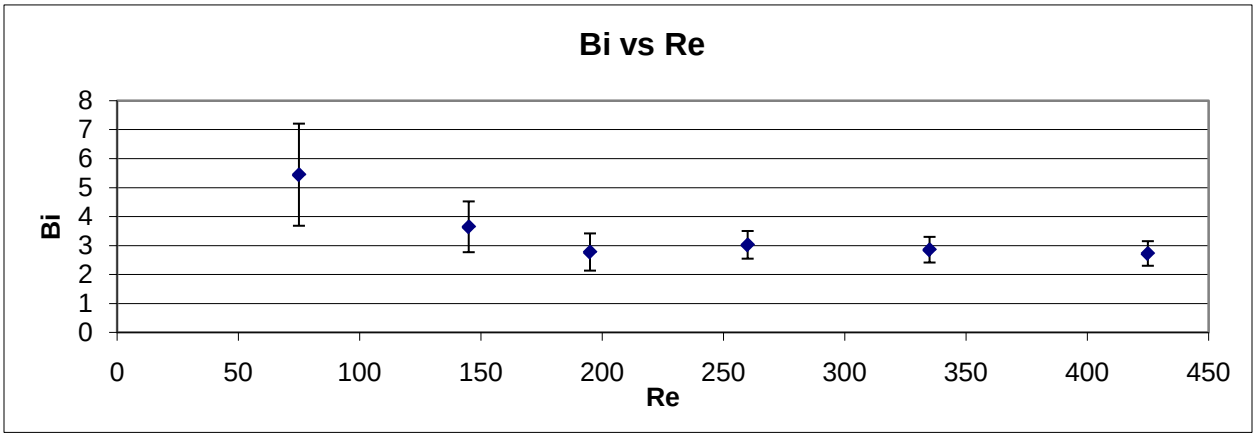

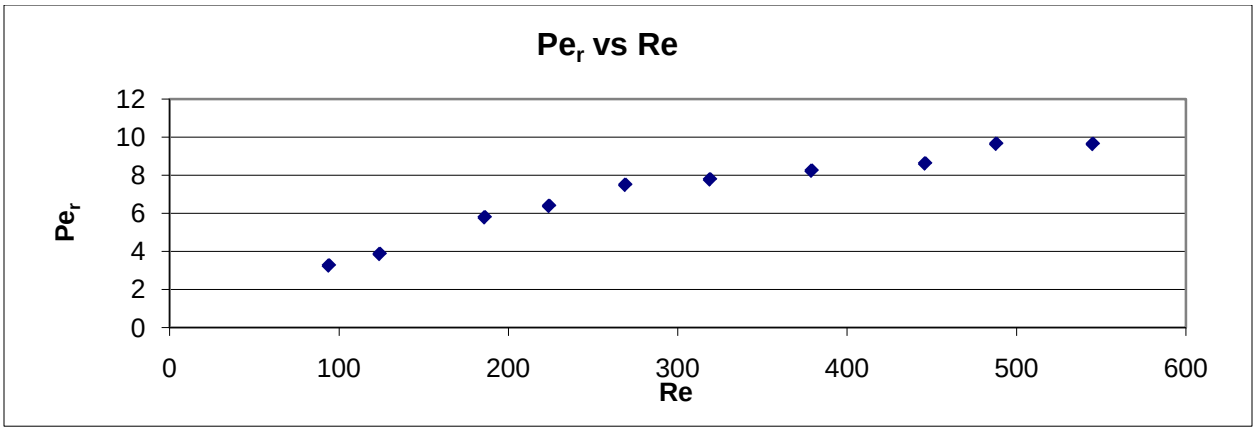
Pe_r vs Re
Pe_r
Re
0
2
4
6
8
10
12
0
100
200
300
400
500
600

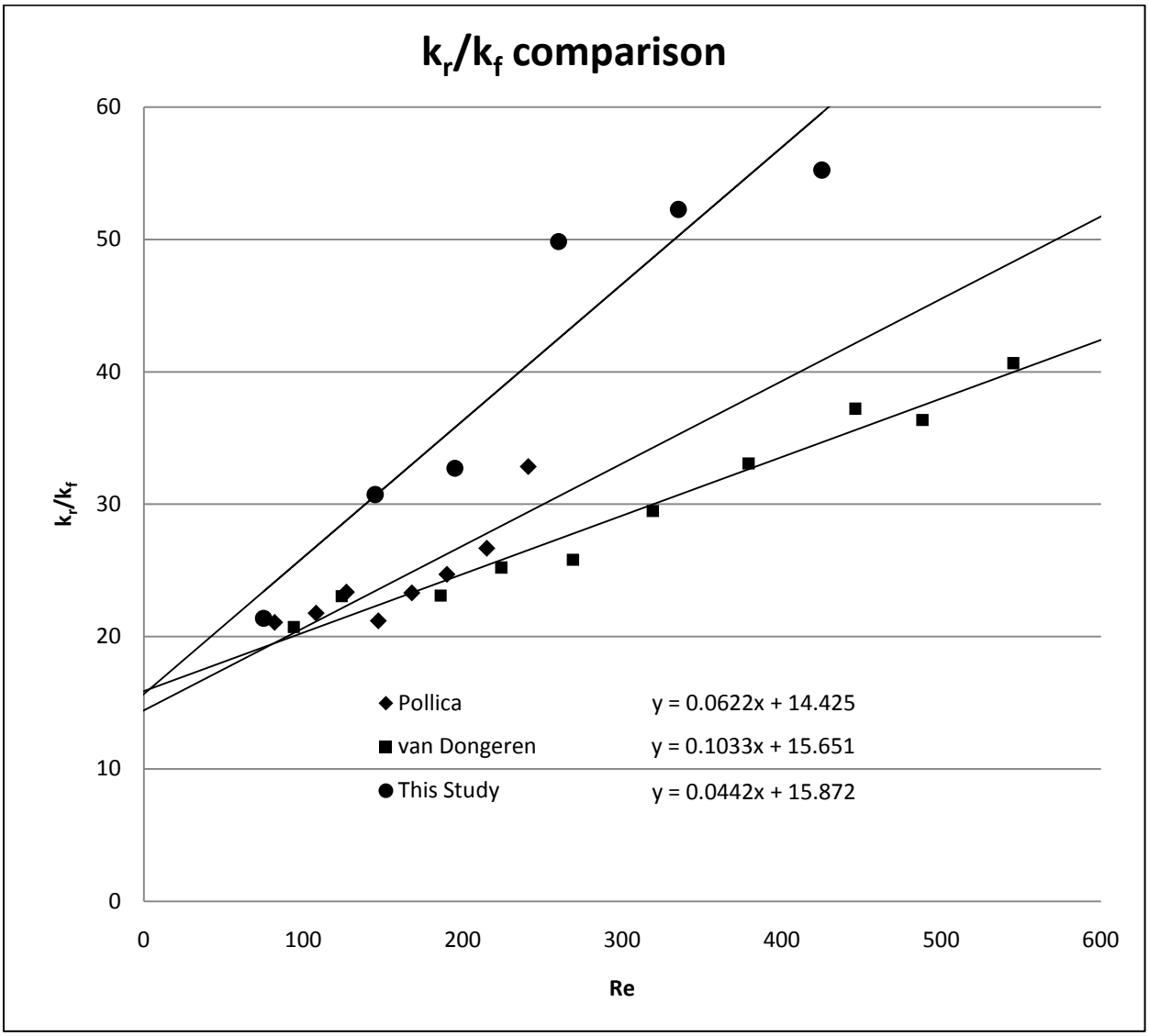
k_r/k_f comparison
k_r/k_f
Re
0
10
20
30
40
50
60
0
100
200
300
400
500
600
Pollica
y = 0.0622x + 14.425
van Dongeren
y = 0.1033x + 15.651
This Study
y = 0.0442x + 15.872

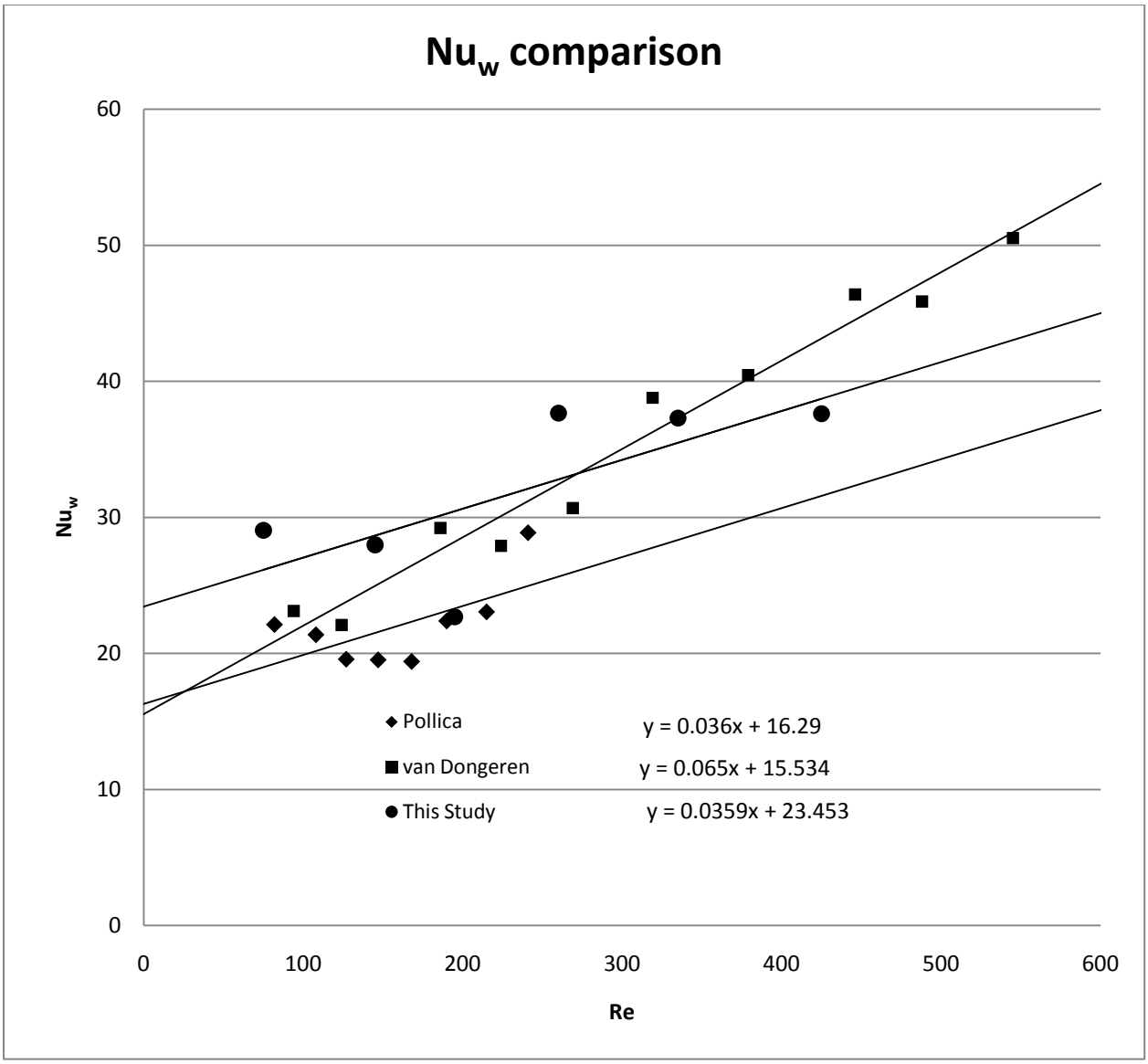
Nu$_w$ comparison
60
50
40
30
20
10
0
Nu$_w$
0
100
200
300
400
500
600
Re
Pollica
van Dongeren
This Study
y = 0.036x + 16.29
y = 0.065x + 15.534
y = 0.0359x + 23.453

4 inch column Spheres (Van Dongeren)

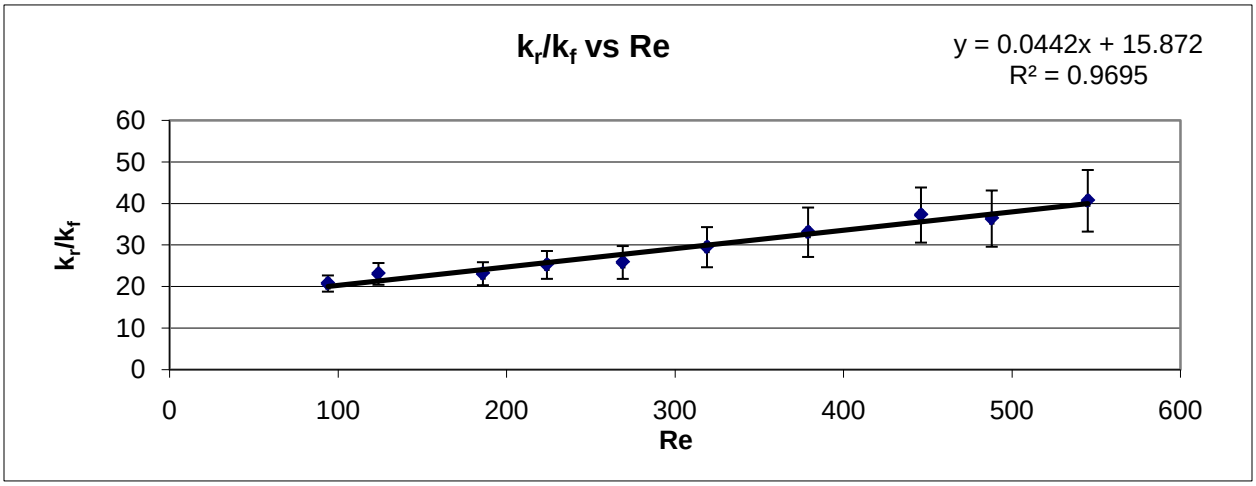

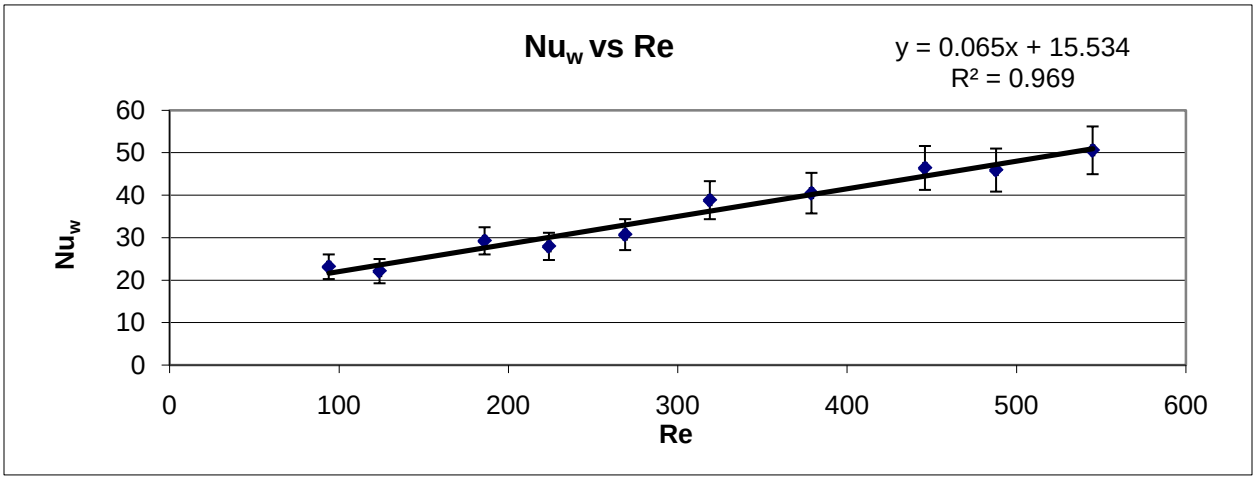

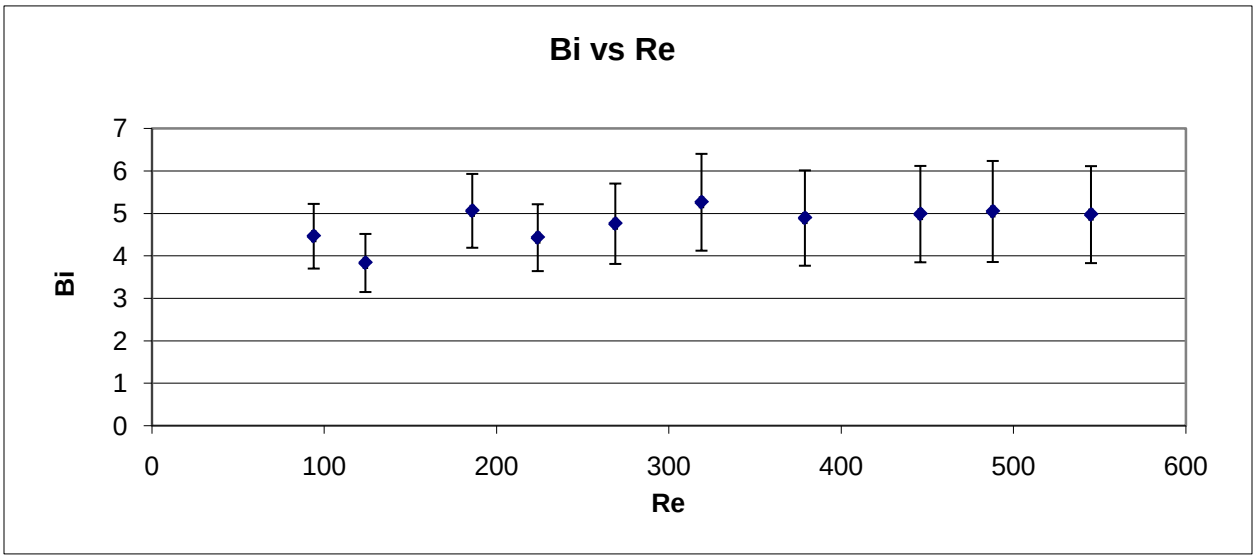

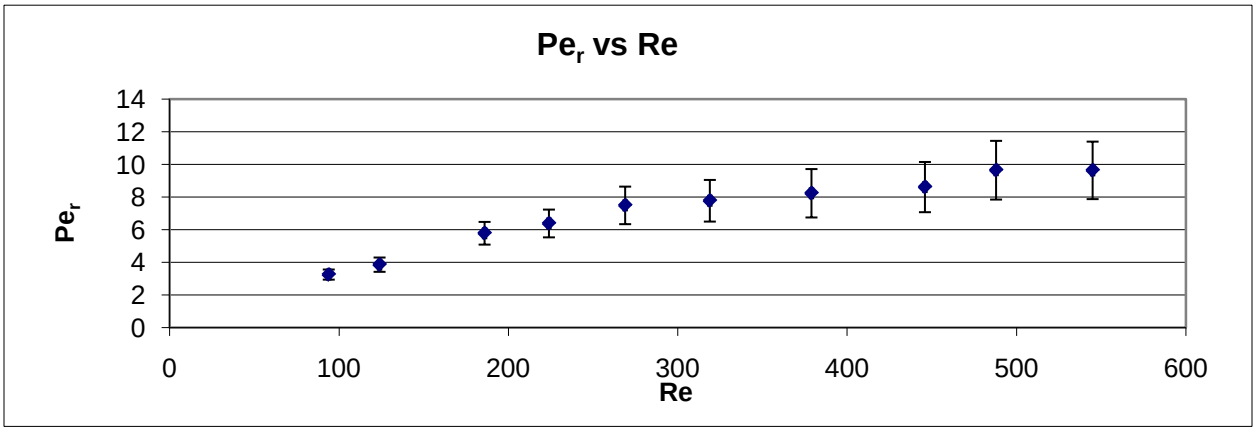
Per vs Re
Per
14
12
10
8
6
4
2
0
0
100
200
300
400
500
600
Re

4 inch column Spheres (Pollica)

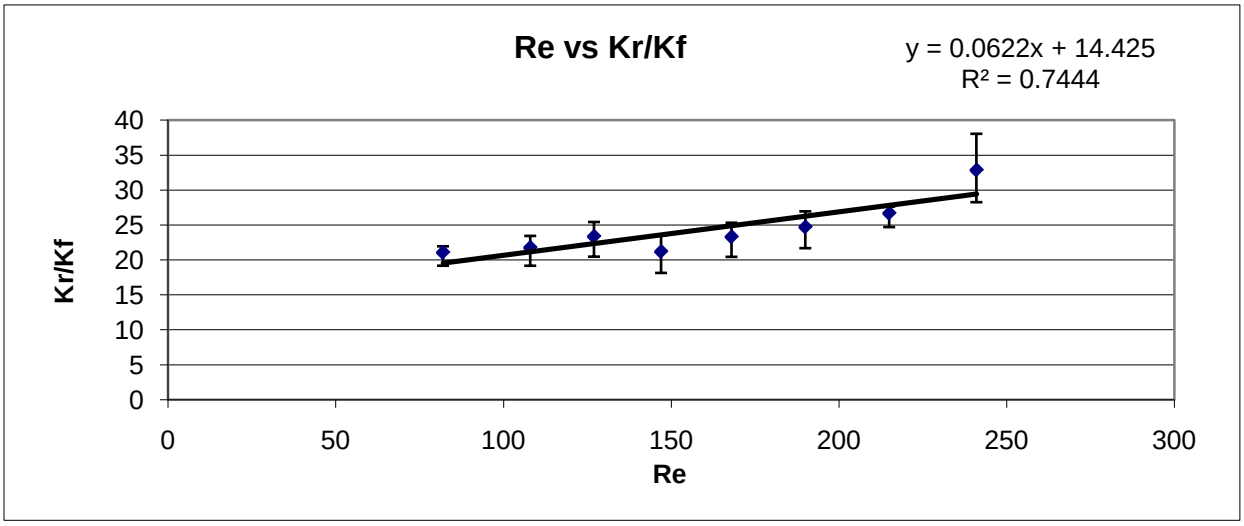

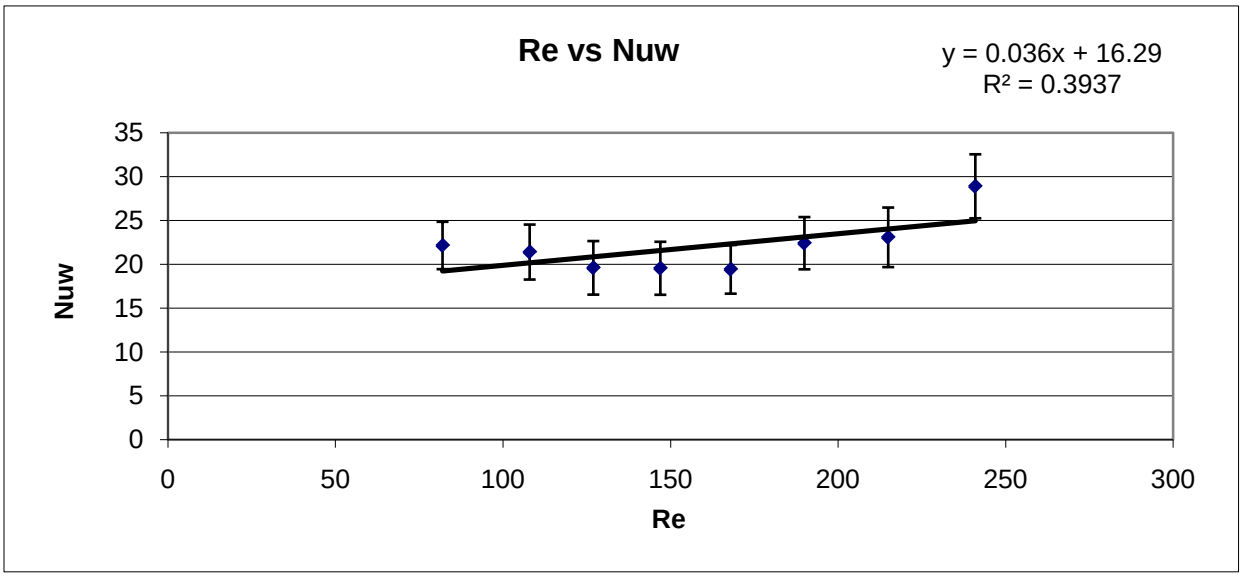

4 inch column Raschig Rings

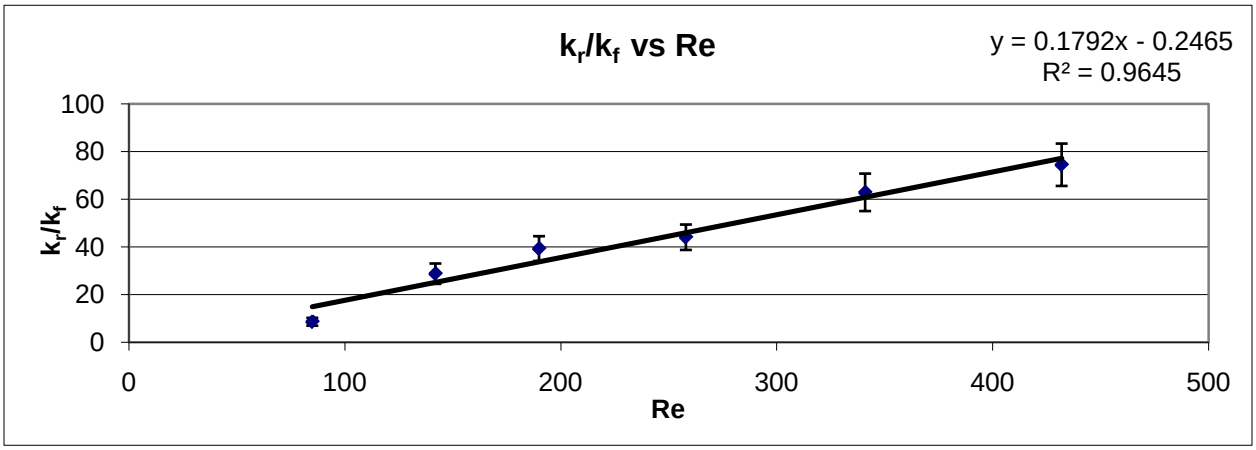

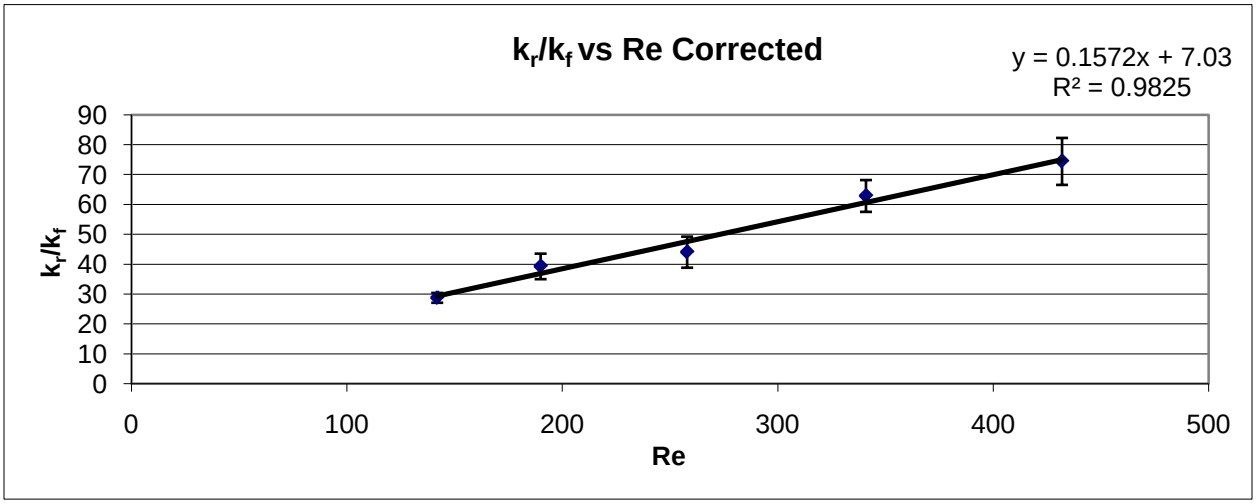

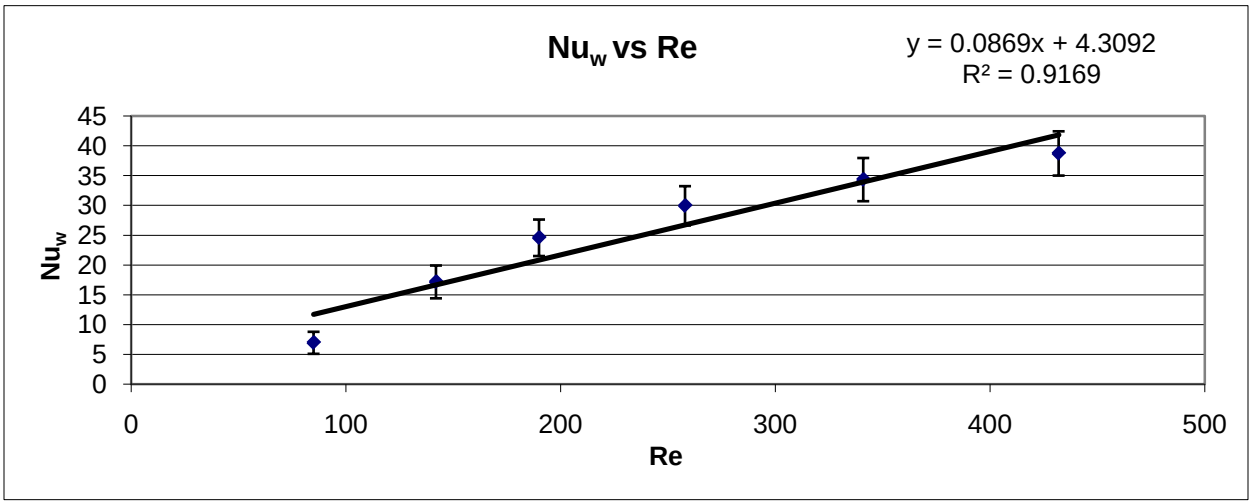

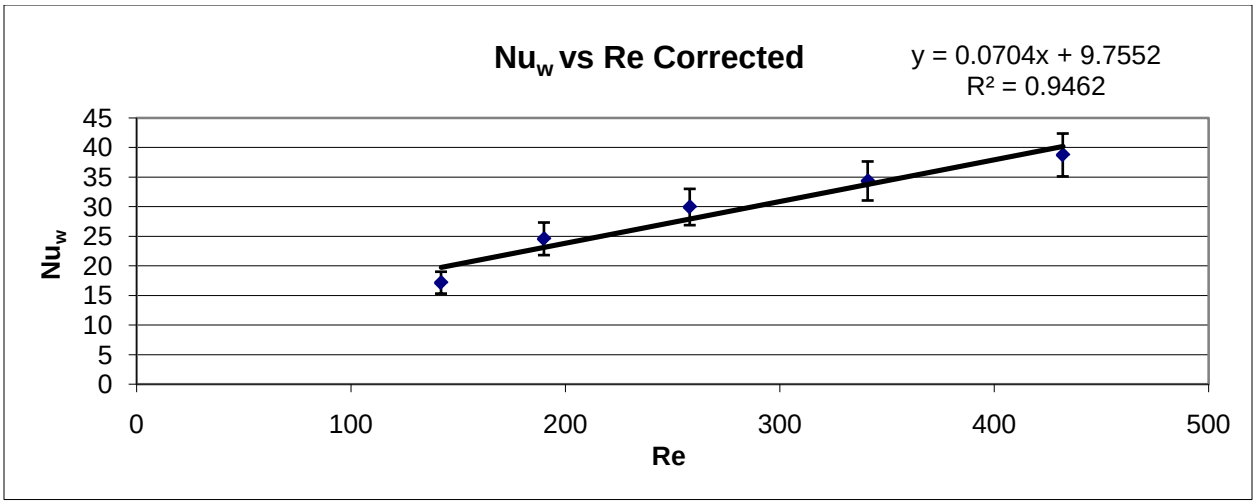
Nu_w vs Re Corrected
y = 0.0704x + 9.7552
R² = 0.9462
Nu_w
45
40
35
30
25
20
15
10
5
0
0
100
200
300
400
500
Re

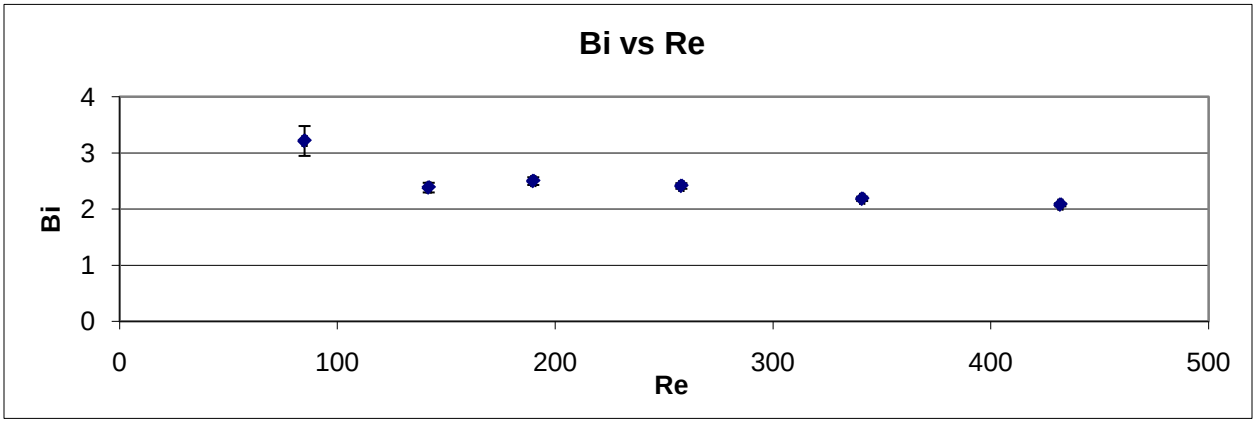
Bi vs Re
Bi
4
3
2
1
0
0
100
200
300
400
500
Re

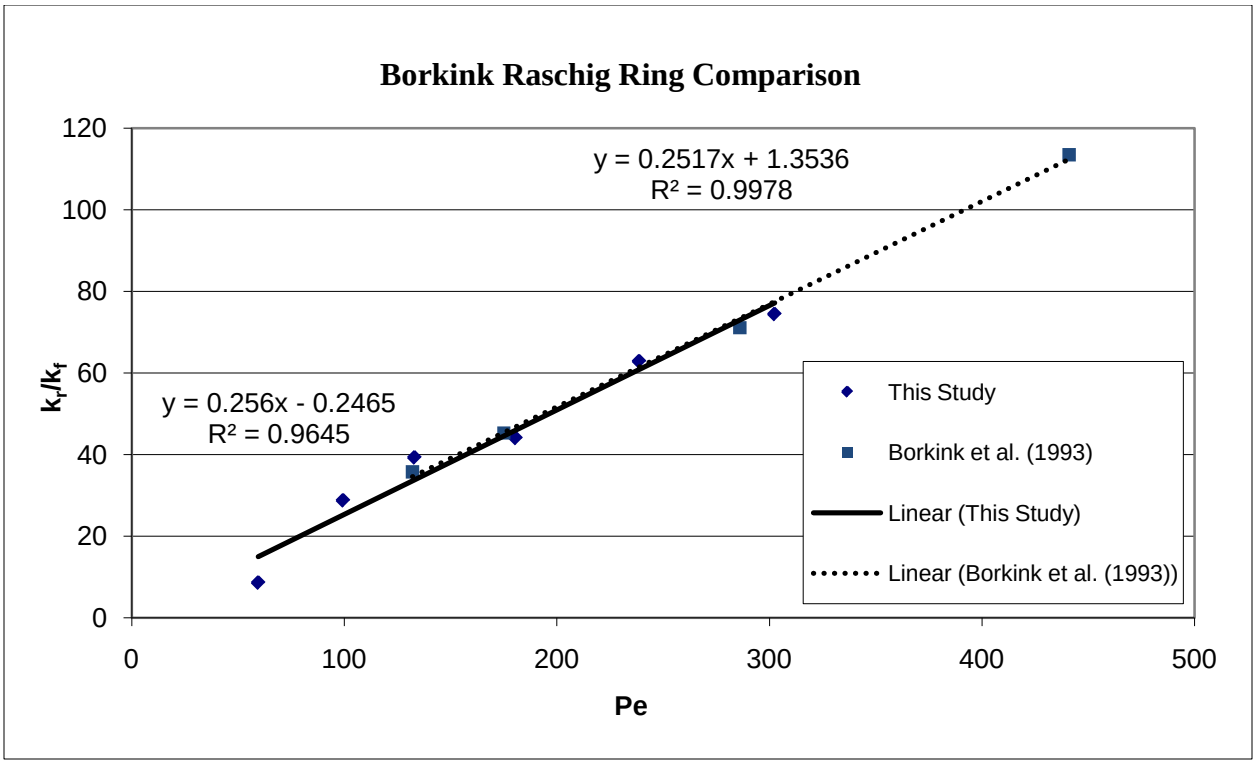
Borkink Raschig Ring Comparison
y = 0.2517x + 1.3536
R² = 0.9978
y = 0.256x - 0.2465
R² = 0.9645
This Study
Borkink et al. (1993)
Linear (This Study)
Linear (Borkink et al. (1993))
kc/kf
Pe
0
20
40
60
80
100
120
0
100
200
300
400
500

4 inch column JM 4-hole cylinders

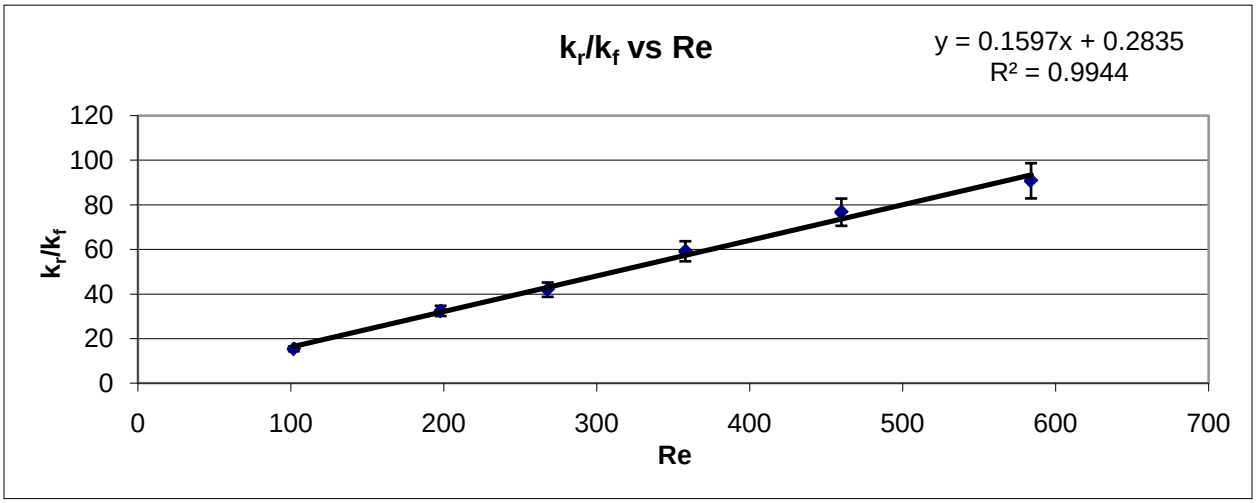

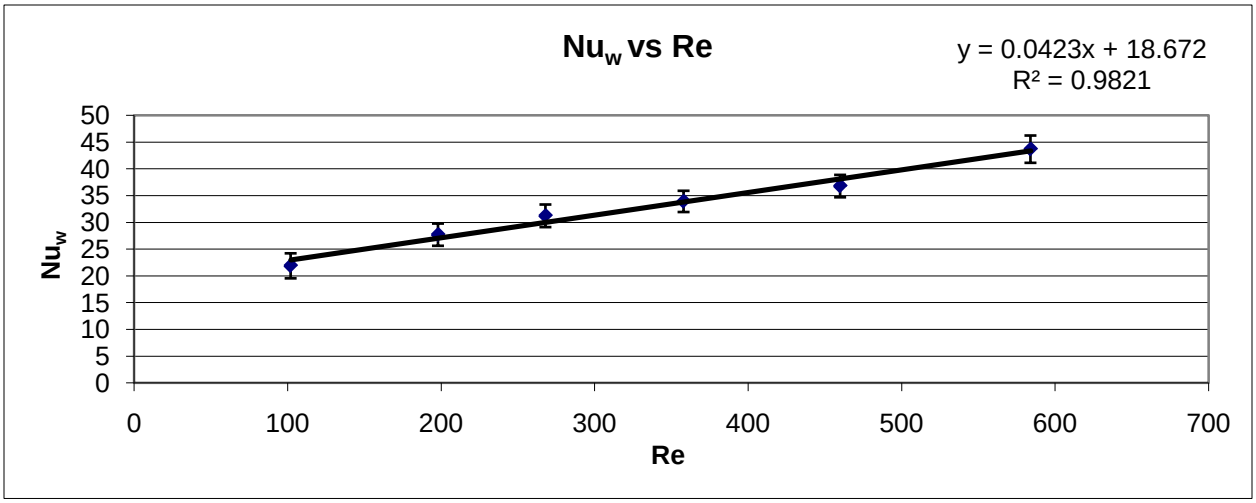

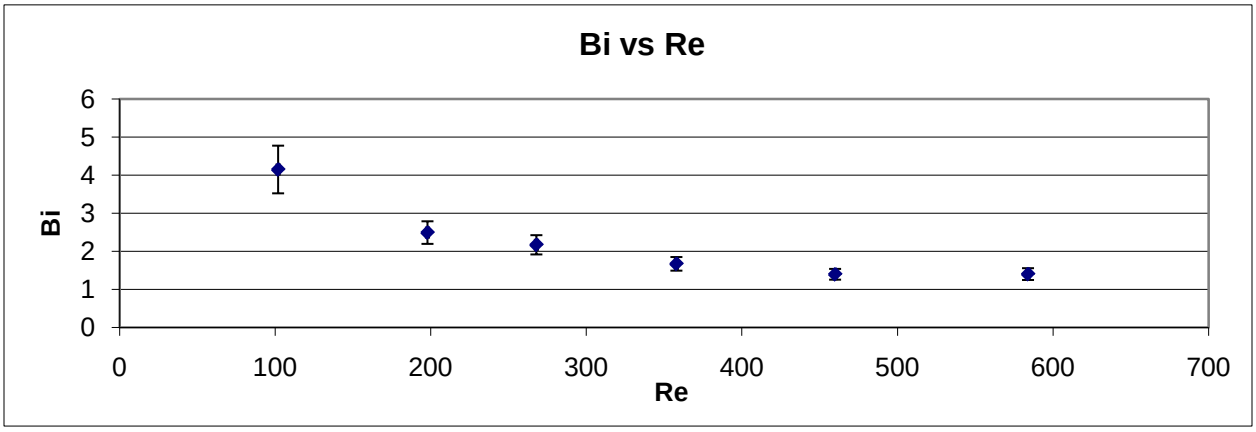

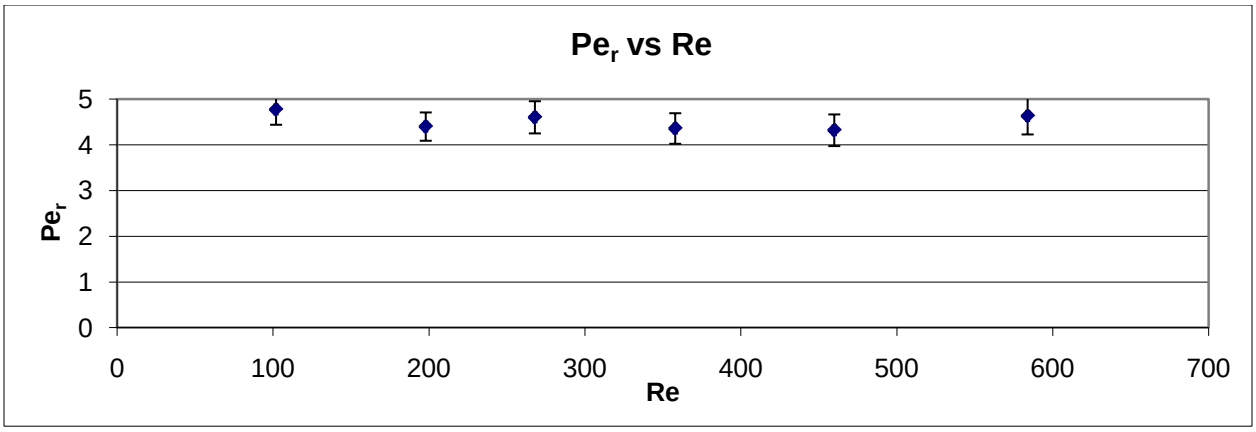
Per vs Re
Per
5
4
3
2
1
0
0
100
200
300
400
500
600
700
Re

4 inch column Monoliths

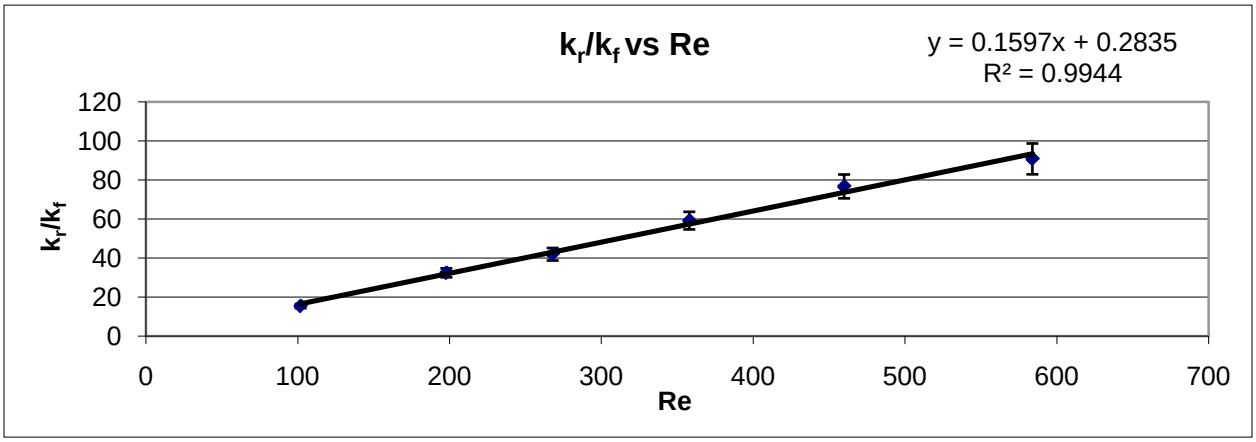

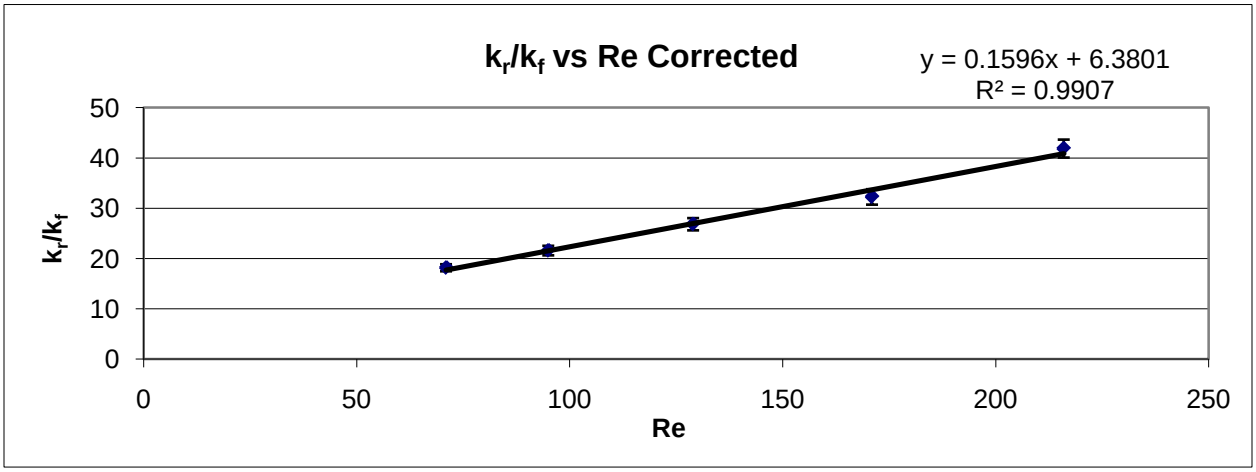

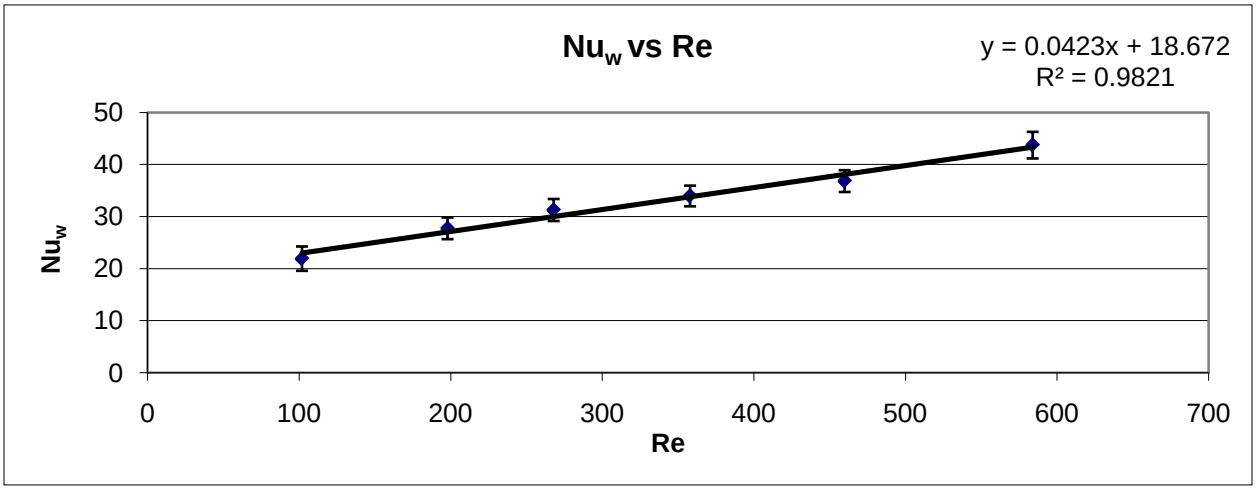

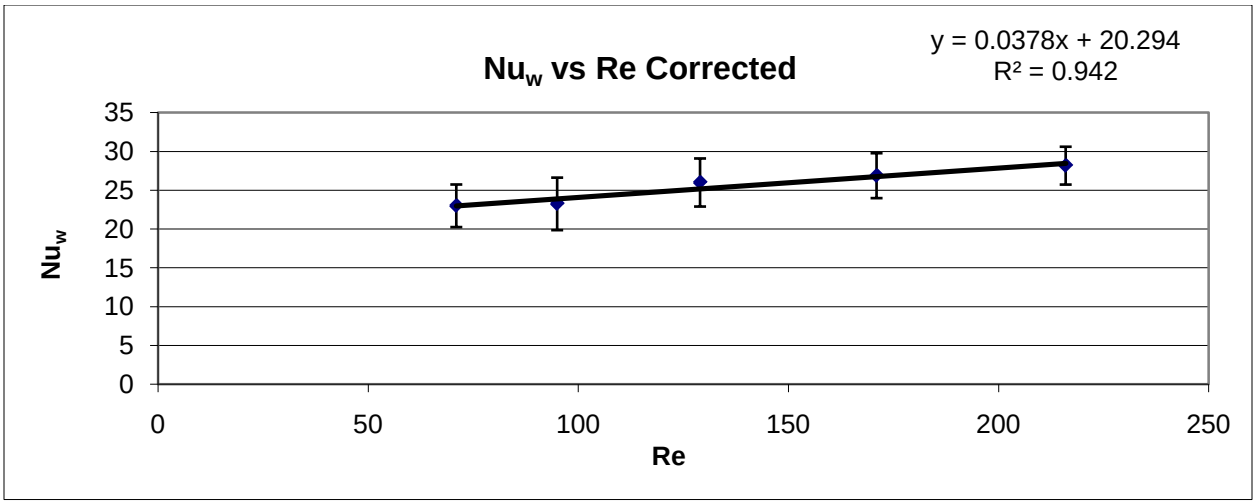
Nu_w vs Re Corrected
y = 0.0378x + 20.294
R² = 0.942
Nu_w
Re
0
5
10
15
20
25
30
35
0
50
100
150
200
250

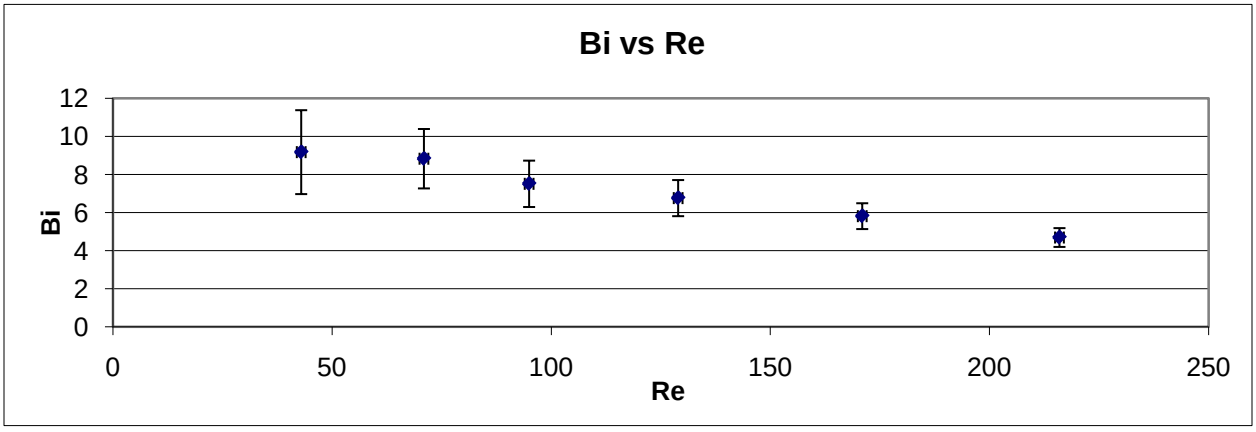
Bi vs Re
Bi
Re
0
2
4
6
8
10
12
0
50
100
150
200
250

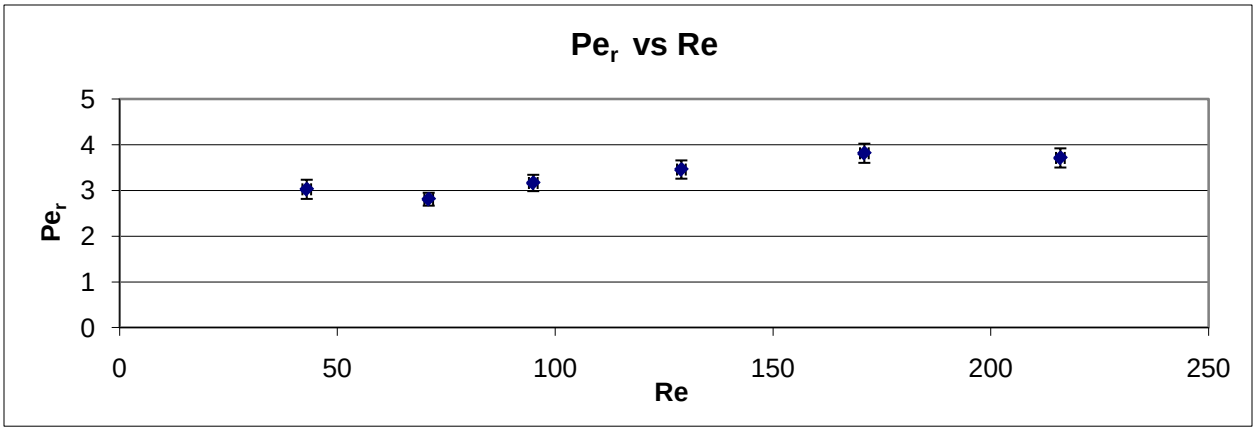
Pe_r vs Re
Pe_r
Re
0
1
2
3
4
5
0
50
100
150
200
250

2 inch column Raschig Rings

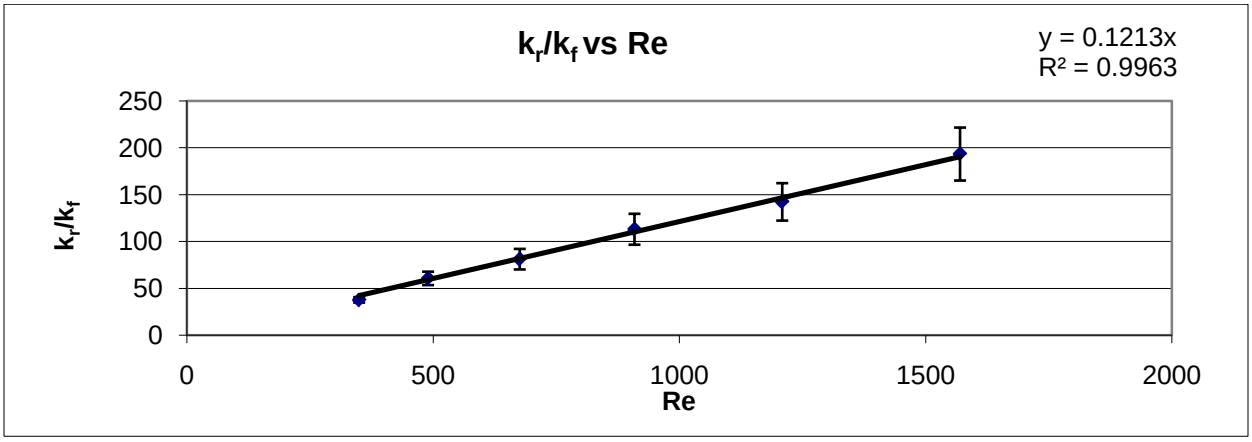

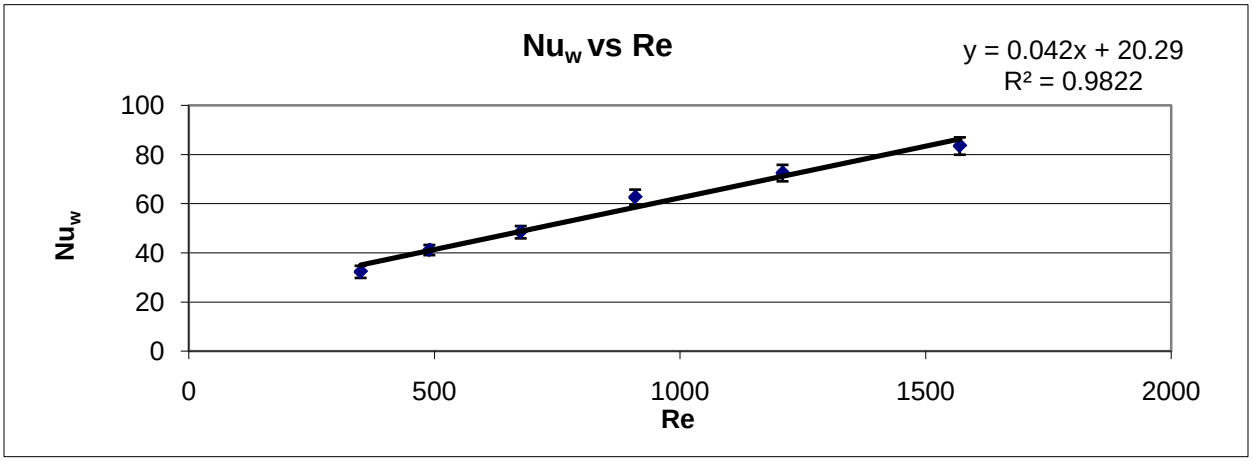

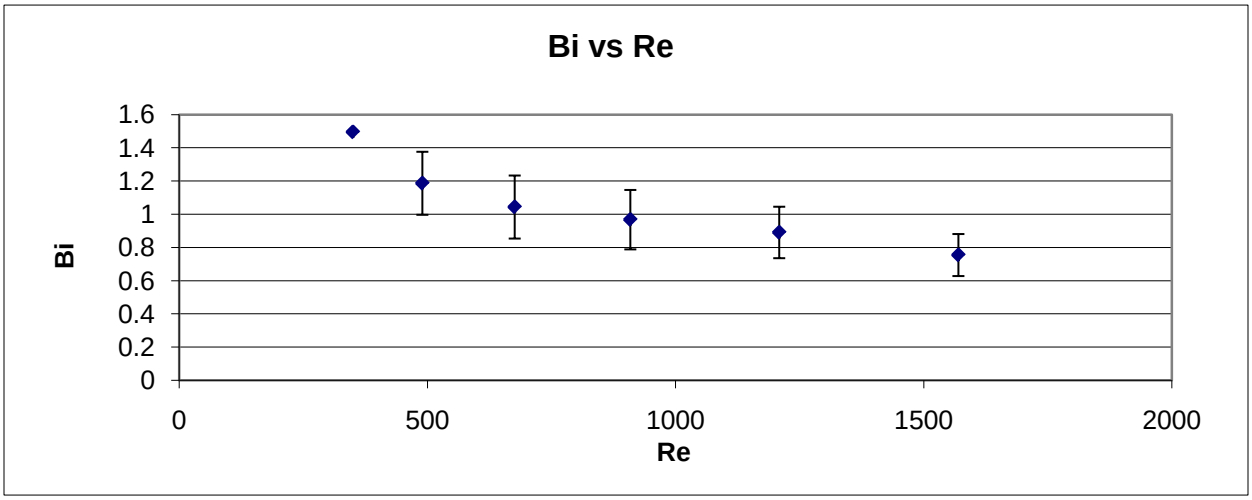

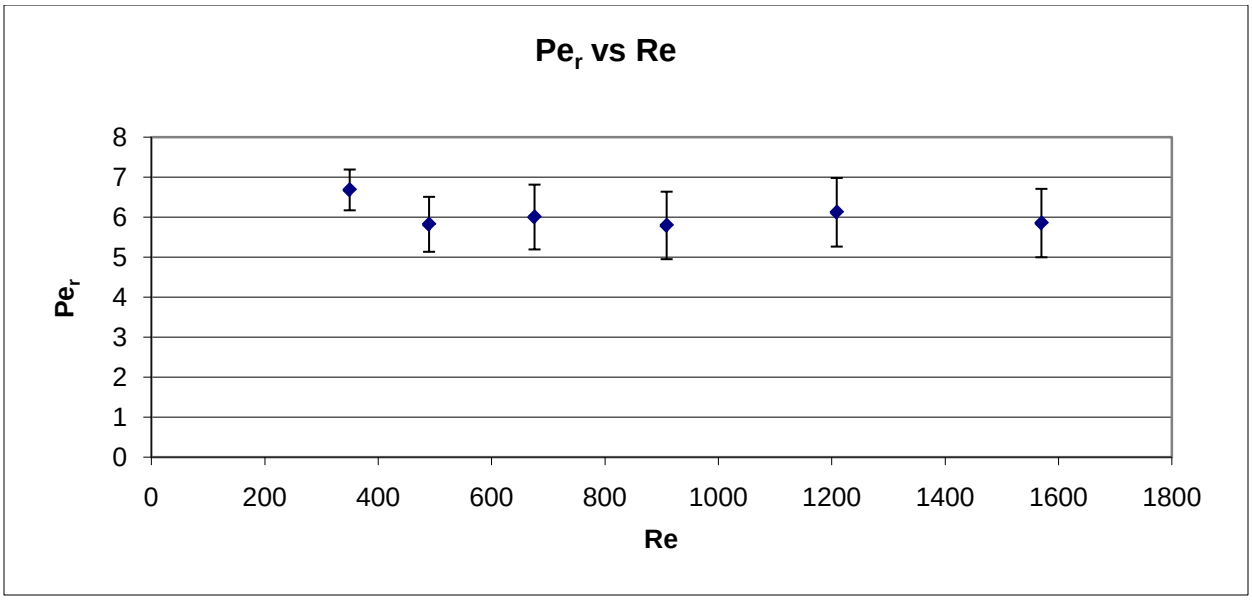
Per vs Re
8
7
6
5
4
3
2
1
0
Per
0
200
400
600
800
1000
1200
1400
1600
1800
Re

2 inch column 4-hole cylinders

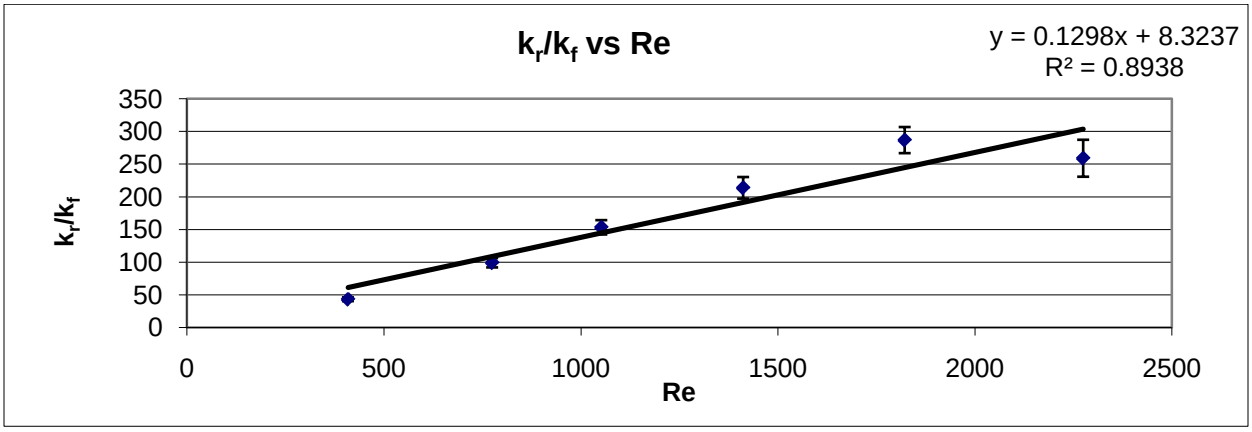

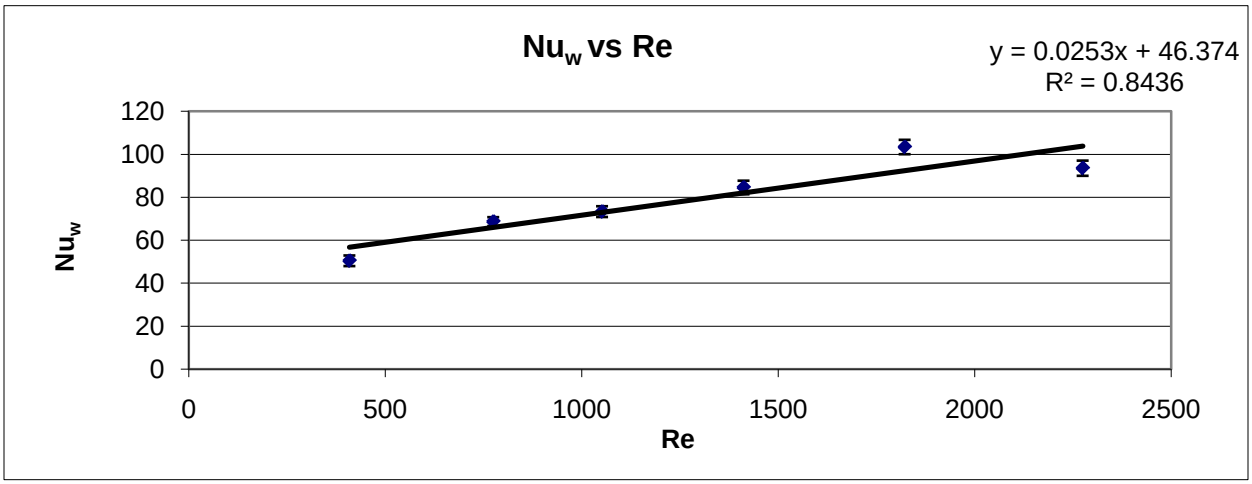

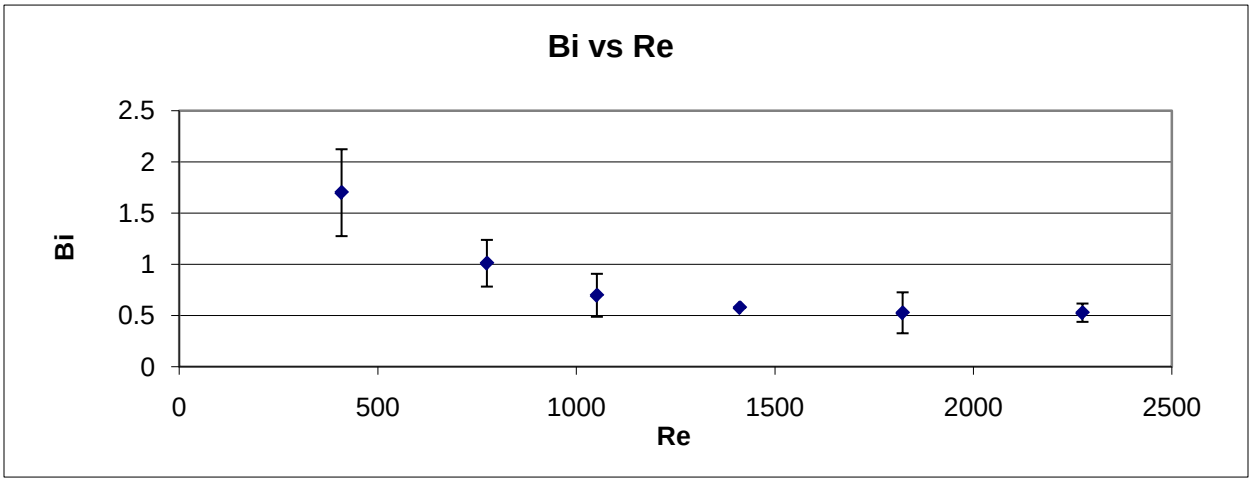

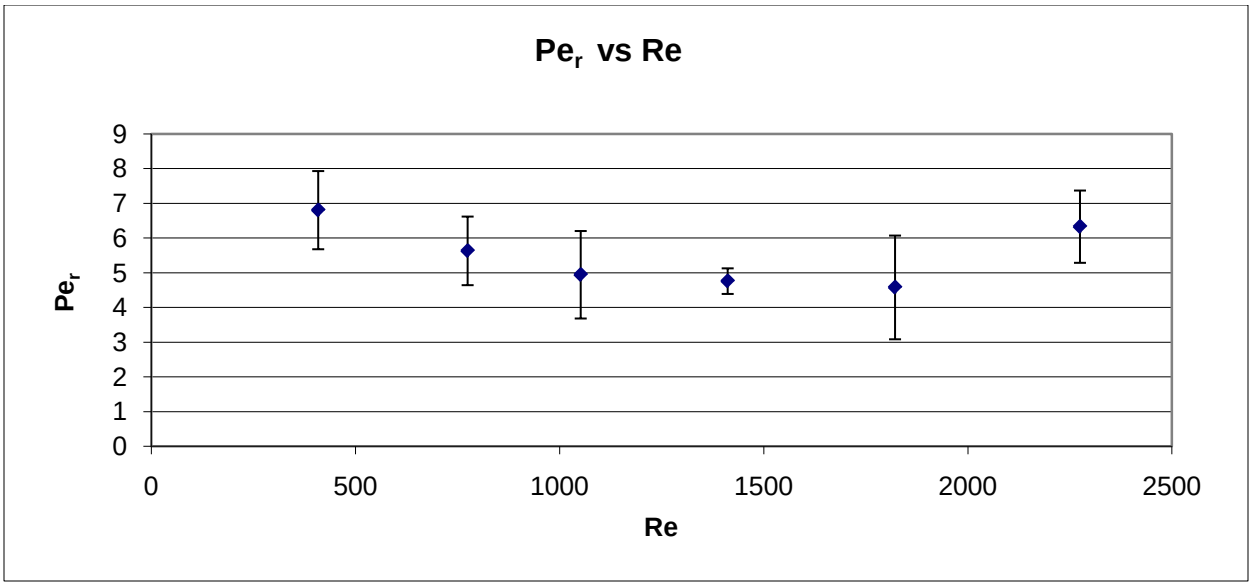
Per vs Re
Per
9
8
7
6
5
4
3
2
1
0
0
500
1000
1500
2000
2500
Re

2 inch column Monoliths

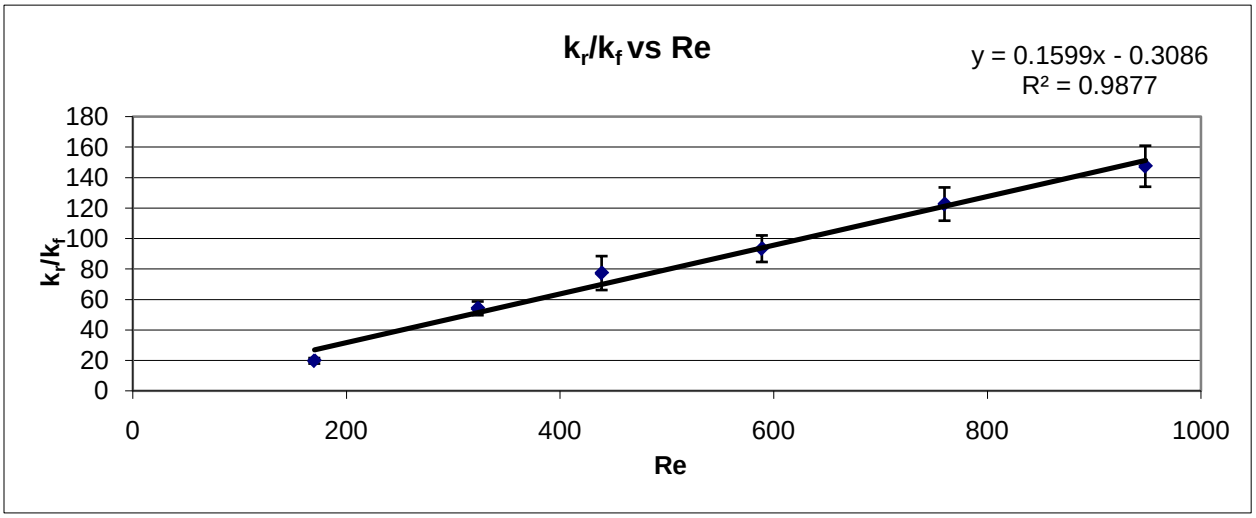

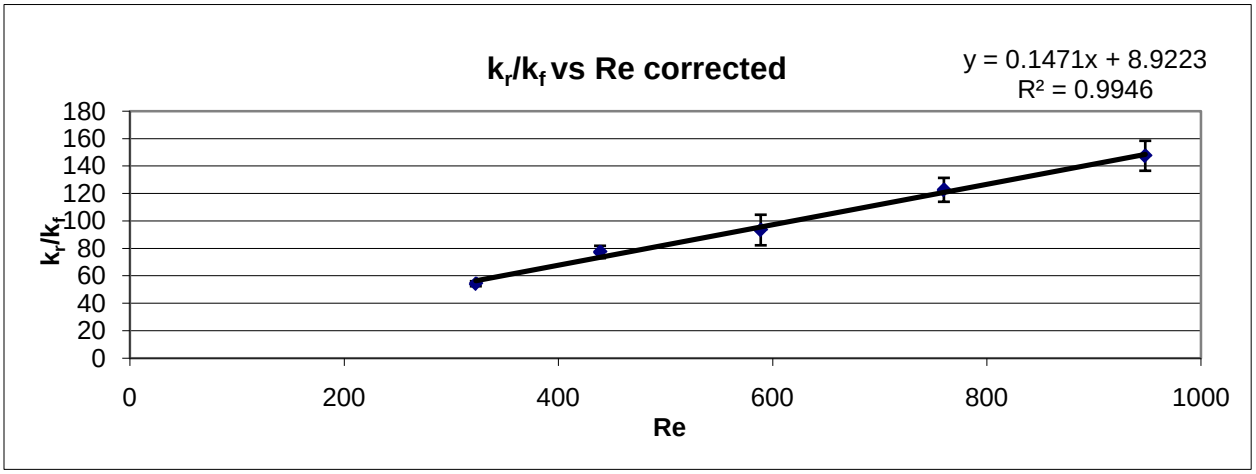

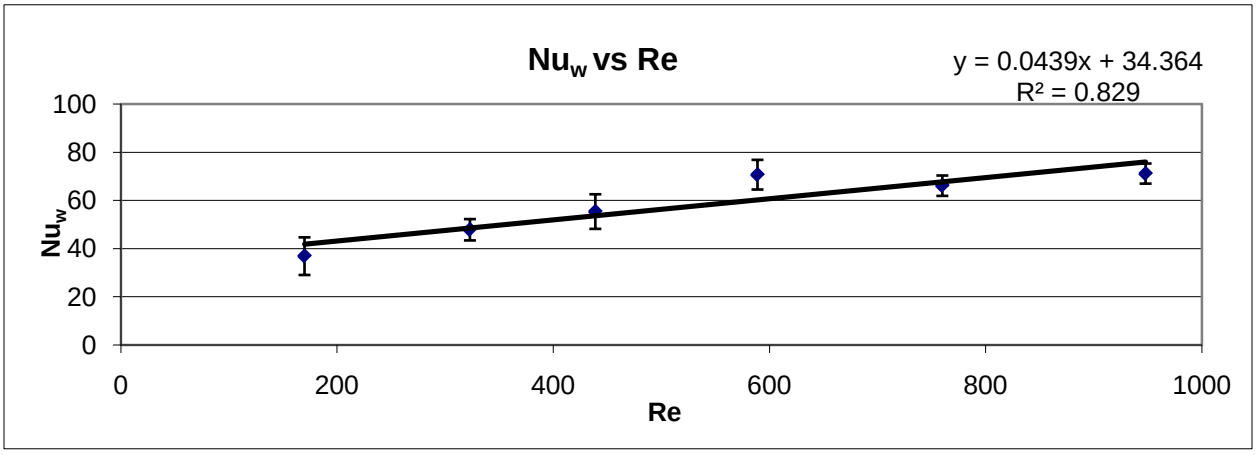

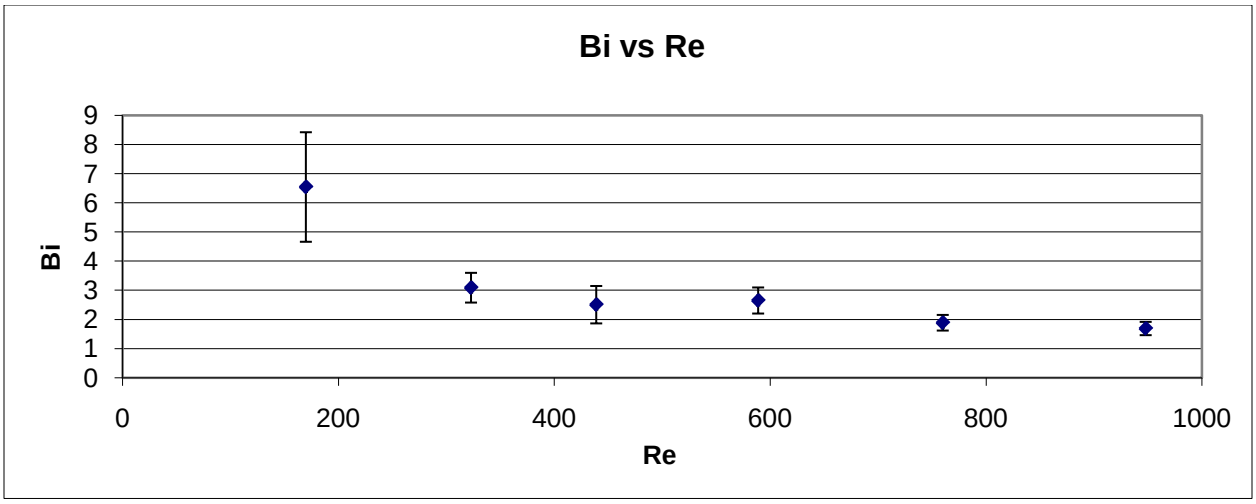
Bi vs Re
Bi
9
8
7
6
5
4
3
2
1
0
0
200
400
600
800
1000
Re

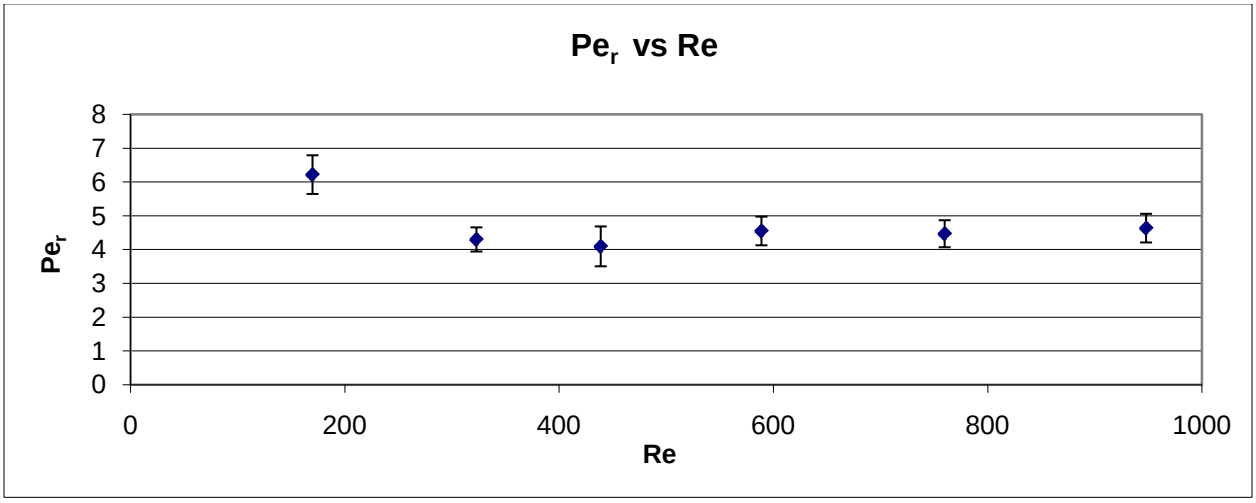
Pe$_r$ vs Re
Pe$_r$
8
7
6
5
4
3
2
1
0
0
200
400
600
800
1000
Re

Appendix F: F-test values

Column	Packing	Re	F/F95
4 Inch Column	Spheres	75	0.384578
		145	1.008367
		195	0.671051
		260	0.53057
		335	0.307174
		425	0.210865
	Raschig Rings	85	0.42928
		142	0.338531
		190	0.377891
		258	0.331282
		341	0.386067
		432	0.424467
	4-hole Cylinders	102	0.806354
		198	0.641854
		268	0.481158
		358	0.558235
		460	0.727119
		584	0.493383
	Monoliths	43	4.647282
		71	1.305055
		95	0.983003
		129	0.629038
		171	0.886185
		216	1.336643
2 Inch Column	Raschig Rings	350	3.912612
		490	2.507197
		676	3.358442
		909	5.43473
		1209	4.867726
		1570	3.886017
	4-hole Cylinders	409	0.82748
		775	2.000006
		1052	0.668281
		1412	1.207582
		1822	1.15873
		2275	1.615775
	Monoliths	170	2.37015
		323	3.674283
		439	10.36014
		589	2.966539
		760	0.986552
		948	1.847035